THE UNIVERSITY OF CHICAGO

SYNTHESIS AND OLEFIN POLYMERIZATION BEHAVIOR OF ELECTRONICALLY-UNSYMMETRICAL PD(II)-ALKYL CATALYSTS

A DISSERTATION SUBMITTED TO

THE FACULTY OF THE DIVISION OF THE PHYSICAL SCIENCES

IN CANDIDACY FOR THE DEGREE OF

DOCTOR OF PHILOSOPHY

DEPARTMENT OF CHEMISTRY

BY

ALISON JOHNSON WILDERS

CHICAGO, ILLINOIS

JUNE 2019

TABLE OF CONTENTS

LIST OF TABLES

CHAPTER TWO

CHAPTER THREE

CHAPTER FOUR

LIST OF FIGURES

CHAPTER TWO

CHAPTER THREE

CHAPTER FOUR

LIST OF SCHEMES

CHAPTER ONE

CHAPTER TWO

CHAPTER THREE

CHAPTER FOUR

LIST OF CHARTS

LIST OF EQUATIONS

CHAPTER ONE

CHAPTER THREE

ACKNOWLEDGEMENTS

First, I thank my advisor, Professor Richard Jordan, for his invaluable guidance and instruction throughout my graduate studies. It has been a privilege to learn from his example of both scientific rigor and professionalism. I also thank the other members of my thesis committee, Professors Michael Hopkins and John Anderson, for their advice and helpful discussions.

I have been fortunate to work with fantastic chemists in the Jordan group. I am especially grateful to Dr. Qian Liu for her mentorship when I first joined the group and for continuing to provide advice and insight throughout graduate school. I would like to thank former and current group members who made for a welcoming environment and enjoyable experience, including Dr. Rebecca Black, Erik Reinhart, Dr. Frank Olechnowicz, Joseph Solomon, James Earl, Dr. Ka Cheong (Tim) Lau, Dr. Feng Zhai, Dr. Ge (David) Feng, Dr. Jia Wei, Amanda Waterbury, Max Weinberg, and Isabel Jensen. I would also like to thank the Anderson group, especially those sharing the Jordan lab space, for also providing an enjoyable lab environment as our group has gotten smaller.

I am grateful to my undergraduate research advisor, Professor Matthew Young at Hillsdale College, for giving me the opportunity to become involved in research and his support in my decision to pursue graduate school.

The research described in this thesis relied heavily on departmental facilities, and I thank Dr. Antoni Jurkiewicz for his assistance with NMR Spectroscopy, Dr. Chang-Jin Qin for his assistance with mass spectrometry, and Dr. Alexander Filatov for his assistance with X-ray crystallography.

I thank my family and friends who have provided tremendous support throughout graduate school, especially my parents, Nancy and Dave Johnson, and my siblings, Hayley, Kerry, Brian, and Jen. I would also like to thank Becca Remmes, Tess Loniewski, Kate Smith, Carley Ross, and Emily Kupa for providing great memories during my time in graduate school. Finally, I thank my husband, Steven, for his love and continued support since the beginning of my studies and into the future.

ABSTRACT

This thesis describes new Pd(II)-alkyl catalysts for ethylene polymerization and strategies for enhancing their catalytic performance. These catalysts feature chelating, electronically-asymmetric ligands that contain strong phosphine and weak sulfonate or phosphonate donor groups. The effects of the phosphonate donor group and the remote binding of Lewis acids to the phosphonate on catalyst performance was explored. Synthetic studies on the self-assembly of Pd(II)-alkyl complexes containing phosphine-*bis*-arenesulfonate ligands to tetrameric cage structures that can polymerize ethylene to high molecular weight polyethylene is also described.

Chapter One introduces Pd(II)-alkyl complexes that contain ancillary phosphine-arenesulfonate (PO) ligands. (PO)PdRL catalysts are unique in their ability to copolymerize ethylene and a wide variety of polar vinyl monomers to highly linear functionalized polyethylene. The ability to produce new types of functionalized polymers with enhanced properties motivates the development of new PO-type Pd catalysts and new strategies for enhancing the catalytic performance of these catalysts.

Chapter Two describes Pd(II)-alkyl complexes containing phosphine-monoalkyl phosphonate ligands ([1-PAr_2-2-PO_2(OR)-Ph]$^-$ $[PPO]^-$). The complexes (κ^2-1-*P*Ar_2-2-P*O*$_2$(OR)-Ph)PdMeL ((PPO)PdMeL) were prepared and characterized in the solid state and in solution. The reaction of the Pd complexes with one or two equiv of $B(C_6F_5)_3$ generates the borane adduct (κ^2-1-*P*Ar_2-2-P(*O*)(O-B(C_6F_5)$_3$)(OR)-Ph)PdMeL or the base-free, borane adduct {(κ^2-1-*P*Ar_2-2-P(*O*)(O-B(C_6F_5)$_3$)(OR)-Ph)PdMe}$_2$, respectively. The borane adducts were characterized by X-ray crystallography and in solution. The reactivity of the (PPO)PdMeL complexes with other

Lewis acids is also described.

Chapter Three describes the ethylene polymerization performance of the complexes prepared in Chapter Two. Remote binding of $B(C_6F_5)_3$ to (PPO)PdMeL (L =pyridine or lutidine) or $\{(PPO)PdMe\}_2$ ethylene polymerization catalysts that contain phosphine-monoalkyl phosphonate ligands significantly increases the catalyst activity and the molecular weight of the polyethylene (PE) product. X-ray structural data, trends in ligand lability, and comparative studies of BF_3 activation suggest that these allosteric effects are primarily electronic in origin. The $B(C_6F_5)_3$ binding enhances R_{growth} by increasing the degree of positive charge on the Pd center. This effect does not result in the large increase in $R_{transfer}$ and concomitant reduction in PE molecular weight seen in previous studies of analogous (PO)PdRL catalysts that contain phosphine-arenesulfonate ligands, because of the operation of an unusual dissociative chain transfer process, which is inhibited by the increased charge at Pd.

Chapter Four describes synthetic studies that were undertaken to further probe the factors that influence the self-assembly of four (Li-OPO)PdRL units containing phosphine-*bis*-arenesulfonate $[Li\text{-}OPO]^-$ ligands into tetranuclear cage structures. The factors that favor the self-assembly of the (Li-OPO)PdRL units around the periphery of a central $Li_4S_4O_{12}\bullet Li_2Cl_2$ expanded core over a $Li_4S_4O_{12}$ double-four-ring (D4R) core were explored. New $[Li\text{-}OPO]^-$ ligands were synthesized with either *meta*- or *para*-substituents, and the generation of tetrameric Pd assemblies based on $Li_4S_4O_{12}\bullet Li_2(OAc)_2$ and $Li_4S_4O_{12}\bullet Li_2Br_2$ cores was explored to determine if cage core expansion can be achieved using other M_2X_2 units besides Li_2Cl_2.

PREFACE

Each chapter has an independent numbering system for compounds. A given compound may have a different number in different chapters. For each chapter, the relevant experimental information, references and notes are provided at the end of the chapter.

(Phosphine-Arenesulfonate)Pd-Alkyl Olefin Polymerization Catalysts

1.1 Introduction

In 2002, Pugh and Drent reported that a Pd(II) catalyst formed *in situ* from 1-PH^+(2-OMe-Ph)$_2$-2-SO_3^--Ph (H[PO]) and $Pd(OAc)_2$ or $Pd(dba)_2$ could uniquely copolymerize ethylene and alkyl acrylates to highly-linear, ester-functionalized polyethylene (Scheme 1.1).[1] This kind of copolymerization is not possible with the highly oxophilic early transition metal catalysts that are traditionally used for ethylene polymerization. Current routes commonly used to copolymerize ethylene and polar vinyl monomers are summarized in Scheme 1.2. Free radical processes are used commercially to produce functionalized polymers (Scheme 1.2a), but require high temperatures and pressures, are uncontrolled, and generally produce highly-branched polymers with low crystallinity.[2,3] Pd catalysts with α-diimine ligands were reported by Brookhart to copolymerize ethylene and several polar monomers (Scheme 1.2b).[4–7] However, these catalysts also produce highly branched polymers with the functional groups generally incorporated at the end of branches. A catalyst system that can tolerate a wide range of polar groups is desirable for developing new types of functionalized polymers with enhanced properties, including controlled surface polarity, compatibility in polymer blends, printability, dye retention, and degradability.

Scheme 1.1. Copolymerization of ethylene and alkyl acrylates by an *in situ* generated Pd(II) catalyst containing a phosphine-arenesulfonate ligand.

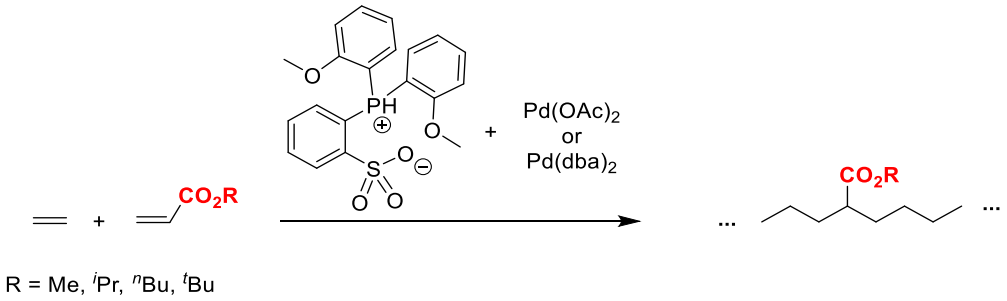

R = Me, ^{i}Pr, ^{n}Bu, ^{t}Bu

Scheme 1.2. Common routes for the copolymerization of ethylene and polar vinyl monomers.

a) free radical

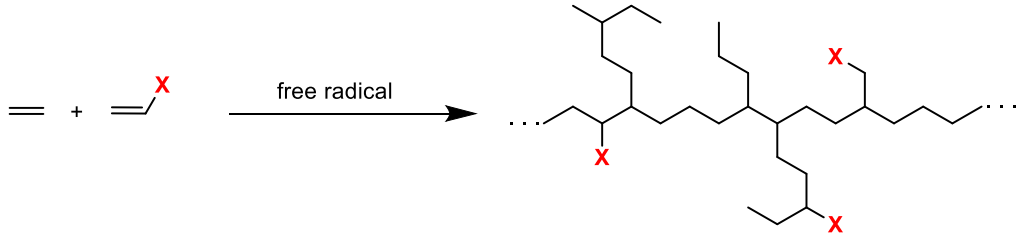

b) Brookhart-type catalysts

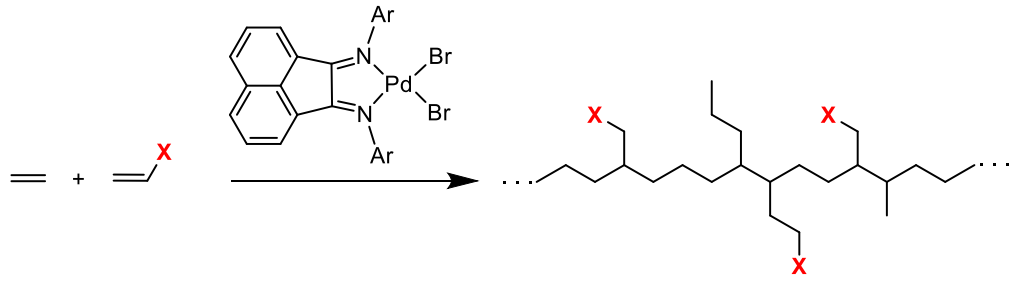

c) (PO)Pd catalysts

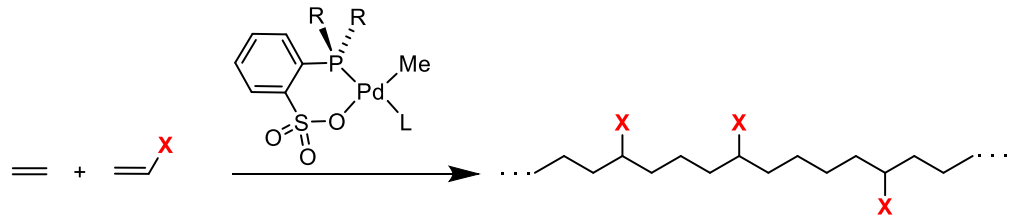

The discovery by Pugh and Drent has motivated extensive studies of the polymerization behavior of discrete (PO)Pd(II)-alkyl catalysts by Claverie,[8–19] Jordan,[20–34] Mecking,[35–61] Nozaki,[62–77] Rieger,[78–82] Sen,[83–86] Chen,[87–95] and others (Scheme 1.2c).[96–102] Many polar monomers have been successfully incorporated in copolymerization using PO-type catalysts,[103–105] including vinyl ethers,[21] vinyl fluoride,[22,23,31] vinyl chloride (terminal incorporation only),[47] acrylonitrile,[63,69] vinyl acetate,[67] acrylates,[1,8,11,15,16,36,39,41,106,107] acrylic acid,[12,14,40] vinyl ketone,[85] styrene,[85] acrylamides,[10,43] N-vinyl-2-pyrrolidinone,[10] vinyl sulfone,[38] vinyl phosphonic acid and vinyl phosphonate,[108] norbornene,[8,84,99] 3,3,3-trifluoropropene,[82] allyl monomers,[57,70] diallyl ether,[53] and norbornene anhydride.[60] (PO)PdR-type complexes can also catalyze the non-alternating copolymerization of ethylene and CO,[79,83,86,97,98,109,110] and the alternating copolymerization of CO with vinyl acetate or methyl acrylate.[64,65,71,75]

A simplified mechanism for olefin polymerization by (PO)PdMeL catalysts is shown in Scheme 1.3.[66,111] Chain growth is initiated by displacement of a labile ligand (e.g. pyridine) by an olefin. The catalyst undergoes an isomerization,[25,66,103,104,112] putting the olefin *trans* the sulfonate, followed by rapid migratory insertion. This provides an open coordination site for a new olefin to bind and continue the chain growth process. Alternatively, the catalyst may undergo an associative chain transfer through β-H elimination into the new open coordination site. After β-H elimination, a new olefin coordinates in the axial position, the catalyst undergoes

a series of Berry pseudorotations, and the vinyl-capped polymer chain is released from the opposite axial position.[25,96,103,104,112] The Pd(II)-hydride complex re-enters the chain growth cycle by migratory insertion.

Scheme 1.3. Simplified mechanism of olefin polymerization by (PO)PdRL catalysts. Ancillary ligands are not shown, and R denotes the growing polymer chain.

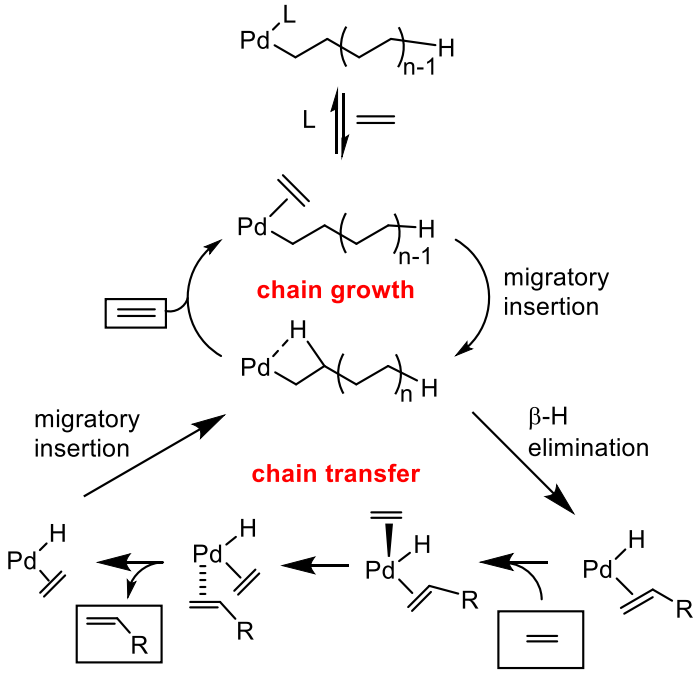

In terms of catalyst performance, the rate of chain growth (R_{growth}) is typically independent of ethylene pressure and corresponds to the insertion rate (activity), and the PE MW is determined by the $R_{growth}/R_{transfer}$ ratio, where $R_{transfer}$ is the rate of chain transfer (Eq 1.1).

$$M_n = \frac{R_{growth} \cdot 28}{R_{transfer}} \qquad \textbf{Eq. 1.1}$$

Electronic asymmetry is created by the strong and weak donors within the phosphine-sulfonate ligand which have different *trans* influence strengths within the square planar catalyst.[96] The soft Pd metal center leads to highly covalent metal-ligand bonds which enhances the *trans* influence. β-H elimination and β-X elimination in the case of polar monomers are key steps in chain transfer and are inhibited by the electronic asymmetry (Scheme 1.4). Both β-H and β-X elimination would lead to a less favorable arrangement of strong and weak donors around the Pd square plane compared to coordination of an olefin in the open coordination site. Thus, chain growth is favored over chain transfer in polymerization and deactivation in copolymerization.

Scheme 1.4. Electronic asymmetry of (PO)PdR olefin polymerization catalysts. Red letters refer to *trans*-influence (vs-very strong, s-strong, m-medium, w-weak, vw-very weak).

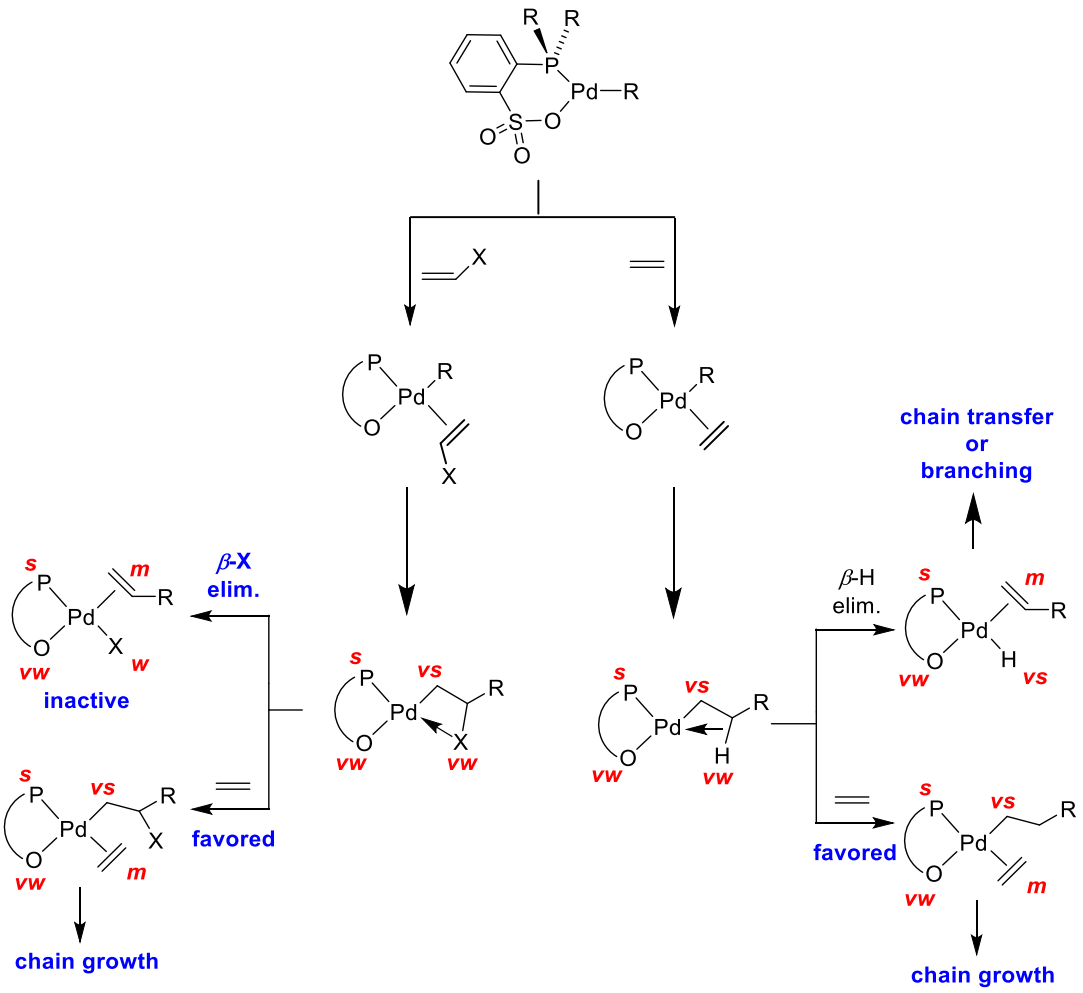

1.2 Modifications to (Phosphine-Arenesulfonate)PdRL Catalysts

Some of the disadvantages to (PO)PdMeL catalysts (**1**, Chart 1.1) compared to other single-site catalyst systems are low activities, formation of polymers with low MWs, and low incorporation of polar monomers.[113,114] The addition of polar monomers in copolymerization

reduces activities and MWs further. Attempts to address these issues have largely focused on modifying the phosphine substituents of the ancillary ligand.[13,46,49,76] Generally, increasing the electron-donating ability of the phosphine substituents of **1** increases catalyst activity, and increasing the size of the phosphine substituents increases the MW of the polymer product. The latter effect has been attributed to steric blocking of the Pd axial sites which inhibits associative chain transfer by blocking the coordination of an olefin.[76]

Modification of the weak donor group has also been explored.[115–126] In general, (PO)-type catalysts with cationic metal centers generate low-MW polymers or oligomers with moderate activity. For example, catalysts of type **2** containing a phosphine-diphenylphosphine oxide (R= Ph) or phosphine-diethylphosphonate (R= OEt) ligand exhibit reasonable activities (63–125 kg mol^{-1} h^{-1}), but only produce oligomers (M_n = 0.3–0.8 kDa).[120,122] Zwitterionic catalyst **3** containing a phosphine-trifluoroborane ligand only dimerizes ethylene because of its high rate of chain transfer.[115,116]

More recently, several PO-type catalysts containing a P(V) oxide group have exhibited interesting polymerization properties. Catalyst **4** containing a phosphine-di-*tert*-butylphosphine oxide ligand exhibits high activity (2800 kg mol^{-1} h^{-1}) and copolymerizes ethylene with allyl acetate, allyl chloride, tert-butyl vinyl ether, vinyl acetate, and acrylonitrile.[120,121] Catalyst **5** containing a phosphine-phosphonamide ligand exhibits high activity (6000 kg mol^{-1} h^{-1}) and

produces high-MW PE (M_n = 130 kDa).[123] **5** also copolymerizes ethylene with methyl acrylate, allyl acetate, and butyl vinyl ether.

Chart 1.1. Examples of (PO)Pd-type complex modifications.

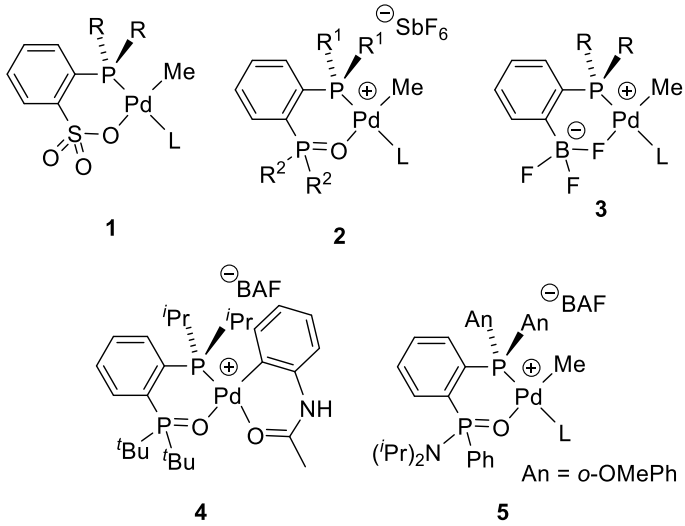

Modification of the weak donor group by coordination of a Lewis acid to the sulfonate group can have a significant impact on catalytic performance.[26] Addition of 1 equiv of $B(C_6F_5)_3$ to **1** will trap the labile ligand (pyridine) and form the base-free complex **6** which dimerizes in the absence of another coordinating species (Scheme 1.5). In ethylene polymerization, **6** exhibits high activity (1570 kg mol^{-1} h^{-1}) and produces moderate-MW PE (M_n = 29 kDa). A second equivalent of $B(C_6F_5)_3$ coordinates to an oxygen of the sulfonate group to form the base-free, borane-coordinated complex **7**. Catalyst **7** is more active (5650 kg mol^{-1} h^{-1}) than **6**, but the MW

of the produced PE is significantly lower (M_n = 3 kDa). A quantitative analysis showed that coordination of the borane to the sulfonate group effects a 40 to 80-fold increase in $R_{transfer}$ but only a 3 to 4-fold increase in R_{growth}, depending on the structure of the Ar substituent. It has been proposed that the enhanced electrophilicity of the cationic Pd metal center in **7** leads to higher rates of β-H elimination.

Scheme 1.5. Synthesis of a base-free, borane-coordinated {(PO)PdMe}$_2$ complex.

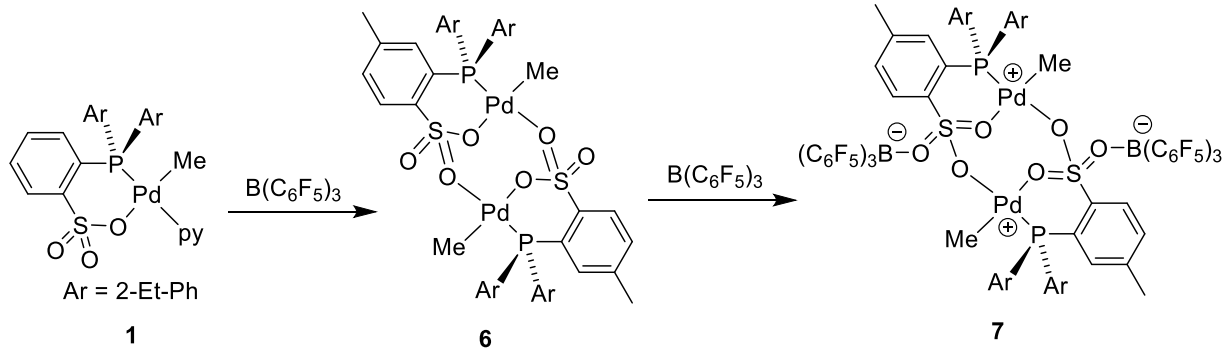

(Li-OPO)PdMe(py') complexes that contain phosphine-*bis*-arenesulfonate (OPO^{2-}) ligands self-assemble to tetrameric structures (Scheme 1.6, **8**). The additional $-SO_3Li$ group forms a central $Li_4S_4O_{12}$ double-four-ring (D4R) core with four (Li-OPO)PdMeL units arranged around the periphery.[23,33] The multinuclear assembly **8** polymerizes ethylene to higher-MW PE than **1** (M_w = 1000 kDa vs 20 kDa) and can incorporate higher levels of vinyl fluoride in ethylene/vinyl fluoride copolymerizations compared to **1** (2.4% vs 0.6% under 120 psi vinyl

fluoride and 130 psi ethylene).[24] Other tetranuclear (M-OPO)PdMeL catalysts based on zinc-phosphonate and $Li_4S_4O_{12}$•Li_2Cl_2 expanded cages have also been explored, and also produce ultra-high-MW PE (M_w > 1000 kDa).[127,128]

Scheme 1.6. Self-assembly of (Li-OPO)PdMeL complexes. The lower (Li-OPO)PdMe(py') units of **A** are denoted by "Pd".

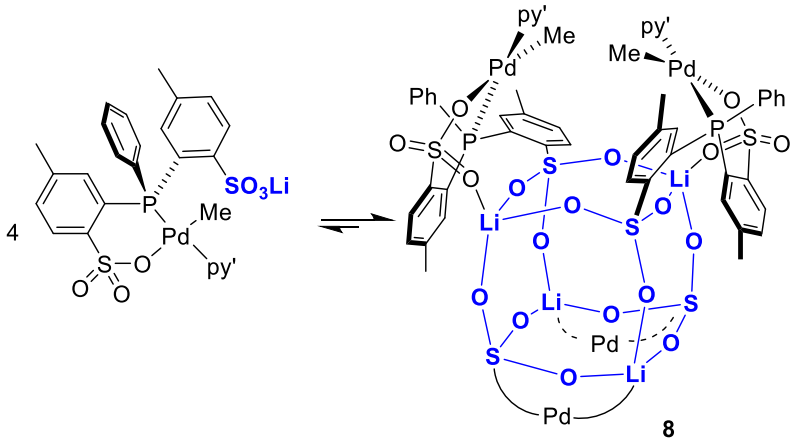

1.3 Thesis Objectives

Although PO-type catalysts exhibit unique polymerization properties, there are still challenges to be addressed before they can be useful for practical applications, including generally low activities, formation of low-MW polymers, and low incorporation of polar monomers in copolymerization. The objectives of this thesis are to investigate strategies to address the limitations of (PO)PdRL catalysts, especially low activity and low PE MW. The

strategies described include (i) ligand modification, (ii) allosteric effects, and (iii) self-assembly of multinuclear catalysts.

Chapter Two describes Pd(II)-alkyl complexes containing phosphine-monoalkyl phosphonate ligands ([1-PAr_2-2-PO_2(OR)-Ph]$^-$ [PPO]$^-$). The complexes (κ^2-1-*P*Ar_2-2-P*O*$_2$(OR)-Ph)PdMeL ((PPO)PdMeL) were prepared and characterized in the solid state and in solution. The reaction of the Pd complexes with one or two equiv of $B(C_6F_5)_3$ generates the borane adduct (κ^2-1-*P*Ar_2-2-P(*O*)(O-B(C_6F_5)$_3$)(OR)-Ph)PdMeL or the base-free, borane adduct {(κ^2-1-*P*Ar_2-2-P(*O*)(O-B(C_6F_5)$_3$)(OR)-Ph)PdMe}$_2$, respectively. The borane adducts were characterized by X-ray crystallography and in solution. The reactivity of the (PPO)PdMeL complexes with other Lewis acids is also described.

Chapter Three describes the ethylene polymerization performance of the complexes prepared in Chapter Two. Remote binding of $B(C_6F_5)_3$ to (PPO)PdMeL (L =pyridine or lutidine) or {(PPO)PdMe}$_2$ ethylene polymerization catalysts that contain phosphine-monoalkyl phosphonate ligands significantly increases the catalyst activity and the molecular weight of the polyethylene (PE) product. X-ray structural data, trends in ligand lability, and comparative studies of BF_3 activation suggest that these allosteric effects are primarily electronic in origin. The $B(C_6F_5)_3$ binding enhances R_{growth} by increasing the degree of positive charge on the Pd center. This effect does not result in the large increase in $R_{transfer}$ and concomitant reduction in PE

molecular weight seen in previous studies of analogous (PO)PdRL catalysts that contain phosphine-arenesulfonate ligands, because of the operation of an unusual dissociative chain transfer process, which is inhibited by the increased charge at Pd.

Chapter Four describes synthetic studies that were undertaken to further probe the factors that influence the self-assembly of four (Li-OPO)PdRL units containing phosphine-*bis*-arenesulfonate $[Li\text{-}OPO]^-$ ligands into tetranuclear cage structures. The factors that favor the self-assembly of the (Li-OPO)PdRL units around the periphery of a central $Li_4S_4O_{12}$•Li_2Cl_2 expanded core over a $Li_4S_4O_{12}$ double-four-ring (D4R) core were explored. New $[Li\text{-}OPO]^-$ ligands were synthesized with either *meta*- or *para*-substituents, and the generation of tetrameric Pd assemblies based on $Li_4S_4O_{12}$•$Li_2(OAc)_2$ and $Li_4S_4O_{12}$•Li_2Br_2 cores was explored to determine if cage core expansion can be achieved using other M_2X_2 units besides Li_2Cl_2.

1.4 References and Notes

(1) Drent, E.; van Dijk, R.; van Ginkel, R.; van Oort, B.; Pugh, R. I. *Chem. Commun.* **2002**, 744.

(2) Doak, K. W. In Encyclopedia of Polymer Science and Engineering, Kroschwitz, J. I., Ed.; John Wiley & Sons: New York, 1986; Vol. 6, p 386.

(3) Boaen, N. K.; Hillmyer, M. A. *Chem. Soc. Rev.* **2005**, *34*, 267.

(4) Ittel, S. D.; Johnson, L. K.; Brookhart, M. *Chem. Rev.* **2000**, *100*, 1169.

(5) Johnson, L. K.; Killian, C. M.; Brookhart, M. *J. Am. Chem. Soc.* **1995**, *117*, 6414.

(6) Johnson, L. K.; Mecking, S.; Brookhart, M. *J. Am. Chem. Soc.* **1996**, *118*, 267.

(7) Mecking, S.; Johnson, L. K.; Wang, L.; Brookhart, M. *J. Am. Chem. Soc.* **1998**, *120*, 888.

(8) Skupov, K. M.; Marella, P. R.; Hobbs, J. L.; McIntosh, L. H.; Goodall, B. L.; Claverie, J. P. *Macromolecules* **2006**, *39*, 4279.

(9) Skupov, K. M.; Marella, P. R.; Simard, M.; Yap, G. P. A.; Allen, N.; Conner, D.; Goodall, B. L.; Claverie, J. P. *Macromol. Rapid Commun.* **2007**, *28*, 2033.

(10) Skupov, K. M.; Piche, L.; Claverie, J. P. *Macromolecules* **2008**, *41*, 2309.

(11) Skupov, K. M.; Hobbs, J.; Marella, P.; Conner, D.; Golisz, S.; Goodall, B. L.; Claverie, J. P. *Macromolecules* **2009**, *42*, 6953.

(12) Kryuchkov, V. A.; Daigle, J.-C.; Skupov, K. M.; Claverie, J. P.; Winnik, F. M. *J. Am. Chem. Soc.* **2010**, *132*, 15573.

(13) Piche, L.; Daigle, J.-C.; Poli, R.; Claverie, J. P. *Eur. J. Inorg. Chem.* **2010**, *2010*, 4595.

(14) Daigle, J.-C.; Piche, L.; Claverie, J. P. *Macromolecules* **2011**, *44*, 1760.

(15) Daigle, J.-C.; Piche, L.; Arnold, A.; Claverie, J. P. *ACS Macro Lett.* **2012**, *1*, 343.

(16) Piche, L.; Daigle, J. C.; Rehse, G.; Claverie, J. P. *Chem. Eur. J.* **2012**, *18*, 3277.

(17) Daigle, J.-C.; Arnold, A. A.; Piche, L.; Claverie, J. P. *Polym. Chem.* **2013**, *4*, 449.

(18) Piche, L.; Daigle, J.-C.; Claverie, J. P. *Chem. Commun.* **2011**, *47*, 7836.

(19) Bashir, O.; Piche, L.; Claverie, J. P. *Organometallics* **2014**, *33*, 3695.

(20) Luo, S.; Vela, J.; Lief, G. R.; Jordan, R. F. *J. Am. Chem. Soc.* **2007**, *129*, 8946.

(21) Vela, J.; Lief, G. R.; Shen, Z.; Jordan, R. F. *Organometallics* **2007**, *26*, 6624.

(22) Weng, W.; Shen, Z.; Jordan, R. F. *J. Am. Chem. Soc.* **2007**, *129*, 15450.

(23) Shen, Z.; Jordan, R. F. *J. Am. Chem. Soc.* **2010**, *132*, 52.

(24) Shen, Z.; Jordan, R. F. *Macromolecules* **2010**, *43*, 8706.

(25) Conley, M. P.; Jordan, R. F. *Angew. Chem. Int. Ed. Engl.* **2011**, *50*, 3744.

(26) Cai, Z.; Shen, Z.; Zhou, X.; Jordan, R. F. *ACS Catal.* **2012**, *2*, 1187.

(27) Feng, G.; Conley, M. P.; Jordan, R. F. *Organometallics* **2014**, *33*, 4486.

(28) Zhou, X.; Lau, K.-C.; Petro, B. J.; Jordan, R. F. *Organometallics* **2014**, *33*, 7209.

(29) Zhou, X.; Bontemps, S.; Jordan, R. F. *Organometallics* **2008**, *27*, 4821.

(30) Lau, K.-C.; Petro, B. J.; Bontemps, S.; Jordan, R. F. *Organometallics* **2013**, *32*, 6895.

(31) Wada, S.; Jordan, R. F. *Angew. Chem. Int. Ed.* **2017**, *56*, 1820.

(32) Black, R. E.; Jordan, R. F. *Organometallics*, **2017**, *36*, 3415.

(33) Wei, J.; Shen, Z.; Filatov, A. S.; Liu, Q.; Jordan, R. F. *Organometallics* **2016**, *35*, 3557.

(34) Kleinsasser, J. F.; Reinhart, E. D.; Estrada, J.; Jordan, R. F.; Lavallo, V. *Organometallics*, **2018**, *37*, 4773.

(35) Guironnet, D.; Rünzi, T.; Göttker-Schnetmann, I.; Mecking, S. *Chem. Commun.* **2008**, 4965.

(36) Guironnet, D.; Roesle, P.; Rünzi, T.; Göttker-Schnetmann, I.; Mecking, S. *J. Am. Chem. Soc.* **2009**, *131*, 422.

(37) Zhang, D.; Guironnet, D.; Göttker-Schnetmann, I.; Mecking, S. *Organometallics* **2009**, *28*, 4072.

(38) Bouilhac, C.; Rünzi, T.; Mecking, S. *Macromolecules* **2010**, *43*, 3589.

(39) Guironnet, D.; Caporaso, L.; Neuwald, B.; Göttker-Schnetmann, I.; Cavallo, L.; Mecking, S. *J. Am. Chem. Soc.* **2010**, *132*, 4418.

(40) Rünzi, T.; Fröhlich, D.; Mecking, S. *J. Am. Chem. Soc.* **2010**, *132*, 17690.

(41) Rünzi, T.; Guironnet, D.; Göttker-Schnetmann, I.; Mecking, S. *J. Am. Chem. Soc.* **2010**, *132*, 16623.

(42) Wucher, P.; Caporaso, L.; Roesle, P.; Ragone, F.; Cavallo, L.; Mecking, S.; Göttker-Schnetmann, I. *Proc. Natl. Acad. Sci. USA* **2011**, *108*, 8955.

(43) Friedberger, T.; Wucher, P.; Mecking, S. *J. Am. Chem. Soc.* **2012**, *134*, 1010.

(44) Neuwald, B.; Ölscher, F.; Göttker-Schnetmann, I.; Mecking, S. *Organometallics* **2012**, *31*, 3128.

(45) Rünzi, T.; Tritschler, U.; Roesle, P.; Göttker-Schnetmann, I.; Möller, H. M.; Caporaso, L.; Poater, A.; Cavallo, L.; Mecking, S. *Organometallics* **2012**, *31*, 8388.

(46) Wucher, P.; Goldbach, V.; Mecking, S. *Organometallics* **2013**, *32*, 4516.

(47) Leicht, H.; Göttker-Schnetmann, I.; Mecking, S. *Angew. Chem. Int. Ed.* **2013**, *52*, 3963.

(48) Neuwald, B.; Caporaso, L.; Cavallo, L.; Mecking, S. *J. Am. Chem. Soc.* **2013**, *135*, 1026.

(49) Neuwald, B.; Falivene, L.; Caporaso, L.; Cavallo, L.; Mecking, S. *Chem. Eur. J.* **2013**, *19*, 17773.

(50) Wucher, P.; Schwaderer, J. B.; Mecking, S. *ACS Catal.* **2014**, *4*, 2672.

(51) Jian, Z.; Wucher, P.; Mecking, S. *Organometallics* **2014**, *33*, 2879.

(52) Jian, Z.; Mecking, S. *Angew. Chem. Int. Ed. Engl.* **2015**, *54*, 15845.

(53) Jian, Z.; Mecking, S. *Angew. Chem. Int. Ed. Engl.* **2015**, *127*, 16071.

(54) Jian, Z.; Baier, M. C.; Mecking, S. *J. Am. Chem. Soc.* **2015**, *137*, 2836.

(55) Leicht, H.; Göttker-Schnetmann, I.; Mecking, S. *J. Am. Chem. Soc.* **2017**, *139*, 6823.

(56) Schuster, N.; Rünzi, T.; Mecking, S. *Macromolecules* **2016**, *49*, 1172.

(57) Jian, Z.; Leicht, H.; Mecking, S. *Macromol. Rapid Commun.* **2016**, *37*, 934.

(58) Jian, Z.; Mecking, S. *Macromolecules* **2016**, *49*, 4057.

(59) Jian, Z.; Mecking, S. *Macromolecules* **2016**, *49*, 4395.

(60) Schuster, N.; Krumova, M.; Richter, F.; Schneller, A.; Mecking, S. *Macromol. Mater. Eng.* **2018**, *303*, 1700276.

(61) Wimmer, F. P.; Caporaso, L.; Cavallo, L.; Mecking, S.; Falivene, L. *Macromolecules* **2018**, *51*, 4525.

(62) Kochi, T.; Yoshimura, K.; Nozaki, K. *Dalton Trans.* **2006**, 25.

(63) Kochi, T.; Noda, S.; Yoshimura, K.; Nozaki, K. *J. Am. Chem. Soc.* **2007**, *129*, 8948.

(64) Kochi, T.; Nakamura, A.; Ida, H.; Nozaki, K. *J. Am. Chem. Soc.* **2007**, *129*, 7770.

(65) Nakamura, A.; Munakata, K.; Kochi, T.; Nozaki, K. *J. Am. Chem. Soc.* **2008**, *130*, 8128.

(66) Noda, S.; Nakamura, A.; Kochi, T.; Chung, L. W.; Morokuma, K.; Nozaki, K. *J. Am. Chem. Soc.* **2009**, *131*, 14088.

(67) Ito, S.; Munakata, K.; Nakamura, A.; Nozaki, K. *J. Am. Chem. Soc.* **2009**, *131*, 14606.

(68) Noda, S.; Kochi, T.; Nozaki, K. *Organometallics* **2009**, *28*, 656.

(69) Nozaki, K.; Kusumoto, S.; Noda, S.; Kochi, T.; Chung, L. W.; Morokuma, K. *J. Am. Chem. Soc.* **2010**, *132*, 16030.

(70) Ito, S.; Kanazawa, M.; Munakata, K.; Kuroda, J.; Okumura, Y.; Nozaki, K. *J. Am. Chem. Soc.* **2011**, *133*, 1232.

(71) Nakamura, A.; Munakata, K.; Ito, S.; Kochi, T.; Chung, L. W.; Morokuma, K.; Nozaki, K. *J. Am. Chem. Soc.* **2011**, *133*, 6761.

(72) Kageyama, T.; Ito, S.; Nozaki, K. *Chem. Asian. J.* **2011**, *6*, 690.

(73) Kanazawa, M.; Ito, S.; Nozaki, K. *Organometallics* **2011**, *30*, 6049.

(74) Ito, S.; Ota, Y.; Nozaki, K. *Dalton Trans.* **2012**, *41*, 13807.

(75) Nakamura, A.; Kageyama, T.; Goto, H.; Carrow, B. P.; Ito, S.; Nozaki, K. *J. Am. Chem. Soc.* **2012**, *134*, 12366.

(76) Ota, Y.; Ito, S.; Kuroda, J.; Okumura, Y.; Nozaki, K. *J. Am. Chem. Soc.* **2014**, *136*, 11898.

(77) Ota, Y.; Ito, S.; Kobayashi, M.; Kitade, S.; Sakata, K.; Tayano, T.; Nozaki, K. *Angew. Chem. Int. Ed. Engl.* **2016**, *55*, 7505.

(78) Nowack, R. J.; Hearley, A. K.; Rieger, B. *Z. anorg. allg. Chem.* **2005**, *631*, 2775.

(79) Hearley, A. K.; Nowack, R. J.; Rieger, B. *Organometallics* **2005**, *24*, 2755.

(80) Anselment, T. M. J.; Wichmann, C.; Anderson, C. E.; Herdtweck, E.; Rieger, B. *Organometallics* **2011**, *30*, 6602.

(81) Anselment, T. M. J.; Anderson, C. E.; Rieger, B.; Boeddinghaus, M. B.; Fässler, T. F. *Dalton Trans.* **2011**, *40*, 8304.

(82) Lanzinger, D.; Giuman, M. M.; Anselment, T. M. J.; Rieger, B. *ACS Macro Lett.* **2014**, *3*, 931.

(83) Newsham, D. K.; Borkar, S.; Sen, A.; Conner, D. M.; Goodall, B. L. *Organometallics* **2007**, *26*, 3636.

(84) Liu, S.; Borkar, S.; Newsham, D.; Yennawar, H.; Sen, A. *Organometallics* **2007**, *26*, 210.

(85) Borkar, S.; Newsham, D. K.; Sen, A. *Organometallics* **2008**, *27*, 3331.

(86) Luo, R.; Newsham, D. K.; Sen, A. *Organometallics* **2009**, *28*, 6994.

(87) Chen, M.; Yang, B.; Chen, C. *Angew. Chem. Int. Ed.* **2015**, *54*, 15520.

(88) Wu, Z.; Chen, M.; Chen, C. *Organometallics* **2016**, *35*, 1472.

(89) Chen, M.; Yang, B.; Chen, C. *Synlett* **2016**, *27*, 1297.

(90) Chen, M.; Chen, C. *ACS Catal.* **2017**, *7*, 1308.

(91) Song, G.; Pang, W.; Li, W.; Chen, M.; Chen, C. *Polym. Chem.* **2017**, *8*, 7400.

(92) Liang, T.; Chen, C. *Organometallics* **2017**, *36*, 2338.

(93) Wu, Z.; Hong, C.; Hongxu Du; Pang, W.; Chen, C. *Polymers* **2017**, *9*, 168.

(94) Yang, B.; Xiong, S.; Chen, C. *Polym. Chem.* **2017**, *8*, 6272.

(95) Liang, T.; Chen, C. L. *Inorg. Chem.* **2018**, *57*, 14913.

(96) Haras, A.; Anderson, G. D. W.; Michalak, A.; Rieger, B.; Ziegler, T. *Organometallics* **2006**, *25*, 4491.

(97) Haras, A.; Michalak, A.; Rieger, B.; Ziegler, T. *Organometallics* **2006**, *25*, 946.

(98) Chen, C.; Anselment, T. M. J.; Fröhlich, R.; Rieger, B.; Kehr, G.; Erker, G. *Organometallics* **2011**, *30*, 5248.

(99) Ravasio, A.; Boggioni, L.; Tritto, I. *Macromolecules* **2011**, *44*, 4180.

(100) Perrotin, P.; McCahill, J. S. J.; Wu, G.; Scott, S. L. *Chem. Commun.* **2011**, *47*, 6948.

(101) Friedberger, T.; Ziller, J. W.; Guan, Z. *Organometallics* **2014**, *33*, 1913.

(102) Rezabal, E.; Ugalde, J. M.; Frenking, G. *J. Phys. Chem. A* **2017**, *121*, 7709.

(103) Nakamura, A.; Ito, S.; Nozaki, K. *Chem. Rev.* **2009**, *109*, 5215.

(104) Nakamura, A.; Anselment, T. M. J.; Claverie, J.; Goodall, B.; Jordan, R. F.; Mecking, S.; Rieger, B.; Sen, A.; van Leeuwen, P. W. N. M.; Nozaki, K. *Acc. Chem. Res.* **2013**, *46*, 1438.

(105) Ito, S.; Nozaki, K. *Chem. Rec.* **2010**, *10*, 315.

(106) Yasuda, H.; Nakano, R.; Ito, S.; Nozaki, K. *J. Am. Chem. Soc.* **2018**, *140*, 1876.

(107) Mitsushige, Y.; Yasuda, H.; Carrow, B. P.; Ito, S.; Kobayashi, M.; Tayano, T.; Watanabe, Y.; Okuno, Y.; Hayashi, S.; Kuroda, J.; Okumura, Y.; Nozaki, K. *ACS Macro Lett.* **2018**, *7*, 305.

(108) Rünzi, T.; Baier, M. C.; Negele, C.; Krumova, M.; Mecking, S. *Macromol. Rapid Commun.* **2015**, *36*, 165.

(109) Drent, E.; van Dijk, R.; van Ginkel, R.; van Oort, B.; Pugh, R. I. Ch*em. Commun.* ***2*****002,** 964.

(110) Bettucci, L.; Bianchini, C.; Claver, C.; Suarez, E. J. G.; Ruiz, A.; Meli, A.; Oberhauser, W. *Dalton Trans.* **2007**, 5590.

(111) Nakano, R.; Chung, L. W.; Watanabe, Y.; Okuno, Y.; Okumura, Y.; Ito, S.; Morokuma, K.; Nozaki, K. *ACS Catalysis* **2016** *6*, 6101.

(112) Zhou, X.; Jordan, R. F. *Organometallics* **2011**, *30*, 4632.

(113) Britovsek, George J. P.; Gibson, V. C.; Wass, D. F. *Angew. Chem. Int. Ed.* **1999**, 428.

(114) Gibson, V. C.; Spitzmesser, S. K. *Chem. Rev.* **2003**, *103*, 283.

(115) Kim, Y.; Jordan, R. F. *Organometallics* **2011**, *30*, 4250.

(116) Gott, A. L.; Piers, W. E.; Dutton, J. L.; McDonald, R.; Parvez, M. *Organometallics* **2011**, *30*, 4236.

(117) Zhang, Y.; Cao, Y.; Leng, X.; Chen, C.; Huang, Z. *Organometallics* **2014**, *33*, 3738.

(118) Jian, Z.; Falivene, L.; Wucher, P.; Roesle, P.; Caporaso, L.; Cavallo, L.; Gottker-Schnetmann, I.; Mecking, S. *Chem. ‐Eur. J.* **2015**, *21*, 2062.

(119) Jian, Z.; Mecking, S. *Macromolecules* **2016**, *49*, 4057.

(120) Carrow, B. P.; Nozaki, K. *J. Am. Chem. Soc.* **2012**, *134*, 8802.

(121) Carrow, B. P.; Nozaki, K. *Macromolecules* **2014**, *47*, 2541.

(122) Contrella, N. D.; Sampson, J. R.; Jordan, R. F. *Organometallics* **2014**, *33*, 3546.

(123) Sui, X.; Dai, S.; Chen, C. *ACS Catal.* **2015**, *5*, 5932.

(124) Mitsushige, Y.; Yasuda, H.; Carrow, B.; Ito, S.; Kobayashi, M.; Tayano, T.; Watanabe, Y.; Okuno, Y.; Hayashi, S.; Kuroda, J.; Okumura, Y.; Nozaki, K. *ACS Macro Lett.* **2018**, *7*, 305.

(125) Zhang, W.; Waddell, P. M.; Tiedemann, M. A.; Padilla, C. E.; Mei, J.; Chen, L.; Carrow, B. P. *J. Am. Chem. Soc.* **2018**, *140*, 8841.

(126) Cai, Z.; Do, L. H. *Organometallics* **2018**, *37*, 3874.

(127) Liu, Q.; Jordan, R. F. *Organometallics*, **2018**, *37*, 4664.

(128) Defoe, J., J. Doctoral dissertation, The University of Chicago, **2011**.

Chapter Two

Synthesis and Characterization of Palladium(II) Alkyl Complexes that Contain Phosphine-monoalkyl Phosphonate Ligands and Allosteric Binding of Lewis Acids

2.1 Introduction

As described in Chapter One, Pd(II) alkyl complexes that contain ancillary *ortho*-phosphine-arenesulfonate (PO^-) ligands (**A**, Chart 1) polymerize ethylene to linear polyethylene (PE) and copolymerize ethylene with a wide variety of polar vinyl monomers.[1–25] While the broad functional group tolerance of these catalysts is unique, their activities and the molecular weights (MWs) of the polymers they produce are generally much lower than those of other single-site catalysts,[26–31] which has motivated extensive modifications of the PO^- ligand structure to enhance catalyst performance. Noteworthy examples of superior (PO)PdMeL catalysts include (*o*-P^{t}BuPh-benzenesulfonate)PdMe(lut) (lut = 2,6-lutidine), which exhibits high ethylene polymerization activity for this class of catalysts (4714 kg mol^{-1} h^{-1}, 85 ^{o}C),[18] (*o*-P(menthyl)$_2$-benzenesulfonate)PdMe(lut), which produces PE with high MW (M_n = 169,000 Da, 80 ^{o}C),[13] and (*o*-P(2',6'-(OMe)$_2$-2-biphenyl)$_2$-benzenesulfonate)PdMe(lut), which displays a good balance of activity and MW (1040 kg mol^{-1} h^{-1}; M_n = 227,000 Da, 90 ^{o}C).[19] Analogues of (PO)PdMeL catalysts in which the sulfonate group has been replaced by other weak donors have also been

explored,[32–40] including systems that contain phosphine-trifluoroborate,[32–33] phosphine-sulfonamide,[34–36] phosphine-phosphine oxide,[37–38] phosphine-dialkyl phosphonate,[39] and phosphine-phosphonamide (**B**) ligands.[40] The phosphine-phosphonamide complex **B** with R^1 = *o*-OMe-Ph, R^2 = ^{i}Pr, and R^3 = Ph is one of most active (PO)Pd-type catalysts for ethylene polymerization (6000 kg mol^{-1} h^{-1}, 80 ^{o}C) reported to date and produces PE with high MW (130,000 Da).[41]

An alternative approach to improving catalytic performance is allosteric regulation, i.e. binding of a small "effector" molecule at a location remote from the active site to induce structural/conformational changes that regulate activity.[42–61] This concept has been implemented in synthetic catalysts for asymmetric hydrogenation,[49] asymmetric hydroformylation,[50] Diels-Alder reactions,[51] and other reactions,[52–59] as well as olefin polymerization catalysis.[60–79] In particular, Bazan reported that coordination of $B(C_6F_5)_3$ to (*o*-PPh_2-benzoate)Ni(η^3-CH_2CMeCH_2) to form zwitterionic complex **C** results in a significant increase in the ethylene oligomerization activity of this system.[62,63] Similar binding of $B(C_6F_5)_3$ to inactive (α-iminocarboxamide)Ni(η^3-CH_2Ph) complexes to form adducts **D** activates these species for ethylene polymerization.[64] More recently, binding of $B(C_6F_5)_3$ to the sulfonate oxygen of (PO)PdRL complexes to form zwitterionic {PO•$B^-(C_6F_5)_3$}Pd^+RL species (**E**)[80] was found to increase the rate of chain growth (R_{growth}) in ethylene polymerization, leading to higher activities.

However, the borane coordination in **E** also results in larger increases in the rate of chain transfer ($R_{transfer}$), so that the $R_{growth}/R_{transfer}$ ratio and hence the MW of the PE that is produced is substantially reduced. For example, coordination of $B(C_6F_5)_3$ to a sulfonate oxygen of (*o*-P(2-Et-Ph)$_2$-benzenesulfonate)PdMe(py) leads to a 4-fold increase in R_{growth} but a 42-fold increase in $R_{transfer}$ and thus a ca. 10-fold reduction in M_n. In contrast, coordination of $B(C_6F_5)_3$ to (PO)Ni(allyl) complexes to form $\{PO•B^-(C_6F_5)_3\}Ni^+$(allyl) complex (**F**) has very little effect on the ethylene polymerization performance.[61]

Recently, Reiger reported the synthesis of an anionic phosphine-phenylphosphinate ligand (PPO^-),[81] and Nathan Contrella synthesized the corresponding neutral Pd-alkyl complex **G**. **G** reacts with ethylene but exhibits very low activity (0.7 kg mol^{-1} h^{-1}) and produces PE with low MW (1340 Da). Interestingly, the zwitterionic complex **H**, formed by coordination of $B(C_6F_5)_3$ to the phosphinate group of **G**, exhibits higher activity (35 kg mol^{-1} h^{-1}) and also produces higher MW PE (7700 Da) than **G**.

In this chapter, the synthesis of simple (PPO)PdMeL complexes that contain phosphine-monoalkyl phosphonate (**I**, R = Et, ^{i}Pr) ligands is described. We also report the allosteric binding of $B(C_6F_5)_3$ to the P=*O* group of **I** to generate zwitterionic $(PPO•B^-(C_6F_5)_3Pd^+MeL$ adducts as well as the synthesis of the base-free, borane-coordinated dimeric complexes $\{(PPO•B^-(C_6F_5)_3Pd^+Me\}_2$. The reactivity of these complexes with ethylene and the effect of borane

coordination on R_{growth} and $R_{transfer}$ was also explored.

Chart 2.1. (PO)PdR complexes

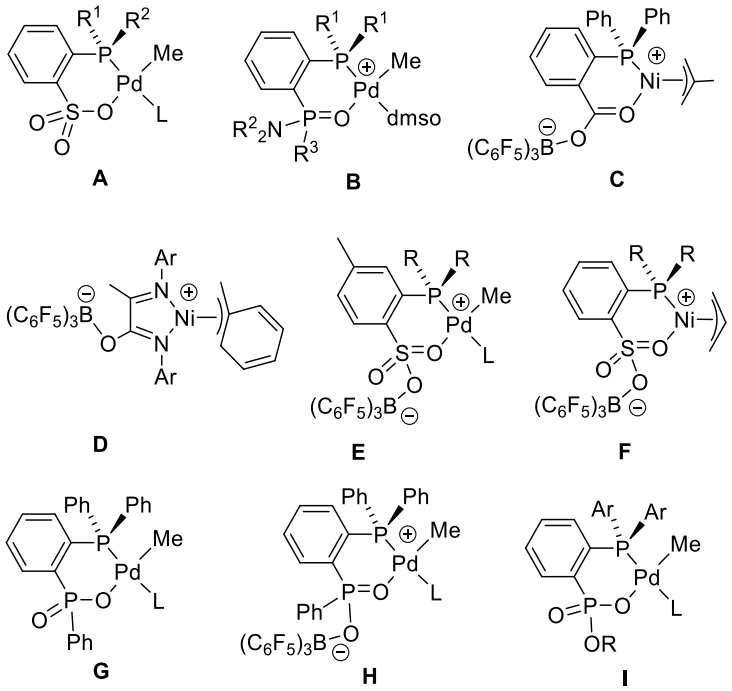

2.2 Results and Discussion

Synthesis of (κ^2-1-*P*Ar_2-2-P(=O)(*O*)(OR)-Ph)PdMeL Complexes. The phosphine-phosphonate diester 1-PAr_2-2-P$O(OR)_2$-Ph (**1a**: Ar = Ph, R = Et) was synthesized as reported by Reiger and Pringle and **1b** (Ar = Ph, R = ^{i}Pr) was synthesized analogously (Scheme 2.1a).[81,82] **1c** (Ar = 2-OMe-Ph = An, R = ^{i}Pr) was synthesized by a Cu-catalyzed P–N coupling reaction[83] and a lithium-halogen exchange followed by reaction with bis(2-methoxyphenyl)chlorophosphine (Scheme 2.1b). **1a–c** were mono-dealkylated by reaction with LiBr in refluxing CH_3CN,

affording Li[**2a**–**c**] (Scheme 2.2),[84] and then acidified with HCl to generate the phosphine-phosphonate monoester proligands H[**2a–c**].

Scheme 2.1. Synthesis of phosphine-phosphonate ligands

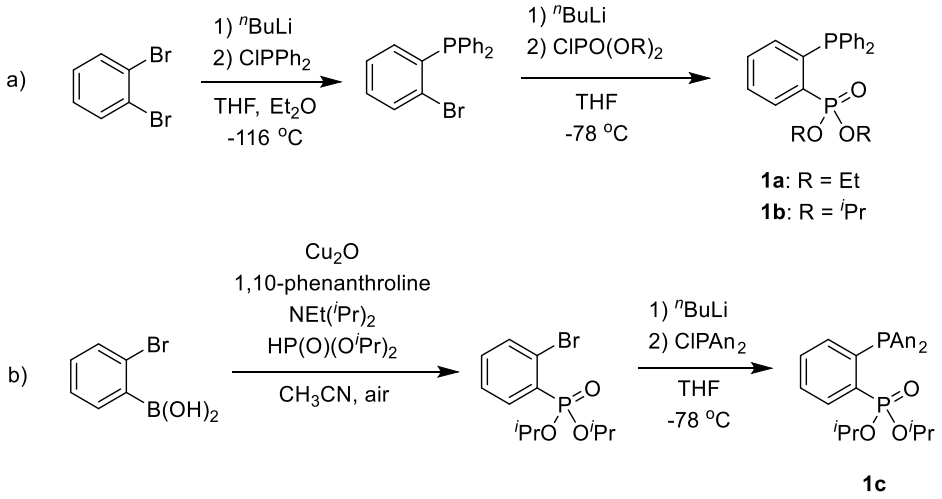

Scheme 2.2. Synthesis of phosphine-phosphonate ligands

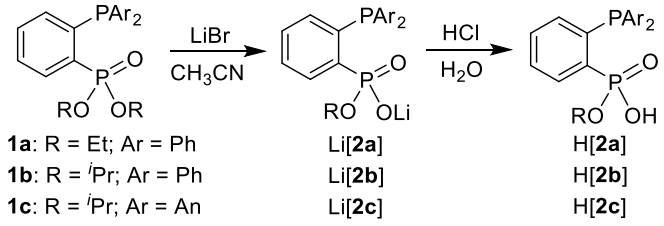

The sequential reaction of H[**2a**], H[**2b**], or H[**2c**] with (TMEDA)$PdMe_2$ followed by 2,6-lutidine or pyridine affords the corresponding (PPO)PdMeL complexes (L = 2,6-lutidine: **3a-lut**, **3b-lut**; L = pyridine: **3a-py**, **3b-py**, **3c-py**) as shown in Scheme 2.3. Chelation of the PPO^-

ligand is indicated by the presence of P–P coupling in the $^{31}P\{^{1}H\}$ NMR spectra of **3a-lut/py**, **3b-lut/py**, and **3c-py** ($^{3}J_{PP}$ = 14–17 Hz), which is not observed in the spectra of the free ligands. Selectively decoupled $^{1}H\{^{31}P\}$ NMR of **3b-py** was used to distinguish between the phosphine (δ 8.6) and phosphonate (δ 32.4) ^{31}P resonances. The solid-state molecular structures of **3a-lut** and **3b-lut** are shown in Figures 2.1 and 2.2 and are similar to that of **G**, with the P-*OR* groups occupying axial positions on the chelate ring. **3a-lut** and **3b-lut** undergo partial dissociation of 2,6-lutidine in CD_2Cl_2 solution, which is indicated by the presence of minor signals for free 2,6-lutidine and minor broad signals ascribed to base-free $\{(PPO)PdMe\}_n$ species in the ^{1}H NMR spectra. Exchange of the Pd-bound (O1, Figures 2.1 and 2.2) and non-Pd-bound oxygen (O2) atoms is fast on the NMR time scale for **3a-lut/py**, **3b-lut/py**, and **3c-py** at room temperature, resulting in the presence of a single set of ^{1}H resonances for the P*Ar*$_2$ groups, as well as for the diastereotopic -OC*H*$_2$CH$_3$ hydrogens in **3a-lut/py** and the diastereotopic -OCH*Me*$_2$ groups in **3b-lut/py** and **3c-py**. The barrier to this exchange process for **3a-py** was determined to be $\Delta G^{\neq}$ = 10.5 kcal mol^{-1} from the coalescence of the -OC*H*$_2$CH$_3$ resonances (500 MHz, δ 3.47, 2.49, T_c = 238 K). *Cis*/*trans* isomerization of (PO)PdR(CH_2=CH_2) species is believed to precede the migratory insertion step in chain growth by (PO)PdR catalysts. One proposed isomerization mechanism, which was predicted to have a low barrier, involves coordination of a second sulfonate oxygen atom to Pd to generate a (κ^3-*P,O,O*-PO)PdR(CH_2=CH_2) species, followed by

Berry pseudorotations and formation of the isomerized (κ^2-*P,O*-PO)PdR(CH_2=CH_2) product. While the exchange of Pd-bound and non-Pd-bound sulfonate oxygen atoms has not been experimentally observed in (PO)PdMeL systems, the present results suggest that this process is indeed facile.[1–3,23–25,85,86]

Scheme 2.3. Synthesis of phosphine-phosphonate Pd complexes.

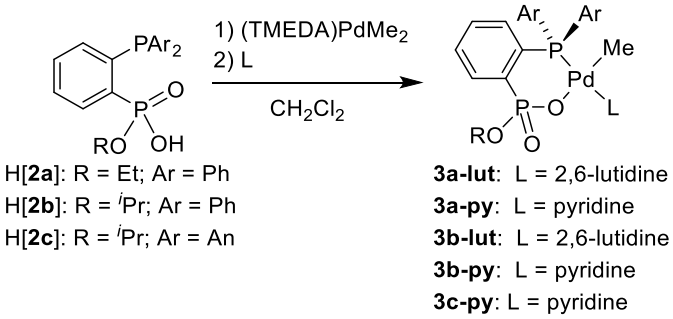

H[**2a**]: R = Et; Ar = Ph
H[**2b**]: R = ^{i}Pr; Ar = Ph
H[**2c**]: R = ^{i}Pr; Ar = An

3a-lut: L = 2,6-lutidine
3a-py: L = pyridine
3b-lut: L = 2,6-lutidine
3b-py: L = pyridine
3c-py: L = pyridine

Figure 2.1. Molecular structure of **3a-lut**•CH_2Cl_2. The CH_2Cl_2 molecule and hydrogen atoms are not shown. Bond lengths (Å) and angles (deg): C1–Pd1 2.016(10), N1–Pd1 2.096(9), O1–Pd1 2.103(7), P1–Pd1 2.197(3), O2–P2 1.462(8), O1–P2 1.497(8), C1–Pd1–N1 84.5(4), N1–Pd1–O1 90.6(3), O1–Pd1–P1 94.9(2), P1–Pd1–C1 90.3(3).

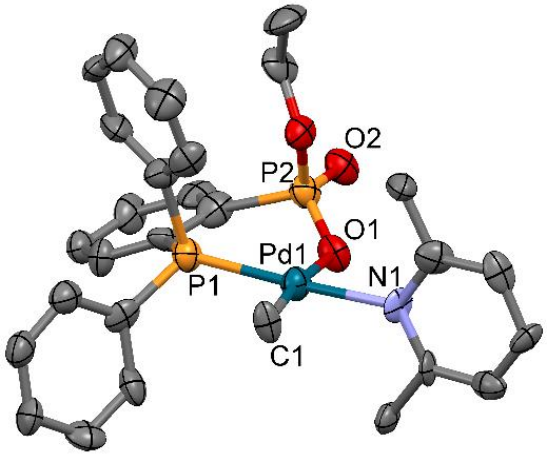

Figure 2.2. Molecular structure of **3b-lut**•CH_2Cl_2•0.5H_2O. The CH_2Cl_2 and H_2O molecules and hydrogen atoms are not shown. Bond lengths (Å) and angles (deg): C1–Pd1 2.030(3), N1–Pd1 2.124(3), O1–Pd1 2.138(2), P1–Pd1 2.2104(9), O2–P2 1.487(2), O1–P2 1.507(2), C1–Pd1–N1 87.98(12), N1–Pd1–O1 86.96(9), O1–Pd1–P1 96.73(6), P1–Pd1–C1 88.76(10).

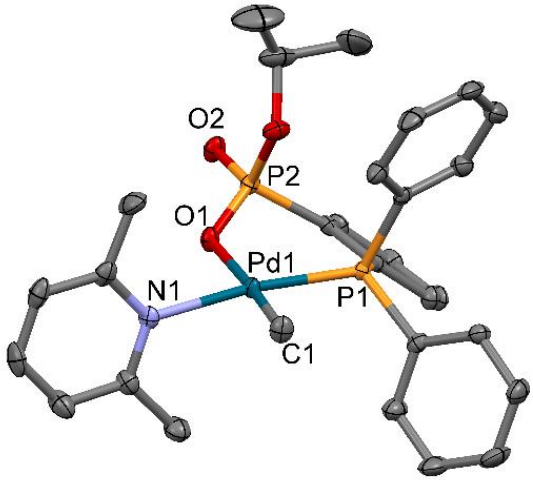

$B(C_6F_5)_3$ Binding to 3a-lut. The reaction of **3a-lut** with $B(C_6F_5)_3$ affords the *O*-bound borane adduct {**2a**•$B(C_6F_5)_3$}PdMe(lut) (**4a-lut**, Scheme 2.4). The $^{31}P\{^1H\}$ NMR spectrum of **4a-lut** displays two sharp doublets at δ 29.6 and 9.8 ($^3J_{PP}$ = 18 Hz). The preservation of resonances for Pd-coordinated 2,6-lutidine in the ^1H NMR spectrum indicate that $B(C_6F_3)_3$ binds to a phosphonate oxygen atom, as shown in Scheme 2.4. The solid-state structure of **4a-lut** was confirmed by X-ray diffraction (Figure 2.3). Consistent with the results for **G** and **H** and the resonance structure in Scheme 2.4, the Pd1–O1 distance in **4a-lut** is ca. 0.04 Å longer than that in **3a-lut** due to the decreased donor ability of the $B(C_6F_5)_3$-coordinated phosphonate group.

However, in this case, the borane does not induce a change in the conformation of the (PPO)Pd chelate ring, and the ethoxy group occupies an axial site.

Scheme 2.4. Synthesis of $B(C_6F_5)_3$-coordinated complexes.

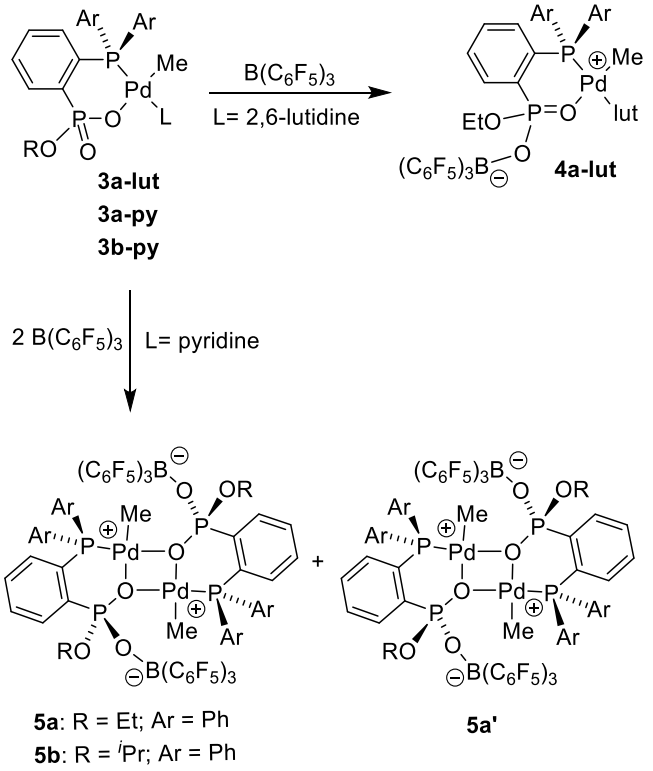

Figure 2.3. Molecular structure of **4a-lut**•CH_2Cl_2. The CH_2Cl_2 molecule and hydrogen atoms are omitted. Bond lengths (Å) and angles (deg): C1–Pd1 2.034(3), N1–Pd1 2.115(2), O1–Pd1 2.1400(19), P1–Pd1 2.2166(8), O1–P2 1.483(2), O2–P2 1.573(2), C1–Pd1–N1 89.49(11), N1–Pd1–O1 85.25(8), O1–Pd1–P1 94.92(6), P1–Pd1–C1 90.51(9).

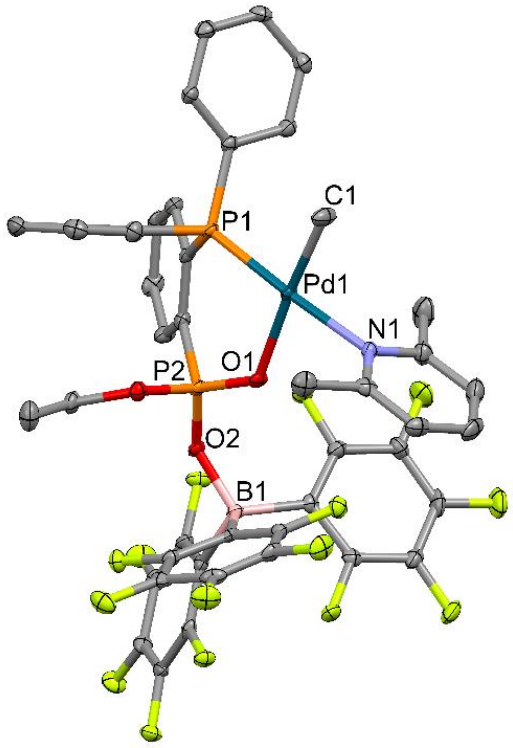

Synthesis of Base-free $B(C_6F_5)_3$-coordinated {[PPO•$B(C_6F_5)_3$]PdMe}$_2$ Complexes. The reaction of **3a-py** with 2 equiv of $B(C_6F_5)_3$ yields the base-free, borane-coordinated species {[**2a**•$B(C_6F_5)_3$]PdMe}$_2$ as a mixture of two diastereomers, **5a** and **5a'**, which differ in the relative configurations of the phosphonate phosphorus atoms (Scheme 2.4). The $^{19}F\{^1H\}$ and ^1H NMR spectra of **5a/5a'** each contain two sets of resonances in an 80/20 intensity ratio for the two isomers. Isomer **5a'**, which has *S,S* (*ent-R,R*) configurations at the phosphonate centers, was

isolated by recrystallization from $CHCl_2CHCl_2/CH_2Cl_2$/hexanes as a racemic conglomerate and identified by X-ray diffraction (Figure 2.4).[87] The two [**2a**•$B(C_6F_5)_3$]PdMe units are linked through a four-membered Pd1–O1−Pd1A–O1A ring. A similar structure was observed previously for {2-P(3,5-^{t}Bu$_2$-Ph)$_2$-*p*-toluenesulfonate)PdMe}$_2$.[80] The conformation of the (PPO)Pd chelate ring in **5a'** is similar to that in **H**, with the ethoxy group occupying an axial position. Addition of 1 equiv of 2,6-lutidine or a coordinating solvent converts **5a**/**5a'** back to the corresponding {**2a**•$B(C_6F_5)_3$}PdMeL species.

Figure 2.4. Molecular structure of **5a'**•CH_2Cl_2•$CHCl_2CHCl_2$. The CH_2Cl_2 and $CHCl_2CHCl_2$ molecules and hydrogen atoms are omitted. Bond lengths (Å) and angles (deg): C1–Pd1 2.005(3), O1–Pd1 2.1539(19), P1–Pd1 2.1802(8), O1A–Pd1 2.2049(19), P2–O1 1.512(2), P2–O2 1.511(2), O1–Pd1–O1A 79.16(8), O1A–Pd1–C1 93.12(11), C1–Pd1–P1 89.14(10), O1–Pd1–P1 98.59(5), Pd1–O1–Pd1A 94.14(7).

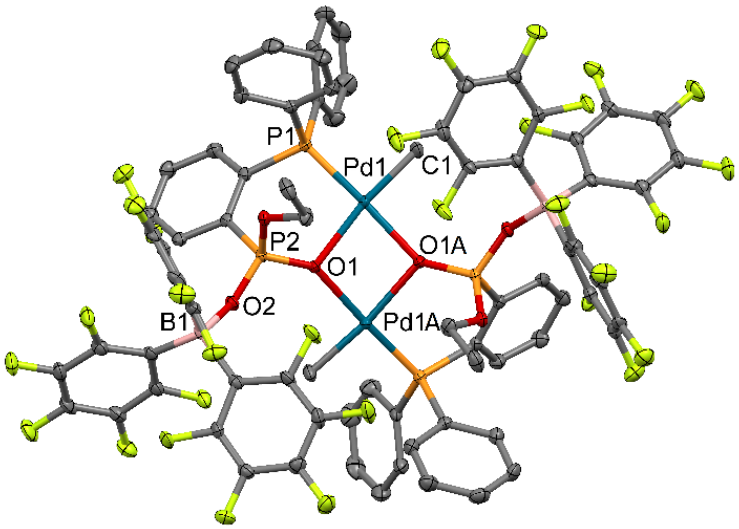

Similarly, the base-free dimer {[**2b**•$B(C_6F_5)_3$]PdMe}$_2$ (**5b**) was synthesized by the reaction of **3b-py** with 2 equiv of $B(C_6F_5)_3$ in CH_2Cl_2 (Scheme 2.4). In this case, only one isomer is observed in the NMR spectra. An X-ray diffraction analysis shows that **5b** has *S*,*R* configurations at the phosphonate centers (Figure 2.5). The borane coordination induces a significant change in the conformation of the (PPO)Pd chelate from the boat observed for **3b-lut** to an envelope in which the –O^{i}Pr and –O$B(C_6F_5)_3$ groups lie above and below Pd1-O1-P2-C9-C8 plane (Figure 2.7). A π-stacking interaction between a C_6F_5 ring (C23–C28) and the backbone arene ring of the PPO^- ligand (C8–12) is associated with this conformational change. The C23–C28 C_6F_5 ring and the C8–C13 Ph ring are organized in an eclipsed parallel arrangement with a distance of 3.58 Å between the ring centroids.

Figure 2.5. Molecular structure of **5b**. Hydrogen atoms are omitted. Bond lengths (Å) and angles (deg): C1–Pd1 2.021(3), O1–Pd1 2.2057(19), P1–Pd1 2.1876(8), O1A–Pd1 2.2284(19), P2–O1 1.513(2), P2–O2 1.510(2), O1–Pd1–O1A 82.90(8), O1A–Pd1–C1 96.38(10), C1–Pd1–P1 89.64(9), O1–Pd1–P1 91.55(5), Pd1–O1–Pd1A 97.10(8).

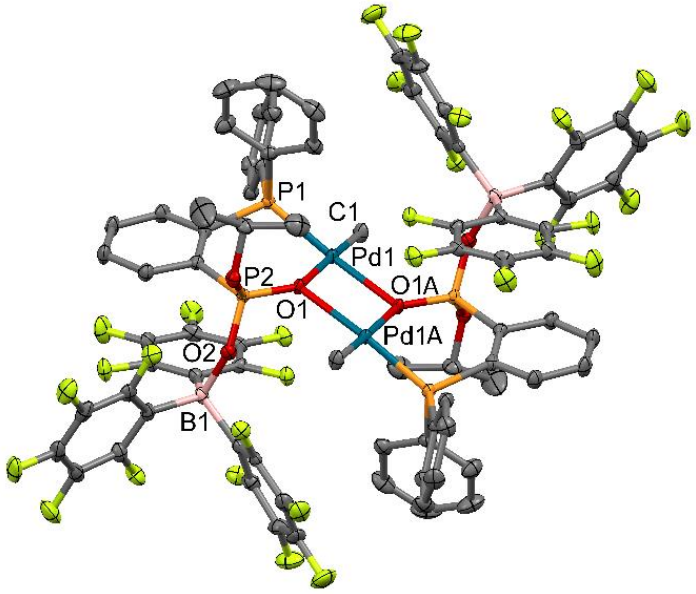

Figure 2.6. Molecular structures highlighting the change in the (κ^2-*P*,*O*)Pd chelate ring conformation from (a) boat in **3b-lut** to (b) envelope in **5b**. Hydrogens, P*Ph*$_2$ groups, 2,6-lutidine carbons in **3b-lut**, and half of dimer in **5b** have been removed for clarity.

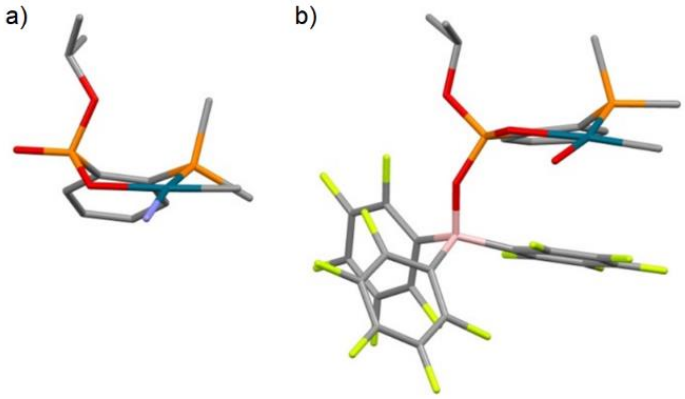

Synthesis of Other Lewis Acid Adducts. Other Lewis acids with varying steric and electronic profiles may produce different allosteric effects on (PPO)PdMeL complexes and therefore, the synthesis of these Lewis acid-coordinated complexes was explored. tris(2,2',2"-perfluorobiphenyl)borane (PBB), has a similar Lewis acidity to $B(C_6F_5)_3$ but is significantly larger. In particular, the placement of the $–C_6F_5$ ring in the *ortho*-position would likely increase steric crowding near the active site significantly. Blocking the Pd axial site may inhibit chain transfer and has been reported to significantly increase PE MW.[13,19] However, the reaction of **3a-lut** with PBB produces a very complex reaction mixture, the components of which could not be identified by $^{31}P\{^1H\}$, ^{19}F and ^1H NMR spectroscopy. The steric bulkiness of PBB likely precludes coordination to **3a-lut**.[88–90]

BF_3 also has a similar Lewis acidity to $B(C_6F_5)_3$ but is significantly smaller.[91–96] The reaction of **3a-py** with 2 equiv BF_3•Et_2O in CD_2Cl_2 produces a major product by $^{31}P\{^1H\}$, $^{19}F\{^1H\}$, ^1H NMR that is consistent with the base-free, BF_3-coordinated $\{[\mathbf{2a}•BF_3]PdMe\}_2$ complex. Two major resonances are observed by ^{19}F NMR that correlate to the $\{[\mathbf{2a}•BF_3]PdMe\}_2$ (δ –146.3) and BF_3•py (δ –151.8) products. However, the product could not be isolated on a larger scale. For polymerization experiments, **3a-py** + 2 equiv BF_3•Et_2O was used to form the expected $\{[BF_3•\mathbf{2a}]PdMe\}_2$ and BF_3•py products *in situ*, and the results are described in Chapter Three.

The reaction of **Li[2a]**, (COD)PdMeCl, $AgPF_6$, and 2,6-lutidine afforded the PF_5-coordinated complex **6a-lut** as shown in Scheme 2.5. $LiPF_6$ is initially produced and decomposes to LiF and PF_5, which coordinates to the O atom of the phosphonate group. A single crystal was isolated for X-ray diffraction from a CH_2Cl_2 solution layered with hexanes and left at –40 °C for ca. 8 weeks (Figure 2.7). **6a-lut** is structurally similar to **4a-lut**, with the ethoxy group occupying an axial site. The Pd1−O1 distance in **6a-lut** is ca. 0.06 Å longer than that in **3a-lut** due to the decreased donor ability of the PF_5-coordinated phosphonate group and ca. 0.02 Å longer than that in **4a-lut**. The $^{31}P\{^1H\}$ NMR spectrum contains two sharp resonances at δ 29.6 ad 6.2 for the phosphine and phosphonate groups and a sextet of doublets for the PF_5 group (δ –147.3, $^1J_{PF}$ = 713, $^2J_{PP}$ = 17). The $^{19}F\{^1H\}$ NMR contains a doublet of doublets corresponding to the coordinated PF_5 group (δ –60.0 ($^3J_{PF}$ = 55, $^1J_{PF}$ = 743). Unreacted $LiPF_6$ is also observed by $^{31}P\{^1H\}$ and $^{19}F\{^1H\}$ NMR. One Pd–C*H*$_3$ resonance (δ 0.22) is observed by ^1H NMR. Unfortunately, **6a-lut** could not be replicated or isolated on a larger scale for polymerization.

Scheme 2.5. Synthesis of **6a-lut**.

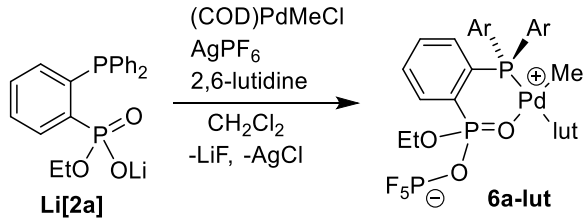

Figure 2.7. Molecular structure of **6a-lut**. Hydrogen atoms are omitted. Bond lengths (Å) and angles (deg): C1–Pd1 2.025(2), O1–Pd1 2.1580(14), P1–Pd1 2.2284(6), N1–Pd1 2.1177(17), P2–O1 1.4879(14), P2–O2 1.5377(15), O1–Pd1–N1 85.57(6), N1–Pd1–C1 89.22(8), C1–Pd1–P1 88.52(7), O1–Pd1–P1 96.74(4).

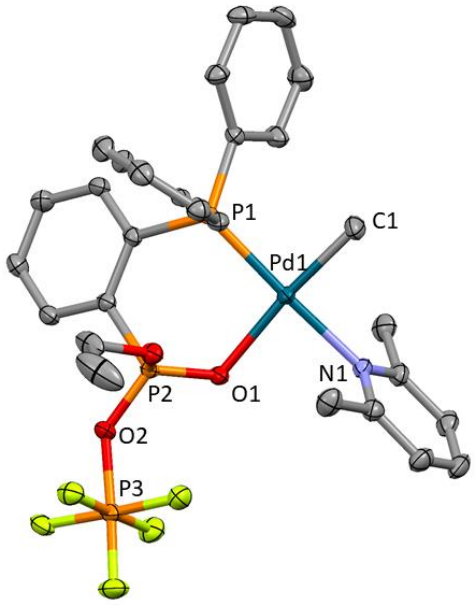

2.3 Conclusions

A novel series of phosphine-monoalkyl phosphonate ligands (**Li[2a–c]**)and the analogous Pd(II) alkyl complexes (**3a–c**) were synthesized. The reaction of **3a-lut** with 1 equiv $B(C_6F_5)_3$ affords the zwitterionic, borane-coordinated complex {**2a**•$B(C_6F_5)_3$}PdMe(lut) (**4a-lut**). The reaction of **3a-py** or **3b-py** with 2 equiv $B(C_6F_5)_3$ affords the base-free, borane-coordinated dimers [{**2a**•$B(C_6F_5)_3$}PdMe]$_2$ and [{**2b**•$B(C_6F_5)_3$}PdMe]$_2$ (**5a/5a'** and **5b**). The solution and solid-state structures of these complexes are discussed in detail. The $B(C_6F_5)_3$ adduct increases

the steric profile of the weak donor group and decreases the donating ability of the phosphonate group to Pd. The reactivity of these complexes with ethylene is discussed in Chapter Three. The reaction of (PPO)PdMeL with other Lewis acids (BF_3, $B(o\text{-}C_6F_5\text{-}C_6F_4)_3$, and PF_5) was also explored, and the PF_5-coordinated complex **6b-lut** was characterized by X-ray crystallography.

2.4 Experimental Section

General Procedures. All experiments were performed under a nitrogen atmosphere or vacuum using drybox or Schlenk techniques. Nitrogen was purified by passage over Q-5 oxygen scavenger and activated molecular sieves. Methylene chloride, diethyl ether and THF were dried by passage over activated alumina. Pentane was purified by passage over BASF R3-11 oxygen scavenger and activated alumina. **1a**,[81,82] bis(2-methoxyphenyl)chlorophosphine[81] and (TMEDA)$PdMe_2$[88] were prepared by literature procedures. $B(C_6F_5)_3$ was donated by Boulder Scientific.

NMR spectra were acquired on Bruker DRX-500 or DRX-400 spectrometers at ambient temperature unless otherwise indicated. ^1H and ^{13}C chemical shifts are reported relative to $SiMe_4$ and are internally referenced to residual ^1H and ^{13}C solvent resonances. ^{31}P and ^{19}F chemical shifts are reported relative to 85% H_3PO_4 and $CFCl_3$, respectively. Coupling constants are reported in Hz. Elemental analyses were performed by Robertson Microlit Laboratories.

Residual solvent in elemental analysis samples was quantified by ^{1}H NMR. Mass spectrometry was performed on an Agilent 6224 TOF-MS instrument (high resolution) or an Agilent 6130 LC-MS (low resolution).

2-BrPh-P(O)(O^{i}Pr)$_2$. The following procedure was adapted from Ref 83. 2-bromophenylboronic acid (20.0 g, 99.6 mmol), copper(I) oxide (1.44 g, 10.2 mmol), and 1,10-phenanthroline (3.78 g, 20.9 mmol) were dissolved in acetonitrile (200 mL). Diisopropylphosphate (8.3 mL, 49 mmol) and NEt(^{i}Pr)$_2$ (26.0 mL, 152 mmol) were added. The mixture stirred in air for 6 d, filtered and stripped of solvent under vacuum. The resulting oil was dissolved in Et_2O (250 mL) and washed with 1 M HCl (250 mL). The organic layer was extracted with Et_2O (3 x 200 mL). The combined organic layers were dried over $MgSO_4$ and the solvent was removed under vacuum to afford a red oil. The crude product was purified by column chromatography (silica; 70:29:1 hexanes:acetone:NEt_3), affording an orange oil (8.19 g, 52 %). ^{31}P{^{1}H} NMR (CD_2Cl_2): δ 12.4 (s, *P*=O). ^{1}H NMR (CD_2Cl_2): δ 8.01 (ddd, $^{3}J_{PH}$ = 7.5, $^{3}J_{HH}$ = 14.5, $^{4}J_{HH}$ = 2, 1H, H^{D}), 7.66 (m, 1H, H^{A}), 7.39 (m, 2H, H^{B} and H^{C}), 4.69 (dq, $^{3}J_{HH}$ = $^{3}J_{PH}$ = 7, 2H, –OC*H*(CH_3)$_2$), 1.37 (d, $^{3}J_{HH}$ = 6.5 , 6H, –OCH(C*H*$_3$)$_2$), 1.26 (d, $^{3}J_{HH}$ = 6.0, 6H, –OCH-(C*H*$_3$)$_2$). ^{13}C{^{1}H} NMR (CD_2Cl_2): δ 136.5 (d, $^{2}J_{PC}$ = 8.3, C^{D}), 134.7 (d, $^{2}J_{PC}$ = 10.9, C^{A}), 133.7 (d, $^{3}J_{PC}$ = 2.8, C^{B}), 131.5 (d, $^{1}J_{PC}$ = 191, C^{E}), 127.3 (d, $^{3}J_{PC}$ = 13.5, C^{C}), 125.5 (d, $^{1}J_{PC}$ = 3.6, C^{F}), 71.7 (d, $^{2}J_{PC}$ = 5.8, –O*C*H(CH_3)$_2$), 24.2 (d, $^{3}J_{PC}$ = 4.3, –OCH(*C*H$_3$)$_2$), 23.9 (d, $^{3}J_{PC}$ = 5.0, –

OCH(CH_3)$_2$). HRMS: calcd. for $[C_{12}H_{19}O_3PBr]^+$ *m/z* 321.02554. Found: 321.0246.

Figure 2.8. Numbering scheme for 2-BrPh-P(O)(O^{i}Pr)$_2$.

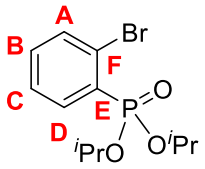

Figure 2.9. NMR spectra of 2-BrPh-P(O)(O^{i}Pr)$_2$.

(a) $^{31}P\{^1H\}$ NMR (CD_2Cl_2, 202 MHz)

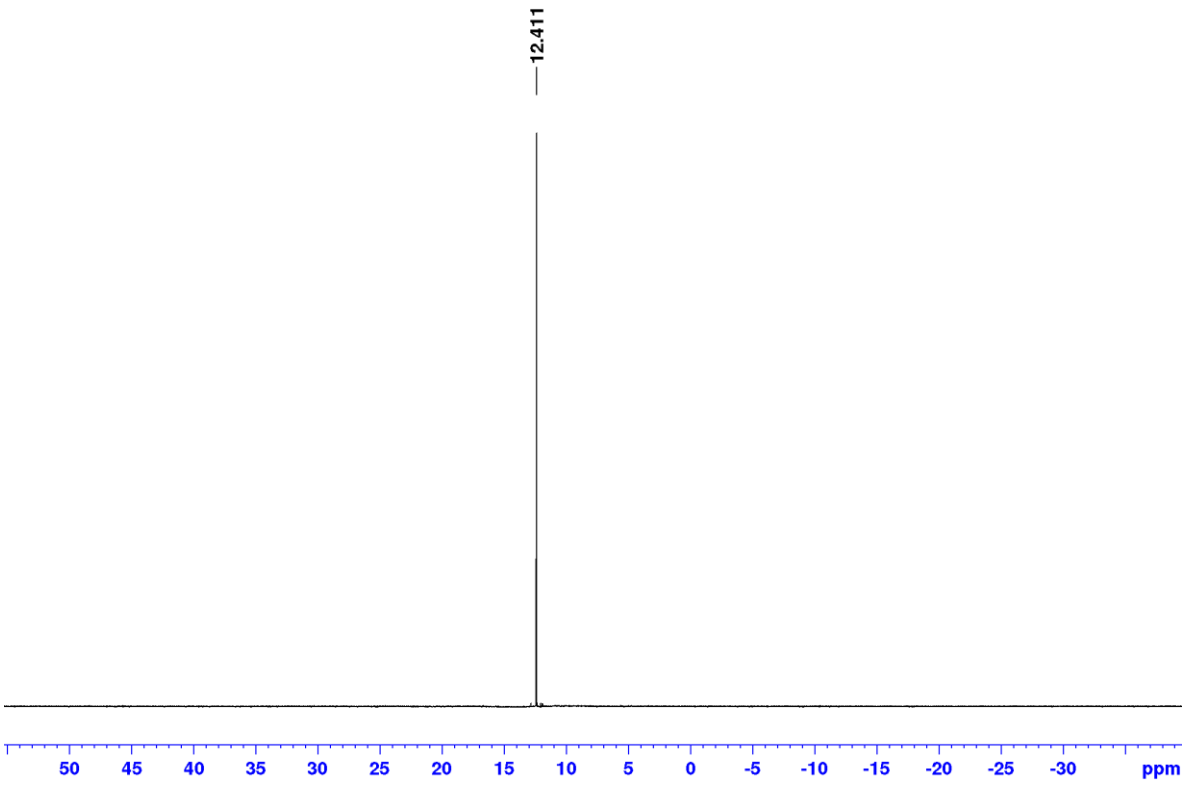

Figure 2.9, continued.

(b) ^{1}H NMR (CD_2Cl_2, 500 MHz)

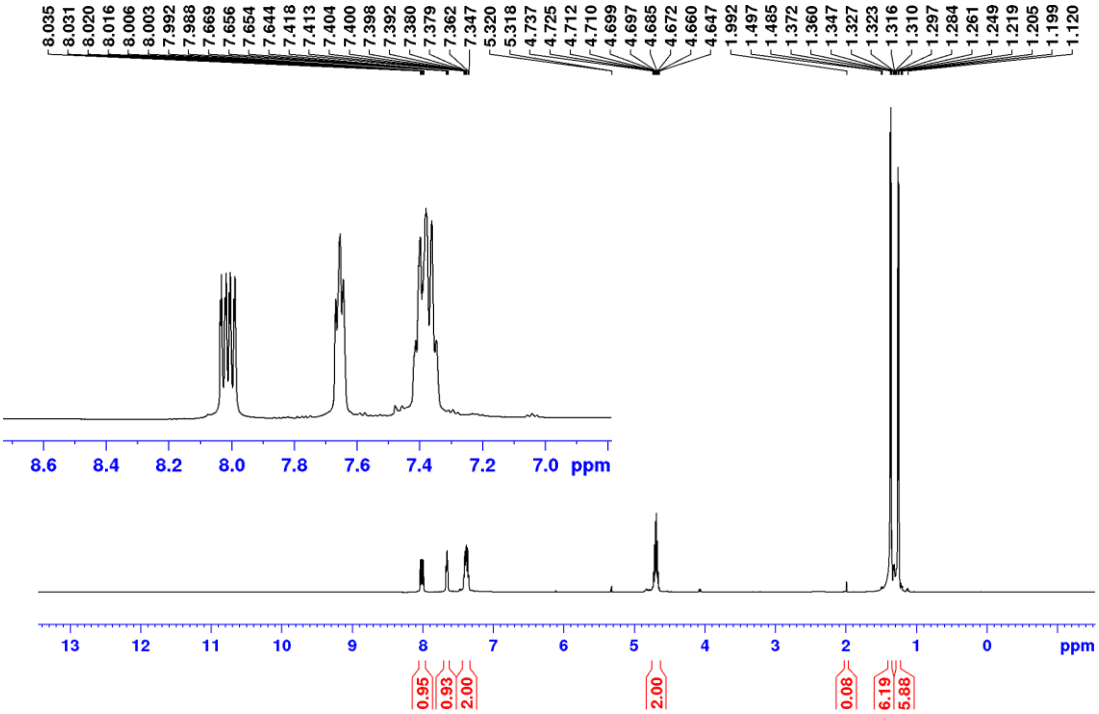

(c) ^{13}C{^{1}H} NMR (CD_2Cl_2, 126 MHz)

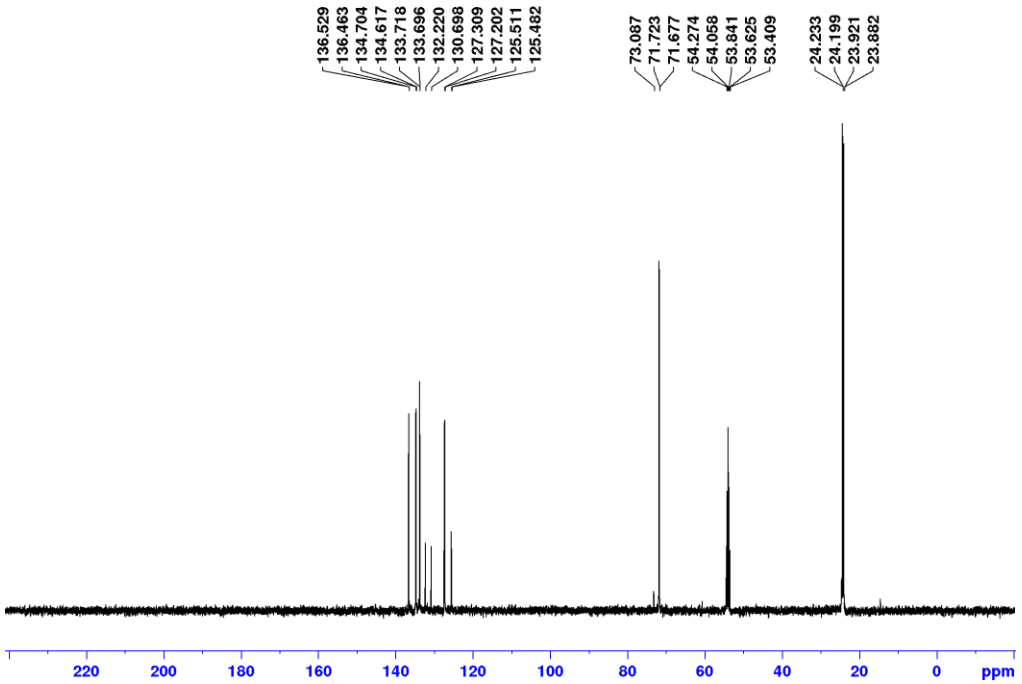

Figure 2.9, continued.

(d) COSY NMR (CD_2Cl_2, 500 MHz)

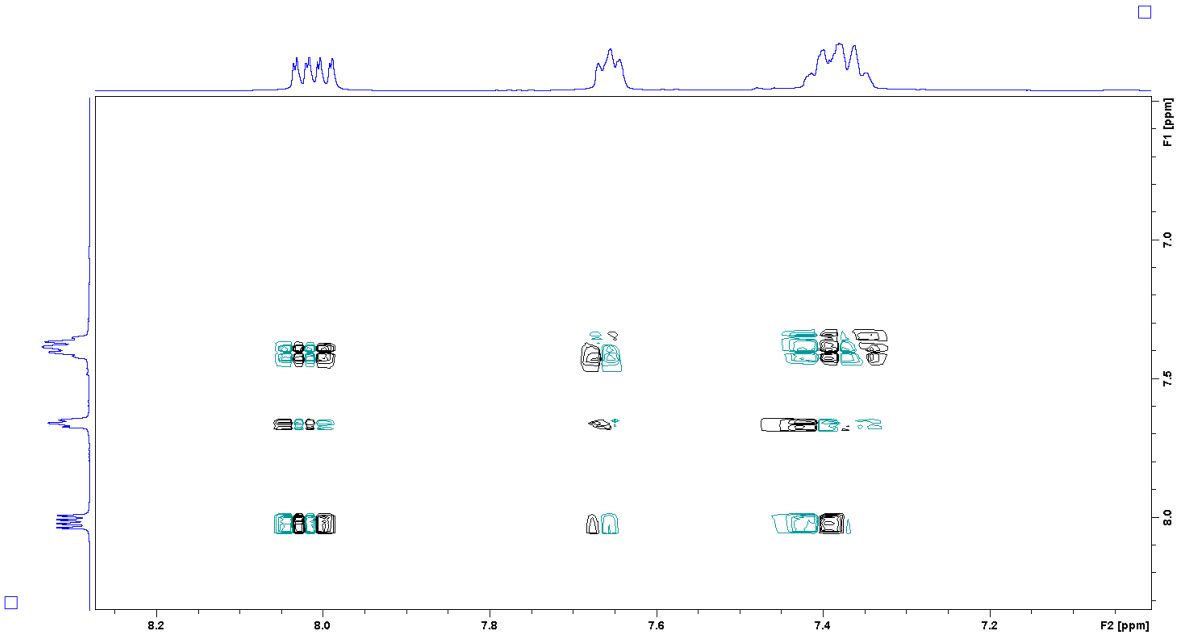

(e) HMQC NMR (CD_2Cl_2, 500 MHz, 125 MHz).

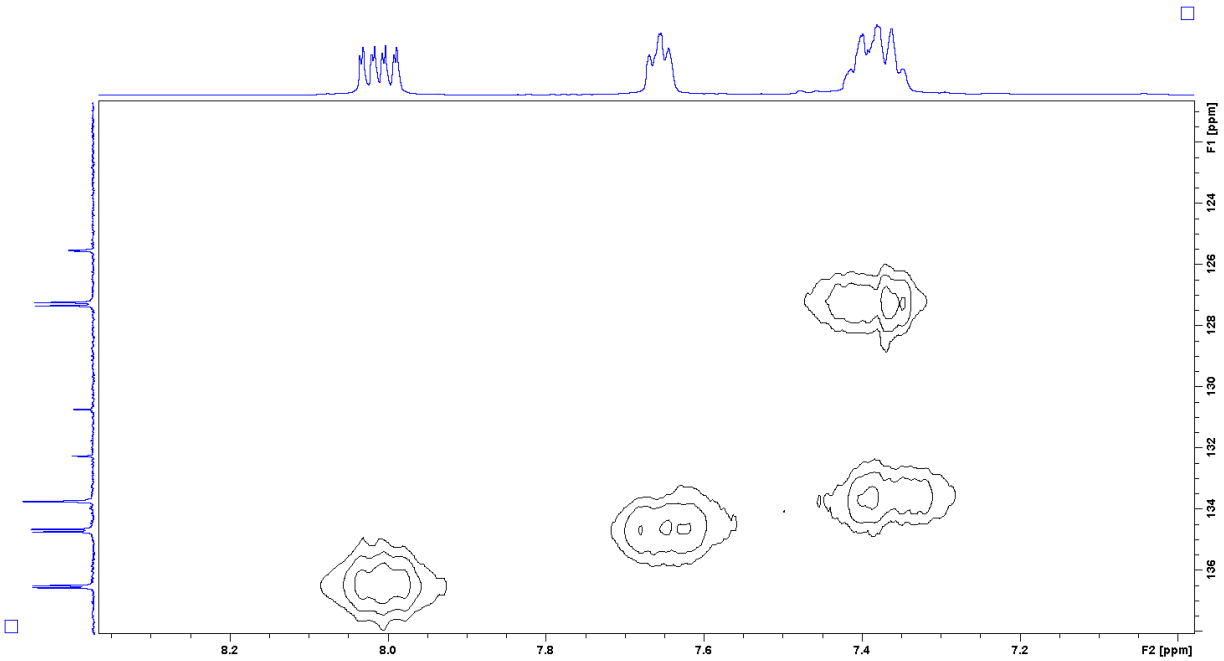

1-PPh_2-2-$P(O)(O^iPr)_2$-benzene (1b). This procedure was adapted from the procedure for **1a**, as reported by Rieger.[81] A solution of 2-bromophenyl-diphenylphosphine (2.24 g, 6.56 mmol) in THF (60 mL) was cooled to -78 °C, and *n*-BuLi (10.5 mL, 6.56 mmol) was added dropwise. The solution was stirred for 1 h at -78 °C. A solution of chlorodiisopropylphosphate (1.32 g, 6.56 mmol) in THF (20 mL) was added dropwise to this mixture. The resulting mixture was allowed to warm to room temperature slowly overnight. The solvent was removed under vacuum. The resulting orange oil was taken up in Et_2O (75 mL) and washed with H_2O (75 mL). The aqueous layer was extracted with Et_2O (3 x 50 mL). The combined organic layers were dried over $MgSO_4$ and stripped under vacuum to afford a yellow oil. The oil was washed with pentane and crystallized from a solution of THF/pentane to give a white solid (1.72 g, 61 %). $^{31}P\{^1H\}$ NMR (CD_2Cl_2): δ 15.9 (s, *P*=O), -9.3 (s, *P*). ^1H NMR (CD_2Cl_2): δ 8.06 (m, 1H, H^D), 7.43 (m, 2H, H^C and H^B), 7.32 (m, 6H, *p*-Ph and *o*-Ph), 7.21 (m, 4H, *m*-Ph), 7.14 (m, 1H, H^A), 4.70 (m, 1H, –OC*H*$(CH_3)_2$) 1.28 (d, $^3J_{HH}$ = 6.0, 6H, –OCH(C*H*$_3)_2$), 1.09 (d, $^3J_{HH}$ = 6.5, 6H, –OCH(C*H*$_3)_2$). $^{13}C\{^1H\}$ NMR (CD_2Cl_2): δ 141.1 (dd, $^1J_{PC}$ = 25.2, $^2J_{PC}$ = 12.8, C^F), 138.1 (d, $^1J_{PC}$ = 13.7, *ispo*-Ph), 137.2 (d, $^1J_{PC}$ = 188, $^2J_{PC}$ = 32.4, C^E), 135.9 (d, $^2J_{PC}$ = 15, C^A), 133.9 (dd, J_{PC} = 10.4, 7.9, C^D), 133.6 (d, $^2J_{PC}$ = 20, *o*-Ph), 131.6 (d, $^3J_{PC}$ = 3.1, C^B), 128.4 (d, $^3J_{PC}$ = 11.4, C^C), 128.3 (d, $^3J_{PC}$ = 6.4, *m*-Ph), 128.3 (*p*-Ph), 71.0 (d, $^2J_{PC}$ = 6.0, –O*C*H$(CH_3)_2$), 23.8 (d, $^3J_{PC}$ = 4.2, –OCH(*C*H$_3)_2$), 23.5 (d, $^3J_{PC}$ = 4.8, –OCH(*C*H$_3)_2$),. HRMS: calcd. for $[C_{24}H_{29}O_3P_2]^+$, *m/z* 426.15921. Found:

427.1585.

Figure 2.10. Numbering scheme for **1b**.

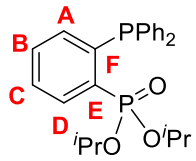

Figure 2.11. NMR spectra of **1b**.

(a) $^{31}P\{^{1}H\}$ NMR (CD_2Cl_2, 202 MHz)

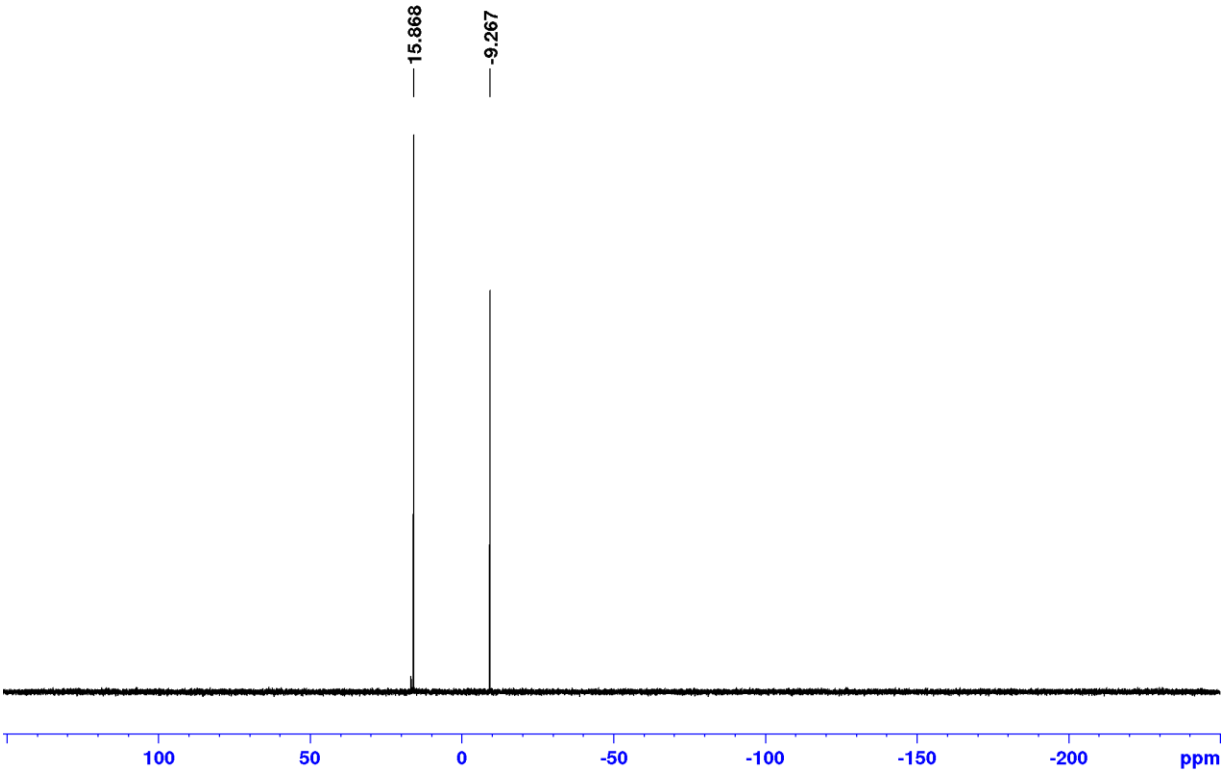

Figure 2.11, continued.

(b) ^{1}H NMR (CD_2Cl_2, 500 MHz)

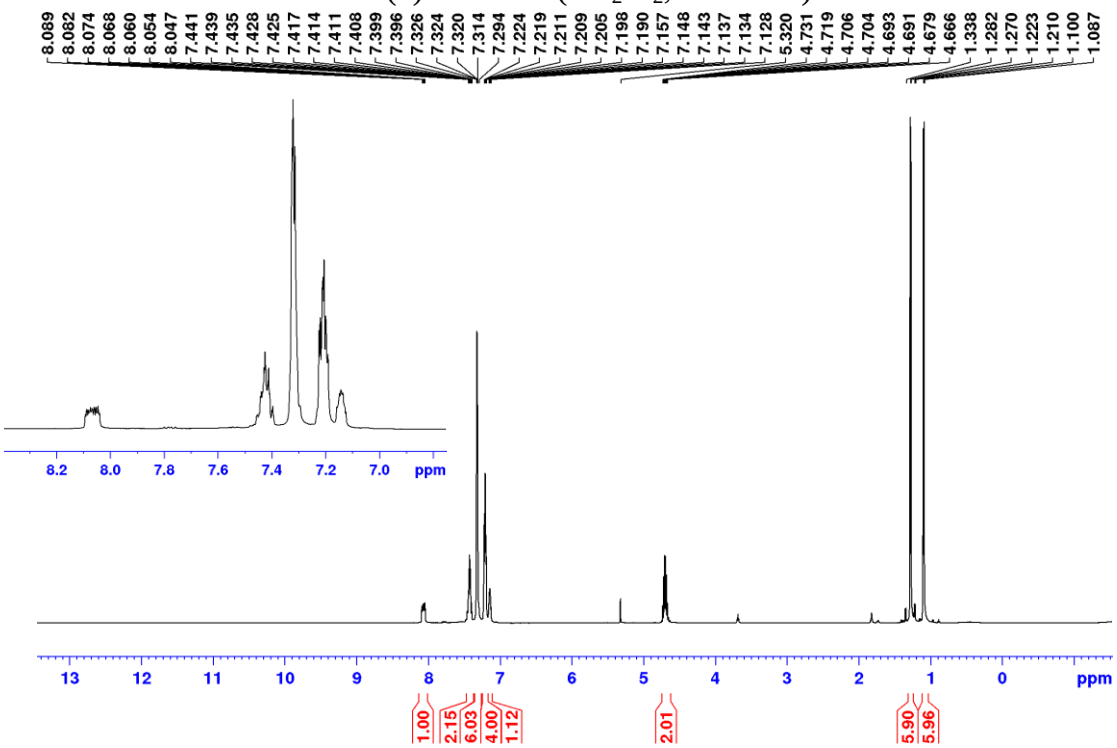

(c) ^{13}C NMR (CD_2Cl_2, 125 MHz)

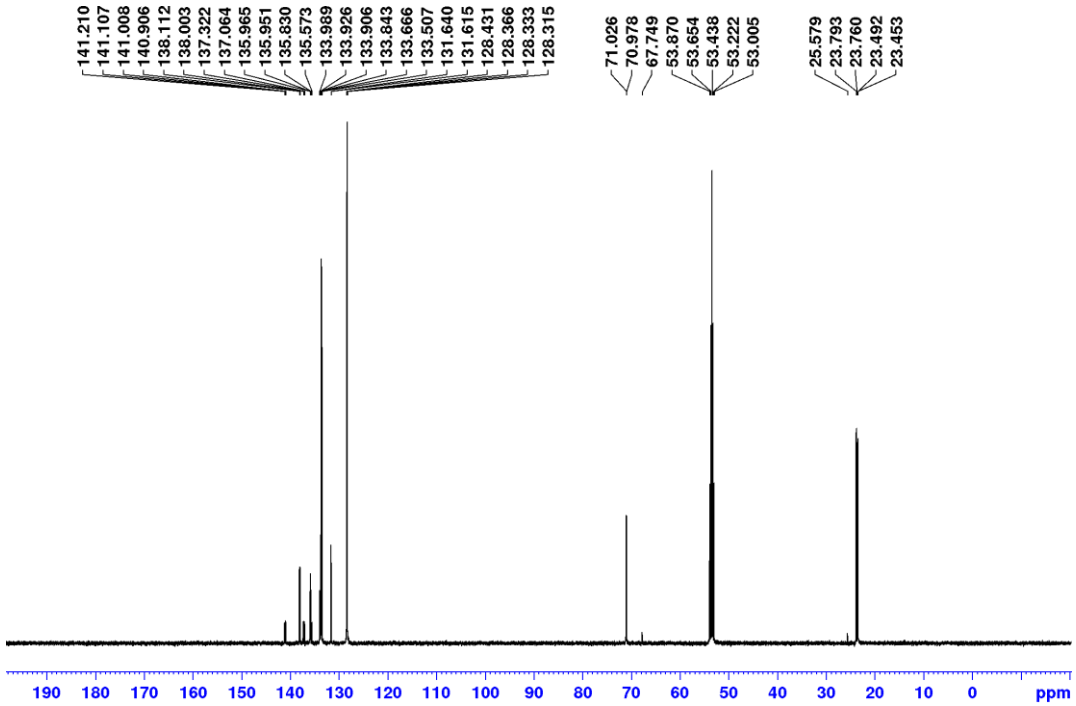

Figure 2.11, continued.

(d) COSY NMR (CD_2Cl_2, 500 MHz)

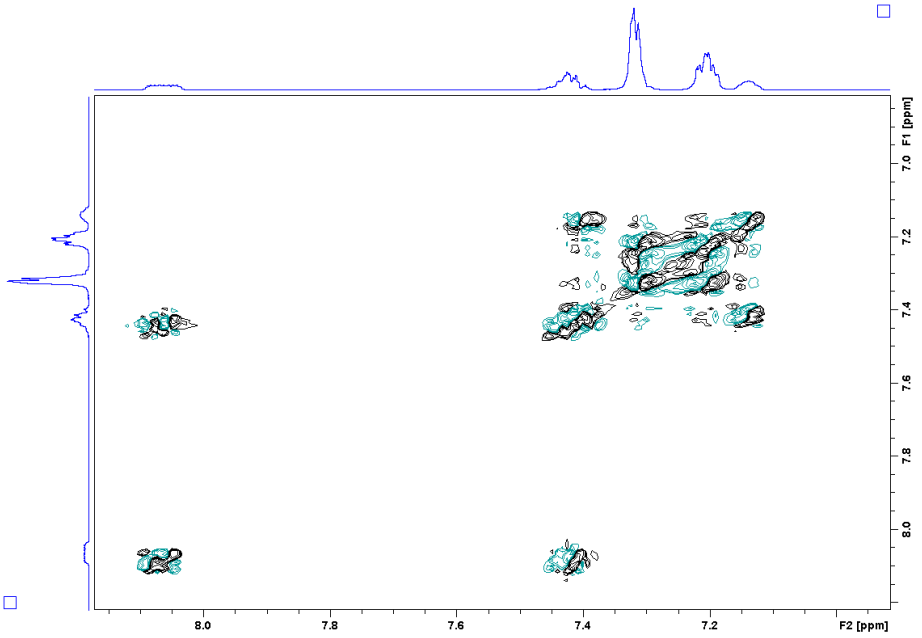

(e) HMQC NMR (CD_2Cl_2, 500 MHZ, 125 MHZ)

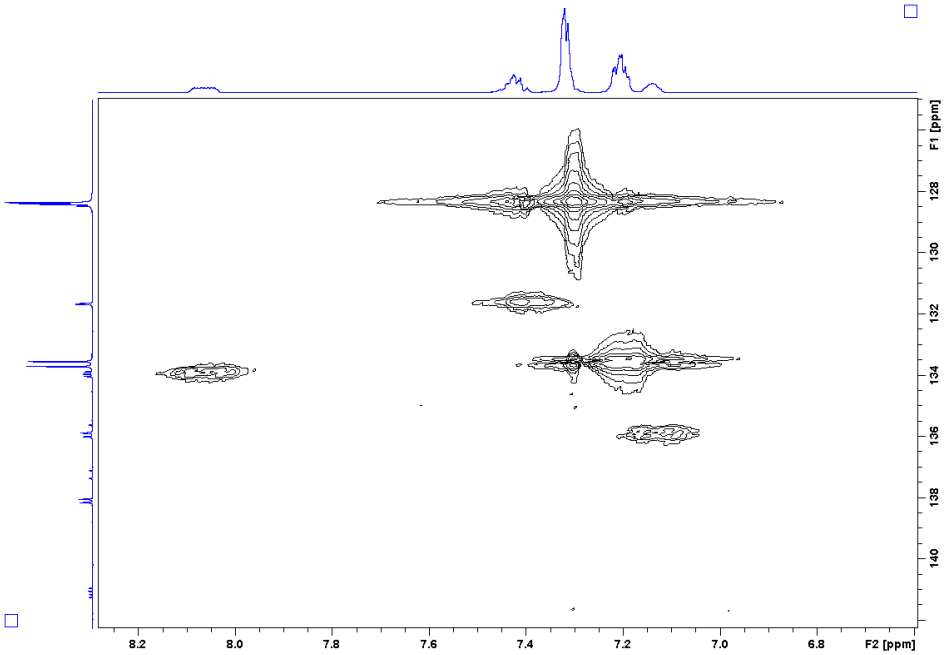

1-PAn$_2$-2-P(O)(O^{i}Pr)$_2$-benzene (1c). A solution of 2-bromophenyl-diisopropylphosphonate (3.37 g, 11.8 mmol) in 1:1 THF:Et_2O (120 mL) was cooled to -78 ^oC and *n*-BuLi (6.6 mL, 10.6 mmol) was added dropwise. The solution was stirred for 1 h at -78 ^oC. A solution of bis(2-methoxyphenyl)chlorophosphine (2.94 g, 10.6 mmol) in THF (20 mL) was added dropwise and the mixture was stirred at room temperature overnight. The solvent was removed under vacuum and the resulting oil was taken up in THF to precipitate the product as a white solid at -40 ^oC (3.93 g, 77 %). $^{31}P\{^1H\}$ NMR (CD_2Cl_2): δ 16.4 (s, *P*=O), -27.8 (s, *P*). ^1H NMR (CD_2Cl_2): δ 8.10 (m, 1H, H^D), 7.41 (m, 1H, H^C), 7.33 (m, 3H, H^H and H^B), 7.00 (m, 1H, H^A), 6.89 (m, 2H, H^G), 6.82 (m, 2H, H^I), 6.53 (br, 2H, H^J), 4.67 (m, 2H, –OC*H*$(CH_3)_2$), 3.69 (s, 6H, –OC*H*$_3$), 1.23 (d, $^3J_{HH}$ = 5.0, 6H, –OCH(C*H*$_3)_2$), 1.05 (br s, 6H, –OCH(C*H*$_3)_2$). $^{13}C\{^1H\}$ NMR (CD_2Cl_2): δ 161.4 (d, $^2J_{PC}$ = 16.7, C^K), 141.5 (dd, $^1J_{PC}$= 25.5, $^2J_{PC}$ = 12.5, C^F), 135.2 (d, $^1J_{PC}$= 187, $^2J_{PC}$ = 33.2, C^E), 135.5 (dd, $^2J_{PC}$= 15.3, $^3J_{PC}$ = 1.3, C^A), 134.5 (d, J_{PC} = 11, 7.8, C^D), 134.4 (C^J), 131.9 (d, $^3J_{PC}$ = 3.1, C^B), 130.2 (C^H), 128.4 (d, $^3J_{PC}$ = 14.3, C^C), 126.3 (d, $^1J_{PC}$ = 16.5, C^L), 121.2 (C^I), 110.5 (d, $^2J_{PC}$ = 1.3, C^G), 71.2 (dd, $^2J_{PC}$ = 6.0,–O*C*H$(CH_3)_2$), 55.8 (–O*C*H$_3$), 24.0 (d, $^3J_{PC}$ = 4.2, –OCH(*C*H$_3)_2$), 23.7 (d, $^3J_{PC}$ = 4.9, –OCH(*C*H$_3)_2$). HRMS: calcd. for $[C_{26}H_{33}O_5P_2]^+$, *m/z* 487.18034. Found: 487.1813.

Figure 2.12. Numbering scheme for **1c**.

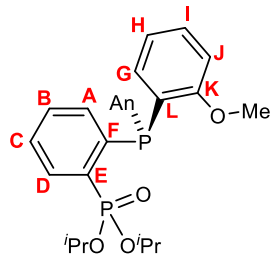

Figure 2.13. NMR spectra of **1c**.

(a) $^{31}P\{^{1}H\}$ NMR (CD_2Cl_2, 202 MHz)

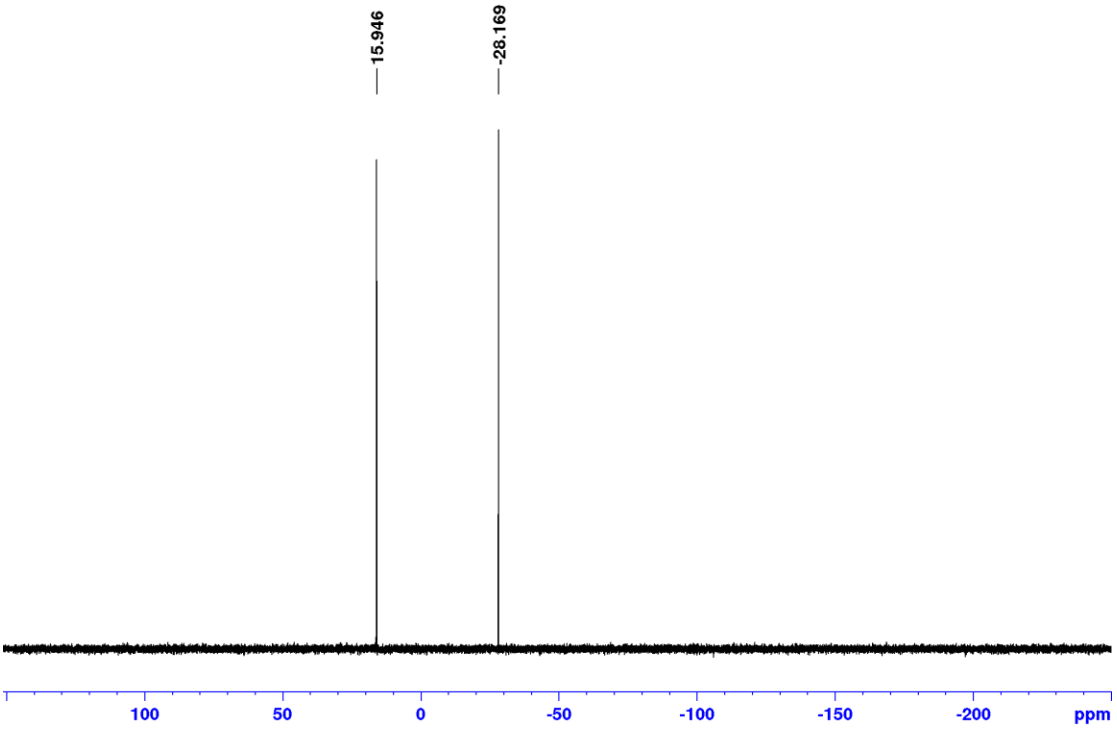

Figure 2.13, continued.

(b) ^{1}H NMR (CD_2Cl_2, 500 MHz)

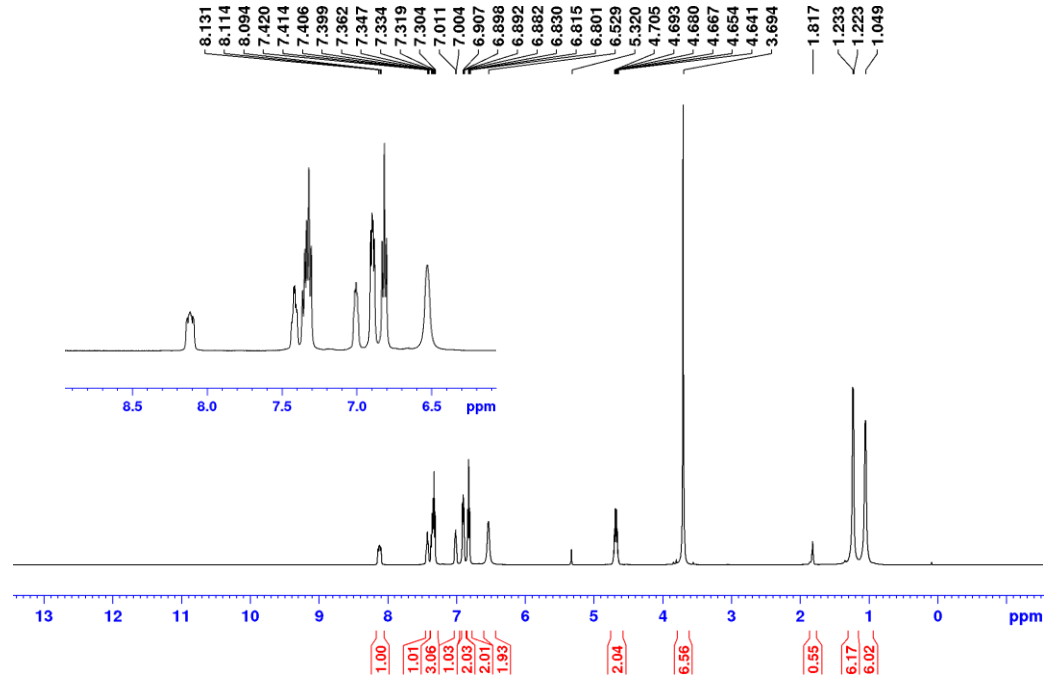

(a) ^{13}C{^{1}H} NMR spectrum (CD_2Cl_2, 125 MHz)

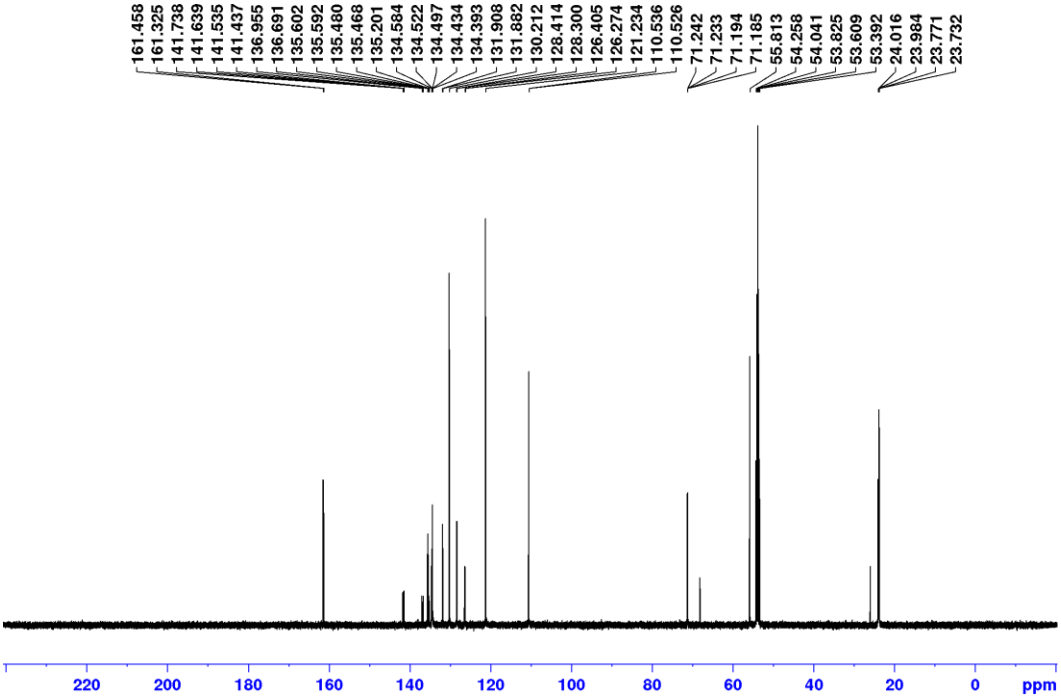

Figure 2.13, continued.

(b) COSY NMR (CD_2Cl_2, 500 MHz)

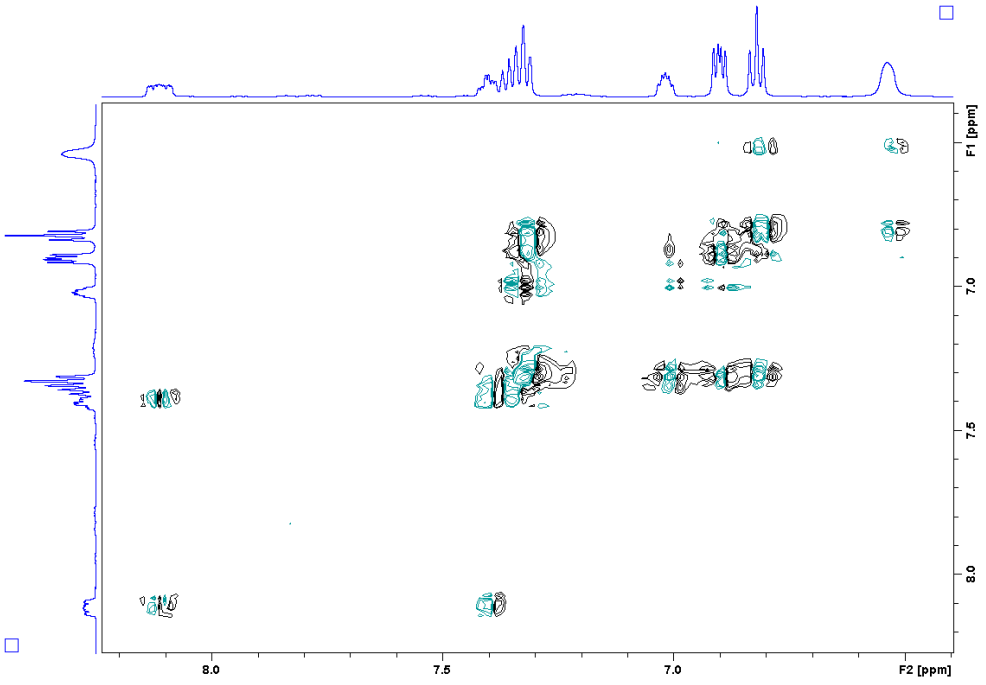

(c) HMQC NMR (CD_2Cl_2, 500 MHz, 125 MHz)

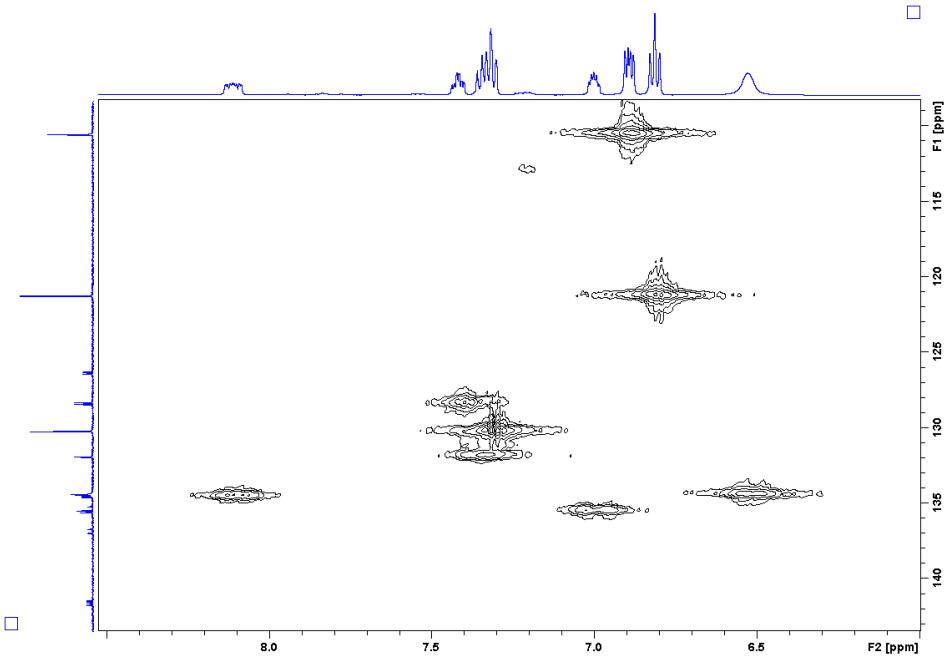

1-PPh$_2$-2-P(O)(OEt)(OLi)-benzene (Li[2a]). A flask was charged with **1a** (3.25 g, 8.17 mmol), lithium bromide (1.20 g, 13.9 mmol), and acetonitrile (30 mL). The mixture was refluxed and stirred. A white solid began to precipitate after approximately 30 min. After ca. 40 h, the suspension was filtered and the white solid was washed with Et_2O (2 x 50 mL) and dried under vacuum (2.67 g, 82 %). A minor impurity formed during the reaction and was identified as the ethylphosphonium zwitterion 1-P(Et)Ph$_2$-2-P(O)(OEt)(OLi)-benzene by ESI-MS, ^{1}H NMR, and ^{31}P{^{1}H} NMR. This material was not purified further but was used directly in the synthesis of H[**6a**]. ^{31}P{^{1}H} NMR (CD_3OD): δ 13.4 (s, *P*=O), -9.3 (s, *P*). ^{1}H NMR (CD_3OD): δ 8.07 (m, 1H, H^D), 7.37-7.22 (m, 12H), 7.08 (m, 1H, H^A), 3.55 (dq, $^3J_{HH}$ = $^3J_{PH}$ = 7, 2H, –O*CH*$_2$CH$_3$), 0.80 (t, $^3J_{HH}$ = 7, 3H, –OCH$_2$*CH*$_3$). ESI-MS (CH_3OH, negative ion scan, *m/z*): 369.1 $[C_{20}H_{19}O_3P_2]^-$.

Figure 2.14. Numbering scheme for **Li[2a]**.

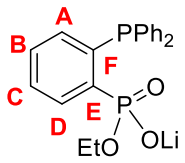

Figure 2.15. NMR spectra of **Li[2a]**.

(a) ^{31}P NMR spectrum (MeOD, 202 MHz)

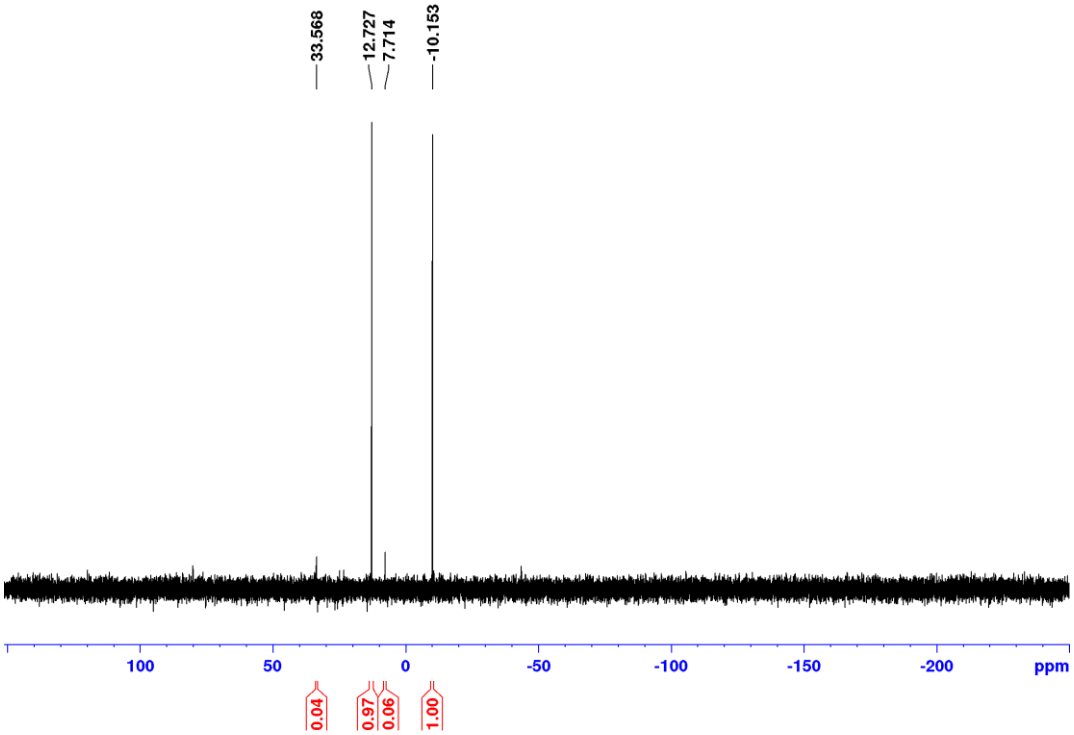

(b) ^{1}H NMR spectrum (MeOD, 500 MHz)

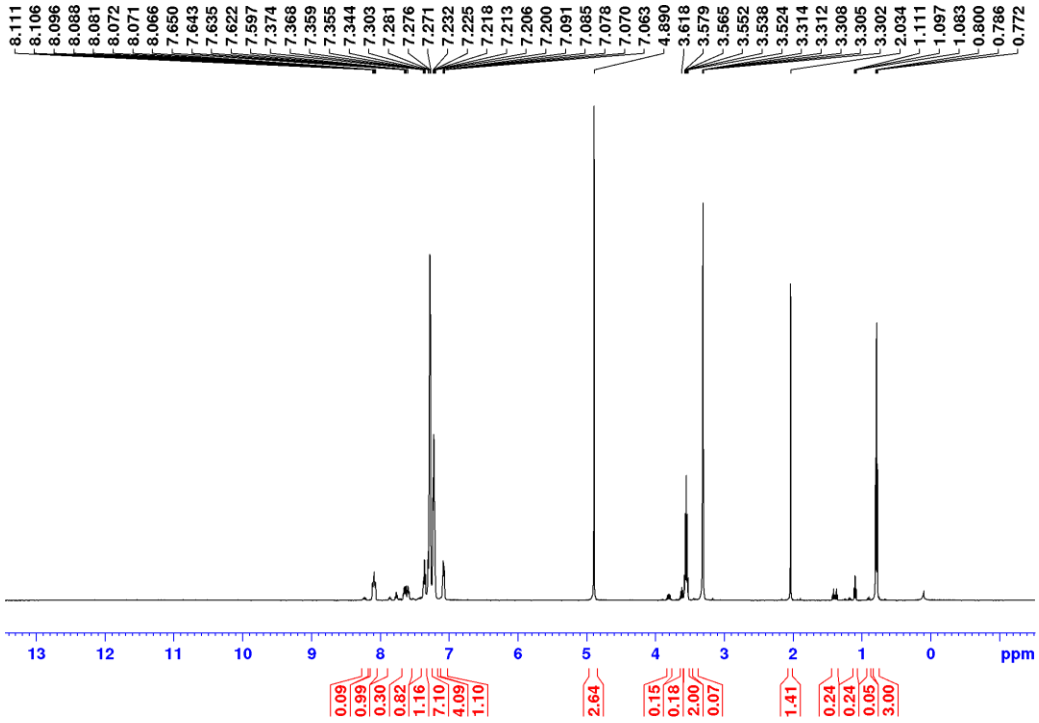

1-PPh$_2$-2-P(O)(O^{i}Pr)(OLi)-benzene (Li[2b]). A flask was charged with **1b** (1.50 g, 3.52 mmol) and acetonitrile (40 mL). The solution was saturated with LiBr at room temperature. The mixture was refluxed and stirred. A white solid began to precipitate after approximately 1 d. After ca. 10 d, the suspension was filtered, and the white solid was washed with acetonitrile (3 x 2 mL) and dried under vacuum (1.26 g, 88 %). ^{31}P{^{1}H} NMR (CD_3OD): δ 12.2 (s, *P*=O), -9.3 (s, *P*). ^{1}H NMR (CD_2Cl_2): δ 8.09 (m, 1H, H^D), 7.34 (m, 1H, H^C), 7.26-7.21 (m, 11H, H^B, Ph–*H* signals), 7.09 (m, 1H, H^A), 4.48 (m, 1H, –OC*H*$(CH_3)_2$) 0.98 (d, $^3J_{HH}$ = 6.5, 6H, –OCH(C*H*$_3)_2$). ^{13}C{^{1}H} NMR (CD_3OD): δ 144.3 (dd, $^1J_{PC}$ = 178, $^2J_{PC}$ = 33.8, C^E), 141.2 (dd, $^1J_{PC}$ = 22.4, $^2J_{PC}$ = 11.5, C^F), 139.7 (d, $^3J_{PC}$ = 15, C^C), 136.9 (dd, $^2J_{PC}$ = 13.8, $^3J_{PC}$ = 2, C^A), 134.7 (d, $^2J_{PC}$ = 19.6, *o*-Ph), 134.3 (dd, $^2J_{PC}$ = $^3J_{PC}$ = 9, C^D), 130.7 (d, $^3J_{PC}$ = 3, C^B), 129.1 (d, $^3J_{PC}$ = 6, *m*-Ph), 129.0 (d, $^1J_{PC}$ = 12.8, *ipso*-Ph), 129.0 (*p*-Ph), 69.0 (d, $^2J_{PC}$ = 5.9, –O*C*H$(CH_3)_2$), 24.5 (d, $^3J_{PC}$ = 4.3, –OCH(*C*H$_3)_2$). HRMS: calcd. for $[C_{21}H_{21}LiO_3P_2 – H_2O]^+$, *m/z* 372.10205. Found: 371.1003.

Figure 2.16. Numbering scheme for Li[**2b**].

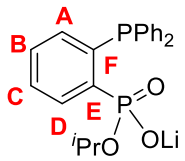

Figure 2.17. NMR spectra of Li[**2b**].

(a) $^{31}P\{^{1}H\}$ NMR (MeOD, 202 MHz)

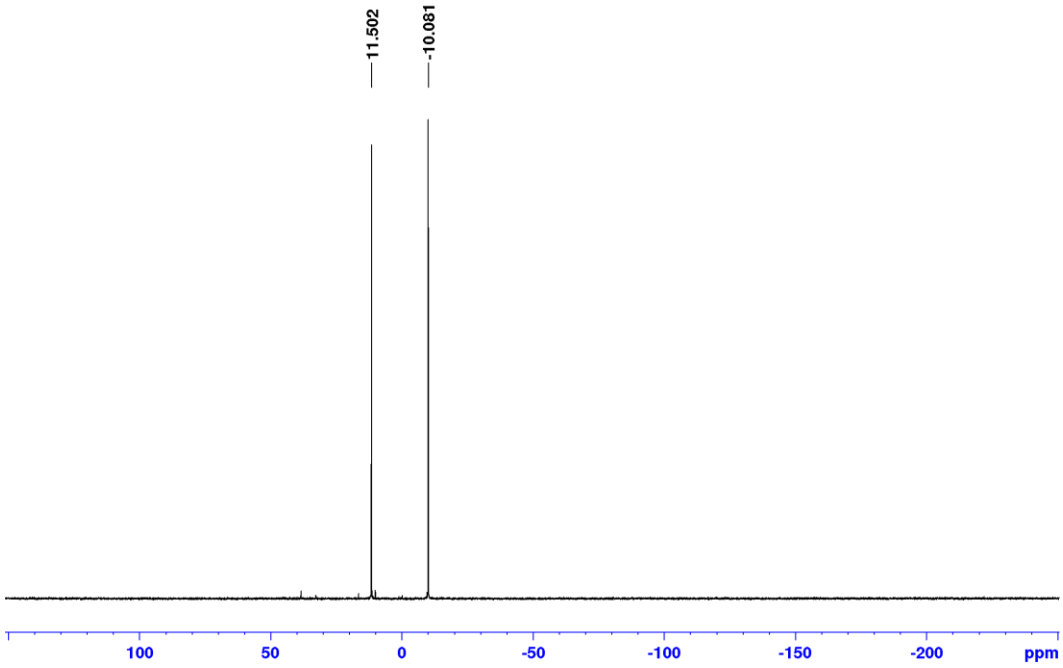

(b) ^{1}H NMR (MeOD, 500 MHz)

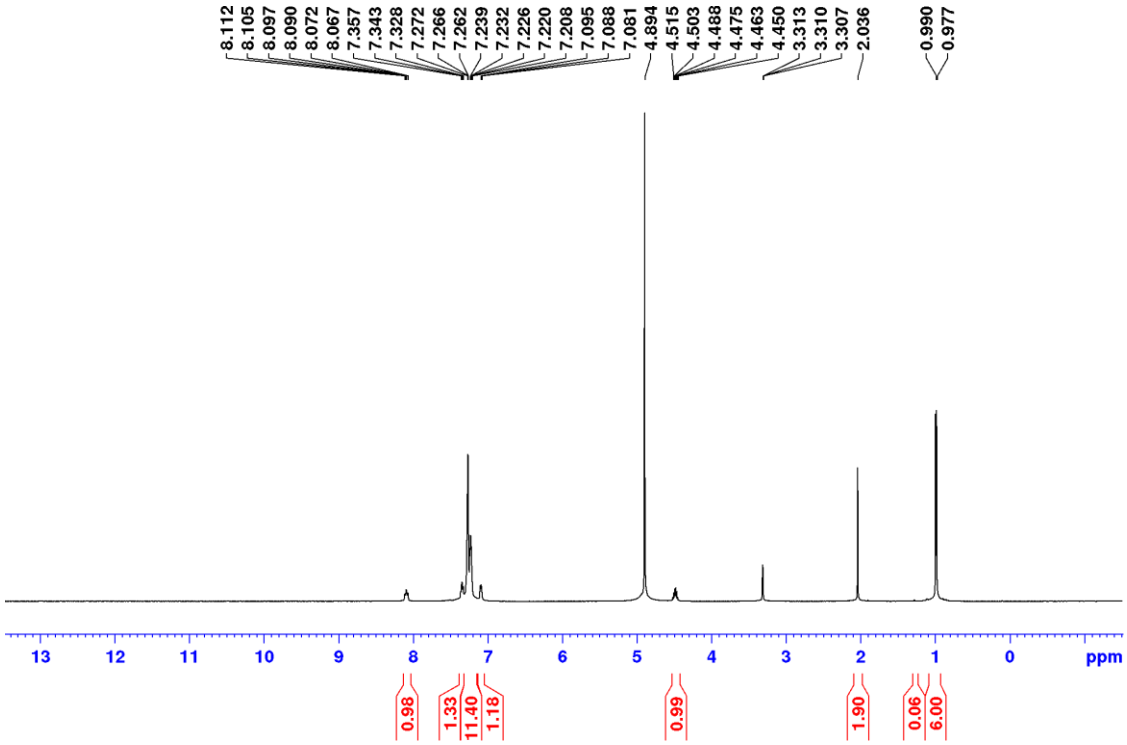

Figure 2.17, continued.

(c) $^{13}C\{^{1}H\}$ NMR (MeOD, 125MHz)

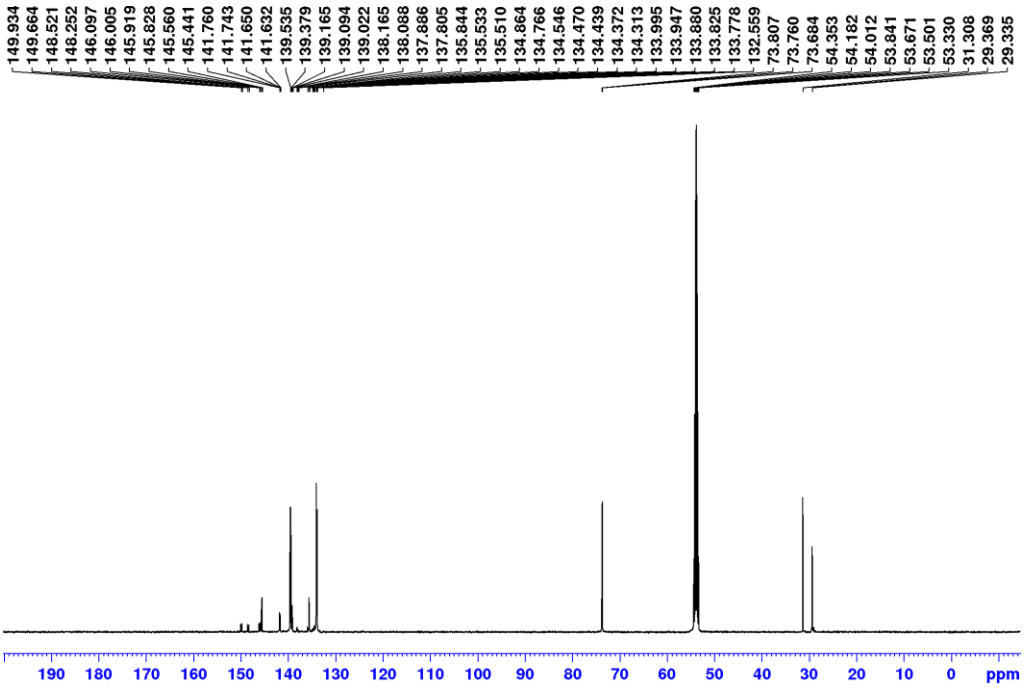

(d) COSY (MeOD, 500 MHz)

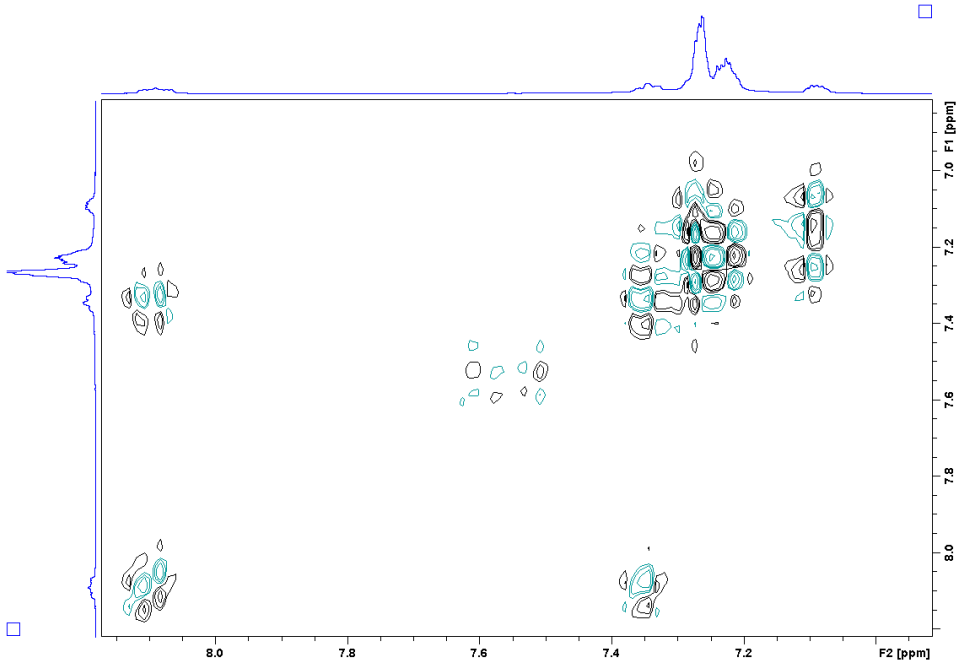

1-PAn$_2$-2-P(O)(O^{i}Pr)(OLi)-benzene (Li[2c]). A flask was charged with **1c** (1.50 g, 3.52 mmol) and acetonitrile (80 mL). The solution was saturated with LiBr at room temperature. The mixture was refluxed and stirred. After ca. 12 days, the volatiles were removed under vacuum. The solid was washed with CH_2Cl_2 and dried under vacuum. Because of similar solubility, Li[**2c**] and LiBr could not be separated and the mixture was used directly in the synthesis of H[**2c**]. $^{31}P\{^1H\}$ NMR (CD_3OD): δ 12.8 (s, *P*=O), -27.9 (s, *P*). ^1H NMR (CD_2Cl_2): δ 8.07 (m, 1H, H^D), 7.34 (m, H), 7.32 (t, H), 7.22 (t, 1H), 6.975(m, 2H), 6.93 (m, 1H), 6.78 (t, 2H, H^I), 6.54 (br, 2H, H^J), 4.46 (m, 1H, –OC*H*$(CH_3)_2$), 3.67 (s, 6H, –OC*H*$_3$), 0.99 (d, $^3J_{HH}$ = 6.5, 6H, –OCH(C*H*$_3$)$_2$). ESI-MS (CH_2Cl_2/MeOH 1:1 volume, pos. scan, *m/z*): 445.1 $[C_{23}H_{27}O_5P_2]^+$.

Figure 2.18. Numbering scheme for Li[**2c**].

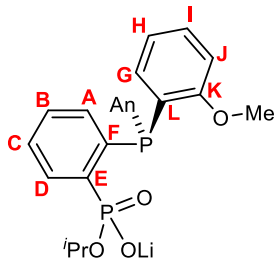

Figure 2.19. NMR spectra of Li[**2c**].

(a) $^{31}P\{^{1}H\}$ NMR spectrum (MeOD, 202 MHz)

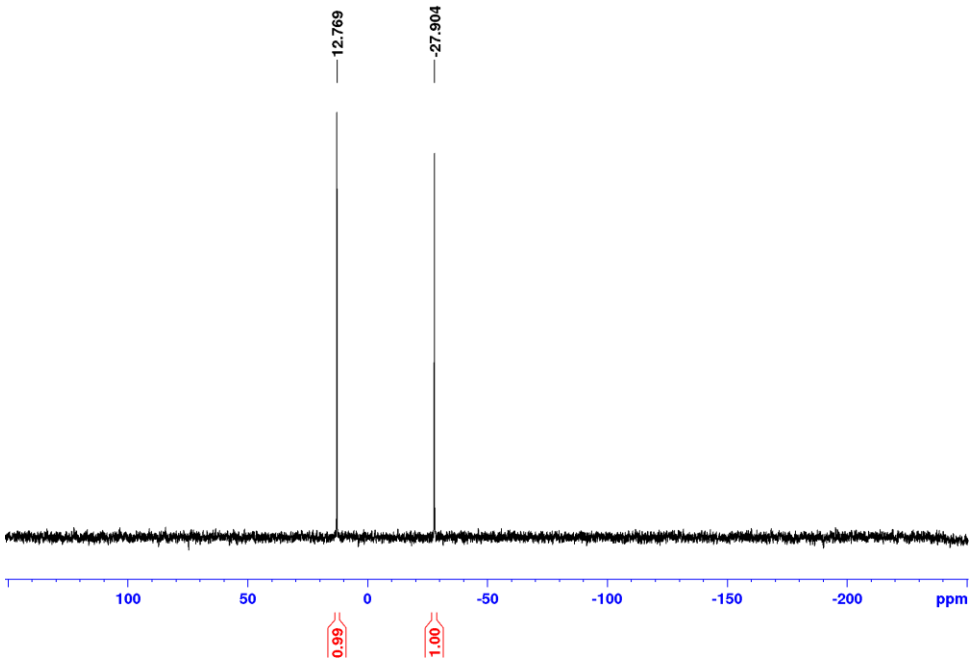

(b) ^{1}H NMR spectrum (MeOD, 500 MHz)

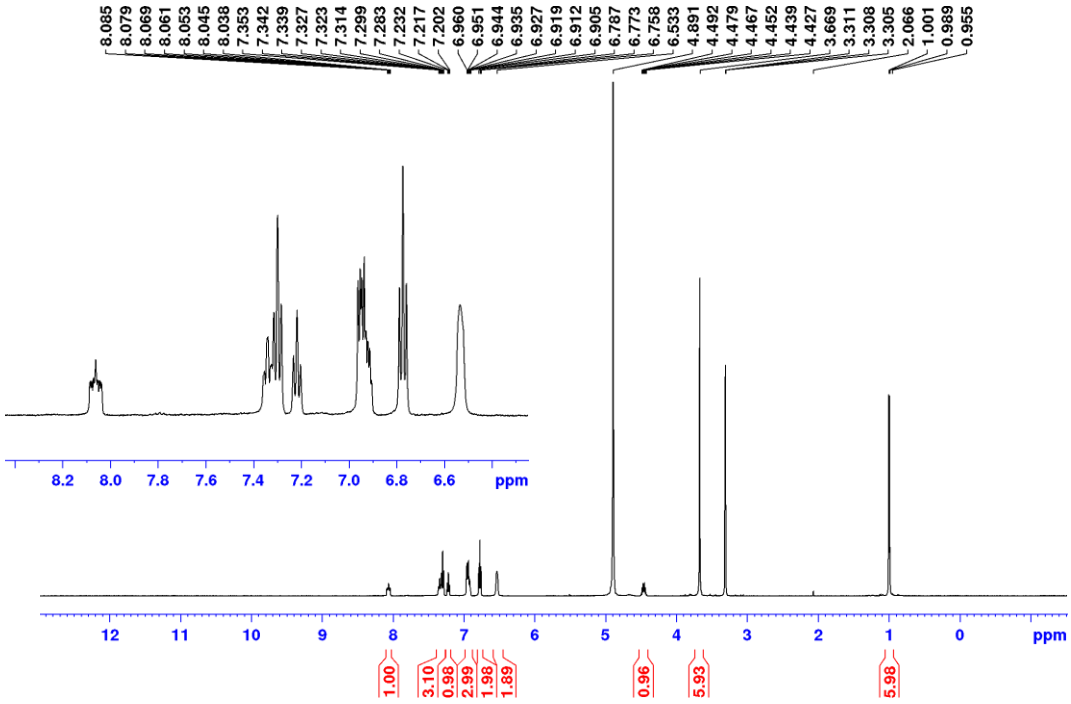

1-PPh$_2$-2-P(O)(OEt)(OH)-benzene (H[2a]). Li[**2a**] (1.70 g, 4.52 mmol) was suspended in distilled water (20 mL) and the mixture was acidified with HCl (2.3 mL, 4.6 mmol, 2.0 M in Et_2O). The mixture was extracted with CH_2Cl_2 (4 x 20 mL) and the solvent was removed under vacuum from the combined extracts to afford a white solid. The solid was recrystallized from THF/Et_2O at -40 ^oC (1.07 g, 64 %). $^{31}P\{^1H\}$ NMR (CD_2Cl_2): δ 20.0 (s, *P*=O), -10.0 (s, *P*). ^1H NMR (CD_2Cl_2): δ 13.29 (s, 1H, –O*H*), 8.1 (m, 1H, H^D), 7.42-7.2 (m, 13H), 4.00 (dq, $^3J_{HH} = {}^3J_{PH}$ = 7, 2H, –OC*H*$_2$CH$_3$), 1.07 (t, $^3J_{HH}$ = 7.0, 3H, –OCH$_2$C*H*$_3$). $^{13}C\{^1H\}$ NMR (CD_2Cl_2): δ 141.2 (dd, $^1J_{PC}$ = 24, $^2J_{PC}$ = 13, C^F), 137.6 (d, $^1J_{PC}$ = 12.7, *ipso*-Ph), 135.9 (dd, $^2J_{PC}$ = 15, $^3J_{PC}$ = 2, C^A), 135.7 (dd, $^1J_{PC}$ = 195, $^2J_{PC}$ = 33, C^E), 134.0 (dd, $^2J_{PC} = {}^3J_{PC}$ = 9, C^D), 133.5 (d, $^2J_{PC}$ = 19.9, *o*-Ph), 132.0 (d, $^3J_{PC}$ = 3, C^B), 128.6 (d, $^3J_{PC}$ = 14.5, C^C), 128.4 (s, *p*-Ph), 128.3 (d, $^3J_{PC}$ = 6.5, *m*-Ph), 62.3 (d, $^2J_{PC}$ = 6, –O*C*H$_2$CH$_3$), 16.1 (d, $^3J_{PC}$ = 7, –OCH$_2$*C*H$_3$). ESI-MS (CH_2Cl_2/MeOH 1:1 volume, pos. scan, *m/z*): 371 $[M+H]^+$ HRMS: calcd. for $[C_{20}H_{21}O_3P_2]^+$ *m/z* 371.09661. Found: 371.0972.

Figure 2.20. Numbering scheme for **H[2a]**.

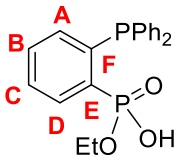

Figure 2.21. NMR spectra of **H[2a]**.

(a) ^{31}P NMR spectrum (CD_2Cl_2, 202 MHz)

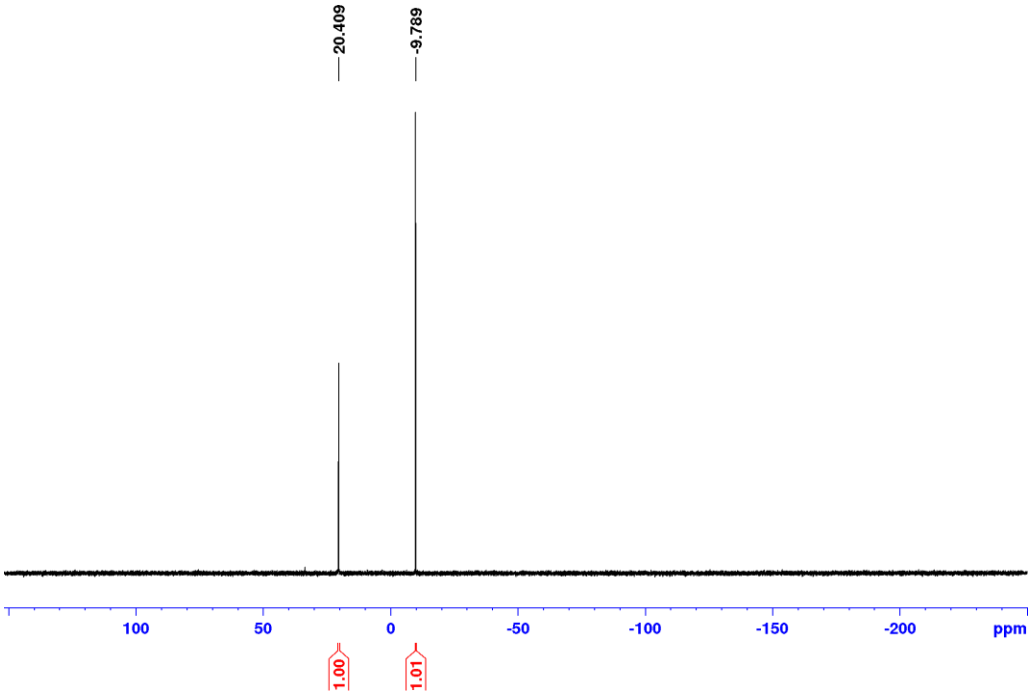

(b) ^{1}H NMR spectrum (CD_2Cl_2, 500 MHz)

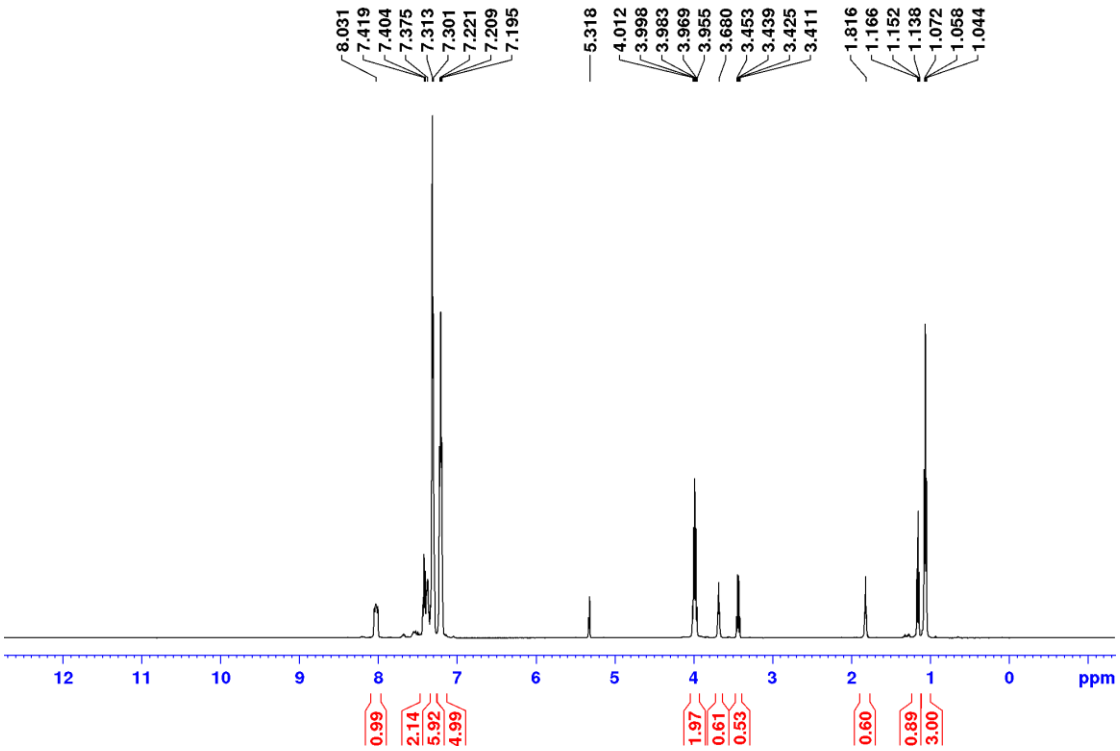

Figure 2.21, continued.

(c) ^{13}C NMR spectrum (CD_2Cl_2, 125 MHz)

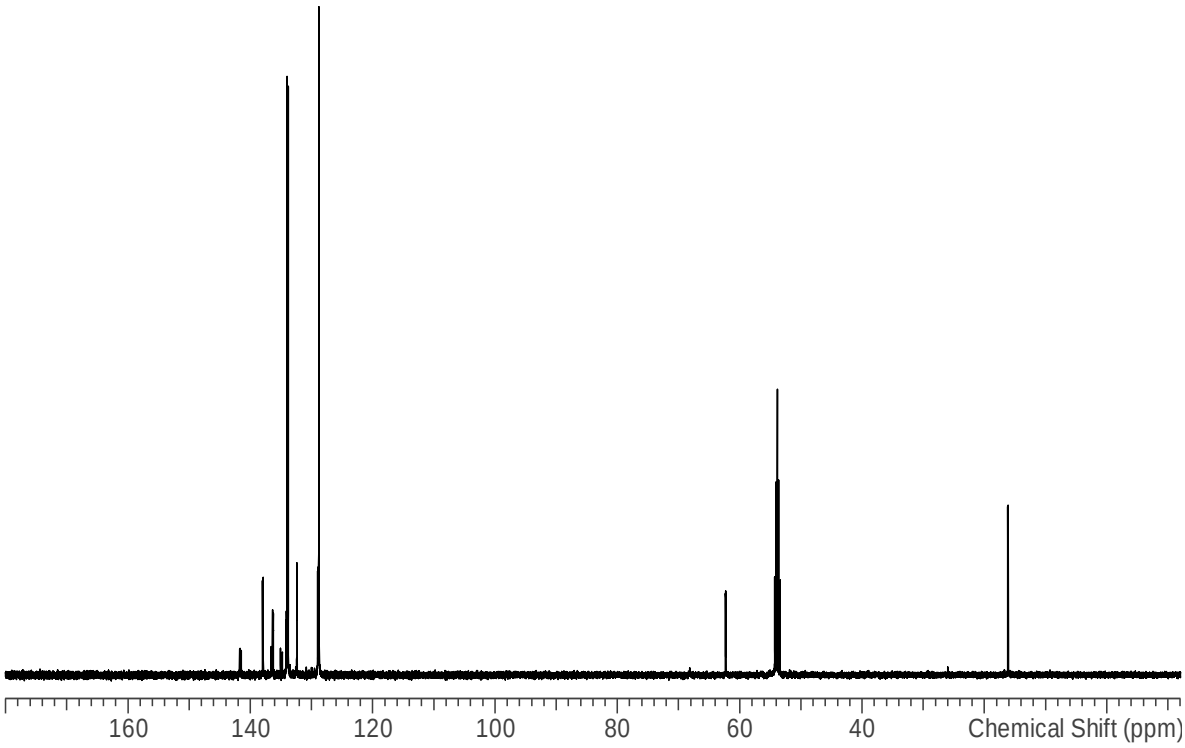

1-PPh_2-2-P(O)(O^iPr)(OH)-benzene (H[2b]). Li[**2b**] (0.35 g, 0.91 mmol) was suspended in distilled water (15 mL) and the mixture was acidified with HCl (0.5 mL, 1.0 mmol, 2.0 M in Et_2O). The mixture was extracted with CH_2Cl_2 (3 x 7 mL) and the solvent was removed under vacuum from the combined extracts to afford a white solid. The solid was recrystallized from THF/Et_2O at -40 °C (0.24 g, 57 %). $^{31}P\{^1H\}$ NMR (CD_2Cl_2): δ 18.7 (s, *P*=O), -10.6 (s, *P*). ^1H NMR (CD_2Cl_2): δ 12.08 (s, 1H, –O*H*), 8.02 (m, 1H, H^D), 7.40 (m, 1H, H^B), 7.35 (m, 1H, H^C), 7.32 (m, 6H, *p*-Ph and *o*-Ph), 7.22-7.18 (m, 5H, *m*-Ph and H^A), 4.75 (m, 1H, –OC*H*(CH_3)$_2$), 1.16

(d, $^{3}J_{HH}$ = 6.0, 6H, –OCH(CH_3)$_2$). $^{13}C\{^{1}H\}$ NMR (CD_2Cl_2): δ 141.3 (dd, $^{1}J_{PC}$ = 24.4, $^{2}J_{PC}$ = 13.7, C^{F}), 138.1 (d, $^{1}J_{PC}$ = 13, *ipso*-Ph), 136.4 (dd, $^{1}J_{PC}$ = 195, $^{2}J_{PC}$ = 32.7, C^{E}), 136.3 (d, $^{2}J_{PC}$ = 15.1, C^{A}), 133.8 (d, $^{2}J_{PC}$ = 19.5, *o*-Ph), 133.8 (dd, obscured by *o*-Ph, C^{D}), 132.2 (d, $^{3}J_{PC}$ = 4, C^{B}), 128.9 (d, $^{3}J_{PC}$ = 14.6, C^{C}), 128.7 (*p*-Ph), 128.7 (d, $^{3}J_{PC}$ = 6, *m*-Ph), 71.8 (d, $^{2}J_{PC}$ = 6.5, –O*C*H(CH$_3$)$_2$), 23.9 (d, $^{3}J_{PC}$ = 4.7, –OCH(*C*H$_3$)$_2$). HRMS: calcd. for $[C_{21}H_{22}O_3P_2]^+$ *m/z* 384.10443. Found: 384.1054. EA: Calcd. for $C_{21}H_{22}O_3P_2$• 0.007 CH_2Cl_2, %: C, 65.5; H, 5.77; N, 0. Found: C, 65.19; H, 5.68; N, <0.02.

Figure 2.22. Numbering scheme for H[**2b**].

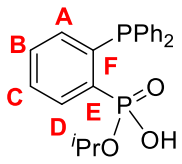

Figure 2.23. NMR spectra of H[**2b**].

(a) ^{31}P NMR spectrum (CD_2Cl_2, 202 MHz)

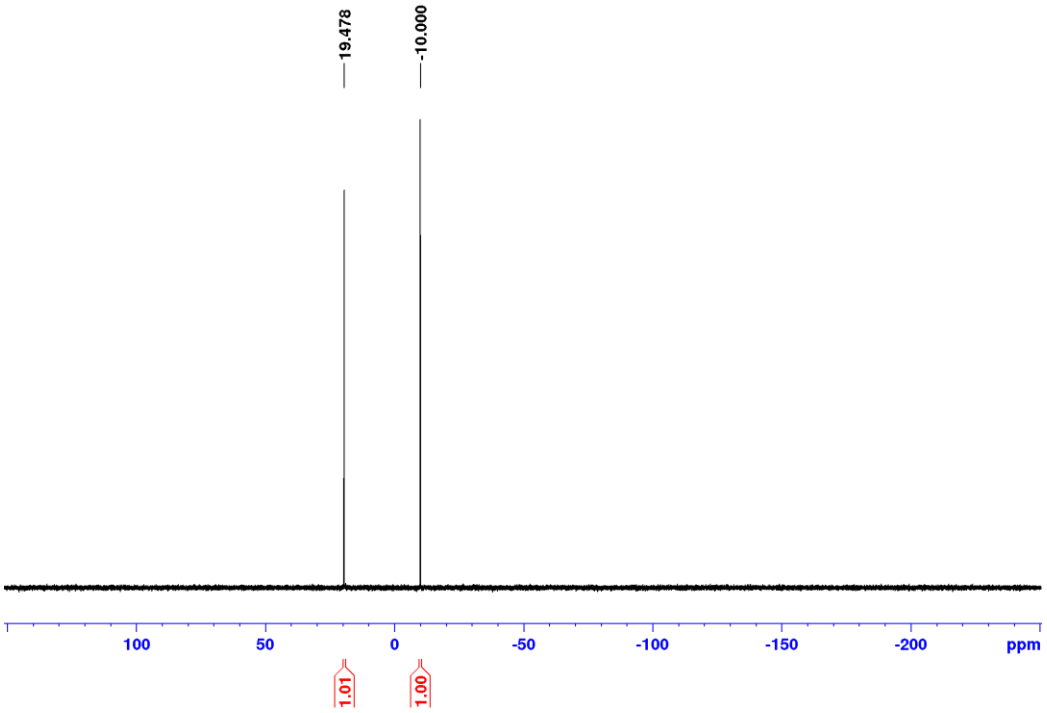

(b) ^{1}H NMR spectrum (CD_2Cl_2, 500 MHz)

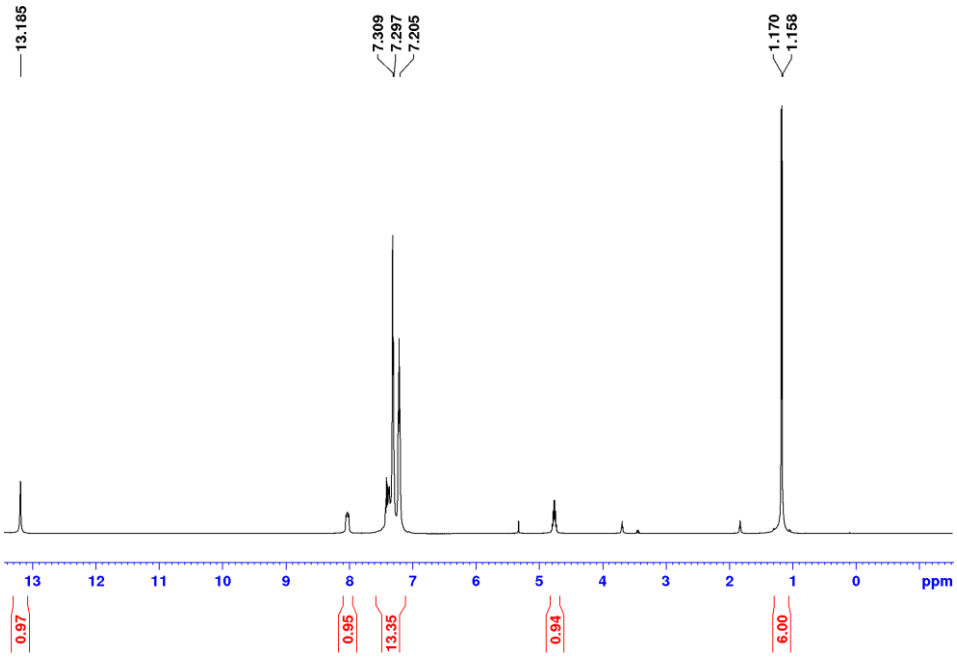

Figure 2.23, continued.

(c) $^{13}C\{^{1}H\}$ NMR spectrum (CD_2Cl_2, 125 MHz)

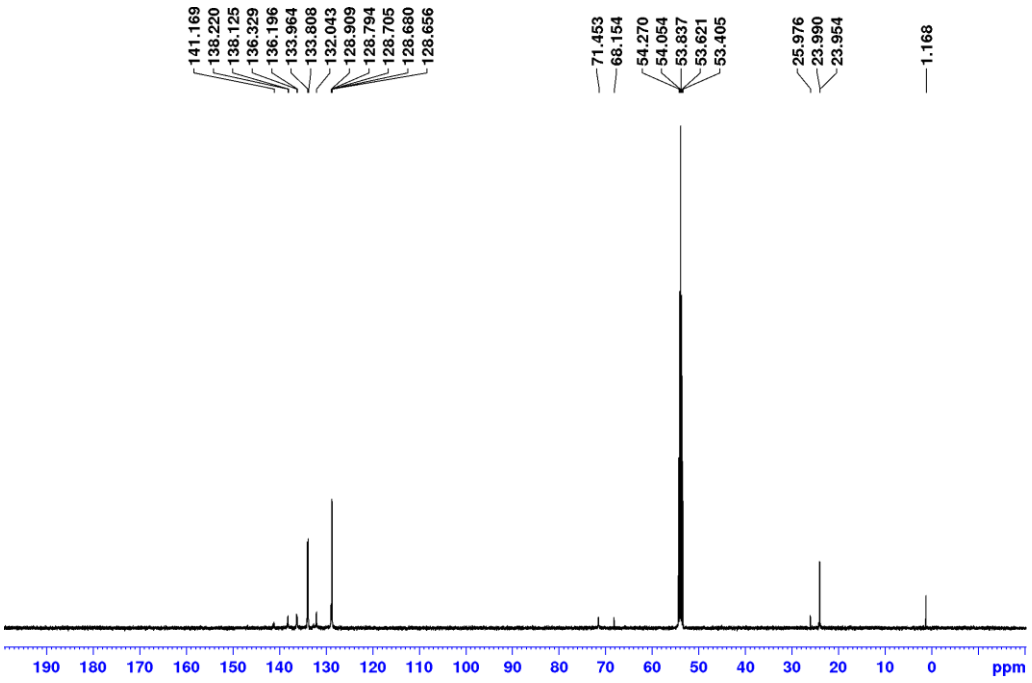

(d) COSY (CD_2Cl_2, 500 MHz)

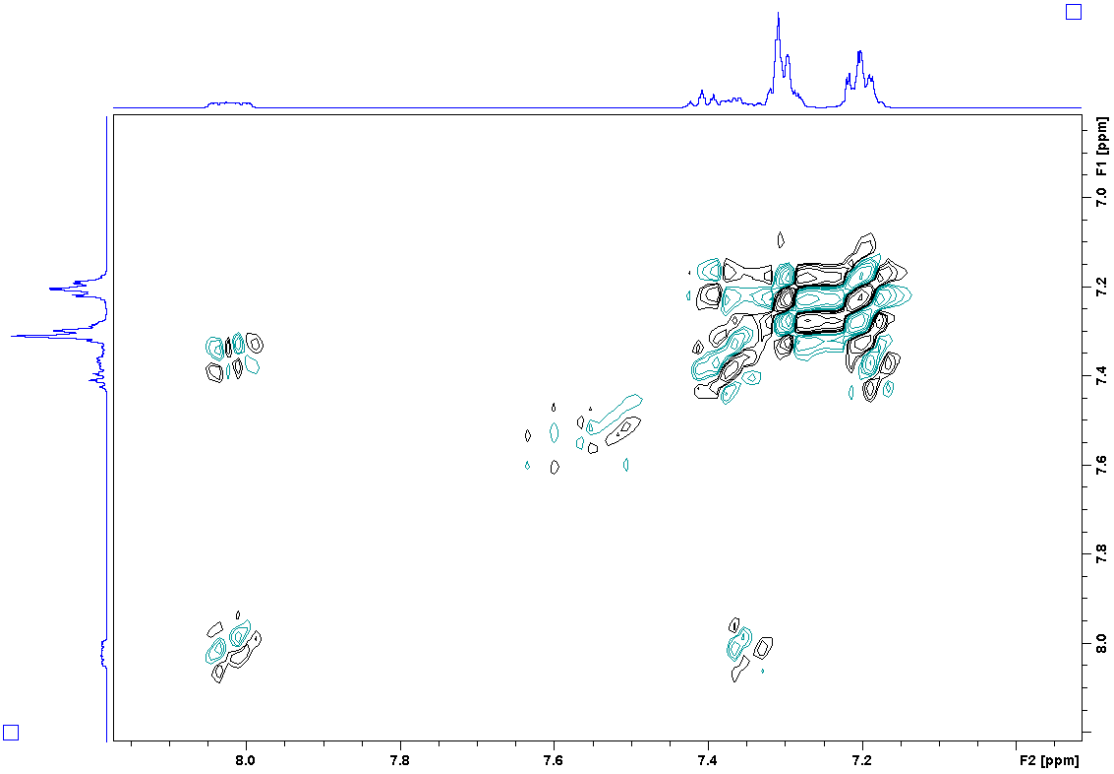

1-PAn$_2$-2-P(O)(O^{i}Pr)(OH)-benzene (H[2c]). Li[**2c**] (1.02 g, 2.3 mmol) was dissolved in H_2O (75 mL). HCl (1.2 mL, 2.4 mmol, 2M in Et_2O) was added dropwise to the solution. H[**2c**] precipitated after 30 min. CH_2Cl_2 (50 mL) was added to the mixture. The organic layer was separated, and the aqueous layer was extracted with CH_2Cl_2 (3 x 10 mL). The combined organic layers were dried under vacuum, affording a white powder (0.585 g, 58 %). $^{31}P\{^1H\}$ NMR (CD_2Cl_2): δ 18.4 (s, *P*=O), -29.1 (s, *P*). ^1H NMR (CD_2Cl_2): δ 12.12 (s, 1H, –O*H*), 8.06 (m, 1H, H^D), 7.36 (m, 4H, H^H, H^B, H^C), 7.09 (m, 1H, H^A), 6.91 (m, 2H, H^G), 6.87 (t, 2H, H^I), 6.68 (t, 2H, H^J), 4.60 (m, 1H, –OC*H*$(CH_3)_2$), 3.66 (s, 6H, –OC*H*$_3$), 1.01 (d, $^3J_{HH}$ = 6, 6H, –OCH(C*H*$_3)_2$). $^{13}C\{^1H\}$ NMR (CD_2Cl_2): δ 161.4 (d, $^2J_{PC}$ = 14.3, C^K), 138.5 (br, C^F), 137.0 (dd, $^1J_{PC}$ = 191, $^2J_{PC}$ = 32.1, C^E), 135.8 (d, $^2J_{PC}$ = 15.1, C^A), 134.3 (s, C^J), 134.0 (dd, $^2J_{PC}$ = $^3J_{PC}$ = 10, C^D), 131.8 (C^B), 131.2 (C^H), 129.3 (d, $^3J_{PC}$ = 13.7, C^C), 123.3 (br, C^L), 121.4 (C^I), 110.9 (C^G), 71.1 (d, $^2J_{PC}$ = 6.3, –O*C*H$(CH_3)_2$), 56.0 (–O*C*H$_3$), 23.8 (d, $^3J_{PC}$ = 4.5, –OCH(*C*H$_3)_2$). ESI-MS (CH_2Cl_2/MeOH 1:1 volume, pos. scan, *m/z*): 445.2. HRMS: calcd. for $[C_{23}H_{27}O_5P_2]^+$, *m/z* 445.1334. Found: 445.1338.

Figure 2.24. Numbering scheme for **H[2c]**.

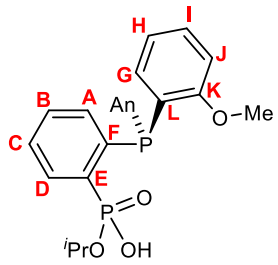

Figure 2.25. NMR spectra for **H[2c]**.

(a) $^{31}P\{^{1}H\}$ NMR spectrum (MeOD, 202 MHz)

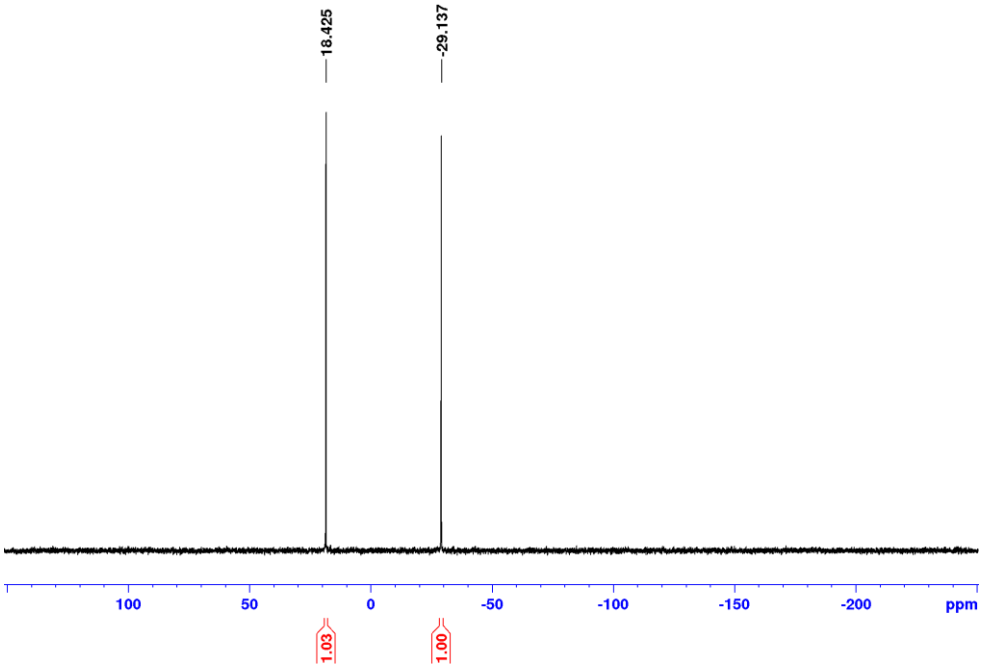

(b) ^{1}H NMR spectrum (MeOD, 500 MHz)

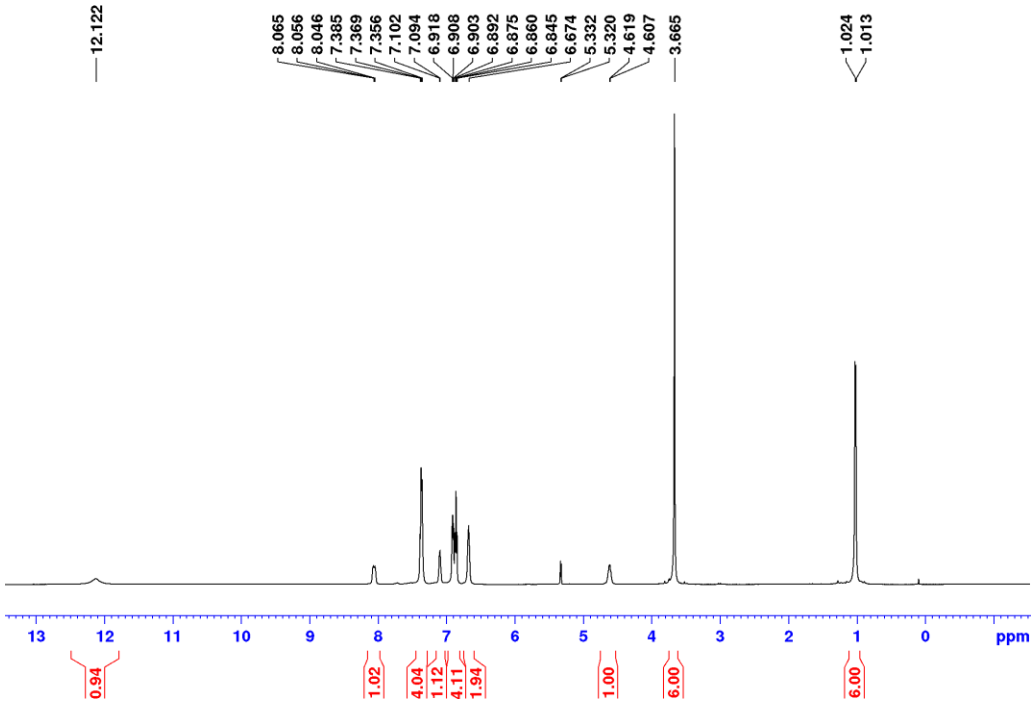

Figure 2.25, continued.

(c) $^{13}C\{^{1}H\}$ NMR spectrum (MeOD, 125 MHz)

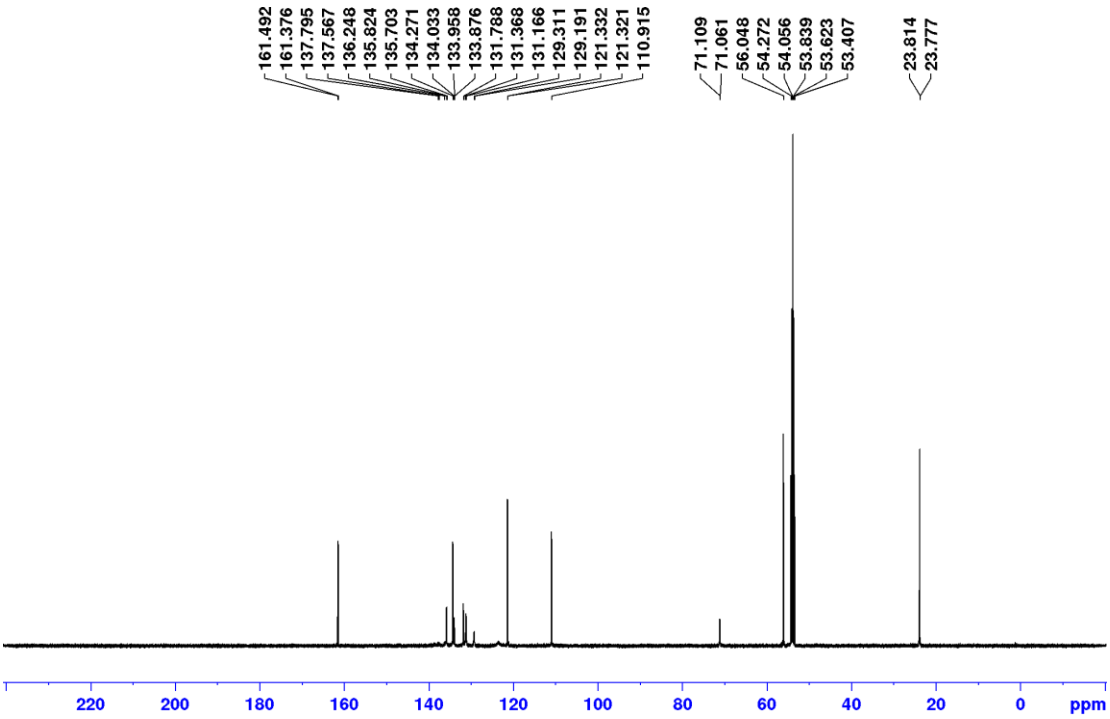

(d) $^{13}C\{^{1}H\}$ NMR spectrum (MeOD, 125 MHz)

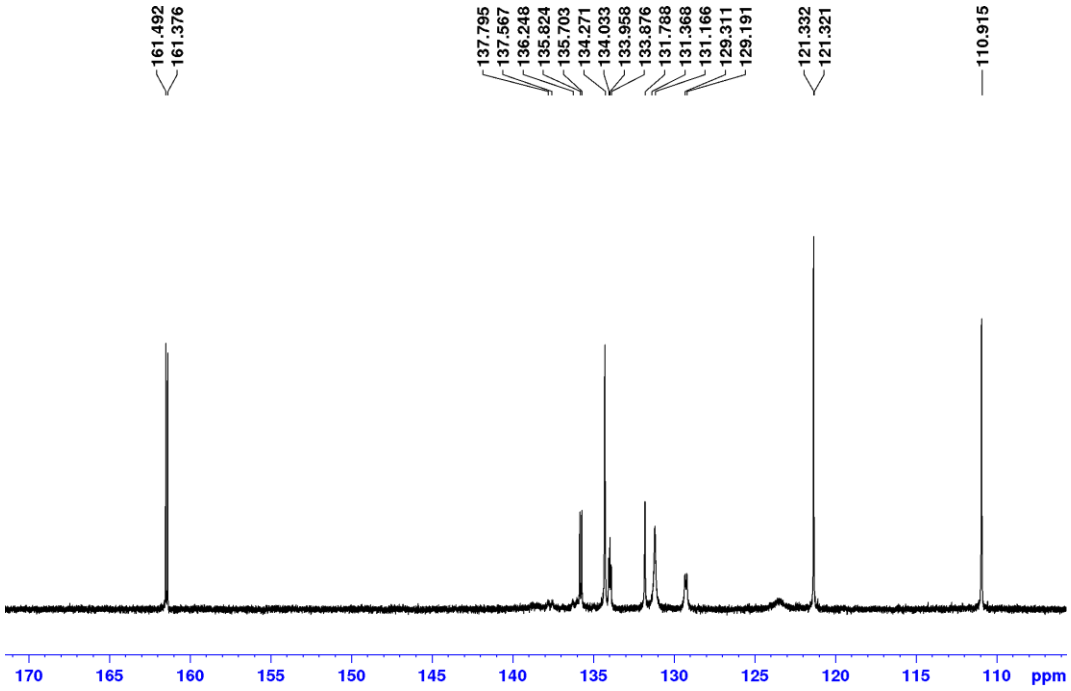

Figure 2.25, continued.

(e) COSY (MeOD, 500 MHz)

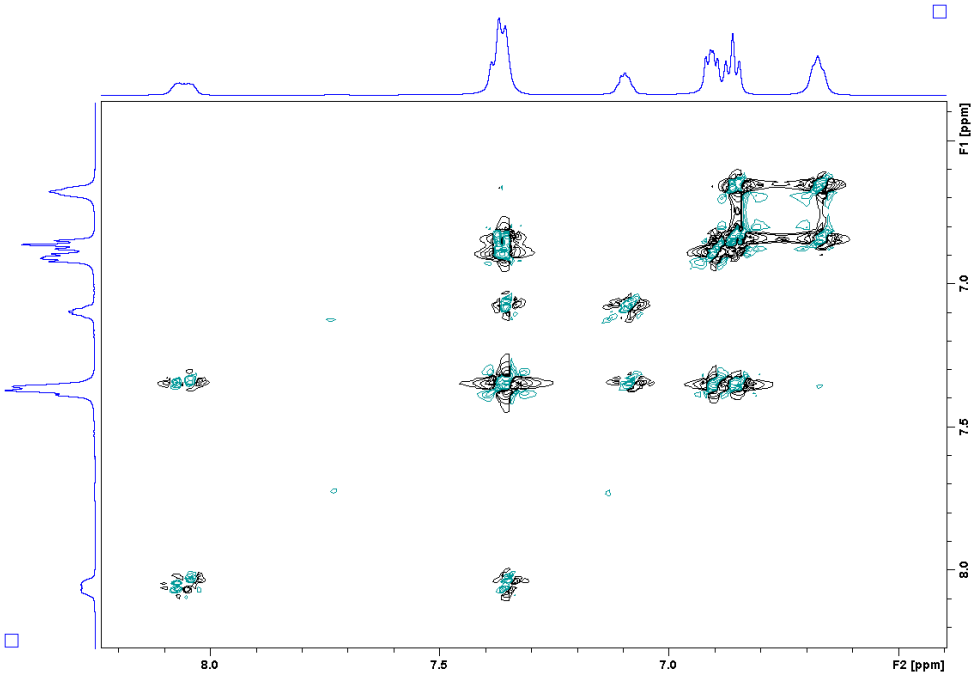

(f) HMQC (MeOD, 500 MHz, 125 MHz)

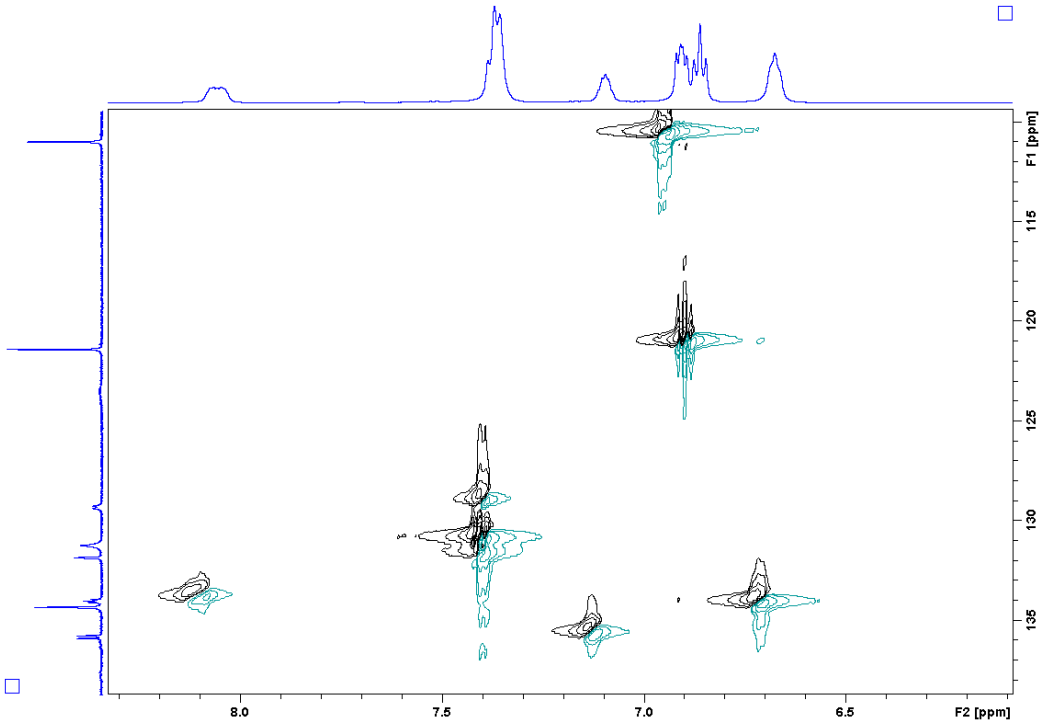

(κ^2-*P,O*-1-PPh_2-2-PO_3Et-Ph)PdMe(2,6-lutidine) (3a-lut). A vial was charged with (TMEDA)$PdMe_2$ (0.147 g, 0.581 mmol), H[**2a**] (0.215 g, 0.581 mmol), 2,6-lutidine (0.12 mL, 1.0 mol) and CH_2Cl_2 (10 mL). The resulting clear solution was stirred for 7 h at room temperature. The volatiles were removed under vacuum to afford a white solid. **3a-lut** was crystallized by Jessica Sampson from CH_2Cl_2/hexanes at –40 ^oC to afford a single crystal for X-ray diffraction (0.174 g, 44 %). $^{31}P\{^1H\}$ NMR (CD_2Cl_2): 28.5 (d, $^3J_{PP}$ = 16, *P*=O), 9.4 (d, $^3J_{PP}$ = 17, *P*–Pd). ^1H NMR (CD_2Cl_2): 8.17 (m, 1H, H^D), 7.65 (t, $^3J_{HH}$ = 7, 1H, *p*-lut), 7.60 (m, 4H, *o*-Ph), 7.47 (m, 7H, H^C, *m*-Ph, and *p*-Ph), 7.34 (m, 1H, H^B), 7.18 (d, $^3J_{HH}$ = 8, 2H, *m*-lut), 7.03 (m, 1H, H^A), 3.15 (br, 8H, –O*C*$H_2$$CH_3$ and lut–C*H*$_3$), 0.56 (t, $^3J_{HH}$ = 7, 3H, –OCH_2C*H*$_3$), 0.04 (d, $^3J_{PH}$ = 3.0, 3H, Pd–C*H*$_3$). $^{13}C\{^1H\}$ NMR (CD_2Cl_2): δ 159.0 (*o*-lut), 143.2 (dd, $^1J_{PC}$ = 163, $^2J_{PC}$ = 19, C^E), 138.6 (*p*-lut), 135.2 (dd, J_{PC} = 21, 8, C^D), 134.7 (dd, $^2J_{PC}$ = 13, 3, C^A), 134.6 (d, $^2J_{PC}$= 12, *o*-Ph), 133.7 (dd, $^1J_{PC}$ = 46, $^2J_{PC}$ = 7, C^F), 131.5 (d, $^1J_{PC}$ = 53, *ipso*-Ph), 130.9 (d, $^4J_{PC}$ = 2, *p*-Ph), 130.3 (dd, J_{PC} = 15, 3, C^C), 129.7 (dd, J_{PC} = 20, 6, C^B), 128.9 (d, $^3J_{PC}$ = 11, *m*-Ph), 122.9 (d, $^4J_{PC}$ = 3, *m*-lut), 60.2 (d, $^2J_{PC}$ = 5, –O*C*$H_2$$CH_3$), 26.5 (lut–*C*$H_3$), 16.1 (d, $^3J_{PC}$ = 7, –OCH_2*C*H_3), -5.2 (d, $^2J_{PC}$ = 4, Pd–*C*H_3). ESI-MS (CH_2Cl_2/MeOH, 1:1 by volume, positive scan, *m/z*): 598.2 $[MH]^+$. HRMS: calcd. for $[C_{28}H_{32}P_2O_3NPd]^+$, *m/z* 598.0892. Found: 598.0897.

Figure 2.26. Numbering scheme for **3a-lut**.

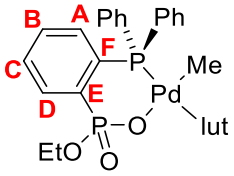

Figure 2.27. NMR spectra of **3a-lut**.

(a) ^{31}P NMR spectrum (CD_2Cl_2, 202 MHz)

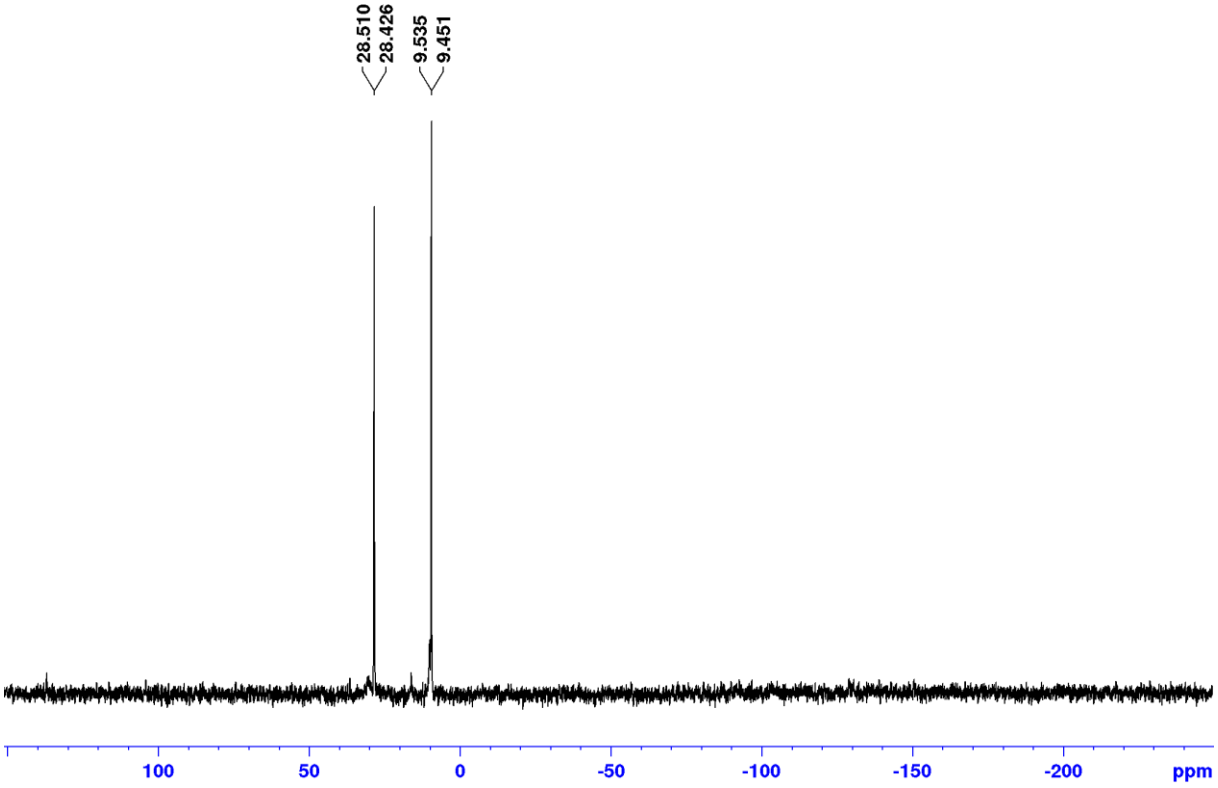

Figure 2.27, continued.

(b) ^{1}H NMR spectrum (CD_2Cl_2, 500 MHz)

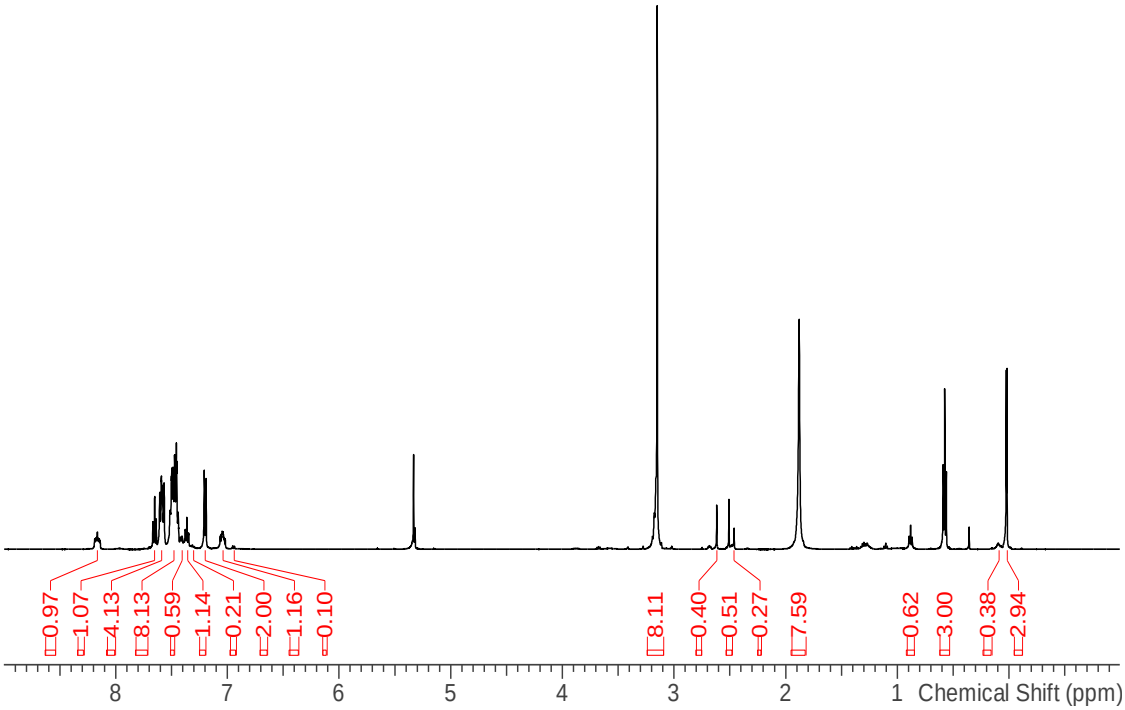

(c) ^{1}H NMR spectrum (CD_2Cl_2, 500 MHz), excess 2,6-lutidine

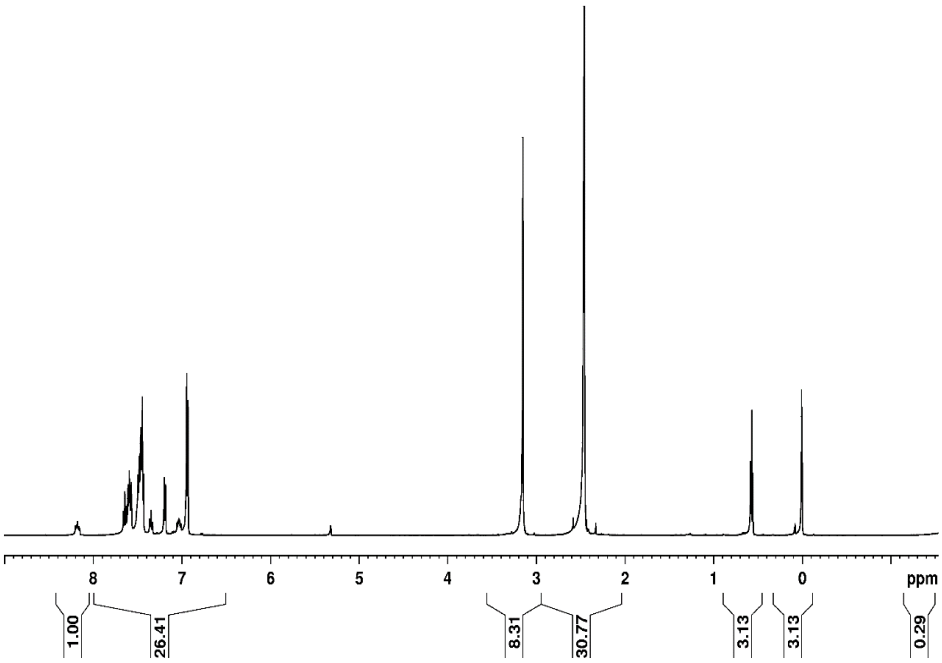

Figure 2.27, continued.

(d) ^{13}C NMR spectrum (CD_2Cl_2, 125 MHz)

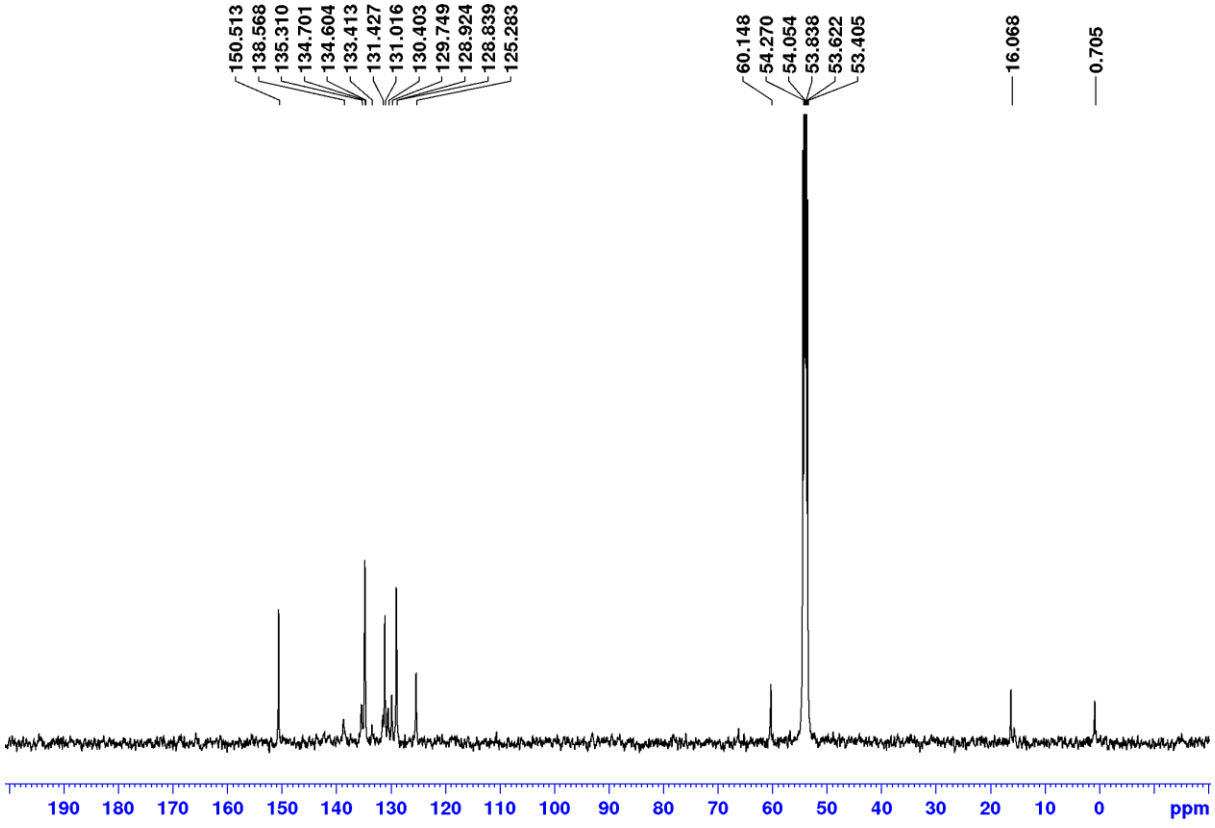

(κ^2-*P,O*-1-PPh_2-2-PO_3Et-Ph)PdMe(pyridine) (3a-py). **3a-py** was synthesized using a similar procedure to **3a-lut** from (TMEDA)$PdMe_2$ (0.055 g, 0.22 mmol), H[**2a**] (0.082 g, 0.22 mmol), pyridine (0.05 mL, 0.6 mmol) and CH_2Cl_2 (10 mL). **3a-py** was obtained as a pale yellow solid (0.040 g, 32 %). $^{31}P\{^1H\}$ NMR ($CDCl_3$): 32.1 (d, $^3J_{PP}$ = 15, *P*=O), 10.4 (d, $^3J_{PP}$ = 15, *P*–Pd). ^1H NMR ($CDCl_3$): 8.85 (2H, *o*-py), 8.19 (m, 1H, H^D), 7.86 (t, $^3J_{HH}$ = 7, 1H, *p*-py), 7.58-7.38 (m, 13H, H^C, *m*-py, Ph signals), 7.34 (td, $^3J_{HH}$ = 7.6, 1.4, 1H, H^B), 7.02 (m, 1H, H^A), 3.35 (dq,

$^{3}J_{HH} = {}^{3}J_{PH}$ = 7, 2H, –O*CH*$_2$CH$_3$), 0.66 (t, $^{3}J_{HH}$ = 7, 3H, –OCH$_2$*CH*$_3$), 0.28 (d, $^{3}J_{PH}$ = 2.5, 3H, Pd–C*H*$_3$). ^{13}C{^{1}H} NMR (CD_2Cl_2): δ 150.5 (*o*-py), 138.6 (*p*-py), 135.3 (d, $^{2}J_{PC}$ =10.3, C^{D}), 134.8 (obscured by *o*-Ph, C^{A}), 134.7 (d, $^{2}J_{PC}$= 12, *o*-Ph), 133.4 (C^{F}), 131.4 (*ipso*-Ph), 131.0 (*p*-Ph), 130.4 (C^{C}), 129.7 (C^{B}), 128.9 (d, $^{3}J_{PC}$ = 10.6, *m*-Ph), 125.3 (*m*-py), 60.1 (–O*C*H$_2$CH$_3$), 16.1 (d, $^{3}J_{PC}$ = 8, –OCH$_2$*C*H$_3$), 0.7 (Pd–*C*H$_3$), C^{E} not observed. HRMS: calcd. for $[C_{26}H_{28}P_2O_3NPd]^{+}$, *m*/*z* 570.0579. Found: 570.0563.

Figure 2.28. Numbering scheme for **3a-py**.

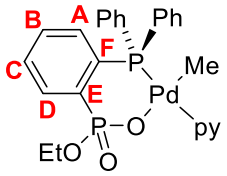

Figure 2.29. NMR spectra of **3a-py**.

(a) ^{31}P NMR spectrum (CD_2Cl_2, 202 MHz)

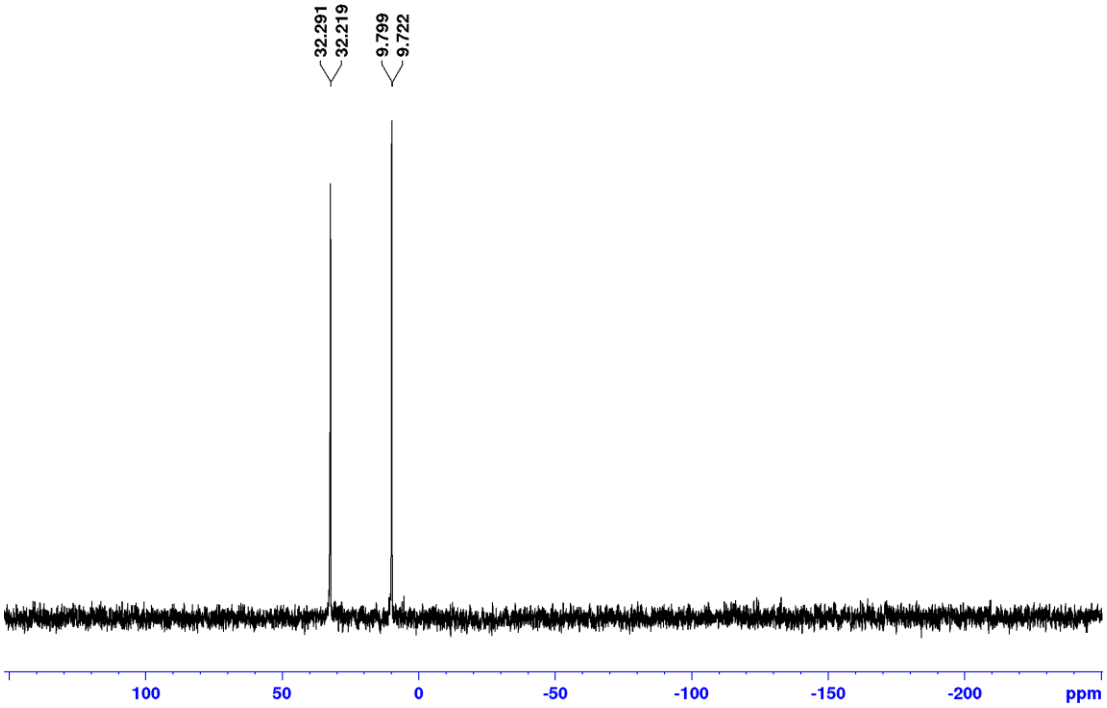

(b) ^{1}H NMR spectrum (CD_2Cl_2, 500 MHz)

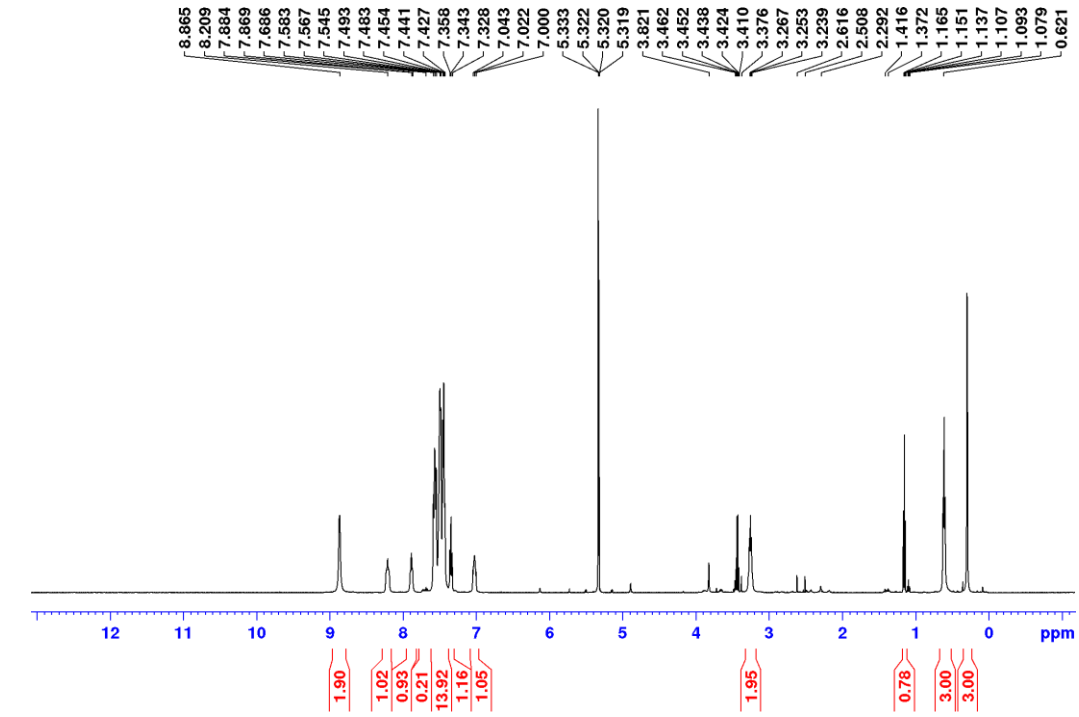

Figure 2.29, continued.

(c) ^{13}C NMR spectrum (CD_2Cl_2, 125 MHz)

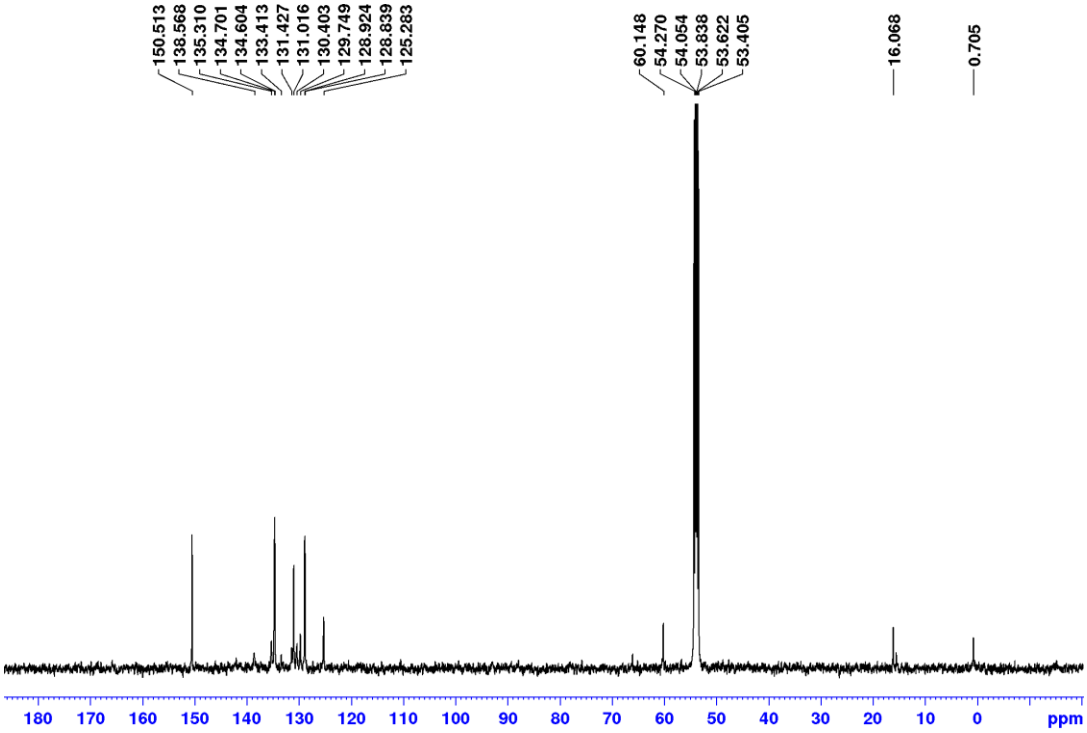

(κ^2-*P,O*-1-PPh_2-2-$PO_3{}^i$Pr-Ph)PdMe(2,6-lutidine) (3b-lut). A flask was charged with (TMEDA)$PdMe_2$ (0.079 g, 0.313 mmol), H[**2b**] (0.120 g, 0.313 mmol) and CH_2Cl_2 (10 mL), and the mixture was stirred rapidly at room temperature for 1 h to give a pale yellow solution. 2,6-lutidine (0.04 mL, 0.313 mmol) was added by syringe and the resulting pale yellow solution was stirred for an additional 1 h. The solution was concentrated under vacuum and washed with 5 mL Et_2O to give a white solid. Colorless crystals were grown from a solution of CH_2Cl_2 layered with pentane at -10 C and were identified as **3b-lut** co-crystallized with 1 equiv of CH_2Cl_2 and 0.5 equiv of H_2O (0.068 g, 36 %). $^{31}P\{^1H\}$ NMR (CD_2Cl_2): δ 28.7 (d, $^3J_{PP}$ = 16, *P*=O), 7.8 (d, $^3J_{PP}$ =

17, *P*–Pd). ^{1}H NMR (CD_2Cl_2): δ 8.17 (m, 1H, H^D), 7.65 (m, 4H, *o*-Ph), 7.55 (br t, 1H, *p*-lut), 7.47 (m, 6H, *m*-Ph, *p*-Ph), 7.42 (m, 1H, H^C), 7.33 (t, $^{3}J_{HH}$ = 7.5, 1H, H^B), 7.20 (d, $^{3}J_{HH}$ = 8, 2H, *m*-lut), 7.08 (m, 1H, H^A), 4.21 (m, 1H, –OC*H*$(CH_3)_2$), 3.16 (s, 6H, lut–C*H*$_3$), 0.56 (d, $^{3}J_{HH}$ = 5.5, 6H, –OCH(C*H*$_3)_2$), -0.05 (d, $^{3}J_{PH}$ = 2.5, 3H, Pd–C*H*$_3$). ^{13}C{^{1}H} NMR (CD_2Cl_2): δ 158.9 (*o*-lut), 144.8 (dd, $^{1}J_{PC}$ = 165, $^{2}J_{PC}$ = 19, C^E), 138.6 (*p*-py), C^D obscured by *o*-Ph, 134.7 (d, $^{2}J_{PC}$ = 12, o-Ph), 134.4 (dd, J_{PC} = 11, 7.8, C^A), 133.5 (dd, $^{1}J_{PC}$ = 45.7, $^{2}J_{PC}$ = 6.5, C^F), 131.4 (d, $^{1}J_{PC}$ = 53.2, *ipso*-Ph), 130.8 (d, $^{4}J_{PC}$ = 2.4, *p*-Ph), 130.4 (dd, J_{PC} = 12, 2.4, C^C), 129.3 (dd, J_{PC} = 7, 2.4, C^B), 128.8 (d, $^{3}J_{PC}$ = 10.9, *m*-Ph), 122.8, (*m*-lut), 68.6 (d, $^{2}J_{PC}$ = 5.8, –O*C*H$(CH_3)_2$), 26.5 (lut–*C*H$_3$), 23.5 (d, $^{3}J_{PC}$ = 4, –OCH(*C*H$_3)_2$), –5.2 (d, $^{2}J_{PC}$ = 4, Pd–*C*H$_3$). HRMS calc. for $[C_{29}H_{34}NO_3P_2Pd]^+$ m/z 612.10488. Found: 612.1036.

Figure 2.30. Numbering scheme for **3b-lut**.

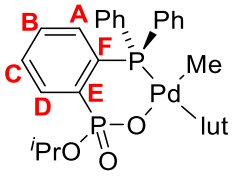

Figure 2.31. NMR spectra of **3b-lut**.

(a) ^{31}P NMR spectrum (CD_2Cl_2, 202 MHz)

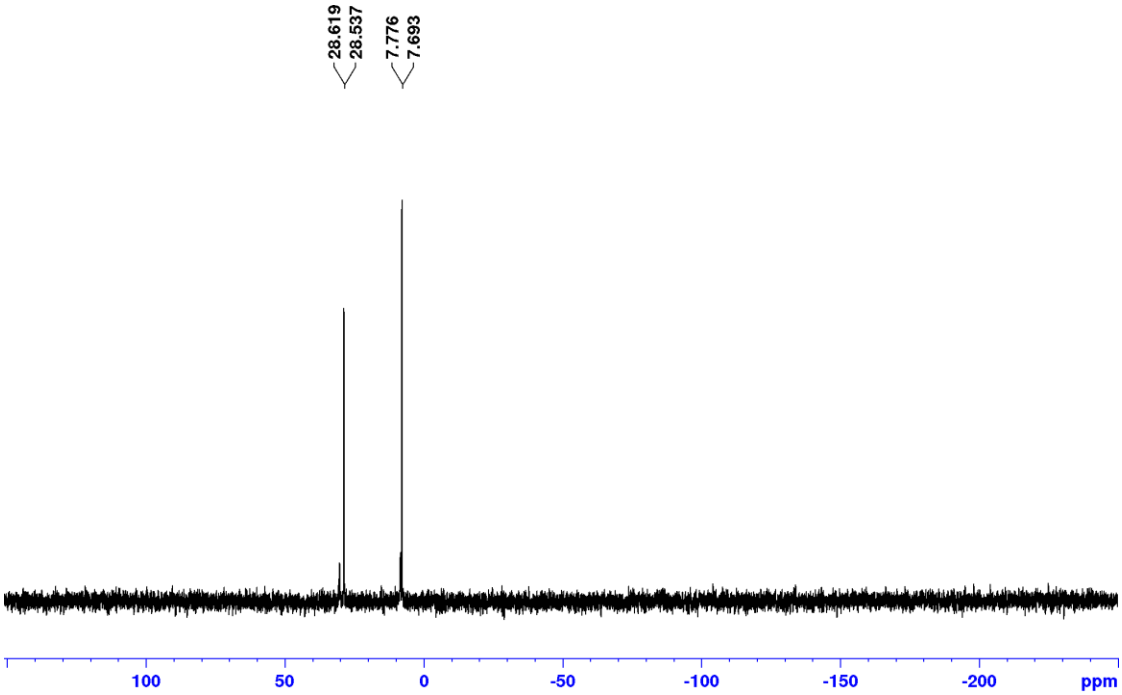

(b) ^{1}H NMR spectrum (CD_2Cl_2, 500 MHz)

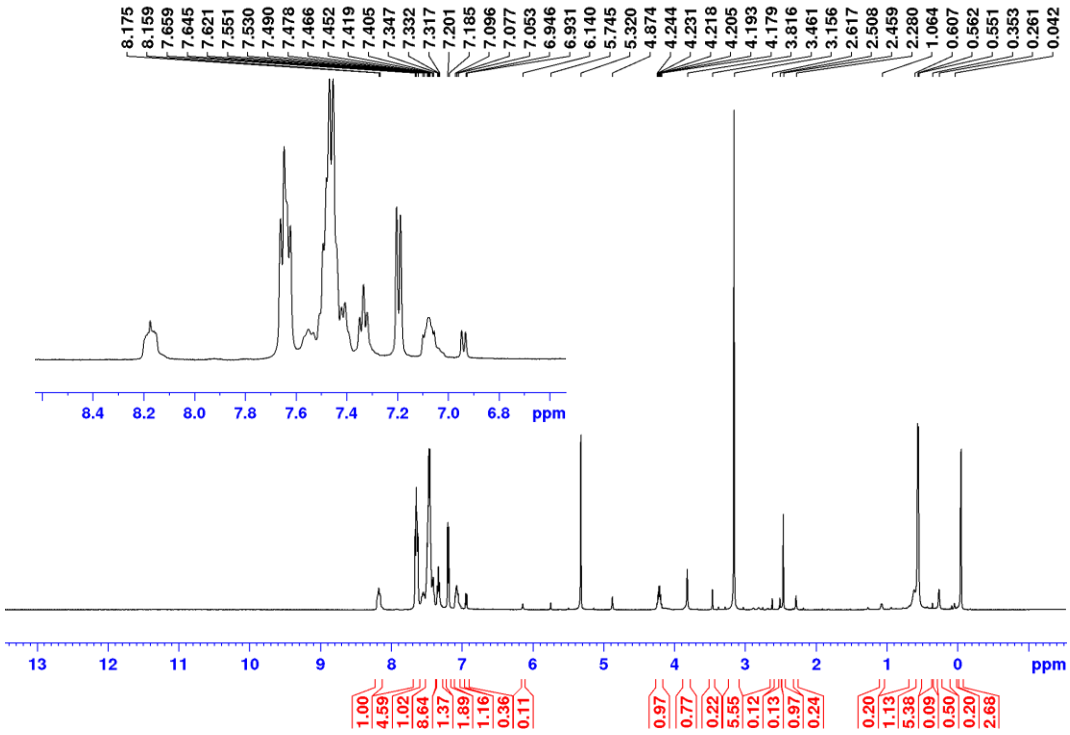

Figure 2.31, continued.

(c) $^{13}C\{^{1}H\}$ NMR spectrum of **3b** (CD_2Cl_2, 125 MHz)

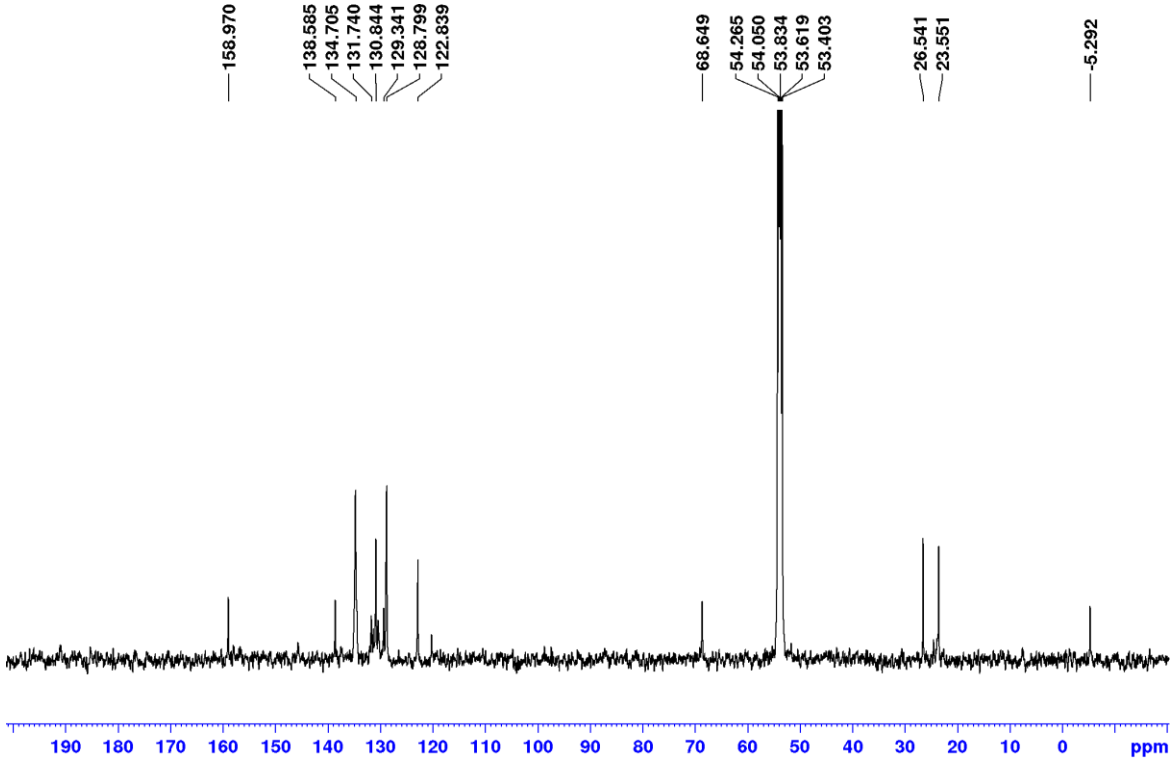

(κ^2-*P,O*-1-PPh_2-2-$PO_3{}^{i}$Pr-Ph)PdMe(pyridine) (3b-py). A flask was charged with (TMEDA)$PdMe_2$ (0.139 g, 0.552 mmol), H[**2b**] (0.212 g, 0.552 mmol), and CH_2Cl_2 (10 mL), and the mixture was stirred rapidly at room temperature for 1 h. Pyridine (0.09 mL, 1.12 mmol) was added by syringe and the resulting pale yellow solution was stirred for an additional 1 h. The solvent was removed under vacuum. The resulting solid was re-dissolved in CH_2Cl_2 (3 mL), and the solvent was removed under vacuum. This procedure was repeated twice to give a white-yellow solid. The solid was dissolved in minimal CH_2Cl_2 (< 1 mL), and the solution was layered

with Et_2O (3 mL) and allowed to stand at -40 °C, affording a white solid. The supernatant was decanted away and a second recrystallization was performed in the same manner (0.128 g, 40%). $^{31}P\{^1H\}$ NMR (CD_2Cl_2): δ 32.4 (d, $^3J_{PP}$ = 14, *P*=O), 8.6 (d, $^3J_{PP}$ = 14, *P*–Pd). ^1H NMR (CD_2Cl_2): δ 8.87 (d, $^3J_{HH}$ = 4, 2H, *o*-py), 8.20 (m, 1H, H^D), 7.87 (br t, $^3J_{HH}$ = 7.5, 1H, *p*-py), 7.60 (m, $^3J_{HH}$ = 7, 4H, *o*-Ph), 7.5-7.42 (m, 9H, H^C, *m*-py, *m*-Ph, *p*-Ph), 7.31 (t, $^3J_{HH}$ = 7.5, 1H, H^B), 7.05 (m, 1H, H^A), 4.23 (m, 1H, –OC*H*$(CH_3)_2$) 0.70 (d, $^3J_{HH}$ = 6.0, 6H, –OCH(C*H*$_3)_2$), 0.25 (d, $^3J_{PH}$ = 2, 3H, Pd–C*H*$_3$). $^{13}C\{^1H\}$ NMR (CD_2Cl_2): δ 150.5 (*o*-py), 144.1 (dd, $^1J_{PC}$ = 168, $^2J_{PC}$ = 19, C^E), 138.4 (*p*-py), C^D obscured by *o*-Ph and C^A, 134.7 (d, $^2J_{PC}$ = 12, o-Ph), 134.6 (dd, J_{PC} = 3.1, 10.3, C^A), 132.8 (d, $^1J_{PC}$ = 44.1, C^F), 131.3 (d, $^1J_{PC}$ = 53.3, *ipso*-Ph), 130.9 (d, $^4J_{PC}$ = 2.1, *p*-Ph), 130.5 (dd, J_{PC} = 11, 4, C^C), 129.5 (dd, J_{PC} = 7.2, 2.3, C^B), 128.8 (d, $^3J_{PC}$ = 10.9, *m*-Ph), 125.2, (*m*-py), 68.3 (d, $^2J_{PC}$ = 5.5, –O*C*H$(CH_3)_2$), 23.9 (d, $^3J_{PC}$ = 4, –OCH(*C*H$_3)_2$), 0.6 (Pd–*C*H$_3$). HRMS calc. for $[C_{27}H_{30}NO_3P_2Pd]^+$ m/z 584.07358. Found: 584.0724.

Figure 2.32. Numbering scheme for **3b-py**.

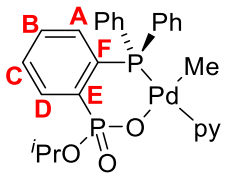

Figure 2.33. NMR spectra of **3b-py**.

(a) ^{31}P NMR spectrum (CD_2Cl_2, 202 MHz)

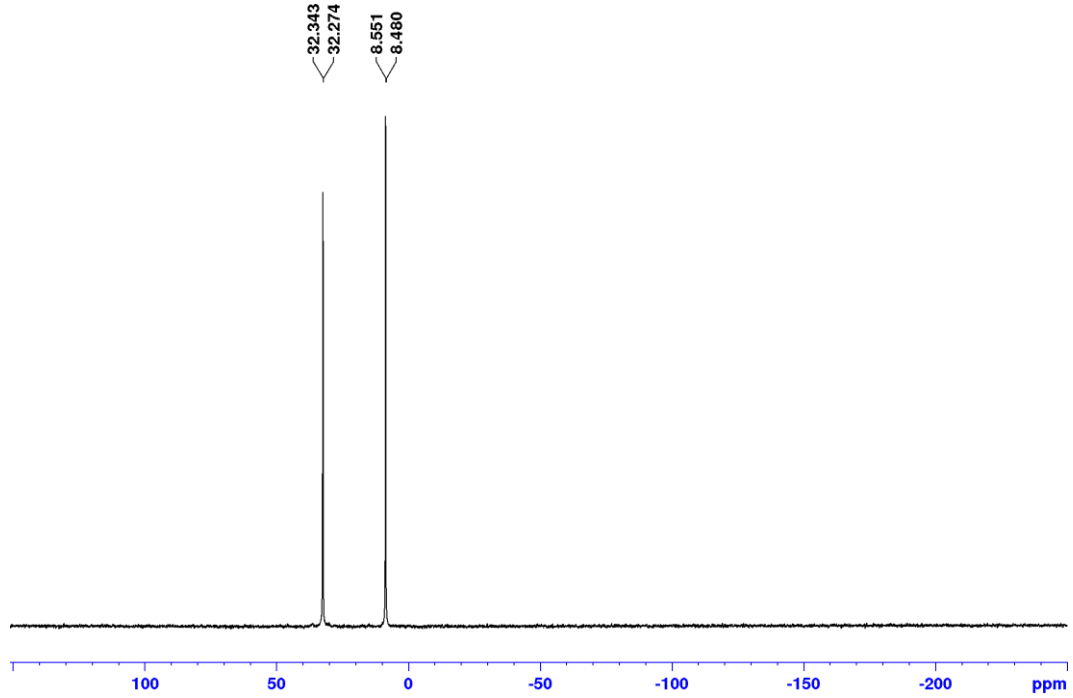

(b) ^{1}H NMR spectrum (CD_2Cl_2, 500 MHz)

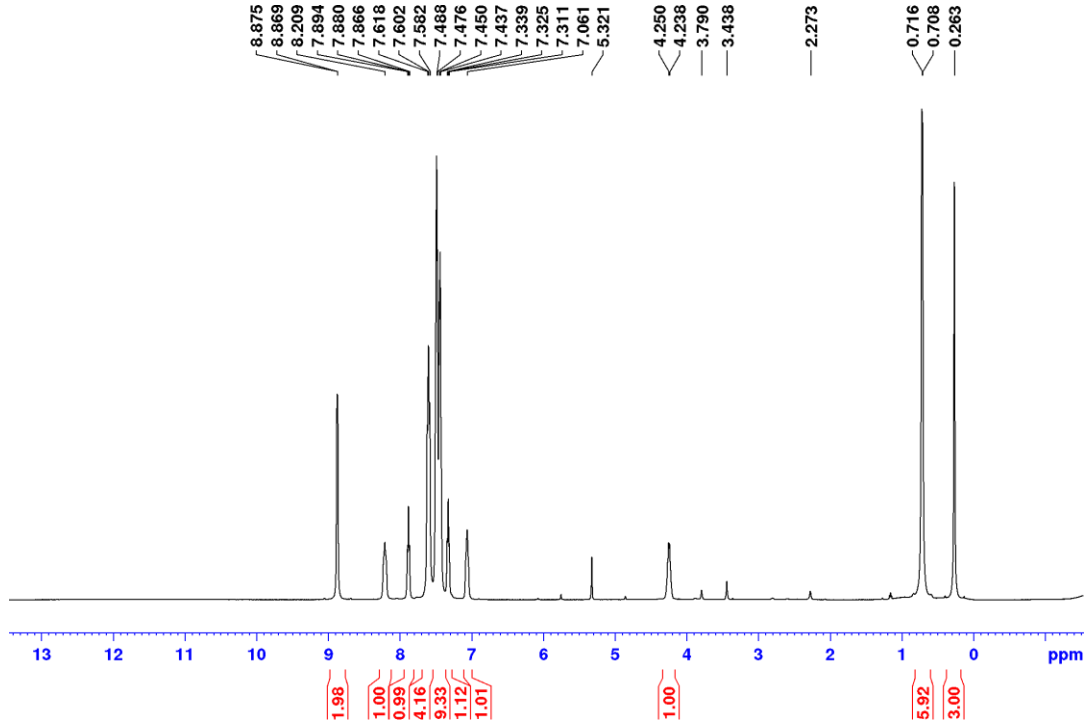

Figure 2.33, continued.

(c) $^{13}C\{^{1}H\}$ NMR spectrum (CD_2Cl_2, 125 MHz)

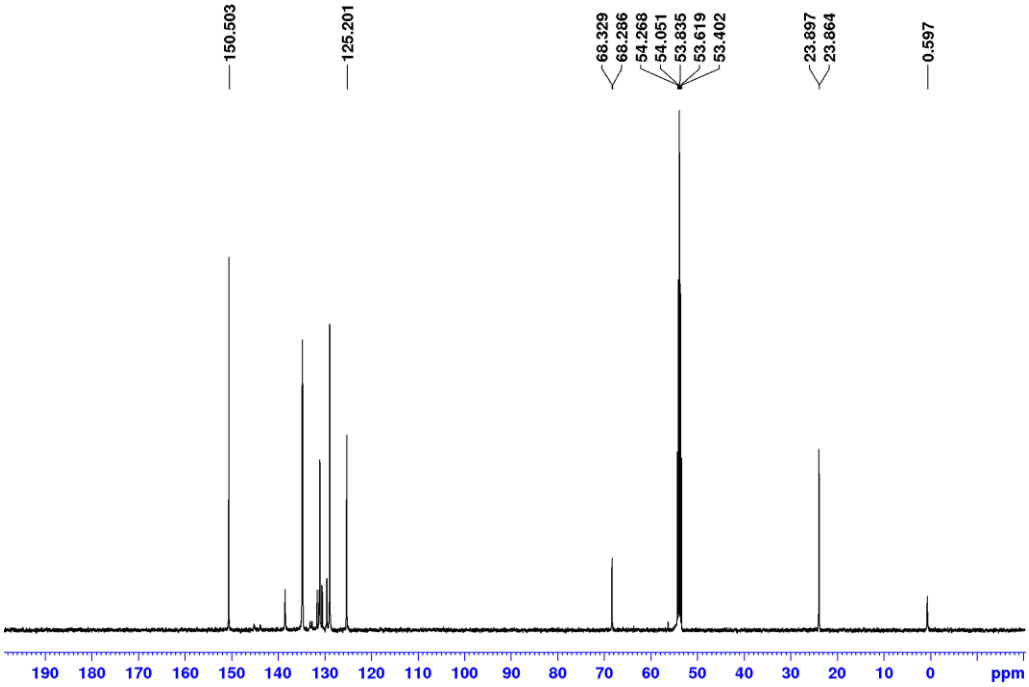

(d) COSY (CD_2Cl_2, 500 MHz)

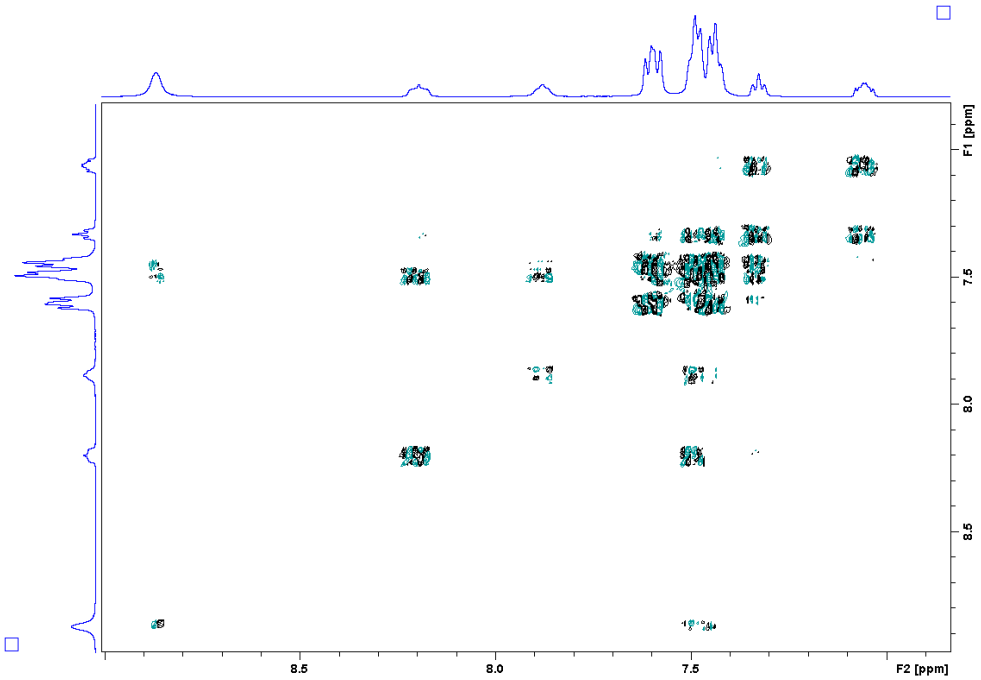

(κ^2-*P,O*-1-PAn$_2$-2-PO$_3$^{i}Pr-Ph)PdMe(pyridine) (3c-py). A flask was charged with (TMEDA)PdMe$_2$ (0.118 g, 0.465 mmol), H[**2c**] (0.206 g, 0.464 mmol), and CH_2Cl_2 (10 mL), and the mixture was stirred rapidly at room temperature for 1 h. Pyridine (80 μL, 0.99 mmol) was added by syringe and the resulting pale yellow solution was stirred for an additional 1 h. The solvent was removed under vacuum. The resulting solid was re-dissolved in CH_2Cl_2 (3 mL), and the solvent was removed under vacuum. This procedure was repeated twice to give a off-white solid. The solid was dissolved in minimal CH_2Cl_2 (1 mL), and the solution was layered with pentane (3 mL) and allowed to stand at -40 °C, affording a yellow solid. The supernatant was decanted away and a second recrystallization was performed in the same manner (0.161 g, 54 %).^{31}P{^{1}H} NMR (CD_2Cl_2): δ 24.6 (br, *P*=O), 9.1 (d, $^3J_{PP}$ = 11.9, *P*–Pd). ^{1}H NMR (CD_2Cl_2): δ 8.89 (d, $^3J_{HH}$ = 3.0, 2H, *o*-py), 8.10 (m, 1H, H^D), 7.84 (t, $^3J_{HH}$ = 7.5, 1H, *p*-py), 7.52 (t, $^3J_{HH}$ = 7.5, 2H, H^H), 7.46-7.41 (m, 5H, m-py, H^J, H^C), 7.23 (t, $^3J_{HH}$ = 7.0, 1H, H^B), 7.19 (m, 1H, H^A), 6.97 (m, 2H, H^I and H^G), 4.15 (m, 1H, –OC*H*(CH$_3$)$_2$), 3.65 (s, 6H, –OC*H$_3$*), 0.73 (d, $^3J_{HH}$ = 5.0, 6H, –OCH(C*H$_3$*)$_2$), 0.12 (d, $^3J_{PH}$ = 2.5, 3H, Pd–C*H$_3$*). ^{13}C{^{1}H} NMR (CD_2Cl_2): δ 161.1 (d, $^2J_{PC}$ = 3.1, C^K), 150.8 (*o*-py), 143.4 (dd, $^1J_{PC}$ = 165, $^2J_{PC}$ = 20.1, C^E), 138.2 (*p*-py), 137.1 (br, C^J), 134.3 (dd, J_{PC} = 18.7, 7.7, C^D), 134.0 (d, $^2J_{PC}$ = 8.4, C^A), 133.2 (C^H), 131.8 (dd, $^1J_{PC}$ = 52, $^2J_{PC}$ = 8.3, C^F), 129.7 (d, $^3J_{PC}$ = 12.1, C^C), 128.3 (d, $^3J_{PC}$ = 7.0, C^B), 125.1 (*m*-py), 120.9 (d, $^2J_{PC}$ = 10.7, C^G), 118.7 (d, $^1J_{PC}$ = 54, C^L), 111.7 (d, $^4J_{PC}$ = 4.4, C^I), 67.8 (d, $^2J_{PC}$ = 5.5, –O*C*H(CH$_3$)$_2$), 55.6 (–

OCH_3), 23.9 (d, $^3J_{PC}$ = 3.3, –OCH(CH_3)$_2$), 0.31 (Pd–CH_3). HRMS calc. for $[C_{29}H_{34}NO_5P_2Pd]^+$ m/z 644.09472. Found: 644.0936.

Figure 2.34. Numbering scheme for **3c-py**.

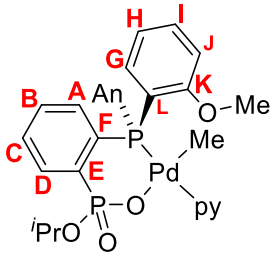

Figure 2.35. NMR spectra of **3c-py**.

(a) ^{31}P NMR spectrum (CD_2Cl_2, 202 MHz)

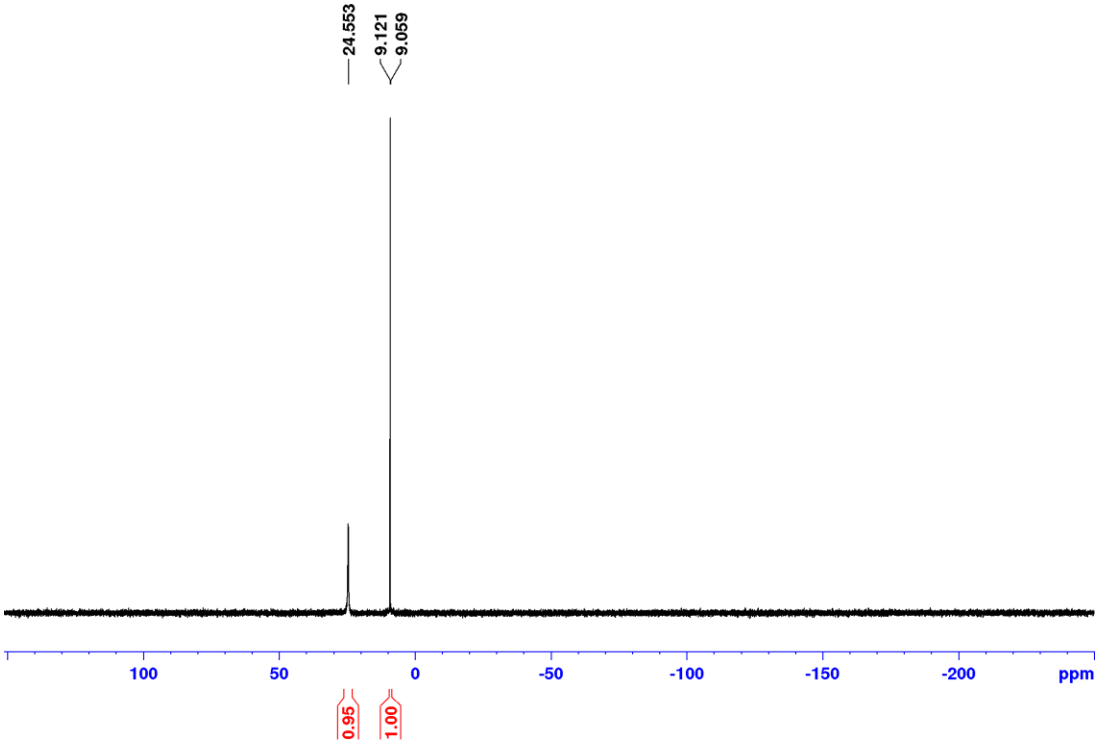

Figure 2.35, continued.

(b) ^{1}H NMR spectrum (CD_2Cl_2, 500 MHz)

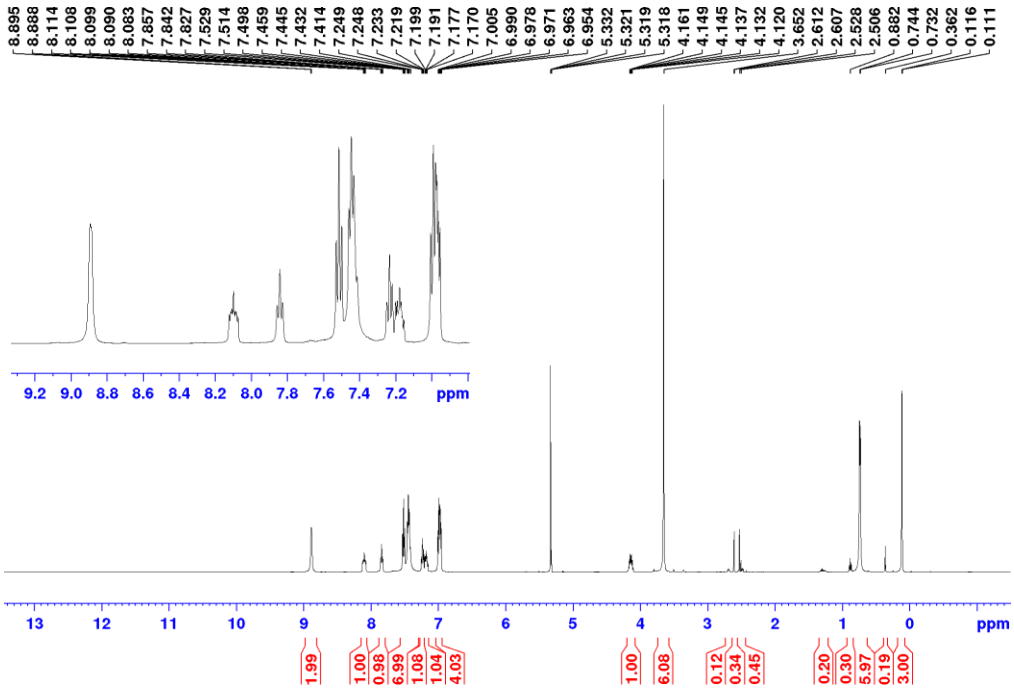

(c) $^{13}C\{^{1}H\}$ NMR spectrum (CD_2Cl_2, 125 MHz)

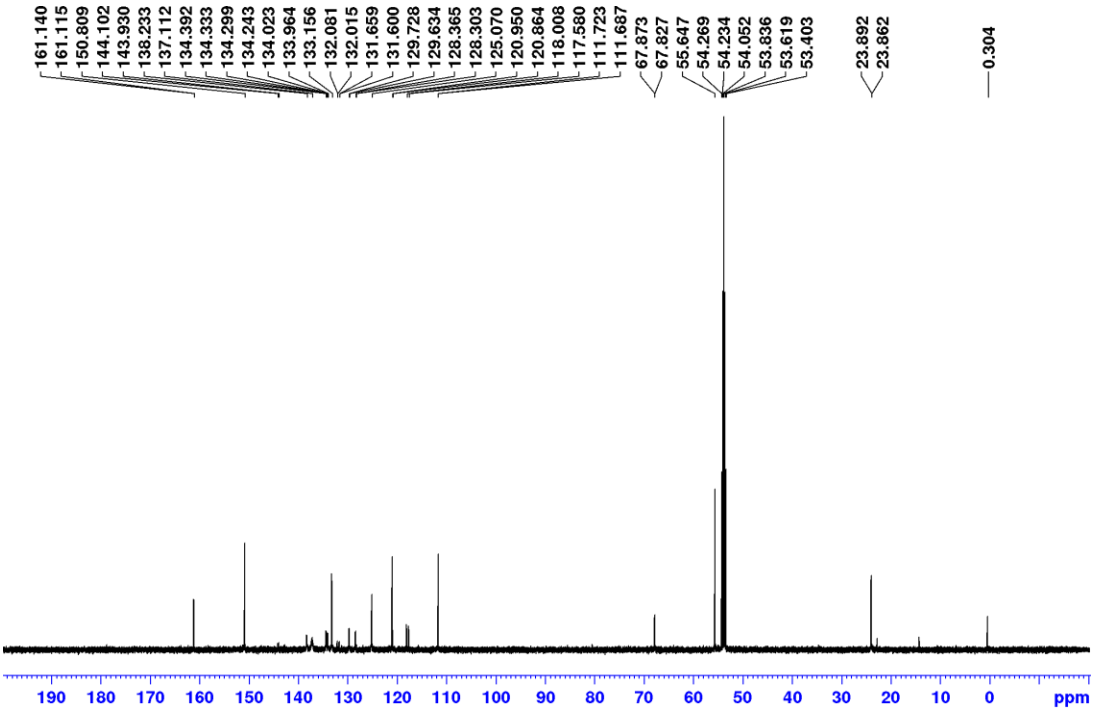

(κ^2-*P,O*-1-PPh_2-2-PO_2Et(O-$B(C_6F_5)_3$)-Ph)PdMe(2,6-lutidine) (4a-lut). A vial was charged with **3a-lut** (0.150 g, 0.248 mmol), $B(C_6F_5)_3$ (0.127 g, 0.250 mmol), and CH_2Cl_2 (5 mL) and the mixture was stirred for 8 h. The resulting yellow mixture was concentrated and layered with pentane, and stored at -40 ^oC for 48 h. A white solid precipitated and was collected by filtration, washed with pentane and purified by Soxhlet extraction into cyclohexane. The product was recrystallized by layering hexanes onto CH_2Cl_2 solution (0.812 g, 29 %). $^{31}P\{^1H\}$ NMR (CD_2Cl_2): δ 29.6 (d, $^3J_{PP}$ = 18, *P*=O), 9.8 (d, $^3J_{PP}$ = 18, *P*–Pd). ^1H NMR (CD_2Cl_2): δ 8.01 (m 1H, H^D), 7.67 (m, 3H, *p*-lut and *o*-Ph), 7.58-7.44 (m, 8H, H^B, H^C, *m*-Ph and *p*-Ph), 7.34 (dd, $^3J_{HH}$ = 7.5, 2H, *o*-Ph), 7.21 (d, $^3J_{HH}$ = 8.0, 1H, *m*-lut), 7.14 (dd, $^3J_{HH}$ = $^3J_{PH}$ = 7.0, 1H, H^A), 7.10 (d, $^3J_{HH}$ = 8.0, 1H, *m*-lut), 3.49 (m, 1H, –OC$H_2$$CH_3$), 3.00 (s, 3H, lut–C$H_3$), 2.86 (s, 3H, lut–C$H_3$), 2.85 (m, 1H, –OC$H_2$$CH_3$) 0.41 (t, $^3J_{HH}$ = 7, 3H, –$OCH_2C$$H_3$), 0.06 (d, $^3J_{PH}$ = 3.5, 3H, Pd–CH_3). $^{13}C\{^1H\}$ NMR (CD_2Cl_2): δ 158.6 (*o*-lut), 158.4 (*o*-lut), 148.4 (dm, $^1J_{FC}$ = 240, *o*-C_6F_5), 139.3 (d, $^1J_{FC}$ = 247, *p*-C_6F_5), 139.0 (*p*-lut), 137.0 (d, $^1J_{FC}$ = 258, *m*-C_6F_5), 135.8 (dd, $^1J_{PC}$ = 192, $^2J_{PC}$ = 16.7, C^E), 135.6 (dd, J_{PC} = 13, 2.4, C^A), 135.1 (d, $^2J_{PC}$ = 13, *o*-Ph), 135.0 (m, C^D), 134.0 (d, $^2J_{PC}$ = 10.7, C^F, partially obscured by *o*-Ph), 133.7 (d, $^2J_{FC}$ = 12, *o*-Ph), 132.1 (d, $^4J_{PC}$ = 2.5, *p*-Ph), 131.7 (dd, J_{PC} = 6.8, 2.8, C^C), 131.1 (d, $^4J_{PC}$ = 2.4, *p*-Ph), 130.9 (d, $^1J_{PC}$ = 56, *ipso*-Ph), 130.7 (dd, J_{PC} = 13, 2.3, C^B), 129.5 (d, $^3J_{PC}$ = 10.9, *m*-Ph), 129.1 (d, $^3J_{PC}$ = 10.7, *m*-Ph), 128.9 (d, $^1J_{PC}$ = 52, *ipso*-Ph), 123.0 (d, $^4J_{PC}$ = 3.1, *m*-lut), 122.6 (d, $^4J_{PC}$ = 3.3, *m*-lut), 121.7 (br s, *ipso*-C_6F_5), 62.5 (d, $^2J_{PC}$

= 5.3, –O*C*H$_2$CH$_3$), 26.1 (s, lut–*C*H$_3$), 25.8 (s, lut–*C*H$_3$), 14.9 (d, $^3J_{PC}$ = 8.8, –OCH$_2$*C*H$_3$), -3.2 (Pd–*C*H$_3$). ^{19}F{^{1}H} NMR (CD_2Cl_2): δ -134.0 (d, $^3J_{FF}$ = 22.1, *o*-C_6F_5), -161.2 (t, $^3J_{FF}$ = 20.7, *p*-C_6F_5), -166.9 (t, $^3J_{FF}$ = 20.7, *m*-C_6F_5). ^{11}B NMR (CD_2Cl_2): δ –2.3. HRMS: calcd. for $[C_{46}H_{31}BF_{15}NO_3P_2Pd]^+$, *m/z* 1109.06672. Found: 1109.067.

Figure 2.36. Numbering scheme for **4a-lut**.

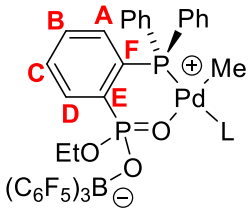

Figure 2.37. NMR spectra of **4a-lut**.

(a) ^{31}P NMR spectrum (CD_2Cl_2, 202 MHz)

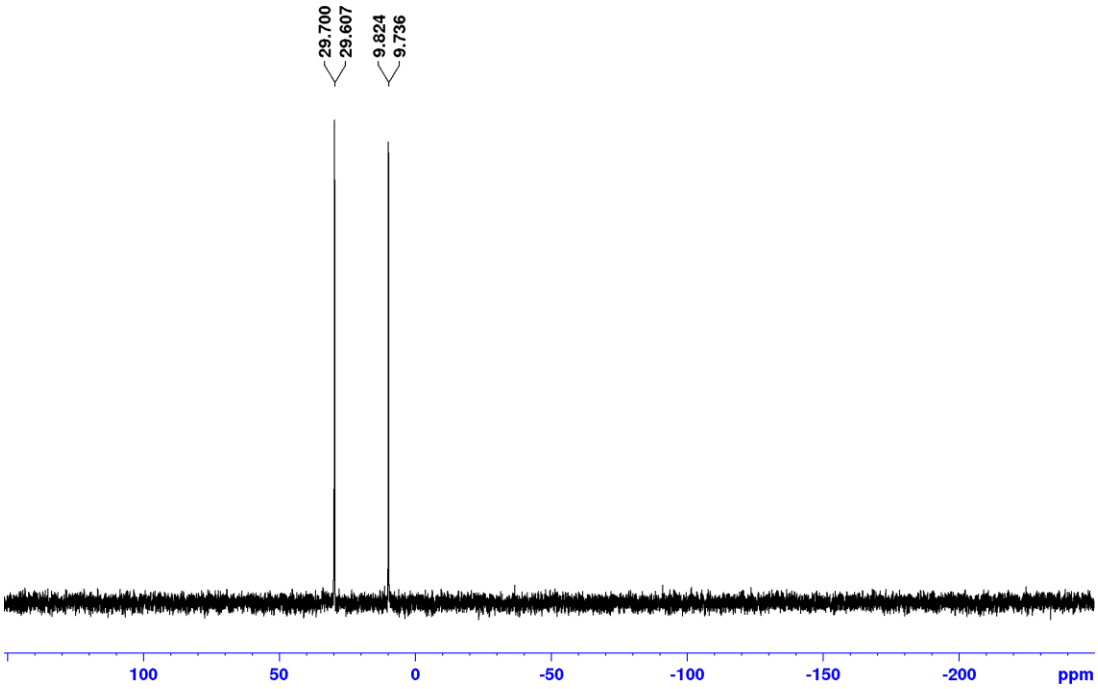

Figure 2.37, continued.

(b) ^{1}H NMR spectrum (CD_2Cl_2, 500 MHz)

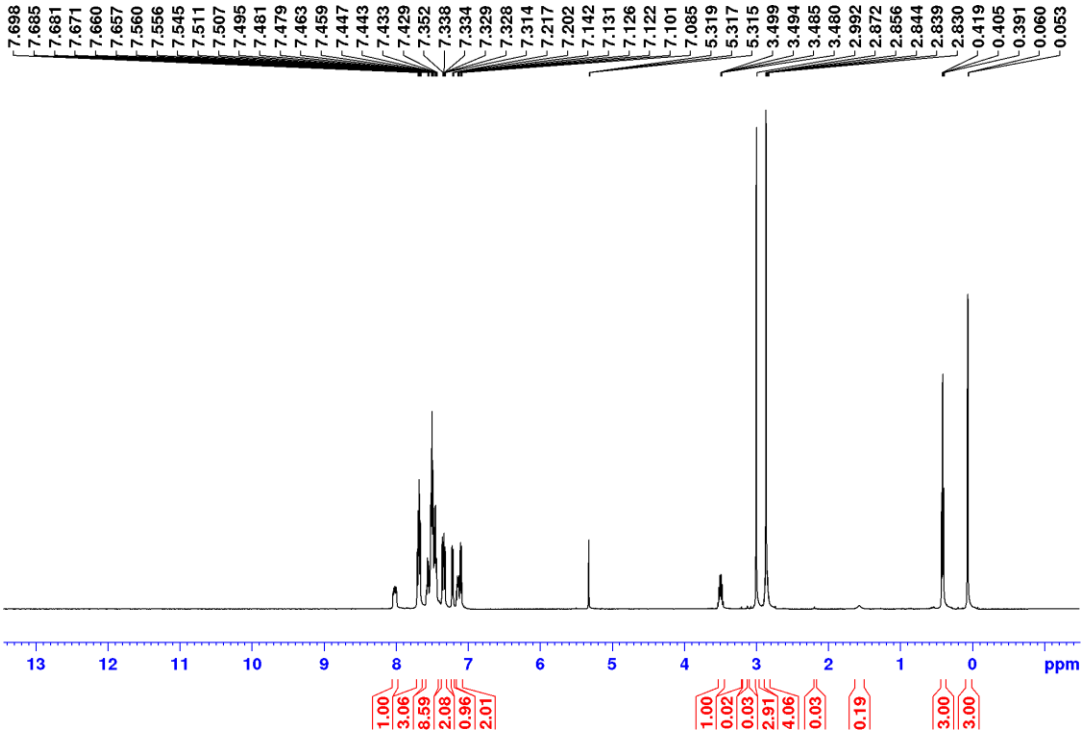

(c) ^{13}C NMR spectrum (CD_2Cl_2, 125 MHz)

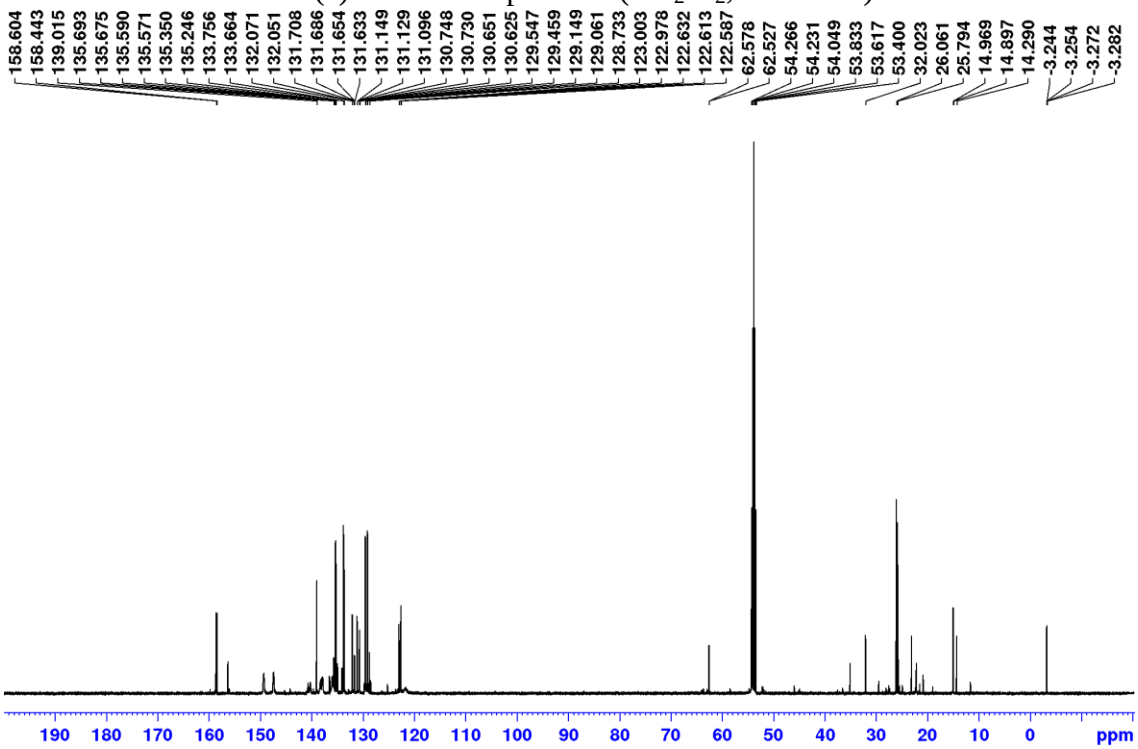

Figure 2.37, continued.

(d) ^{13}C NMR spectrum (CD_2Cl_2, 125 MHz), aryl region

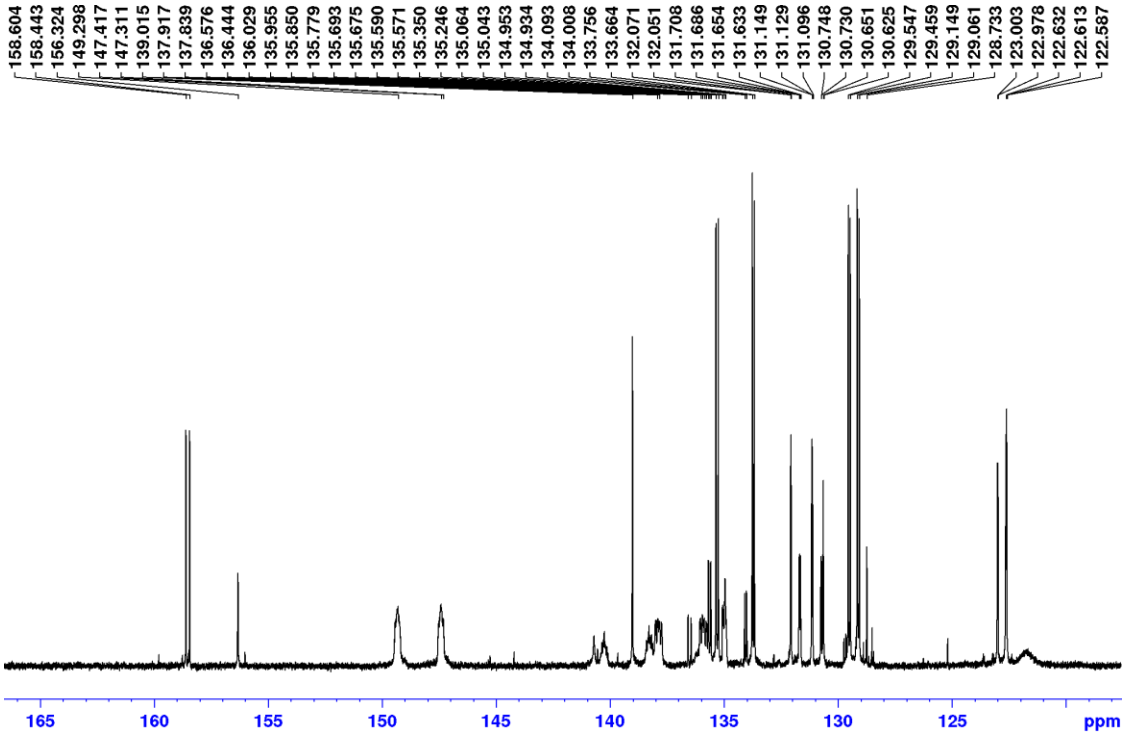

(e) ^{19}F NMR spectrum (CD_2Cl_2, 470 MHz)

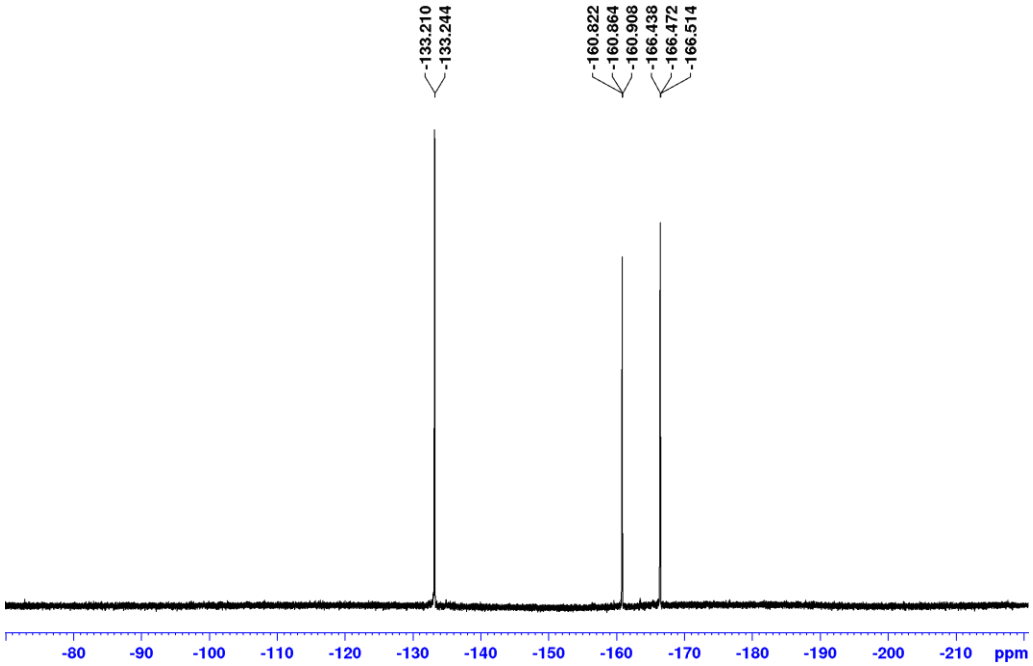

Figure 2.37, continued.

(f) ^{11}B NMR spectrum (CD_2Cl_2, 128 MHz)

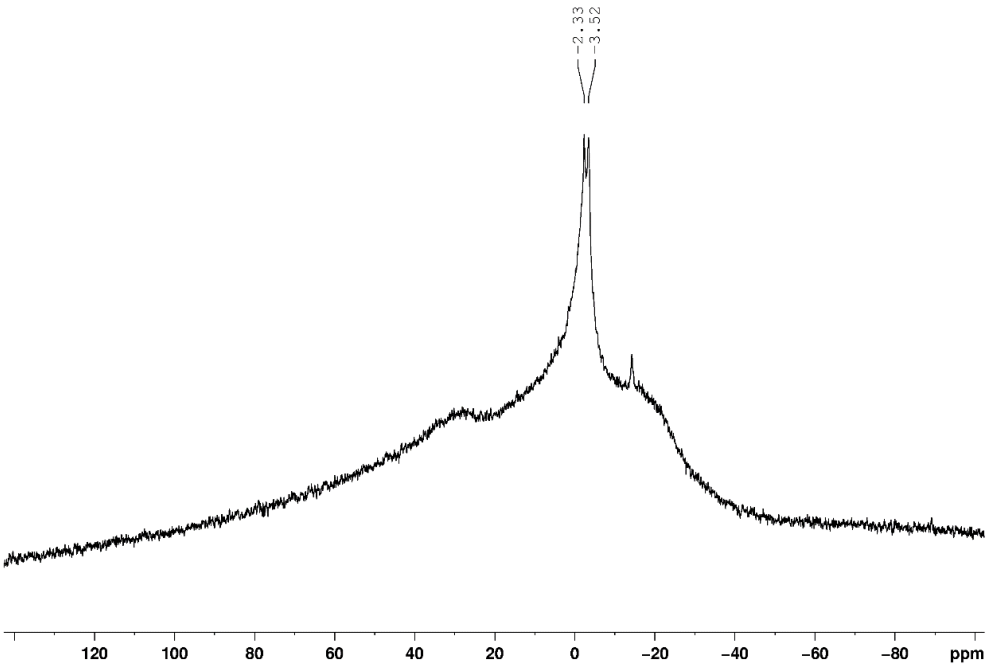

(g) COSY (CD_2Cl_2, 500 MHz)

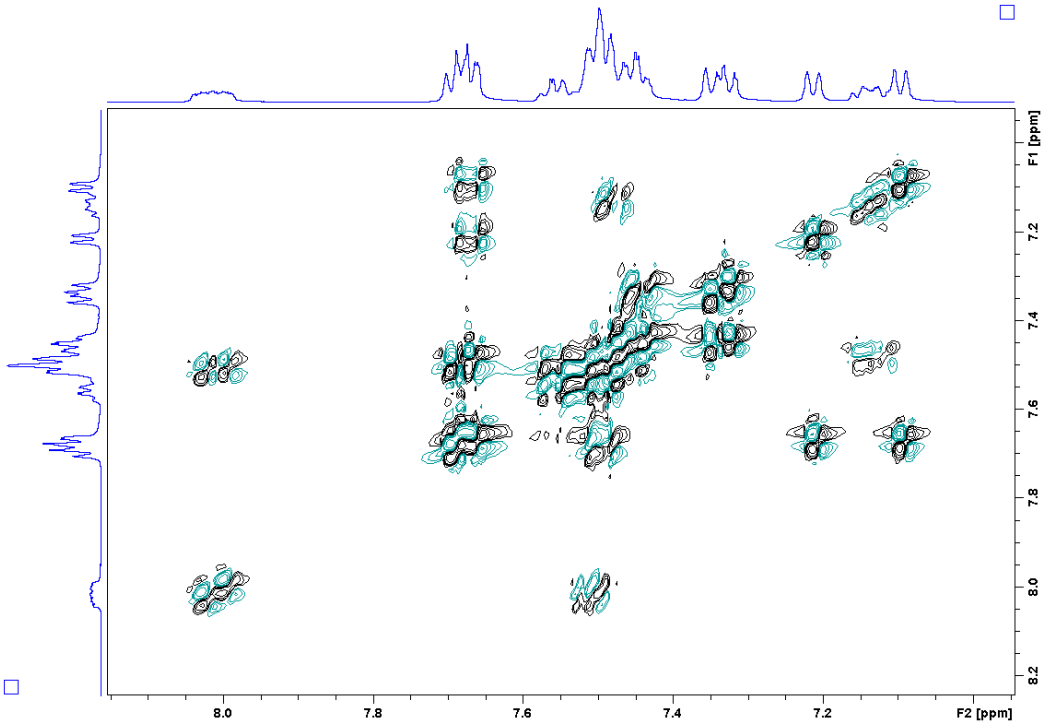

Figure 2.37, continued.

(h) HMQC (CD_2Cl_2, 500 MHz, 125 MHz)

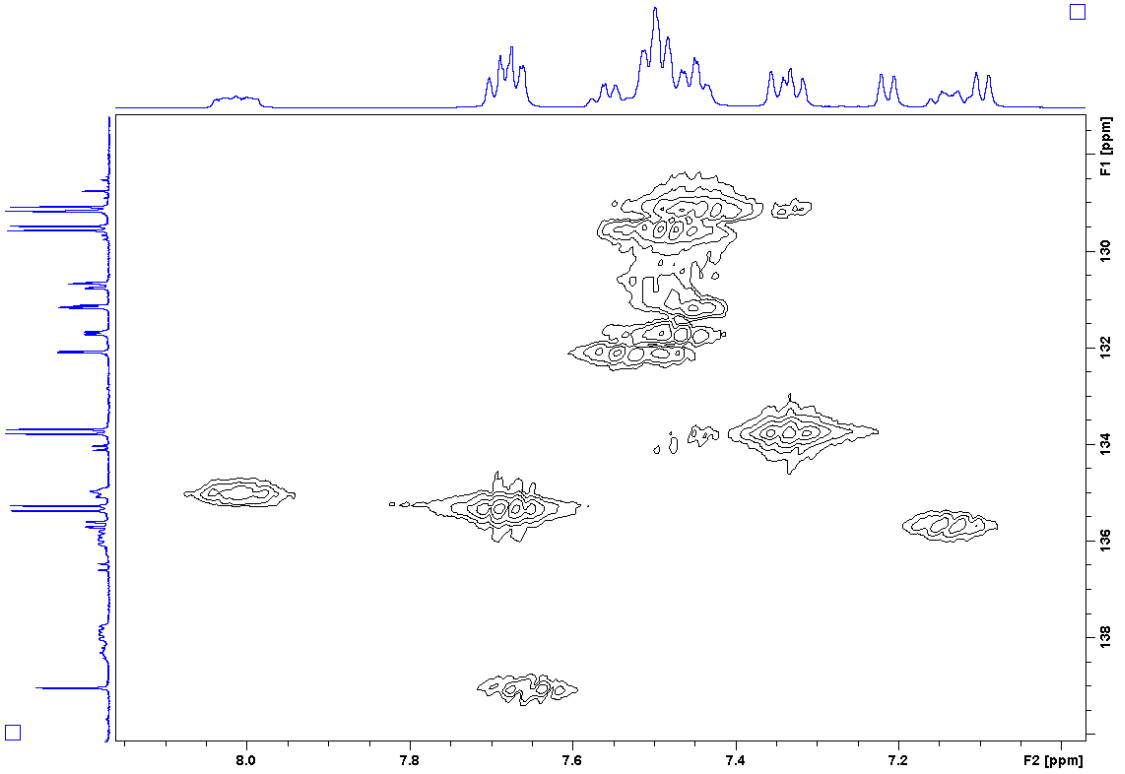

{(κ^2-*P,O*-1-PPh_2-2-PO_2Et(O-$B(C_6F_5)_3$)-Ph)PdMe}$_2$ (5a/5a'). A vial was charged with **3a-py** (0.201 g, 0.351 mmol), $B(C_6F_5)_3$ (0.360 g, 0.704 mmol), and CH_2Cl_2 (7 mL), and the mixture was stirred for 1 h, resulting in bright yellow solution. The mixture was concentrated, layered with hexanes, and stored at -40 °C for 48 h and a white solid precipitated. The solid was collected by filtration and recrystallized again from a CH_2Cl_2/hexanes solution at -40 °C. X-ray quality crystals were grown from $C_2H_2Cl_4$/hexanes solution at room temperature (0.184 g, 52 %). **5a.** $^{31}P\{^1H\}$ NMR (CD_2Cl_2): δ 37.3 (br, *P*=O), 11.3 (br, *P*–Pd). ^1H NMR (CD_2Cl_2): δ 7.8 (br, 1H, H^D), 7.6-7.23 (br, 12H, *H*–Ph), 6.93 (br, 1H, H^A), 4.45 (br, 2H, –O*C*H_2CH_3), 3.7 (br, 2H, –

OCH_2CH$_3$), 0.71 (br t, 6H, –OCH$_2$CH_3) -0.03 (br d, 6H, Pd–CH_3). ^{19}F{^{1}H} NMR (CD_2Cl_2): δ -133.0 (br, *o*-C_6F_5), -159.5 (br, *p*-C_6F_5), -165.7 (br, *m*-C_6F_5). **5a'**. ^{31}P{^{1}H} NMR (CD_2Cl_2): δ 37.0 (br, *P*=O), 9.7 (br, *P*–Pd). ^{1}H NMR (CD_2Cl_2): δ 7.90 (br, 1H, H^D), 7.6-7.3 (br, 12H, *H*–Ph), 7.13, (br, 1H, H^A), 3.63 (br, 2H, –OCH_2CH$_3$), 2.99 (br, 2H, –OCH_2CH$_3$), 0.51 (br, 6H, –OCH$_2$CH_3), 0.40 (br, 6H, Pd–CH_3). ^{19}F{^{1}H} NMR (CD_2Cl_2): δ -133.7 (br, *o*-C_6F_5), -160.8 (br, *p*-C_6F_5), -166.3 (br, *m*-C_6F_5). ^{13}C{^{1}H} and ^{11}B NMR too broad to make assignments. HRMS: calcd. for [$C_{78}H_{44}B_2F_{30}O_6P_4Pd_2$+ 2Na]$^{2+}$ *m/z* 2005.990218. Found: 2005.9978.

Figure 2.38. Numbering scheme for **5a/5a'**.

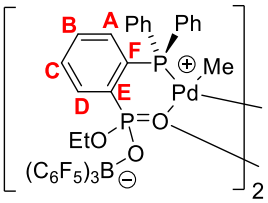

Figure 2.39. NMR spectra of **5a/5a'**.

(a) ^{31}P NMR spectrum (CD_2Cl_2, 202 MHz)

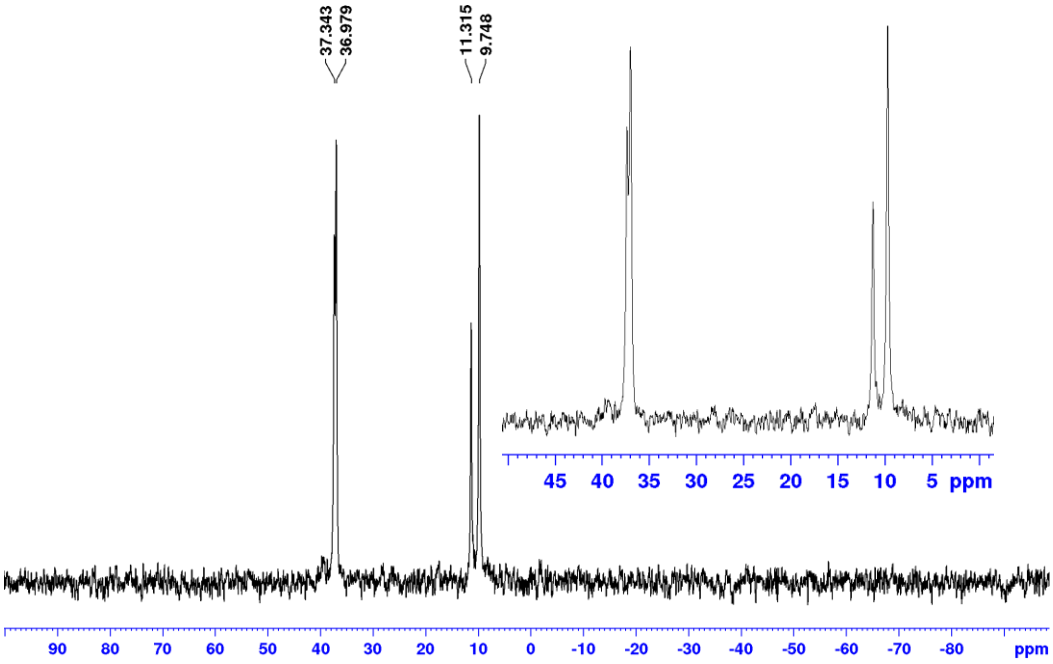

(b) ^{1}H NMR spectrum (CD_2Cl_2, 500 MHz)

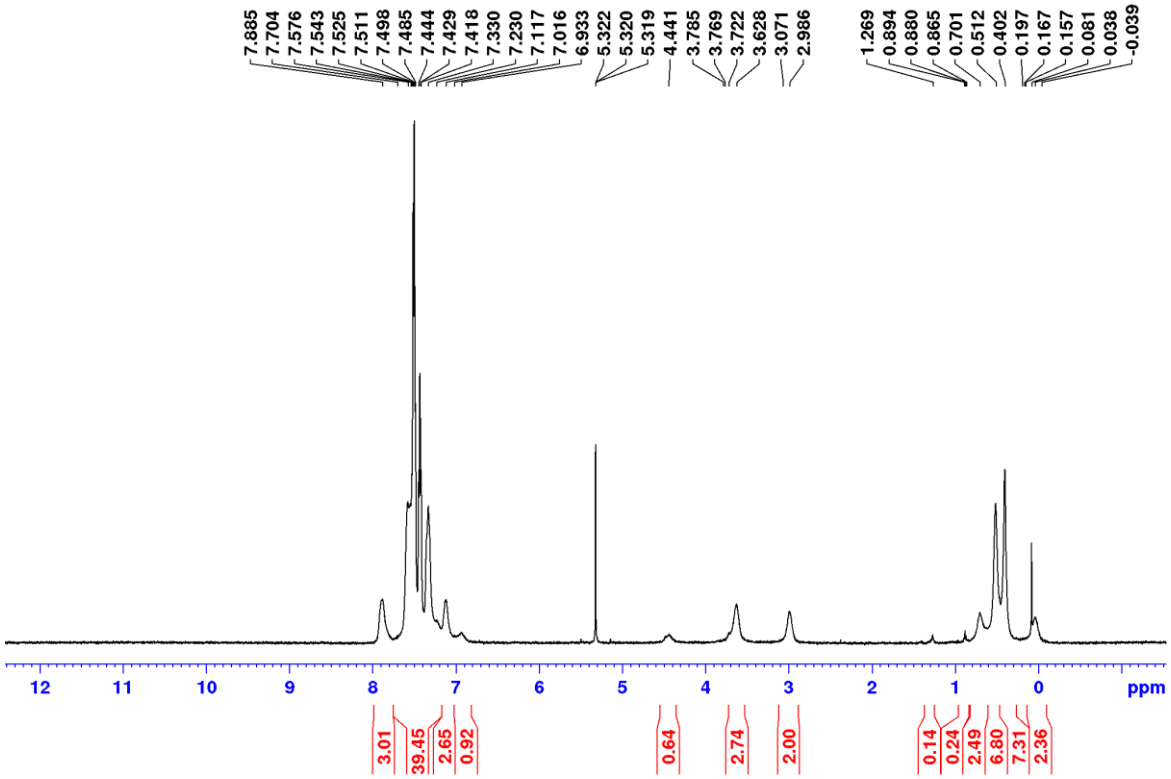

Figure 2.39, continued.

(c) ^{19}F NMR spectrum (CD_2Cl_2, 470 MHz)

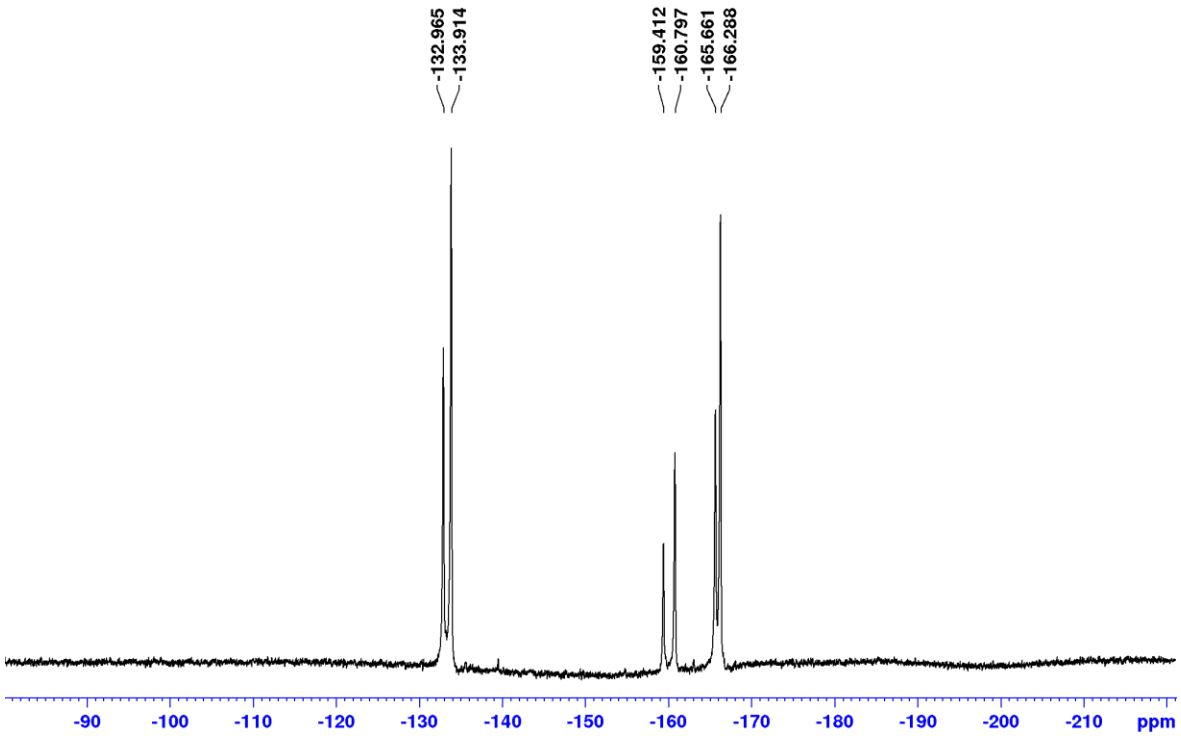

{(κ^2-*P,O*-1-PPh$_2$-2-PO$_2$^{i}Pr(O-B(C$_6$F$_5$)$_3$-Ph)PdMe}$_2$ (5b). A vial was charged with **3b-py** (0.104 g, 0.178 mmol), $B(C_6F_5)_3$ (0.182 g, 0.356 mmol), and CH_2Cl_2 (5 mL) and the mixture was stirred for 1 h, resulting in a bright yellow solution. The mixture was concentrated, layered with hexanes, and stored at -40 °C for 48 h and a white solid precipitated. The solid was collected by filtration and recrystallized again from a CH_2Cl_2/hexanes solution at -40 °C. X-ray quality crystals were grown from $C_2H_2Cl_4$/hexanes solution at room temperature (0.100 g, 87 %). $^{31}P\{^1H\}$ NMR (CD_2Cl_2): δ 36.6 (br d, *P*=O), 6.1 (d, $^3J_{PP}$ = 13.4, *P*–Pd). ^{1}H NMR (CD_2Cl_2): δ 7.69 (m, 1H, H^D), 7.6-7.36 (m, 12H, *H*–Ph), 7.13 (m, 1H, H^A), 4.36 (m, 1H, –OC*H*(CH$_3$)$_2$), 0.93

(d, $^{3}J_{HH}$ = 6.0, 6H, –OCH(CH_3)$_2$), 0.67 (br d, $^{3}J_{HH}$ = 5, 6H, –OCH(CH_3)$_2$), 0.35 (br, 6H, Pd–CH_3). ^{19}F{^{1}H} NMR (CD_2Cl_2): δ -134.2 (d, $^{3}J_{FF}$ = 19, *o*-C_6F_5), -161.7 (t, $^{3}J_{FF}$ = 20, *p*-C_6F_5), -167.0 (t, $^{3}J_{FF}$ = 17, *m*-C_6F_5). ^{13}C{^{1}H} and ^{11}B NMR too broad to make assignments. HRMS calc. for $[C_{80}H_{49}B_2F_{30}O_6P_4Pd_2–H_2O]^+$ m/z 2017.0154. Found: 2017.0201.

Figure 2.40. Numbering scheme for **5b**.

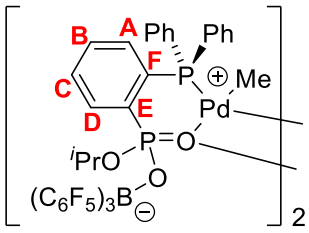

Figure 2.41. NMR spectra of **5b**.

(a) ^{31}P NMR spectrum (CD_2Cl_2, 202 MHz)

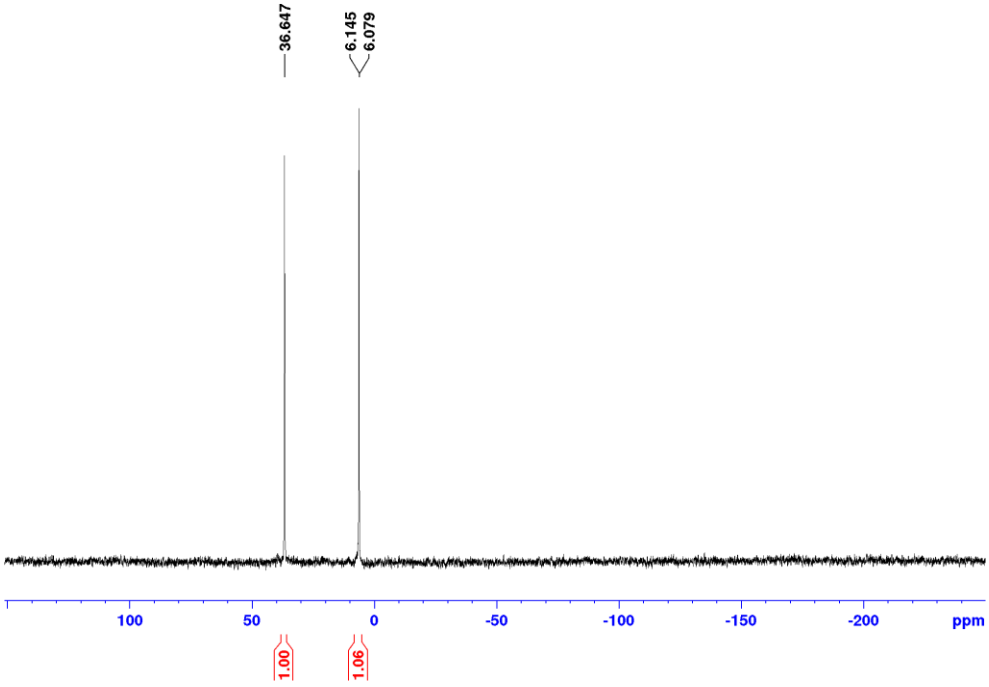

Figure 2.41, continued.

(b) ^{1}H NMR spectrum (CD_2Cl_2, 500 MHz)

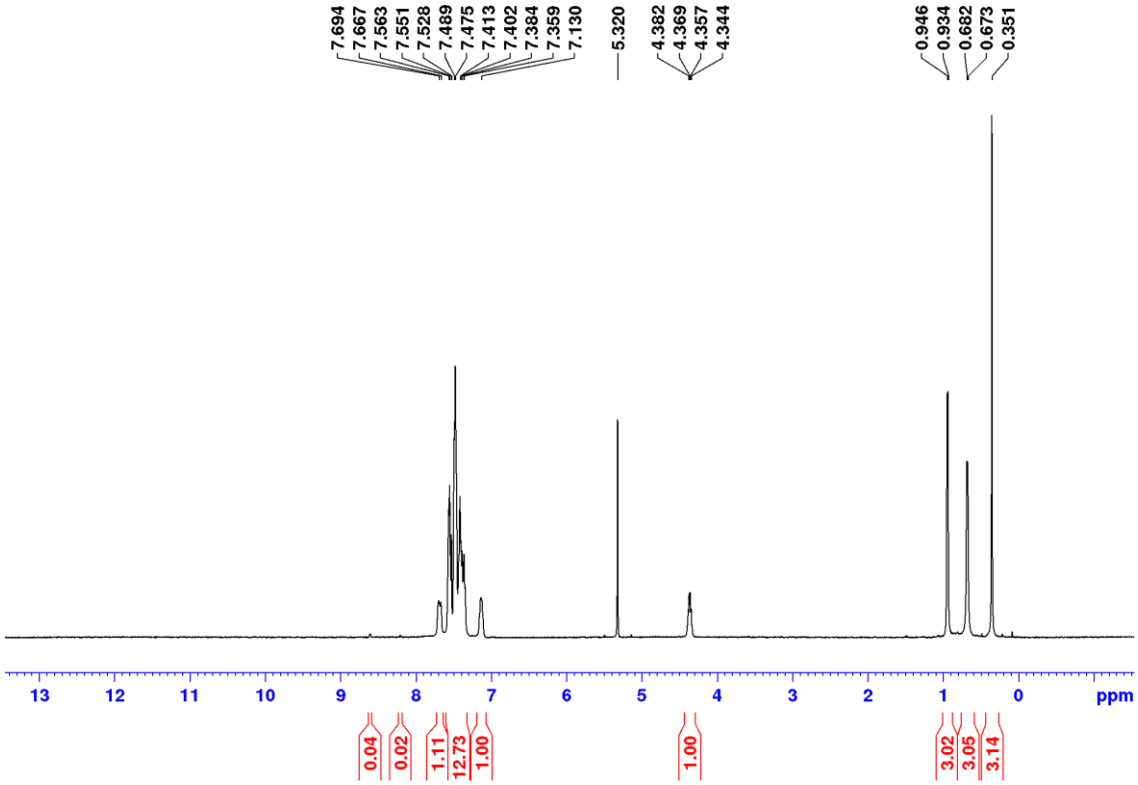

(c) ^{19}F NMR spectrum (CD_2Cl_2, 470 MHz)

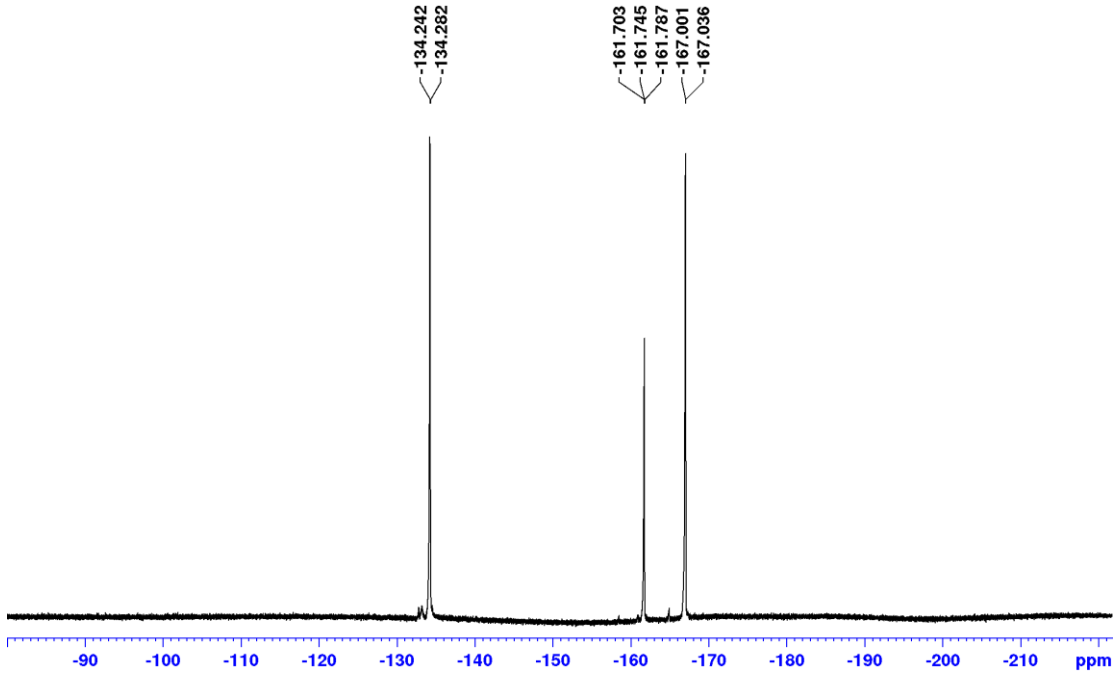

(2a•PF_5)PdMelut (6a-lut). Li[2a] (20.6 mg, 0.055 mmol) and (COD)PdMeCl (14.6 mg, 0.055 mmol) were weighed out to a J Young tube. CD_2Cl_2 (0.4 mL) was vacuum transferred to the tube and the mixture was stirred for 1 h, resulting in a cloudy white solution. $AgPF_6$ (18 mg, 0.0712 mmol) was added. The reaction mixture turned to a clear solution and a gray solid precipitated. 2,6-lutidine (6.4 µL, 0.055 mmol) was added and the mixture was stirred for 1 h. Unreacted PF_6 also present. $^{31}P\{^1H\}$ NMR (CD_2Cl_2): δ 29.6 (d, $^2J_{PP}$ = 17, *P*=O), 6.2 (br, *P*–Pd), –147.3 (sextet of d, $^1J_{PF}$ = 713, $^2J_{PP}$ = 17, *P*F_5). ^1H NMR (CD_2Cl_2): δ 8.18 (m, 1H, H^D), 7.75-7.15 (m, 16H, *H*–Ph), 3.74 (m, 1H, –OC*H*$_2$CH$_3$), 3.23 (m, 1H, –OC*H*$_2$CH$_3$), 3.16 (s, 3H, lut–C*H*$_3$), 3.08 (s, 3H, lut–C*H*$_3$), 0.73 (t, $^3J_{HH}$ = 7, 3H, –OCH$_2$C*H*$_3$), 0.22 (d, $^3J_{PH}$ = 4, 3H, Pd–C*H*$_3$). $^{19}F\{^1H\}$ NMR (CD_2Cl_2): δ –60.0 (dd, $^3J_{PF}$ = 55, $^1J_{PF}$ = 743, P*F*$_5$).

Figure 2.42. Numbering scheme for **6a-lut**.

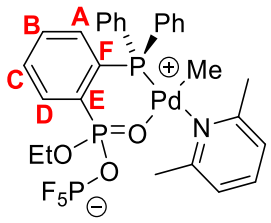

Figure 2.43. NMR spectra of **6a-lut**.

(a) ^{31}P NMR spectrum (CD_2Cl_2, 202 MHz)

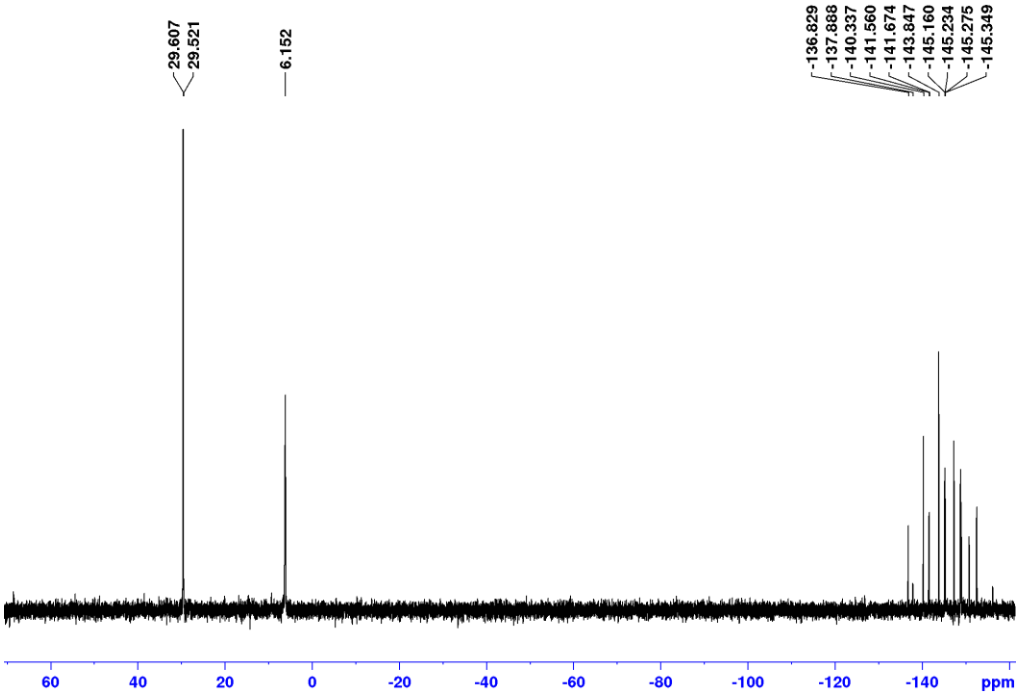

(b) ^{1}H NMR spectrum (CD_2Cl_2, 500 MHz)

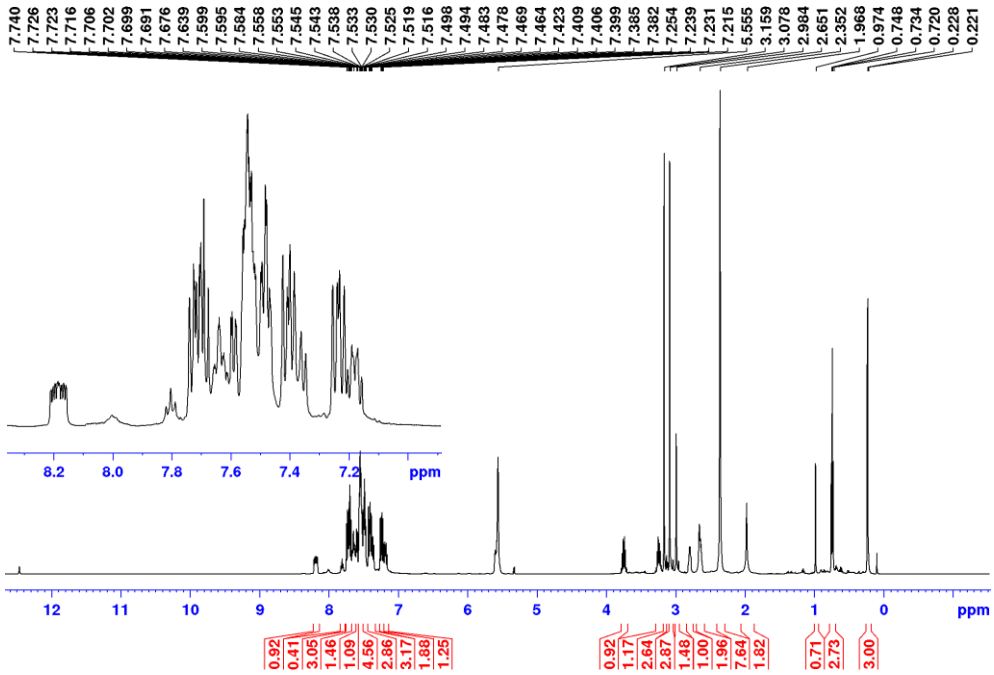

Figure 2.43, continued.

(c) ^{19}F NMR spectrum (CD_2Cl_2, 470 MHz)

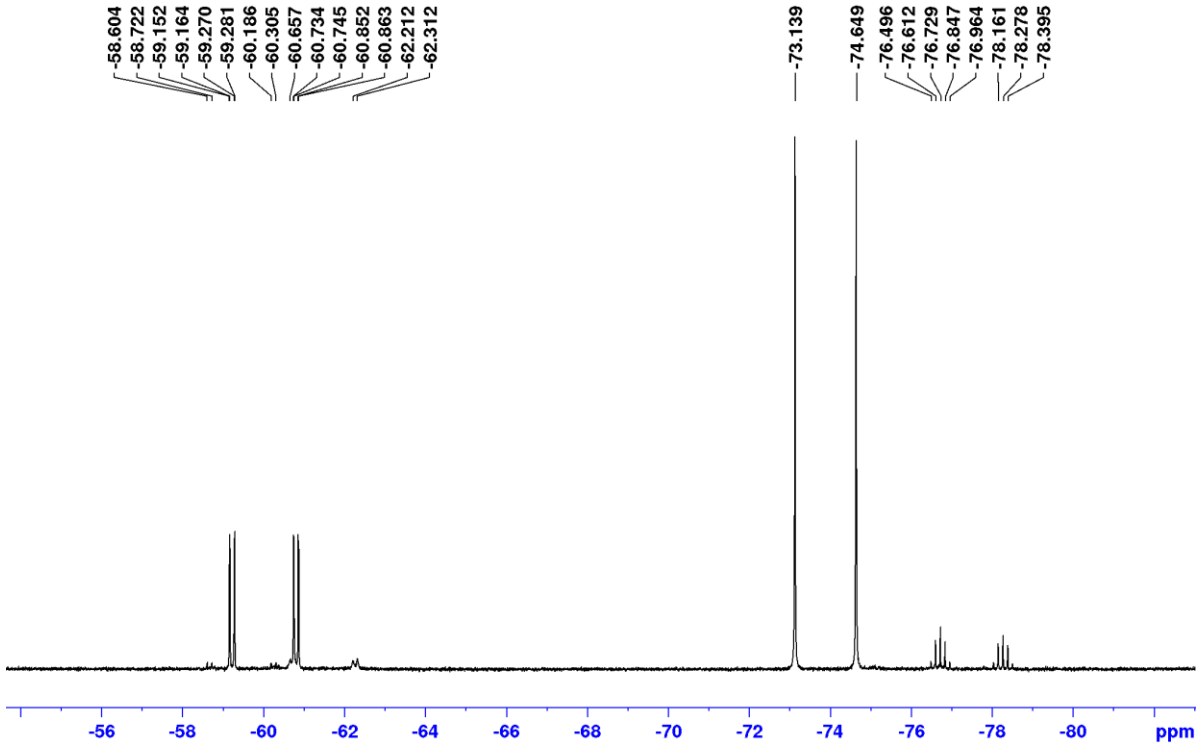

Reaction of 3a-py and BF_3•Et_2O. A J Young tube was charged with **3a-py** (0.02 g, 0.04 mmol) and CD_2Cl_2 (0.4 mL). 2 equiv of BF_3•Et_2O (8.7 µL, 0.08 mmol) was added and the mixture was stirred for 8 h. Stripped down mixture and redissolved in CD_2Cl_2. $^{31}P\{^1H\}$ NMR (CD_2Cl_2): δ 32.0 (br, *P*=O), 9.5 (br, *P*–Pd). ^1H NMR (CD_2Cl_2): δ 8.83 (br, 2H, *o*-py•BF_3), 8.16 (m, 1H), 7.92 (t, 1H, *p*-py•BF_3), 7.69 (m, 1H), 7.75-7.35 (m, 13H, *H*–Ph), 7.04 (m, 1H), 3.29 (m, 1H, –OC*H*$_2$CH$_3$), 0.76 (t, $^3J_{HH}$ = 7, 3H, –OCH$_2$C*H*$_3$), 0.62 (t, $^3J_{HH}$ = 7, 3H, –OCH$_2$C*H*$_3$), 0.47 (br,

3H, Pd–CH_3), 0.34 (br, 3H, Pd–CH_3). $^{19}F\{^1H\}$ NMR (CD_2Cl_2): δ –146.3 (**3a-py**•BF_3), –151.8 (py•BF_3).

Figure 2.44. NMR spectra of product from reaction of **3a-py** and 2 equiv of BF_3•Et_2O.

(a) ^{31}P NMR spectrum (CD_2Cl_2, 202 MHz)

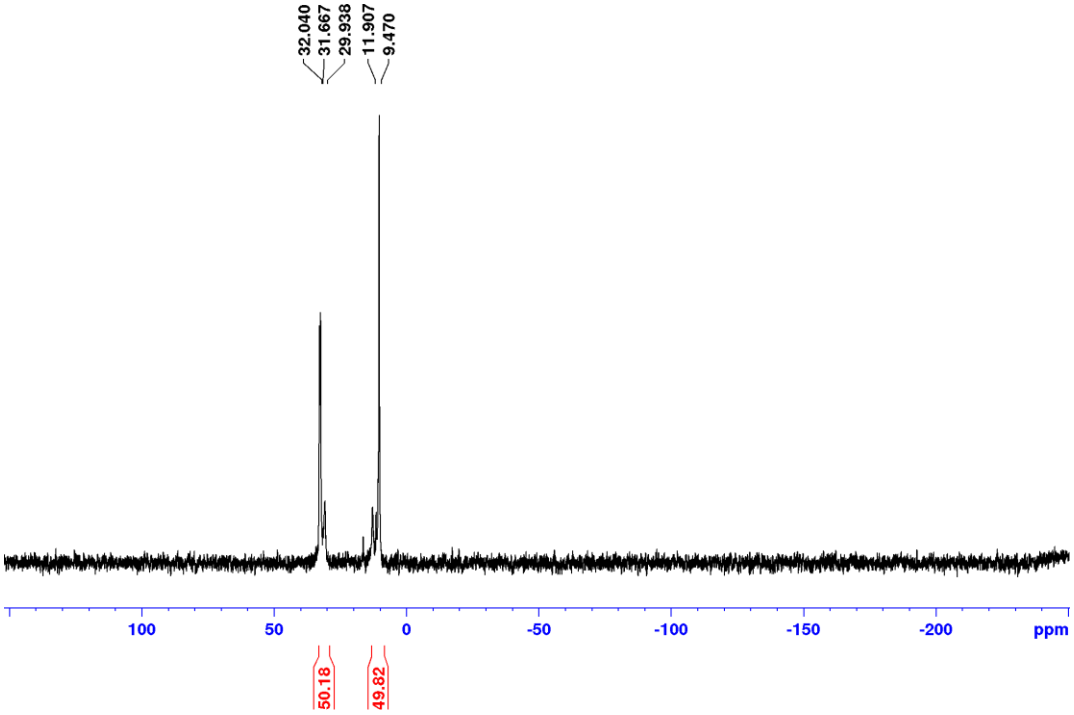

Figure 2.44, continued.

(b) ^{1}H NMR spectrum (CD_2Cl_2, 500 MHz)

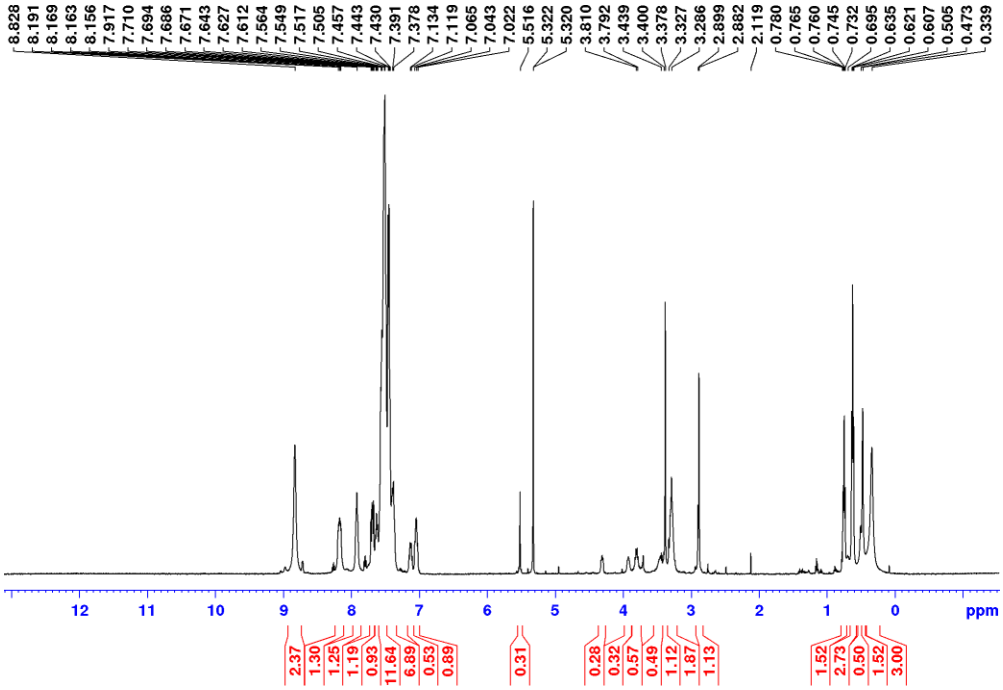

(c) ^{19}F{^{1}H} NMR spectrum (CD_2Cl_2, 470 MHz)

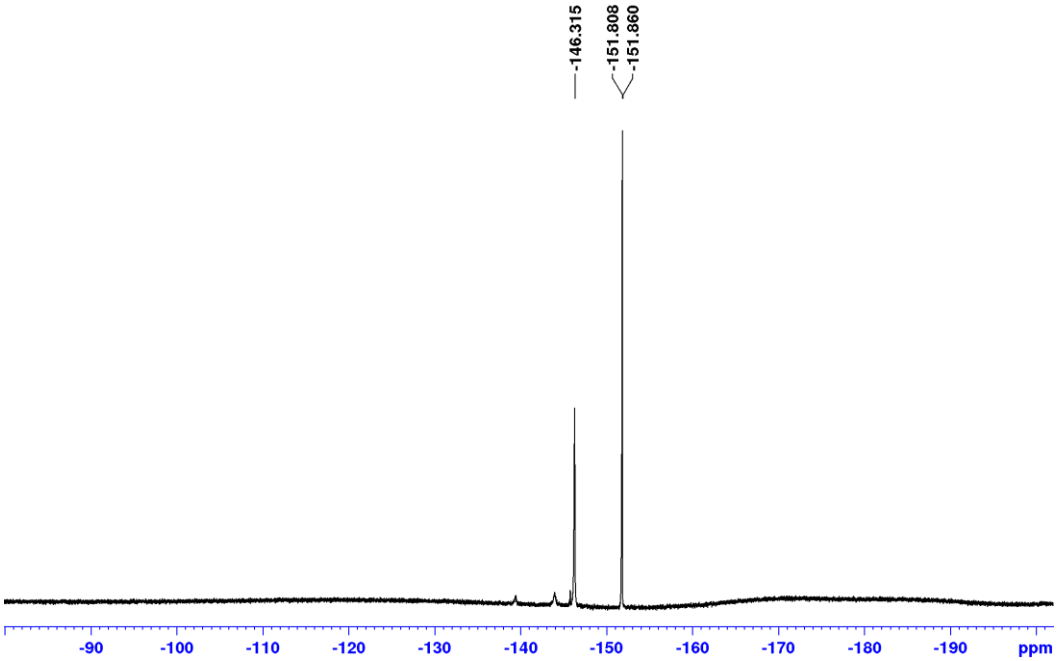

X-ray Crystallography. Data were measured on a Bruker D8 VENTURE diffractometer using a PHOTON 100 CMOS detector system equipped with a Mo-target micro-focus X-ray tube and Kα radiation (0.71073 Å). Direct methods were used to locate many atoms from the E-map. Repeated difference Fourier maps enabled location of all expected non-hydrogen atoms. Following anisotropic refinement of all non-H atoms, ideal H atom positions were calculated. Final refinement was anisotropic for all non-H atoms and isotropic-riding for H atoms. ORTEP diagrams are drawn with 50 % probability ellipsoids.

Specific details for structure refinement for 3b-lut. All atoms were refined with anisotropic thermal parameters. Hydrogen atoms were included in idealized positions for structure factor calculations. All structures are drawn with thermal ellipsoids at 50% probability. i-Pr group, CH_2Cl_2, and water molecules are found to be disordered as shown in the figure below. Water molecule is half-occupied alternatively being at one of the positions. This seems to lead to the additional disorder of a DCM molecule as at one of the orientations Cl-atom becomes too close to the water molecule. So, this provides a possible correlation between the disorders of both molecules.

Specific details for structure refinement for 4a-lut. All atoms were refined with anisotropic thermal parameters. Hydrogen atoms were included in idealized positions for structure factor calculations. All structures are drawn with thermal ellipsoids at 50% probability.

Specific details for structure refinement for 5a'. All atoms were refined with anisotropic thermal parameters. Hydrogen atoms were included in idealized positions for structure factor calculations. All structures are drawn with thermal ellipsoids at 50% probability. Crystal contained many disordered solvent molecules located in large solvent accessible voids. The diffuse contribution to scattering was treated by application of the program SQUEZZE [van der Sluis, P. & Spek, A. L., Acta Cryst. 1990, A46, 194-201; Spek, A.L. *Acta Cryst.* **2015**, *C71*, 9-18] as implemented in Platon [Spek, A. L., Acta Cryst. 2009, D65, 148-155] using the "fab" file construct. SQUEEZE algorithm located 4 voids:

1	0.250	-0.018	0.250	374	83 ' '
2	0.750	0.014	0.750	374	83 ' '
3	0.750	0.245	0.250	182	49 ' '
4	0.250	0.754	0.750	182	49 ' '

with a total solvent accessible volume of 1120 $Å^3$ and the electron count of 264. In terms of electron count, first 2 voids could be occupied by 2 molecules of DCM, and the latter two voids, by one molecule of DCE.

Specific details for structure refinement for 5b. All atoms were refined with anisotropic thermal parameters. Hydrogen atoms were included in idealized positions for structure factor calculations. All structures are drawn with thermal ellipsoids at 50% probability.

Table 2.1. X-ray crystallographic parameters of **3a-lut**.

Empirical formula	$C_{28}H_{31}NO_3P_2Pd + CH_2Cl_2$
Formula weight	682.80
Temperature	100 K
Wavelength	0.71073 Å
Crystal system	Orthorhombic
Space Group	Pccn
Unit cell dimensions	a = 18.659(7) Å $\alpha = 90^o$
	b = 22.632(8) Å $\beta = 90^o$
	c = 14.434(5) Å $\gamma = 90^o$
Volume	6095(4) $Å^3$
Z	8
Density (calculated)	1.488 Mg/m^3
Absorption coefficient	0.920 mm^{-1}
F(000)	2784.0
Crystal size, color, habit	0.44 × 0.06 × 0.06 mm, clear, rod
2Θ range for data collection	4.00 to 50.24^o
Index ranges	$-22 \leq h \leq 22$, $-26 \leq k \leq 26$, $-17 \leq l \leq 17$
Reflections collected	55378
Independent reflections	5419 [R_{int} = 0.0586]
Absorption correction	SADABS based on redundant diffractions
Refinement method	Full-matrix least squares on F2
Data / restraints / parameters	5419/0/347
Goodness-of-fit on F2	0.904
Final R indices [I > 2 sigma(I)]	R_1 = 0.0801, wR_2 = 0.1702
R indices (all data)	R_1 = 0.2107, wR_2 = 0.2141
Largest diff. peak and hole	0.715, -0.902 $eÅ^{-3}$

Table 2.2. X-ray crystallographic parameters of **3b-lut**.

Empirical formula	$C_{30}H_{36}Cl_2NO_{3.5}P_2Pd$
Formula weight	705.84
Temperature	100 K
Wavelength	0.71073 Å
Crystal system	Monoclinic
Space Group	$P2_1/n$
Unit cell dimensions	a = 10.8588(4) Å α = 90 ^{o}
	b = 10.5927(4) Å β = 96.1460(10)^o
	c = 27.6745(12) Å γ = 90^o
Volume	3164.9(2) Å^3
Z	4
Density (calculated)	1.481 Mg/m^3
Absorption coefficient	0.889 mm^{-1}
F(000)	1444.0
Crystal size, color, habit	0.22 × 0.10 × 0.08 mm, colorless, block
2Θ range for data collection	4.854 to 51.522^o
Index ranges	-13 ≤ h ≤ 13, -12 ≤ k ≤ 12, -33 ≤ l ≤ 33
Reflections collected	75624
Independent reflections	6042 [R_{int} = 0.0928, R_{sigma} = 0.0357]
Absorption correction	SADABS based on redundant diffractions
Refinement method	Full-matrix least squares on F2
Data / restraints / parameters	6042/66/408
Goodness-of-fit on F2	1.040
Final R indices [I > 2 sigma(I)]	R_1 = 0.0360, wR_2 = 0.0752
R indices (all data)	R_1 = 0.0542, wR_2 = 0.0818
Largest diff. peak and hole	0.82/-0.88 eÅ^{-3}

Table 2.3. X-ray crystallographic parameters of **4a-lut**.

Empirical formula	$C_{47}H_{33}BCl_2F_{15}NO_3P_2Pd$
Formula weight	1194.79
Temperature	100 K
Wavelength	0.71073 Å
Crystal system	Triclinic
Space Group	P1(bar)
Unit cell dimensions	a = 10.1749(5) Å α = 90.851(2)^o
	b = 15.3276(8) Å β = 102.811(2)^o
	c = 16.2202(8) Å γ = 107.649(2)^o
Volume	2341.4(2) Å^3
Z	2
Density (calculated)	1.695 Mg/m^3
Absorption coefficient	0.683 mm^{-1}
F(000)	1192.0
Crystal size, color, habit	0.32 × 0.18 × 0.06 mm, colorless, plate
2Θ range for data collection	4.324 to 57.446^o
Index ranges	$-13 \leq h \leq 13$, $-20 \leq k \leq 20$, $-21 \leq l \leq 21$
Reflections collected	51386
Independent reflections	10474 [R_{int} = 0.0566, R_{sigma} = 0.0650]
Absorption correction	SADABS based on redundant diffractions
Refinement method	Full-matrix least squares on F2
Data / restraints / parameters	10474/0/653
Goodness-of-fit on F2	1.035
Final R indices [I > 2 sigma(I)]	R_1 = 0.0437, wR_2 = 0.0934
R indices (all data)	R_1 = 0.0758, wR_2 = 0.1040
Largest diff. peak and hole	1.07, -0.72 eÅ^{-3}

Table 2.4. X-ray crystallographic parameters of **5a'**.

Empirical formula	$C_{78}H_{44}B_2F_{30}O_6P_4Pd_2$
Formula weight	2005.43
Temperature	100 K
Wavelength	0.71073 Å
Crystal system	Monoclinic
Space Group	*P*2/*n*
Unit cell dimensions	a = 18.1036(12) Å α = 90°
	b = 11.8008(8) Å β = 96.321(2)°
	c = 21.0899(14) Å γ = 90°
Volume	4478.2(5) Å^3
Z	2
Density (calculated)	1.487 Mg/m^3
Absorption coefficient	0.582 mm^{-1}
F(000)	1984.0
Crystal size, color, habit	0.18 × 0.14 × 0.08 mm, yellow, block
2Θ range for data collection	4.454 to 54.346°
Index ranges	$-23 \leq h \leq 23$, $-15 \leq k \leq 15$, $-27 \leq l \leq 27$
Reflections collected	80374
Independent reflections	9904 [R_{int} = 0.0656, R_{sigma} = 0.0460]
Absorption correction	SADABS based on redundant diffractions
Refinement method	Full-matrix least squares on F2
Data / restraints / parameters	9904/0/552
Goodness-of-fit on F2	1.037
Final R indices [I > 2 sigma(I)]	R_1 = 0.0417, wR_2 = 0.1001
R indices (all data)	R_1 = 0.0647, wR_2 = 0.1095
Largest diff. peak and hole	1.55/-0.73 eÅ^{-3}

Table 2.5. X-ray crystallographic parameters of **5b**.

Empirical formula	$C_{80}H_{48}B_2F_{30}O_6P_4Pd_2$
Formula weight	2033.48
Temperature	100 K
Wavelength	0.71073 Å
Crystal system	Monoclinic
Space Group	$P2_1/c$
Unit cell dimensions	a = 12.6956(10) Å α = 90 ^{o}
	b = 18.0969(15) Å β = 109.684(3)^o
	c = 17.7465(16) Å γ = 90^o
Volume	3839.0(6) Å^3
Z	2
Density (calculated)	1.759 Mg/m^3
Absorption coefficient	0.681 mm^{-1}
F(000)	2016.0
Crystal size, color, habit	0.32 × 0.26 × 0.18 mm, light yellow, block
2Θ range for data collection	4.084 to 55.862^o
Index ranges	$-16 \leq h \leq 14$, $-23 \leq k \leq 21$, $-22 \leq l \leq 23$
Reflections collected	51479
Independent reflections	8988 [R_{int} = 0.0685, R_{sigma} = 0.0530]
Absorption correction	SADABS based on redundant diffractions
Refinement method	Full-matrix least squares on F2
Data / restraints / parameters	8988/0/562
Goodness-of-fit on F2	1.040
Final R indices [I > 2 sigma(I)]	R_1 = 0.0392, wR_2 = 0.0868
R indices (all data)	R_1 = 0.0651, wR_2 = 0.0975
Largest diff. peak and hole	0.97/-0.72 eÅ^{-3}

Table 2.6. X-ray crystallographic parameters of **6b-lut**.

Empirical formula	$C_{29}H_{33}Cl_2F_5NO_3P_3Pd$
Formula weight	808.77
Temperature	100 K
Wavelength	0.71073 Å
Crystal system	Triclinic
Space Group	P-1
Unit cell dimensions	a = 10.5740(9) Å α = 101.266(2) ^{o}
	b = 13.2552(12) Å β = 108.975(2)^o
	c = 14.9620(13) Å γ = 106.512(2)^o
Volume	1803.0(3) Å^3
Z	2
Density (calculated)	1.490 Mg/m^3
Absorption coefficient	0.851 mm^{-1}
F(000)	816.0
Crystal size, color, habit	0.32 × 0.24 × 0.14 mm, light yellow, block
2Θ range for data collection	4.21 to 55.802^o
Index ranges	-13 ≤ h ≤ 13, -17 ≤ k ≤ 17, -19 ≤ l ≤ 19
Reflections collected	37444
Independent reflections	8463 [R_{int} = 0.0297, R_{sigma} = 0.0304]
Absorption correction	SADABS based on redundant diffractions
Refinement method	Full-matrix least squares on F2
Data / restraints / parameters	8463/3/411
Goodness-of-fit on F2	1.079
Final R indices [I > 2 sigma(I)]	R_1 = 0.0315, wR_2 = 0.0777
R indices (all data)	R_1 = 0.0407, wR_2 = 0.0807
Largest diff. peak and hole	0.57/-0.67 eÅ^{-3}

2.5 References and Notes

(1) Nakamura, A.; Ito, S.; Nozaki, K. *Chem. Rev.* **2009**, *109*, 5215.

(2) Nakamura, A.; Anselment, T. M.; Claverie, J.; Goodall, B.; Jordan, R. F.; Mecking, S.; Rieger, B.; Sen, A.; van Leeuwen, P. W.; Nozaki, K. *Acc. Chem. Res.* **2013**, *46*, 1438.

(3) Ito, S.; Nozaki, K. *Chem. Rec.* **2010**, *10*, 315.

(4) Drent, E.; van Dijk, R.; van Ginkel, R.; van Oort, B.; Pugh, R. I. *Chem. Commun.* **2002**, 744.

(5) Guironnet, D.; Roesle, P.; Runzi, T.; Gottker-Schnetmann, I.; Mecking, S. *J. Am. Chem. Soc.* **2009**, *131*, 422.

(6) Kochi, T.; Noda, S.; Yoshimura, K.; Nozaki, K. *J. Am. Chem. Soc.* **2007**, *129*, 8948.

(7) Luo, S.; Vela, J.; Lief, G. R.; Jordan, R. F. *J. Am. Chem. Soc.* **2007**, *129*, 8946.

(8) Ito, S.; Munakata, K.; Nakamura, A.; Nozaki, K. *J. Am. Chem. Soc.* **2009**, *131*, 14606.

(9) Weng, W.; Shen, Z.; Jordan, R. F. *J. Am. Chem. Soc.* **2007**, *129*, 15450.

(10) Leicht, H.; Gottker-Schnetmann, I.; Mecking, S. *Angew. Chem., Int. Ed.* **2013**, *52*, 3963.

(11) Borkar, S.; Newsham, D. K.; Sen, A. *Organometallics* **2008**, *27*, 3331.

(12) Skupov, K. M.; Piche, L.; Claverie, J. P. *Macromolecules* **2008**, *41*, 2309.

(13) Ota, Y.; Ito, S.; Kuroda, J.; Okumura, Y.; Nozaki, K. *J. Am. Chem. Soc.* **2014**, *136*, 11898.

(14) Jian, Z.; Wucher, P.; Mecking, S. *Organometallics* **2014**, *33*, 2879.

(15) Contrella, N. D.; Jordan, R. F. *Organometallics* **2014**, *33*, 7199.

(16) Wucher, P.; Goldbach, V.; Mecking, S. *Organometallics* **2013**, *32*, 4516.

(17) Neuwald, B.; Falivene, L; Caporaso, L.; Cavallo, L.; Meching, S. *Chem.—Eur. J.* **2013**, *19*, 17773.

(18) Piche, L.; Daigle, J. C. Rehse, G.; Claverie, J. P. *Chem.—Eur. J.* **2012**, *18*, 3277.

(19) Skupov, K. M.; Marella, P. R.; Simard, M.; Yap, G. P. A.; Allen, N.; Conner, D.; Goodall, B. L.; Claverie, J. P. *Macromol. Rapid Commun.* **2007**, *28*, 2033.

(20) Wu, Z.; Chen, M.; Chen, C. *Organometallics* **2016**, *35*, 1472.

(21) Wada, S.; Jordan, R.F. *Angew. Chem.* **2017**, *129*, 1846.

(22) Gaikwad, S. R.; Deshmukh, S. S.; Gonnade, R. G.; Rajamohanan, P. R.; Chikkali, S. H. *ACS Macro Lett.* **2015**, *4*, 933.

(23) Noda, S.; Nakamura, A.; Kochi, T.; Chung, L. W.; Morokuma, K.; Nozaki, K. *J. Am. Chem. Soc.* **2009**, *131*, 14088.

(24) Haras, A.; Anderson, G. D. W.; Michalak, A.; Rieger, B.; Ziegler, T. *Organometallics* **2006**, *25*, 4491.

(25) Nozaki, K.; Kusumoto, S.; Noda, S.; Kochi, T.; Chung, L. W.; Morokuma, K. *J. Am. Chem. Soc.* **2010**, *132*, 16030.

(26) Britovsek, G. J. P.; Gibson, V. C.; Wass, D. F. *Angew. Chem., Int. Ed.* **1999**, *38*, 428.

(27) Gibson, V. C.; Spitzmesser, S. K. *Chem. Rev.* **2003**, *103*, 283.

(28) Ittel, S. D.; Johnson, L. K.; Brookhart, M. *Chem. Rev.* **2000**, *100*, 1169.

(29) Camacho, D. H.; Guan, Z. *Chem. Commun.* **2010**, *46*, 7879.

(30) Franssen, N. M. G.; Reek, J. N. H.; de Bruin, B. *Chem. Soc. Rev.* **2013**, *42*, 5809.

(31) Mu, H.; Pan, L.; Song, D.; Li, Y. *Chem. Rev.* **2015**, *115*, 12091.

(32) Kim, Y.; Jordan, R. F. *Organometallics* **2011**, *30*, 4250.

(33) Gott, A. L.; Piers, W. E.; Dutton, J. L.; McDonald, R.; Parvez, M. *Organometallics* **2011**, *30*, 4236.

(34) Zhang, Y.; Cao, Y.; Leng, X.; Chen, C.; Huang, Z. *Organometallics* **2014**, *33*, 3738.

(35) Jian, Z.; Falivene, L.; Wucher, P.; Roesle, P.; Caporaso, L.; Cavallo, L.; Gottker-Schnetmann, I.; Mecking, S. *Chem. Eur. J.* **2015**, *21,* 2062.

(36) Jian, Z.; Mecking, S. *Macromolecules* **2016**, *49*, 4057.

(37) Carrow, B. P.; Nozaki, K. *J. Am. Chem. Soc.* **2012**, *134*, 8802.

(38) Carrow, B. P.; Nozaki, K. *Macromolecules* **2014**, *47*, 2541.

(39) Contrella, N. D.; Sampson, J. R.; Jordan, R. F. *Organometallics* **2014**, *33*, 3546.

(40) Sui, X.; Dai, S.; Chen, C. *ACS Catal.* **2015**, *5*, 5932.

(41) Data from reference 9. Conditions: 1 μmol Pd, 0.5 h, 48 mL of toluene, 2 mL of dichloromethane, 9 atm.

(42) Goodey, N. M.; Benkovic, S. J. *Nature Chemical Biology* **2008**, *4*, 474.

(43) Cornish-Bowden, A. *FEBS Journal* **2014**, *281*, 621.

(44) Tsai, C.-J.; Nussinov, R. *PLoS Comput. Biol.* **2014**, *10*, e1003394.

(45) Motlagh, H. N.; Wrabl, J. O.; Li, J.; Hilser, V. J. *Nature* **2014**, *508*, 331.

(46) Blanco, V.; Leigh, D. A.; Marcos, V. *Chem. Soc. Rev.* **2015**, *44*, 5341.

(47) Kovbasyuk, L.; Krämer, R. *Chem. Rev*. **2004**, *104*, 3161.

(48) Wiester, M. J.; Ulmann, P. A.; Mirkin, C. A.; Wasielewski, M. R.; Mirkin, C. A. *Angew. Chem. Int. Ed.* **2011**, *50*, 114.

(49) Dydio, P.; Rubay, C.; Gadzikwa, T.; Lutz, M.; Reek, J. N. H. *J. Am. Chem. Soc.* **2011**, *133*, 17176.

(50) Mon, I.; Jose, D. A.; Vidal-Ferran, A. *Chem. Eur. J.* **2013**, *19*, 2720.

(51) McGuirk, C. M.; Stern, C. L.; Mirkin, C. A. *J. Am. Chem. Soc*. **2014**, *136*, 4689.

(52) Marcos, V.; Stephens, A. J.; Jaramillo-Garcia, J.; Nussbaumer, A. L.; Woltering, S. L.; Valero, A.; Lemonnier, J. F.; Vitorica-Yrezabal, I. J.; Leigh, D. A. *Science* **2016**, *352*, 155.

(53) Kovbasyuk, L.; Pritzkow, H.; Krämer, R.; Fritsky, I. O. *Chem. Commun.* **2004**, 880.

(54) McGuirk, C. M.; Mendez-Arroyo, J.; d'Aquino, A. I.; Stern, C. L.; Liu, Y.; Mirkin, C. A. *Chem. Sci.* **2016**, *7*, 6674.

(55) Tseng, K. T.; Kampf, J. W.; Szymczak, N. K. *ACS Catal.* **2015**, *5,* 411.

(56) Gianneschi, N. C.; Bertin, P. A.; Nguyen, S. T.; Mirkin, C. A.; Zakharov, L. N.; Rheingold, A. L. *J. Am. Chem. Soc.* **2003**, *125*, 10508.

(57) Kita, M. R.; Miller, A. J. M. *J. Am. Chem. Soc.* **2014**, *136*, 14519.

(58) McGuirk, C. M.; Mendez-Arroyo, J.; Lifschitz, A. M.; Mirkin, C. A. *J. Am. Chem. Soc.* **2014**, *136*, 16594.

(59) Lifschitz, A. M.; Young, R. M.; Mendez-Arroyo1, J.; Stern, C. L.; McGuirk, C. M. *Nat. Commun.* **2015**, *6*, 6541.

(60) Smith, A. J.; Kalkman, E. D.; Gilbert, Z. W.; Tonks, I. A. *Organometallics* **2016**, *35*, 2429.

(61) Chen, M.; Zou, W.; Caib, Z.; Chen, C. *Polym. Chem.* **2015**, *6*, 2669.

(62) Komon, Z. J. A.; Bu, X.; Bazan, G. C. *J. Am. Chem. Soc.* **2000**, *122*, 1830.

(63) Komon, Z. J. A.; Bu, X.; Bazan, G. C. *J. Am. Chem. Soc.* **2000**, *122*, 12379.

(64) Lee, B. Y.; Bazan, G. C.; Vela, J.; Komon, Z. J. A.; Bu, X. *J. Am. Chem. Soc.* **2001**, *123*, 5352.

(65) Lee, B. Y.; Bu, X.; Bazan, G. C. *Organometallics* **2001**, *20*, 5425.

(66) Boardman, B. M.; Bazan, G. C. *Acc. Chem. Res.* **2009**, *42*, 1597.

(67) Lee, B. Y.; Kim, Y. H.; Shin, H. J.; Lee, C. H. *Organometallics* **2002**, *21*, 3481.

(68) Shim, C. B.; Kim, Y. H.; Lee, B. Y.; Dong, Y.; Yun, H. *Organometallics* **2003**, *22*, 4272.

(69) Shim, C. B.; Kim, Y. H.; Lee, B. H.; Shin, D. M.; Chung, Y. K. *J. Organomet. Chem.* **2003**, *675*, 72.

(70) Kim, Y. H.; Kim, T. H.; Lee, B. Y.; Woodmansee, D.; Bu, X.; Bazan, G. C. *Organometallics* **2003**, *21*, 3082.

(71) Boardman, B. M.; Valderrama, J. M.; Munoz, F.; Wu, G.; Bazan, G. C.; Rojas, R. *Organometallics* **2008**, *27*, 1671.

(72) Chen, Y.; Boardman, B. M.; Wu, G.; Bazan, G. C. *J. Organomet. Chem.* **2007**, *692*, 4745.

(73) Azoulay, J. D.; Rojas, R. S.; Serrano, A. V.; Ohtaki, H.; Galland, G. B.; Wu, G.; Bazan, G. C. *Angew. Chem. Int. Ed.* **2009**, *48*, 1089.

(74) Azoulay, J. D.; Koretz, Z. A.; Wu, G.; Bazan, G. C. *Angew. Chem. Int. Ed.* **2010**, *49*, 7890.

(75) Kwon, H. Y.; Lee, S. Y.; Lee, B. Y.; Shin, D. M.; Chung, Y. K. *Dalton Trans*. **2004**, 921.

(76) Chen, Y.; Wu, G.; Bazan, G. C. *Angew. Chem. Int. Ed.* **2005**, *44*, 1108.

(77) Boardman, B. M.; Wua, G.; Rojas, R.; Bazan, G. C. *J. Organomet. Chem.* **2009**, *694*, 1380.

(78) Kim, Y. H.; Kim, T. H.; Lee, B. Y.; Woodmansee, D.; Bu, X.; Bazan, G. C. *Organometallics* **2002**, *21,* 3082.

(79) Kim, Y. H.; Kim, T. H.; Kim, N. Y.; Cho, E. S.; Lee, B. Y.; Shin, D. M.; Chung, Y. K. *Organometallics* **2003**, *22,* 1503.

(80) Cai, Z.; Shen, Z.; Zhou, X.; Jordan, R. F. *ACS Catal.* **2012**, *2*, 1187.

(81) Reisinger, C. M.; Nowack, R. J.; Volkmer, D.; Rieger, B. *Dalton Trans.* **2007**, 272.

(82) Ellis, D. D.; Harrison, G.; Orpen, A. G.; Phetmung, H.; Pringle, P. G.; deVries, J. G.; Oevering, H. *J. Chem Soc, Dalton Trans.* **2000**, 671.

(83) Zhuuang, R.; Xu, J.; Cai, Z.; Tang, G.; Fang, M.; Zhao, Y. *Org. Lett.* 2011, *13*, 2110.

(84) Krawczyk, H. *Syn. Comm.* **1997**, *27*, 3151.

(85) Zhou, X.; Lau, K.; Petro, B. J.; Jordan, R. F. *Organometallics* **2014**, *33*, 7209.

(86) Conley, M. P. Jordan, R. F. *Angew. Chem., Int. Ed.* **2011**, *50*, 3744.

(87) Flack, H.D. *Helvetica Chimica Acta* **2003**, *86*, 905.

(88) Chen, Y.; Metz, M. V.; Li, L.; Stern, C. L.; Marks, T. J. *J. Am. Chem. Soc.* **1998**, *120*, 6287.

(89) Binding, S. C.; Zaher, H.; Chadwick, F. M.; O'Hare, D. *Dalton Trans.,* **2012**, *41*, 9061.

(90) Chen, Y.; Stern, C. L.; Yang, S.; Marks, T. J. *J. Am. Chem. Soc.* **1996**, *118*, 12451.

(91) Massey, A. G.; Park, A. J. *J. Organomet. Chem.* **1966**, *5*, 218.

(92) Beckett, M. A.; Brassington, D. S.; Coles, S. J.; Hursthouse, M. B. *Inorg. Chem. Commun.* **2000**, *3*, 530.

(93) Komon, Z. J. A.; Bazan, G. C.; Fang, C.; Bu, X. *Inorg. Chim. Acta*. **2003**, *345*, 95.

(94) Sivaev, I. B.; Bregadze, V. I. *Coord. Chem. Rev.* **2014**, *270−271*, 75.

(95) Mendez, M.; Cedillo, A. *Comput. Theor. Chem.* **2013**, *1011*, 44.

(96) Jacobsen, H.; Berke, H.; Doring, S.; Kehr, G.; Erker, G.; Frohlich, R.; Meyer, O. *Organometallics* **1999**, *18*, 1724.

(97) De Graaf, W.; Boersma, J.; Smeets, W. J. J.; Spek, A. L.; Van Koten, G. *Organometallics* **1989**, *8*, 2907.

Chapter Three

Ethylene Polymerization Behavior of Palladium(II) Alkyl Complexes that Contain Phosphine-monoalkyl Phosphonate Ligands

3.1 Introduction

The polymerization behavior of (PO)Pd-type complexes is highly dependent on modifications to the PO^- ligand structure, as described in Chapters One and Two. Recently, modification of the weak donor group to phosphorus-containing groups has been effective at improving catalyst activity and increasing polymer MW.[1–4] The phosphine-phosphonamide complex **B** (Chart 2.1, Chapter Two) is one of most active (PO)Pd-type catalysts for ethylene polymerization (6000 kg mol^{-1} h^{-1}, 80 ^oC) reported to date and also produces PE with high MW (130,000 Da).[4] Coordination of $B(C_6F_5)_3$ to PO-type Pd complexes has also been an effective method for improving catalytic activity[5] and, with phosphine-phosphinate Pd complex **G**, also increases PE MW (Chart 2.1, Chapter Two).[6] In this chapter, the reactivity of (PPO)PdMeL (**3a–c**), (PPO)PdMe(lut) (**4a-lut**) and $\{(PPO{\bullet}B(C_6F_5)_3)PdMe\}_2$ (**5a,b**) with ethylene (Chart 3.1), and kinetic studies of ethylene polymerization by **5a/5a'** are described. The synthesis and characterization of **3a–c**, **4a-lut**, and **5a,b** were described in Chapter Two.

Chart 3.1. New (Phosphine-monoalkyl phosphonate)PdR complexes

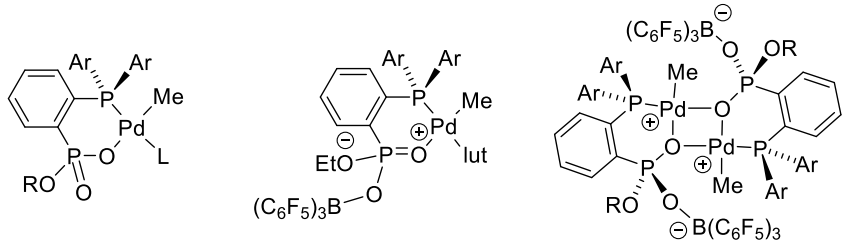

3a-lut: R= Et, Ar = Ph **4a-lut** **5a**
3a-py: R = Et, Ar = Ph **5b**
3b-lut: R= ^{i}Pr, Ar = Ph
3b-py: R= ^{i}Pr, Ar = Ph
3c-py: R= ^{i}Pr, Ar = 2-OMe-Ph

3.2 Results and Discussion

Ethylene polymerization. Ethylene polymerization studies of complexes **3a–c**, **4a-lut** and **5a/b** are summarized in Table 3.1. Complexes **3a-lut/py** and **3b-lut/py** exhibit very low activity for ethylene polymerization (1.8–3.5 kg mol^{-1} h^{-1}) and produce PE with M_n < 5340 Da (Table 3.1, entries 1, 3, 8, 9). Complex **3c-py**, which contains a PAn_2 unit in the PPO^- ligand, is somewhat more active (9.8 kg mol^{-1} h^{-1}) and produces PE with M_n = 9030 Da (entry 11), but the performance of all of these catalysts is quite poor relative to that of analogous (PO)PdRL catalysts.[7,8] Polymerizations run for a longer time with **3a-lut** (entry 2) retained approximately the same activity indicating that these catalysts are reasonably stable under the polymerization conditions. These findings indicate that the catalytic ability of (PPO)PdR complexes is innately poor, consistent with previous results for catalysts bearing a phosphine-phosphinate ligand, including **G** (entry 15).[6,9,10]

However, coordination of $B(C_6F_5)_3$ to **3a-lut** significantly increases the catalytic activity and the MW of the PE product. The $B(C_6F_5)_3$ adduct **4a-lut** exhibits activity of 50 kg mol^{-1} h^{-1} and produce PE with M_n of 7260 Da (entry 5). The activity of **4a-lut** can be further increased 7-fold by adding a second equiv of $B(C_6F_5)_3$ to trap the 2,6-lutidine *in situ* or by using the isolated base-free, borane-coordinated dimer **5a/5a'** (entries 6 and 7 vs. 5). The M_n and α-olefin content (i.e. the polymer microstructure) of the PEs produced by **4a-lut**+$B(C_6F_5)_3$ and **5a/5a'** are similar to those observed in the absence of the additional borane, which implies that the second equiv of $B(C_6F_5)_3$ traps the 2,6-lutidine but does not otherwise affect the active catalytic species. Similar though less pronounced effects on activity and MW are observed in ethylene polymerization by **3a-py** + 2 BF_3•Et_2O, which is expected to form the BF_3-coordinated {**2a**•BF_3}PdMe(Et_2O) species and BF_3•py *in situ* (entry 4 vs 6 and 7).[11] Replacement of the ethoxy group of **5a**/**5a'** by the isopropoxy group in **5b** results in a ca. 65% increase in both the catalyst activity and the MW of the PE product (entry 10 vs 7). The catalyst **3c-py** + 2 $B(C_6F_5)_3$, which is expected to generate a base-free, borane-coordinated {**2c**•$B(C_6F_5)_3$}PdMe species analogous to **5a/5a'** and **5b** *in situ*, displays high activity (3390 kg mol^{-1} h^{-1}) and produces PE with M_n > 90,000 Da (entry 12).

Table 3.1. Ethylene polymerization by (PPO)PdMeL and {PPO•$B(C_6F_5)_3$}PdMeL catalysts[a]

Entry	Catalyst	$B(C_6F_5)_3$ (equiv)	Act.[b]	M_n[c]	PDI[c]	T_m (°C)[d]
1[e]	**3a-lut**	0	3.5	3350	1.84	129.2
2[e]	**3a-lut**[f]	0	2.0	2620	1.81	128.1
3[e]	**3a-py**	0	2.4	1480	1.90	124.3
4[e]	**3a-py**[g]	0	248	4140	2.03	132.6
5[e]	**4a-lut**	0	50	7260	1.98	132.2

Table 3.1, continued.

6[e]	**4a-lut**	1	335	7910	1.91	132.8
7[e]	**5a/5a'**[h]	0	308	6370	2.23	132.1
8[e]	**3b-lut**	0	2.1	5340	1.38	131.0
9[e]	**3b-py**	0	1.8	1360	1.65	123.4
10[e]	**5b**[h,i]	0	529	10300	1.86	133.2
11[e]	**3c-py**	0	9.8	9030	1.34	131.2
12[e]	**3c-py**[h]	2	3390	91200	2.11	135.9
13	**3c-py**[h]	4	5330	96400	2.21	137.0
14	**3c-py**[h]	8	5700	99200	2.14	136.1
15	**G**	0	0.7	1340	1.35	120.0
16[e]	**H**	0	35	7770	1.71	128.5
17[e]	**H**	1	175	6670	1.98	128.6

[a] Conditions: 50 mL toluene, 10 μmol Pd, 80 °C, 410 psi ethylene, 2 h, unless otherwise noted. [b] Activity in kg mol^{-1} h^{-1}. [c] Determined by GPC. [d] Determined by DSC. [e] Average of at least two reactions. [f] 28 μmol Pd, 450 psi, 21 h. [g] 2 equiv BF_3•Et_2O added. [h] 0.88 μmol Pd. [i] 450 psi.

Based on previous studies of {PO•$B(C_6F_5)_3$}PdR borane adducts, it is probable that some dissociation of the borane occurs under the dilute concentration and high temperature conditions of ethylene polymerization reactions described above.[5] When excess $B(C_6F_5)_3$ (4 or 8 equiv) is added to **3c-py**-catalyzed ethylene polymerizations to counteract this effect, the activity and MW of the PE are increased further to 5700 kg mol^{-1} h^{-1} and 99,200 Da (entries 13 and 14).

The **3c-py**+8 $B(C_6F_5)_3$ catalyst is one of the most active (PO)PdR-type catalysts reported to date that also produces high-MW PE (Table 3.2). The base-free borane adduct generated from (*o*-P(2-Et-Ph)$_2$-*p*-toluenesulfonate)PdMe(py) + 4 $B(C_6F_5)_3$ exhibits similar activity but produces PE with low MW (entry 2).[5] Other **A**-type catalysts exhibit either high activity (entries

3,6,7,8)[1,12–14] or produce PE with high MW (entries 4 and 5).[15,16] Under similar conditions to those reported here, the phosphine-phosphonamide complex is the most comparable to **3c-py**+8 $B(C_6F_5)_3$ in terms of both activity and MW (entry 9).[4]

Table 3.2. Examples of high-performance PO-type catalysts for ethylene polymerization.

Entry	Complex	Act.[a]	M_n
1	**3c-py** + 8 $B(C_6F_5)_3$	5700	99200
2[b]	(*o*-P(2-Et-Ph)$_2$-*p*-toluenesulfonate)PdMe(py) + 4 $B(C_6F_5)_3$	5650	2520
3[c]	(*o*-(P^{t}BuPh)-benzenesulfonate)PdMe(lut)	4714	14600
4[d]	(*o*-P(menthyl)$_2$-benzenesulfonate)PdMe(lut)	205	169000
5[e]	(*o*-P(2',6'-(OMe)$_2$-2-biphenyl)$_2$-benzenesulfonate)PdMe(lut)	1040	227000
6[f]	(*o*-P(2',6'-(OMe)$_2$-2-biphenyl)$_2$-benzenesulfonate)PdMe	5330	29000
7[g]	(*o*-PAn$_2$-naphthalenesulfonate)PdMe(dmso)	3900	16000
8[h]	[{*o*-(P^{i}Pr$_2$)C$_6$H$_4$(P(O)^{t}Bu$_2$}Pd(κ^2-*o*-acetanilido)]$^+$ [B(3,5-(CF$_3$)$_2$-Ph)$_4$]$^-$	2800	29000
9[i]	[{*o*-(PAn$_2$)C$_6$H$_4$(P(O)-(N(^{i}Pr)$_2$)Ph)}PdMe(dmso)]$^+$ [B(3,5-(CF$_3$)$_2$-Ph)$_4$]$^-$	3500	190000

[a]Activity in kg mol^{-1} h^{-1}. [b]Conditions: 50 mL toluene, 1.0 μmol Pd, 435 psi ethylene, 80 °C, 1 h, reference [**5**]. [c]Conditions: 200 mL toluene, 6.5 μmol Pd, 300 psi ethylene, 85 °C, 1 h, reference [**12**]. [d]Conditions: 100 mL toluene, 10 μmol Pd, 435 psi ethylene, 80 °C, 1 h, reference [**15**]. [e]Conditions: 5 μmol Pd L^{-1}, 300 psi ethylene, 80 °C, 1 h, reference [**16**]. [f]Conditions: 100 mL toluene, 4 μmol Pd, 5 bar ethylene, 80 °C, 0.5 h, reference [**13**]. [g]Conditions: 48 mL toluene, 2 mL CH_2Cl_2, 0.4 μmol Pd, 9 atm ethylene, 90 °C, 1 h, reference [**14**]. [h]15 mL toluene, 0.75 μmol Pd, 435 psi ethylene, 100 °C, 1 h, reference [**1**]. [i]Conditions: 48 mL toluene, 2 mL CH_2Cl_2, 1 μmol Pd, 132 psi ethylene, 80 °C, 1 h, reference [**4**].

The (PPO)PdR and {PPO•$B(C_6F_5)_3$}PdR catalysts reported here all produce linear PE with one olefin unit per saturated chain-end. The olefins comprise a mixture of terminal (17–46%) and internal (54–83%) olefins (see Experimental Section). The internal olefins were

characterized as 2-(60%), 3-(25%) and 4+-olefins (15%) by $^{13}C\{^{1}H\}$ NMR. To investigate whether these catalysts can isomerize α-olefins, 1-nonene was added to **3b-py** and **5b**-catalyzed ethylene polymerizations. No isomerization of the 1-nonene was detected by GC/MS analysis of the reaction mixtures. This result provides strong evidence that the internal olefins are formed during chain growth and not by post-polymerization isomerization of terminal olefins. These observations imply that (PPO)PdR and {PPO•B(C_6F_5)$_3$}PdR complexes can chain walk, but chain transfer is favored over insertion/growth for the resulting secondary alkyl species.

Influence of ethylene pressure. The ethylene polymerization behavior of **5a/5a'** was studied over a range of ethylene pressures from 50 to 850 psi. In this range, the activity of **5a/5a'** remains constant, with an average value of 306 kg mol^{-1} h^{-1} (Figure 3.1). This result is consistent with the catalyst resting state being the {PPO•B(C_6F_5)$_3$}PdR(CH_2=CH_2) species.[17] Low temperature NMR experiments of **5a/5a'** in the presence of ethylene indicate there is fast exchange of the free and bound ethylene so the bound ethylene resonance is not observed. However, a NOESY correlation between ethylene and the –OC*H*(CH_3)$_2$ group of the ligand at 243 K indicates the {PPO•B(C_6F_5)$_3$}PdR(CH_2=CH_2) species is present (Figure 3.4, Experimental Section). In contrast, the MW of the PE product increases over this pressure range, with M_w increasing from 11870 to 15900 Da (Figure 3.2).

Figure 3.1. Effect of ethylene pressure on activity in ethylene polymerization by **5a**/**5a'**. Conditions: 50 mL toluene, 0.88 μmol Pd, 80 °C, 2 h. Each data point represents the average of two runs with error bars indicating high and low values.

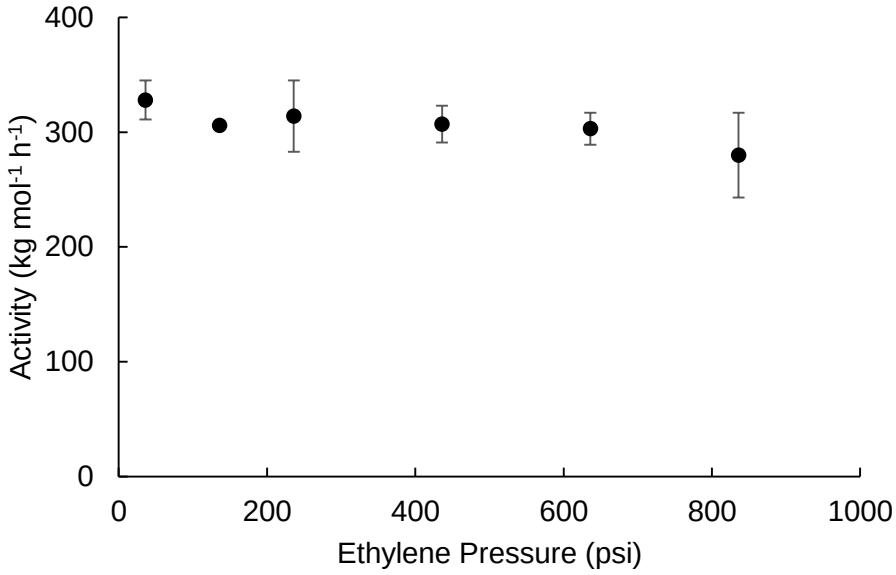

Figure 3.2. Effect of ethylene pressure on the MW of PE produced by **5a**/**5a'**. M_n data are shown as triangles and M_w data are shown as circles. Conditions: 50 mL toluene, 0.88 μmol Pd, 80 °C, 2 h. Each data point represents the average of two runs with error bars indicating high and low values. Molecular weights were determined by GPC.

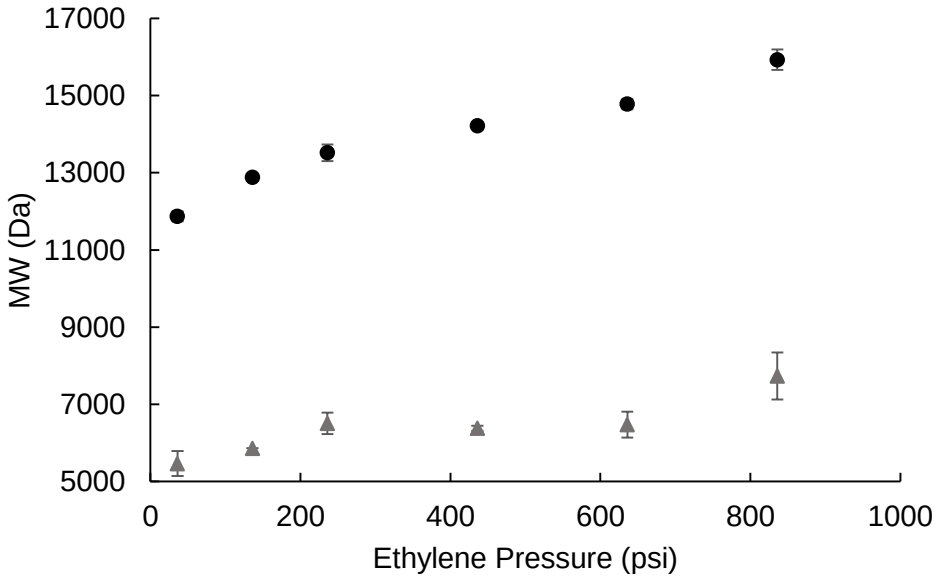

The PE MW is determined by the $R_{growth}/R_{transfer}$ ratio (Eq. 3.1). The chain growth pathway and several possible chain transfer mechanisms for ethylene polymerization by **5a/5a'** are shown in Scheme 3.1. As noted above, the observation that activity is independent of ethylene pressure, i.e. R_{growth} is zero order in ethylene concentration (Eq 3.2), implies that the {PPO•B(C_6F_5)$_3$}PdR(CH_2=CH_2) species **J** is the catalyst resting state. A commonly assumed chain transfer process (mechanism 1) is β-H elimination from **J** followed by dissociation of the unsaturated polymer chain. The rate of this chain transfer process ($R_{transfer,1}$) is zero order in ethylene concentration (Eq 3.3). Alternatively, chain transfer can occur through base-free species **K**, formed by dissociation of ethylene from **J**. From **K**, chain transfer can occur by β-H elimination to form Pd(olefin)(H) species **L**, followed by replacement of the unsaturated polymer chain by ethylene. Assuming pre-equilibrium conditions and k_4 as the rate-determining and irreversible step (mechanism 2), the rate of this chain transfer process ($R_{transfer,2}$) is inverse first order in ethylene concentration (Eq. 3.4; see Experimental Section). If β-H elimination by **J** is reversible and substitution of the unsaturated polymer chain of **L** by ethylene occurs by a dissociative mechanism (mechanism 3), the rate of chain transfer ($R_{transfer,3}$) is also inverse first order in ethylene concentration (Eq 3.5). Finally, if β-H elimination by **K** is reversible and substitution of the unsaturated polymer chain of **L** by ethylene occurs by an associative mechanism (mechanism 4), the rate of chain transfer ($R_{transfer,4}$) is zero order in ethylene concentration (Eq 3.6). Mechanisms 1 and 4 are considered to be associative chain transfer

processes because their rates are independent of ethylene concentration, and mechanisms 2 and 3 are considered to be dissociative chain transfer processes because their rates are inverse first order in ethylene concentration.[18,19]

The increase in MW with increasing ethylene pressure observed for ethylene polymerization by **5a/5a'** indicates that dissociative mechanisms 2 and/or 3 contribute to chain transfer in this system. A similar dependence of MW on ethylene pressure has been observed for (PO)PdR catalysts bearing bulky biaryl, menthyl, or *tert*-butyl substituents on the phosphine unit.[18] DFT computational studies showed that dissociative chain transfer mechanism 3 is competitive with associative chain transfer mechanism 4 for these sterically hindered catalysts, and this is probably the case for **5a**/**5a'** as well.

Additionally, the percentage of olefins that are internal (vs. terminal) in the PE decreases from 60 to 15% as the ethylene pressure is raised from 410 to 850 psi. This result is consistent with a standard chain walking mechanism initiated by 2,1 insertion of intermediate **L** in Scheme 3.1.

Scheme 3.1. Possible chain transfer mechanisms for PO-type catalysts.

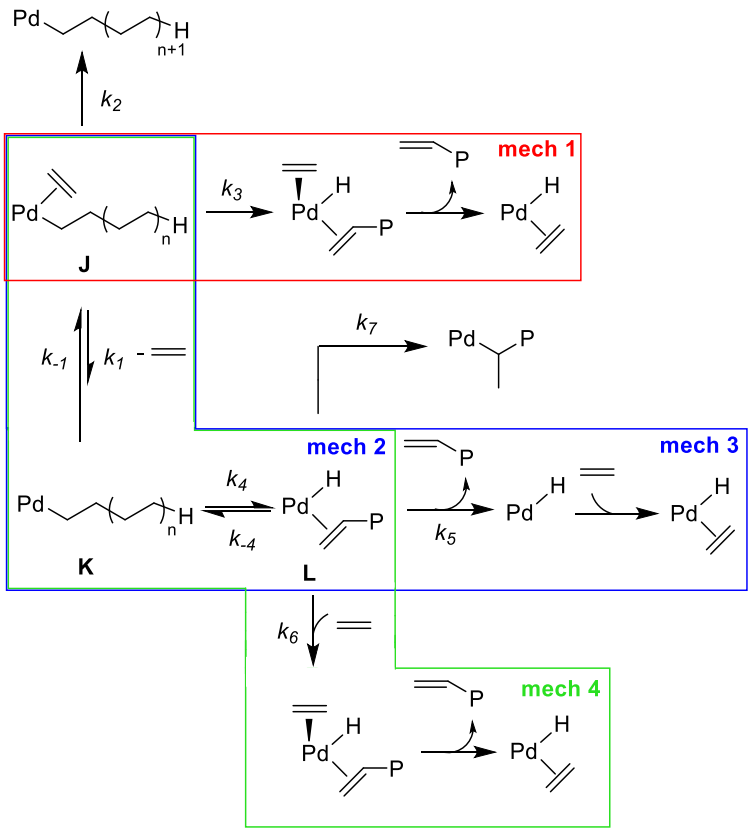

$$M_n = \frac{R_{growth} \cdot 28}{R_{transfer}} \qquad \textbf{Eq. 3.1}$$

$$R_{growth} = k_2[\mathbf{J}] \qquad \textbf{Eq. 3.2}$$

$$R_{transfer,1} = k_3[\mathbf{J}] \qquad \textbf{Eq. 3.3}$$

$$R_{transfer,2} = k_4[\mathbf{K}] = k_4 K_1[\mathbf{J}][C_2H_4]^{-1} \qquad \textbf{Eq. 3.4}$$

$$\text{Where } K_1 = \frac{[\mathbf{K}][C_2H_4]}{[\mathbf{J}]}$$

$$R_{transfer,3} = k_5[\mathbf{L}] = k_5 K_1 K_4[\mathbf{J}][C_2H_4]^{-1} \qquad \textbf{Eq. 3.5}$$

$$\text{Where } K_4 = \frac{[\mathbf{L}]}{[\mathbf{K}]}$$

$$R_{transfer,4} = k_6 K_1 K_4 [\mathbf{J}] \qquad \textbf{Eq. 3.6}$$

Influence of $B(C_6F_5)_3$ on R_{growth} and $R_{transfer}$. The data in Table 3.1 show that the ethylene polymerization performance of (PPO)PdRL catalysts is significantly improved by the binding of $B(C_6F_5)_3$ to the PPO^- ligand. This section addresses this issue in more detail. The rates of chain growth (R_{growth}, R'_{growth}) and chain transfer ($R_{transfer}$, $R'_{transfer}$) for a pair of ethylene polymerization catalysts (cat, cat') are related by Eq. 3.7, where X_n and X'_n are the corresponding number average degrees of polymerization of the PE products. Here we assume that growth rates are equal to activities. X_n data are obtained by GPC analysis ($X_n = M_n/28$). As summarized in Table 3.3, conversion of (PPO)PdRL species to {PPO•$B(C_6F_5)_3$}PdRL adducts results in large increases in R_{growth} and smaller increases in $R_{transfer}$ (column I, entries 1–4). Conversion of {PPO•$B(C_6F_5)_3$}PdRL species to base-free {PPO•$B(C_6F_5)_3$}PdR species further increases R_{growth} and $R_{transfer}$, in this case by a similar amount since the structure of the active {PPO•$B(C_6F_5)_3$}PdR(ethylene) species is not changed (column II). Overall, conversion of a (PPO)PdRL catalyst to a {PPO•$B(C_6F_5)_3$}PdR catalyst results in a substantial increases in both R_{growth} (up to 580-fold) and the $R_{growth}/R_{transfer}$ ratio (up to 11-fold, column III).

$$\frac{R'_{transfer}}{R_{transfer}} = \frac{X_n R'_{growth}}{X'_n R_{growth}} \qquad \textbf{Eq. 3.7}$$

The allosteric binding of $B(C_6F_5)_3$ to (PPO)PdR complexes exerts a significant electronic effect on the catalytic site. $B(C_6F_5)_3$ coordination weakens the donor ability of the PPO^- ligand and converts the neutral (PPO)PdMeL complex to a zwitterionic $\{PPO•B^-(C_6F_5)_3\}Pd^+MeL$ species with increased positive charge at the Pd center.[20] The facile decoordination of 2,6-lutidine from **3a-lut** but not the corresponding $B(C_6F_5)_3$ adduct **4a-lut** in CD_2Cl_2 solution underscores the enhanced electrophilic character at Pd in the latter cases. Based on Mecking's studies of {P(2-OMe-4-X-Ph)$_2$benzenesulfonate}PdMe(dmso) ethylene polymerization catalysts, for which electron-withdrawing X substituents increase activity and decrease the PE MW,[21] and studies of zwitterionic and cationic (PO)PdRL-type catalysts,[5,22–26] the increased charge at Pd in $\{PPO•B^-(C_6F_5)_3\}Pd^+MeL$ species is expected to increase both R_{growth} and $R_{transfer}$, which is observed.

The steric effects of $B(C_6F_5)_3$ binding to (PPO)PdRL complexes are more subtle. Analysis of X-ray structural and Sambvca plots[27] (see Experimental section) for the three sets of structurally characterized complexes – **G**/**H**, **3a-lut**/**4a-lut**/**5a'** and **3b-lut**/**5b** − shows that, in each case, the borane coordination results in a small increase in steric crowding of one axial face, a small decrease in steric crowding of the opposite axial face and a small increase in lateral steric crowding, but little change in the buried volume ($\%V_{bur}$; see Experimental section). The C1–Pd1–N1 angles can be used to assess lateral steric pressure but appear to be influenced by packing forces in these complexes. The presence of a CH_2Cl_2 solvent molecule in the mouth of

the C1–Pd1–N1 angle in **G**, an intermolecular π-stacking interaction between 2,6-lutidine ligands (3.78 Å intercentroid distance) in **3a-lut**, and an intermolecular π-stacking interaction between a C_6F_5 ring and 2,6-lutidine ring (4.0 Å intercentroid distance) in **H** likely influence the C1–Pd1–N1 angles in these complexes and complicate comparison of these parameters. However, in the two structurally-characterized pairs of catalysts for which the allosteric effect is most pronounced, **G**/**H** and **3b-lut**/**5b**, the $B(C_6F_5)_3$ "effector" induces significant changes in the conformation of the (PPO)Pd chelate rings and generates π-stacking interactions that may rigidify the structure and influence reactivity. The observation that conversion of **3a-py** to the {**2a**•$B(C_6F_5)_3$}PdR or {**2a**•BF_3}PdR species results in similar increases in R_{growth} (128 and 103-fold respectively) and the $R_{growth}/R_{transfer}$ ratio (4.3 and 2.8-fold, respectively) for the two cases is consistent a primarily electronic origin for these effects as the Lewis acidities of BF_3 and $B(C_6F_5)_3$.[28–33] Assuming that, for **3c-py**, R_{growth} and $R_{transfer}$ are both increased by a factor of 6 by generation of the base-free species (cf. results for **G** and **3a-lut**), R_{growth} and $R_{transfer}$ are increased by a ca. factor of 100 and 10 respectively by coordination of $B(C_6F_5)_3$ to the PPO^- ligand, which at 80 °C corresponds to $\Delta\Delta G^{\neq}$ of 1.1 kcal mol^{-1}. Given that the $\Delta\Delta G^{\neq}$ values associated with these allosteric effects are quite small (< 2 kcal mol^{-1}) further studies will be required to explain their origin in more detail.

The large increase in R_{growth} and comparatively smaller increase in $R_{transfer}$ resulting from $B(C_6F_5)_3$ binding to (PPO)PdRL catalysts (Table 3.3, entries 1–4) contrasts with the smaller

increase in R_{growth} and larger increase in $R_{transfer}$ observed for (PO)PdRL phosphine-sulfonate catalysts (entries 5,6).[5,7] This difference has the important consequence that $B(C_6F_5)_3$ binding substantially increases both activity and PE MW for (PPO)PdRL catalysts, but only moderately increases activity and substantially *decreases* PE MW for (PO)PdRL catalysts. The smaller increase in $R_{transfer}$ upon $B(C_6F_5)_3$ binding to (PPO)PdRL catalysts vis-à-vis (PO)PdRL catalysts likely reflects the operation of a dissociative chain transfer mechanism in the former case, since the increased charge on Pd in the $\{PPO{\bullet}B^{-}(C_6F_5)_3\}Pd^{+}H(olefin)$ adduct **L** should inhibit olefin dissociation. Similar allosteric effects may be anticipated for other catalysts that undergo dissociative chain transfer.

Table 3.3. Proportional increases in R_{growth} and $R_{transfer}$ in (PPO)PdMeL ethylene polymerization catalysts resulting from conversion of (PPO)PdRL to $\{PPO{\bullet}B(C_6F_5)_3\}$PdRL borane adducts (column I), conversion of $\{PPO{\bullet}B(C_6F_5)_3\}$PdRL to base-free $\{PPO{\bullet}B(C_6F_5)_3\}$PdR species (column II) and overall conversion of (PPO)PdRL to $\{PPO{\bullet}B(C_6F_5)_3\}$PdR species (column III), and comparative data for (PO)PdRL and (PO)Ni(allyl) catalysts.

		I Formation of $B(C_6F_5)_3$ adduct		**II Formation of base-free species**		**III Formation of base-free $B(C_6F_5)_3$ adduct**	
Entry	Complex	R_{growth}	$R_{transfer}$	R_{growth}	$R_{transfer}$	R_{growth}	$R_{transfer}$
1	**G**	50	8.6	5	5.8	250	50
2	**3a-lut**	14	6.6	6.7	6.1	88	48
3	**3b-lut**	-	-	-	-	250	130
4	**3c-py**	-	-	-	-	580	53

Table 3.3, continued.

5	(*o*-P(3,5-^{t}Bu$_2$-Ph)$_2$-*p*-toluenesulfonate)PdMe(py)[a]	4.3	80	-	-	-	-
6	(*o*-P(2-Et-Ph)$_2$-*p*-toluene-sulfonate)PdMe(py)[a,b]	3.6	42	5.3	3.4	19	140

[a]Conditions: 50 mL toluene, 1.0 μmol Pd, 435 psi ethylene, 80 °C, 1 h, reference [**5**]. [b]Conditions: 50 mL toluene, 2.0 μmol Pd, 435 psi, 80 °C, 1 h, reference [**7**].

3.3 Conclusion

Remote binding of $B(C_6F_5)_3$ to (PPO)PdMeL or {(PPO)PdMe}$_2$ ethylene polymerization catalysts that contain phosphine-arenephosphinate or phosphine-arenephosphonate ligands significantly increases the catalyst activity and the molecular weight of the PE product. In the most favorable case, *in situ* conversion of (**2c**)PdMe(py) to the base-free adduct {**2c**•$B(C_6F_5)_3$}PdMe increases the ethylene polymerization activity from 9.8 to 5700 kg mol^{-1} h^{-1} and the M_n of the PE product from 9030 to 99,200 Da (80 °C, 410 psi). X-ray structural data, trends in ligand lability and comparative studies of BF_3 activation suggest that these allosteric effects are primarily electronic in origin. The $B(C_6F_5)_3$ binding enhances R_{growth} by increasing the degree of positive charge on the Pd center. This effect does not result in the large increase in $R_{transfer}$ and concomitant reduction in PE molecular weight seen in previous studies of analogous (PO)PdRL catalysts that contain phosphine-arene*sulfonate* ligands, because of the operation of a dissociative chain transfer process, which is inhibited by the increased charge at Pd. This allosteric strategy for enhancing catalyst performance may be generally applicable to other

catalysts that undergo dissociative chain transfer.

3.4 Experimental Section

General Procedures. All experiments were performed under a nitrogen atmosphere or vacuum using drybox or Schlenk techniques. Nitrogen was purified by passage over Q-5 oxygen scavenger and activated molecular sieves. Methylene chloride, diethyl ether and THF were dried by passage over activated alumina. Pentane was purified by passage over BASF R3-11 oxygen scavenger and activated alumina. $B(C_6F_5)_3$ was donated by Boulder Scientific.

NMR spectra were acquired on Bruker DRX-500 or DRX-400 spectrometers at ambient temperature unless otherwise indicated. ^{1}H and ^{13}C chemical shifts are reported relative to $SiMe_4$ and are internally referenced to residual ^{1}H and ^{13}C solvent resonances.

Ethylene Homopolymerization. Polymerization reactions were run in a stainless steel Parr 300 mL autoclave, which was equipped with a mechanical stirrer, thermocouple, water cooling loop, and a Parr 4842 controller. In a glovebox, the catalyst was weighed directly into a 200 mL glass autoclave liner. When applicable, $B(C_6F_5)_3$ was also weighed directly into the liner. Toluene (50 mL) was added, and the liner was placed in a stainless steel autoclave, which was sealed and removed from the glovebox. The autoclave was heated to 80 °C and then pressurized with ethylene while the contents were stirred at 170 rpm. After 2 h, the autoclave was cooled to 25 °C and vented. Acetone (50 mL) was added to precipitate the polymer. The polymer was collected by filtration, rinsed with acetone, and dried overnight in a vacuum oven.

The oligomer content of the filtrate was determined by GC-MS and ^{1}H NMR analysis. For polymerizations with $B(C_6F_5)_3$•Et_2O and BF_3•Et_2O, the catalyst and activator were injected in a 10 mL toluene solution after the autoclave was heated and pressurized with ethylene.

Table 3.4. Detailed ethylene homopolymerization data.

entry	complex	Pd (μmol)	pressure (psi)	$B(C_6F_5)_3$ (equiv)	yield (g)	T_m (°C)[b]	M_w (Da)[c]	PDI[c]	α-olefin[d]
1	**3a-lut**	10	410	0	0.07	128.9	5790	1.70	34
2	**3a-lut**	10	410	0	0.04	129.9	5880	1.52	46
3	**3a-lut**	10	410	0	0.06	130.0	6300	1.52	
4	**3a-lut**	10	410	0	0.12	128.1	5670	2.34	
5	**3a-lut**[e]	28	450	0	1.20	128.1	4740	1.81	
6	**3a-py**	10	410	0	0.03	123.1	2470	2.02	25
7	**3a-py**	10	410	0	0.07	125.1	3150	1.80	
8	**3a-py**	10	410	0	0.05	124.7	2830	1.89	
9	**3a-py**	10	410	2[f]	254	134.6	14200	1.91	
10	**3a-py**	10	410	0[g]	256	133.4	9910	2.13	
11	**3a-py**	10	410	0[g]	240	131.8	7030	1.94	
12	**4a-lut**	10	410	0	1.01	131.7	13900	1.89	25
13	**4a-lut**	10	410	0	0.92	132.7	14800	2.06	
14	**4a-lut**	10	410	1	6.83	132.8	14500	1.80	17
15	**4a-lut**	10	410	1	7.04	132.7	15600	2.01	
16	**5a/5a'**	0.88	50	0	0.62	125.0	11700	2.28	
17	**5a/5a'**	0.88	50	0	0.56	127.9	12000	2.07	
18	**5a/5a'**	0.88	150	0	0.55	130.3	13300	2.14	
19	**5a/5a'**	0.88	250	0	0.50	132.2	13700	2.03	
20	**5a/5a'**	0.88	250	0	0.62	132.0	13300	2.13	
21	**5a/5a'**	0.88	450	0	0.51	132.6	14200	2.25	
22	**5a/5a'**	0.88	450	0	0.57	131.5	14200	2.21	
23	**5a/5a'**	0.88	650	0	0.51	133.7	14900	2.19	
24	**5a/5a'**	0.88	650	0	0.56	132.8	14600	2.39	
25	**5a/5a'**	0.88	850	0	0.56	133.9	15700	1.88	
26	**5a/5a'**	0.88	850	0	0.43	134.1	16200	2.27	85

Table 3.4, continued.

27	**3b-lut**	10	410	0	0.04	130.7	7310	1.43	
28	**3b-lut**	10	410	0	0.04	131.3	7420	1.33	
29	**3b-py**	10	410	0	0.03	122.7	2070	1.65	
30	**3b-py**	10	410	0	0.04	124.4	2430	1.65	
31	**5b**	0.88	410	0	1.01	132.6	18900	1.85	48
32	**5b**	0.88	410	0	1.03	133.9	19400	1.87	44
33	**3c-py**	10	410	0	0.19	131.6	10800	1.32	47
34	**3c-py**	10	410	0	0.20	130.7	13400	1.36	
35	**3c-py**	0.88	410	2	5.96	136.1	196200	2.17	
36	**3c-py**	0.88	410	2	5.99	135.7	188000	2.05	
37	**3c-py**	0.88	410	4	9.37	137.0	213000	2.21	
38	**3c-py**	0.88	410	8	10.0	136.1	212000	2.14	

[a]Conditions: solvent = 50 mL toluene, 80 °C, 2 h. [b]Determined by DSC. [c]Determined by GPC.[d] % Determined from ^{1}H NMR. [e]21 h. [f]2 equiv $B(C_6F_5)_3$•Et_2O added, injection method. [g]2 equiv BF_3•Et_2O added, injection method.

Polymer Characterization. Gel-permeation chromatography (GPC) data were obtained on a Polymer Laboratories PL-GPC 200 instrument with three PLgel 10 μm Mixed-B LS columns at 150 °C with 1,2,4-trichlorobenzene (stabilized with 125 ppm BHT) as the mobile phase. Molecular weights were calibrated using narrow polystyrene standards (ten-point calibration with M_n from 570 Da to 5670 kDa) and are corrected for linear polyethylene by universal calibration using the following Mark-Houwink parameters: polystyrene, K = 1.75 x 10^{-2} cm^3g^{-1}, α = 0.67; polyethylene, K = 5.90 x 10^{-2} cm^3g^{-1}, α = 0.69.[34] DSC measurements were performed on a TA Instruments 2920 differential scanning calorimeter. Samples (5 mg) were initially annealed by heating to 180 °C at 15 °C/min and cooling to 50 ℃ at 15 °C/min, and then analyzed by heating to 180 ℃ at 15 °C/min.

Figure 3.3. ^{1}H NMR spectrum of polyethylene produced by **5b**, Table 3.1, Entry 10 (393 K, dichlorobenzene-d_4, 500 MHz).

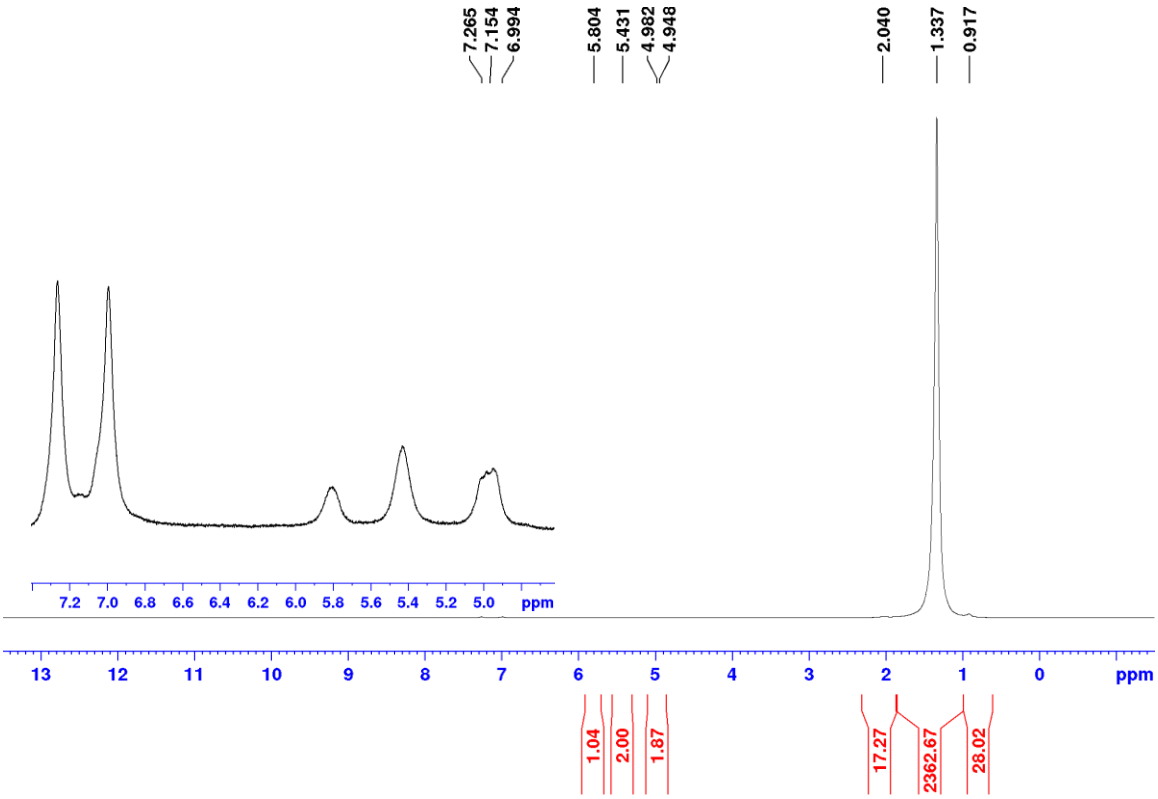

Figure 3.4. NOESY spectrum of **5a/5a'** in the presence of ethylene at 243 K.

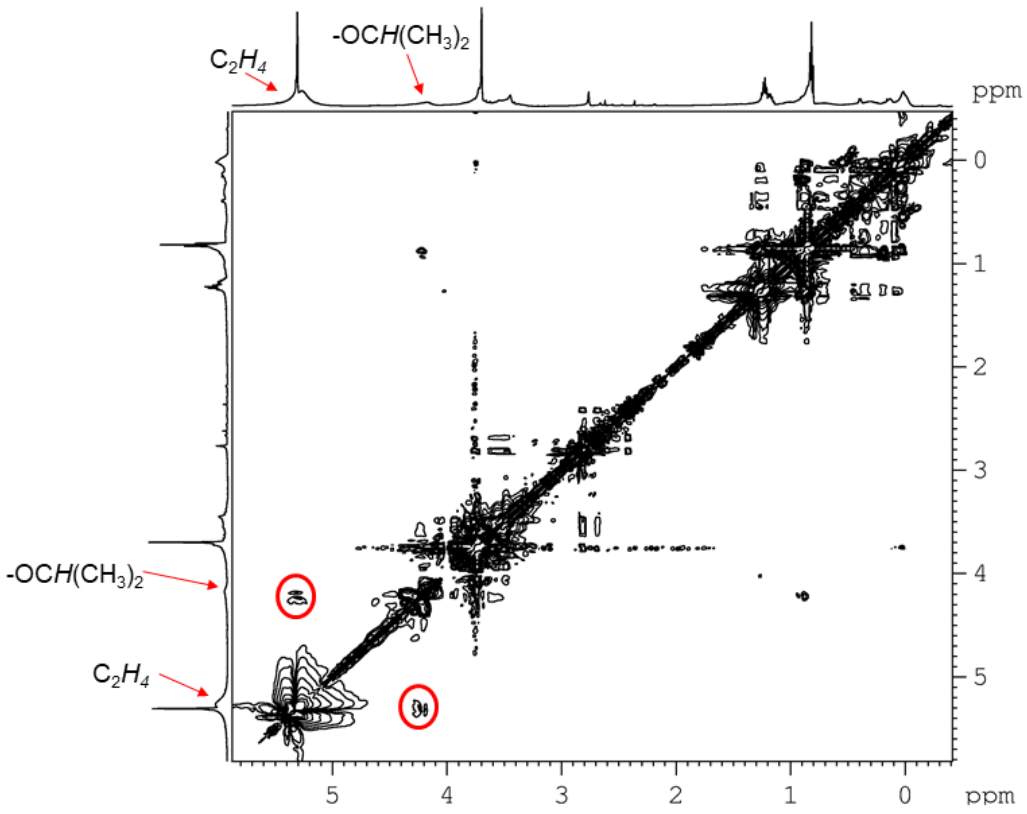

Kinetic Derivations for $R_{transfer,2}$, $R_{transfer,3}$, and $R_{transfer,4}$

Derivation for $R_{transfer,2}$. If k_4 is the rate-determining step,

$$R_{transfer,2} = k_4[\mathbf{K}]$$

And

$$K_1 = [\mathbf{K}][C_2H_4][\mathbf{J}]^{-1} \; ; \; [\mathbf{K}] = K_1[\mathbf{J}][C_2H_4]^{-1}$$

Then

$R_{transfer,2} = k_4[\mathbf{K}] = k_4K_1[\mathbf{J}][C_2H_4]^{-1}$.

Derivation for $R_{transfer,3}$. If K_1 and K_4 are reversible and k_5 is the rate-determining step,

$R_{transfer,3} = k_5[\mathbf{L}]$

And

$K_4 = [\mathbf{L}][\mathbf{K}]^{-1}$; $[\mathbf{L}] = K_4[\mathbf{K}]$

Then

$R_{transfer,3} = k_5[\mathbf{L}] = k_5K_4[\mathbf{K}]$

And

$K_1 = [\mathbf{K}][C_2H_4][\mathbf{J}]^{-1}$; $[\mathbf{K}] = K_1[\mathbf{J}][C_2H_4]^{-1}$

Then

$R_{transfer,3} = k_5K_4[\mathbf{K}] = k_5K_4K_1[\mathbf{J}][C_2H_4]^{-1}$.

Derivation for $R_{transfer,4}$. If K_1 and K_4 are reversible and k_6 is the rate-determining step,

$R_{transfer,3} = k_6[\mathbf{L}][C_2H_4]$

And

$K_4 = [\mathbf{L}][\mathbf{K}]^{-1}$; $[\mathbf{L}] = K_4[\mathbf{K}]$

Then

$R_{transfer,4} = k_6[\mathbf{L}][C_2H_4] = k_6K_4[\mathbf{K}][C_2H_4]$

And

$K_1 = [\mathbf{K}][C_2H_4][\mathbf{J}]^{-1}$; $[\mathbf{K}] = K_1[\mathbf{J}][C_2H_4]^{-1}$

Then

$R_{transfer,4} = k_6K_4[\mathbf{K}][C_2H_4] = k_6K_4K_1[\mathbf{J}]$.

Sample Calculations from Table 3.3:

Entry 1:

G:

R_{growth} = activity = 0.7 kg mol^{-1} h^{-1}

$R_{transfer} = R_{growth}X_n^{-1} = R_{growth} \times 28 \times M_n^{-1}$

= (0.7 kg mol^{-1} h^{-1}) × 28 × (1.340 kDa)$^{-1}$ = 14.6 h^{-1}

H:

R_{growth} = activity = 35 kg mol^{-1} h^{-1}

$R_{transfer} = R_{growth}X_n^{-1} = R_{growth} \times 28 \times M_n^{-1}$

= (35 kg mol^{-1} h^{-1}) × 28 × (7.770 kDa)$^{-1}$ = 126 h^{-1}

H + B(C_6F_5)$_3$:

R_{growth} = activity = 175 kg mol^{-1} h^{-1}

$R_{transfer} = R_{growth}X_n^{-1} = R_{growth} \times 28 \times M_n^{-1}$

$$= (175 \text{ kg mol}^{-1} \text{ h}^{-1}) \times 28 \times (6.670 \text{ kDa})^{-1} = 735 \text{ h}^{-1}$$

Column I: $R_{growth} = \frac{35 \text{ kg mol}^{-1}\text{h}^{-1}}{0.7 \text{ kg mol}^{-1}\text{h}^{-1}} = 50$; $R_{transfer} = \frac{126 \text{ h}^{-1}}{14.6 \text{ h}^{-1}} = 8.6$

Column II: $R_{growth} = \frac{175 \text{ kg mol}^{-1}\text{h}^{-1}}{35 \text{ kg mol}^{-1}\text{h}^{-1}} = 5$; $R_{transfer} = \frac{735 \text{ h}^{-1}}{126 \text{ h}^{-1}} = 5.8$

Column III: $R_{growth} = \frac{175 \text{ kg mol}^{-1}\text{h}^{-1}}{0.7 \text{ kg mol}^{-1}\text{h}^{-1}} = 250$; $R_{transfer} = \frac{735 \text{ h}^{-1}}{14.6 \text{ h}^{-1}} = 5$

Entry 4:

3c-py:

$$R_{growth} = \text{activity} = 9.8 \text{ kg mol}^{-1} \text{ h}^{-1}$$

$$R_{transfer} = R_{growth}X_n^{-1} = R_{growth} \times 28 \times M_n^{-1}$$

$$= (9.8 \text{ kg mol}^{-1} \text{ h}^{-1}) \times 28 \times (9.030 \text{ kDa})^{-1} = 30.4 \text{ h}^{-1}$$

3c-py + 8 $B(C_6F_5)_3$:

$$R_{growth} = \text{activity} = 5700 \text{ kg mol}^{-1} \text{ h}^{-1}$$

$$R_{transfer} = R_{growth}X_n^{-1} = R_{growth} \times 28 \times M_n^{-1}$$

$$= (5700 \text{ kg mol}^{-1} \text{ h}^{-1}) \times 28 \times (99.200 \text{ kDa})^{-1} = 1609 \text{ h}^{-1}$$

Column III: $R_{growth} = \frac{5700 \text{ kg mol}^{-1}\text{h}^{-1}}{9.8 \text{ kg mol}^{-1}\text{h}^{-1}} = 580$; $R_{transfer} = \frac{1609 \text{ h}^{-1}}{30.4 \text{ h}^{-1}} = 53$

SambVca plots[27]

Figure 3.5. Steric maps of (PPO)PdMeL and {PPO•B(C_6F_5)$_3$}PdMeL complexes (a) **G**, (b) **H**, (c) **3a-lut**, (d) **4a-lut**, (e) **5a'**, (f) **3b-lut**, and (g) **5b**. The Pd-atom is placed at the center of the xyz coordinate systems (top). The xz plane is placed in the Pd square plane with the x-axis bisecting the P1–Pd1–C1 angle and the z-axis bisecting the P1−Pd1−O1 angle. The y-axis is orthogonal to the square plane. The methyl, 2,6-lutidine, and Pd atoms are omitted.

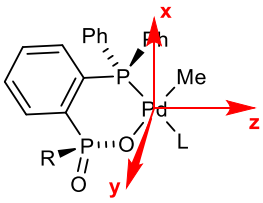

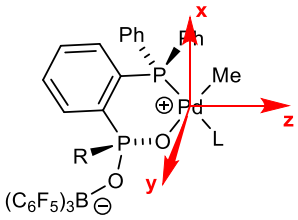

(a) **G** (b) **H**

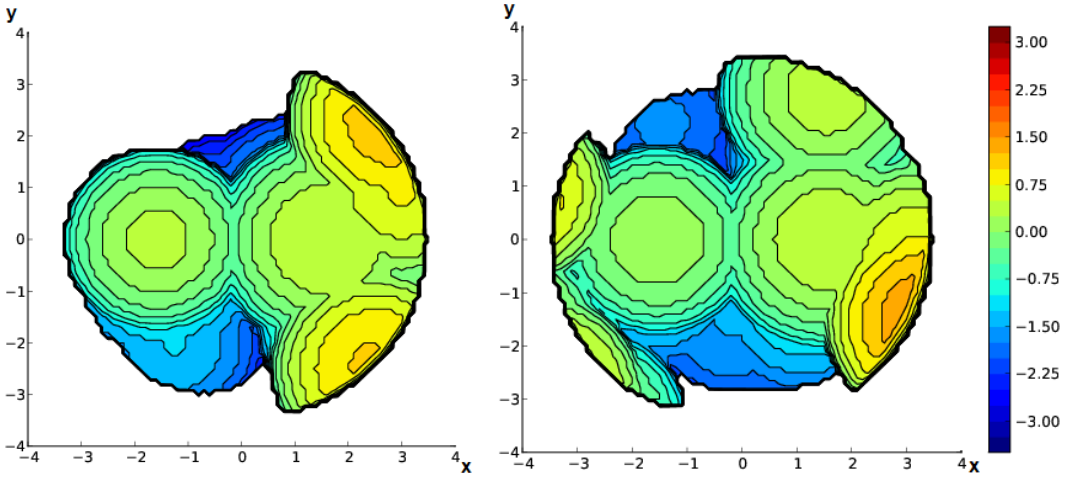

Figure 3.5, continued.

(c) **3a-lut**

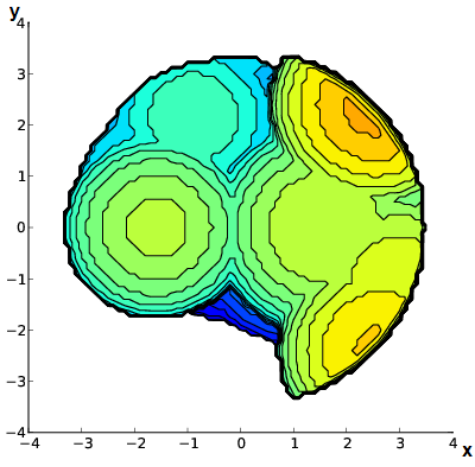

(d) **4a-lut**

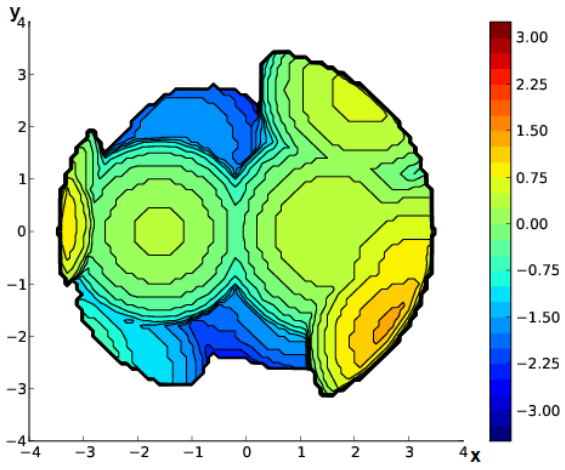

(e) **5a'**

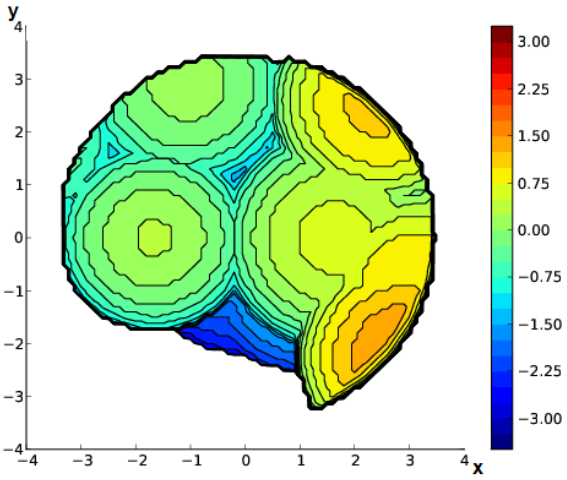

Figure 3.5, continued.

(f) **3b-lut** (g) **5b**

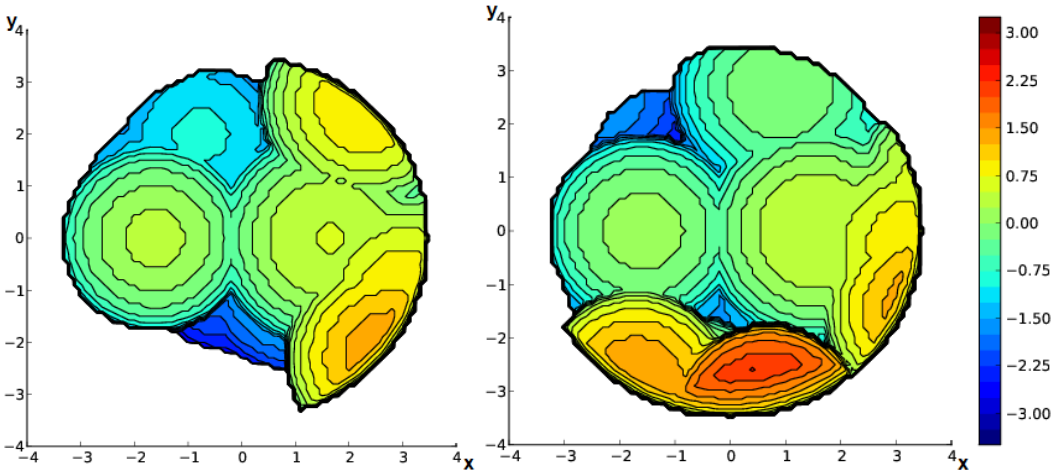

Figure 3.6. Steric maps of (PPO)PdMeL and {PPO•B(C_6F_5)$_3$}PdMeL complexes (a) **G**, (b) **H**, (c) **3a-lut**, (d) **4a-lut**, (e) **5a'**, (f) **3b-lut**, and (g) **5b**. The Pd-atom is placed at the center of the xyz coordinate systems (top).The xy plane is placed in the Pd square plane with the z-axis orthogonal to the xy-plane and passing through the Pd center. The y-axis passes through the Pd1–O1 bond and the x-axis passes through the Pd1–P1 bond. The 2,6-lutidine (except N1) and Pd1 atoms are omitted.

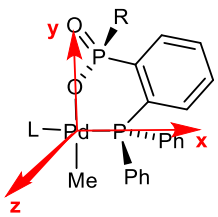

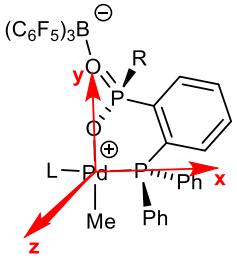

Figure 3.6, continued.

(a) **G**

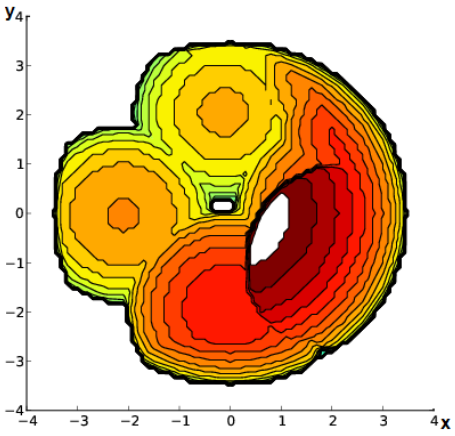

(b) **H**

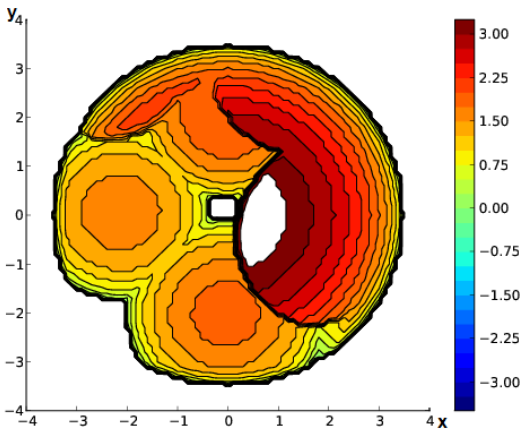

(c) **3a-lut**

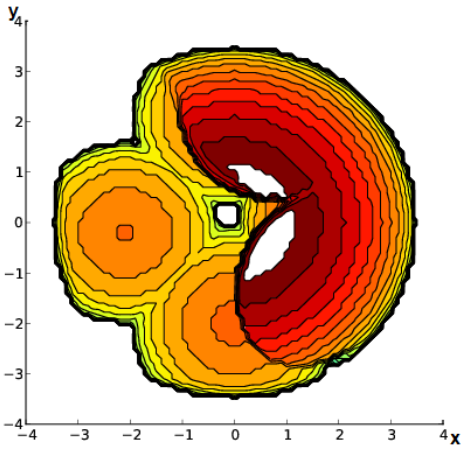

(d) **4a-lut**

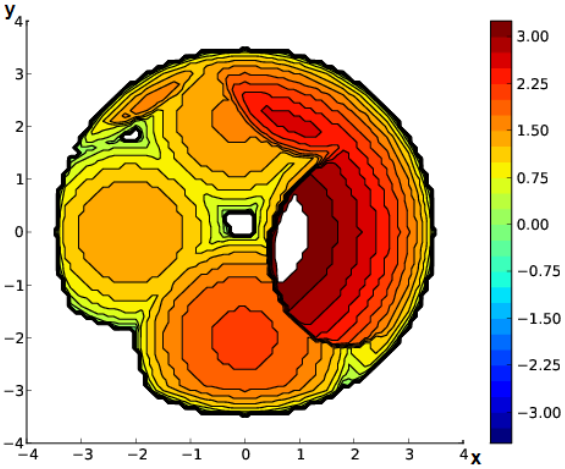

Figure 3.6, continued.

(e) **5a'**

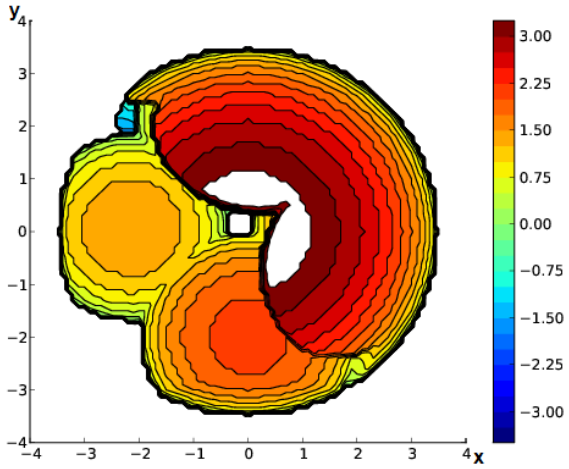

(f) **3a-lut**

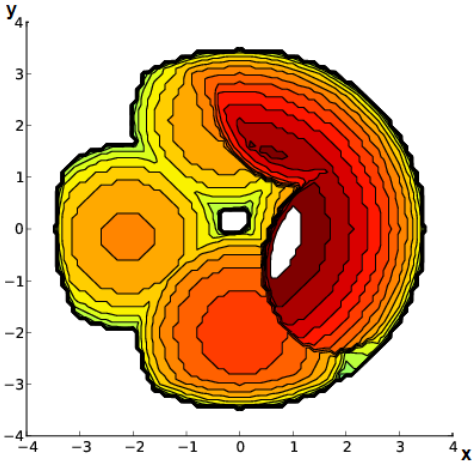

(g) **5b**

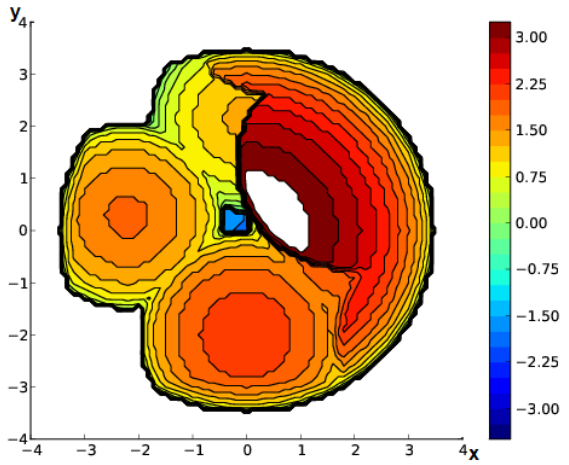

Figure 3.7. Steric maps of (PPO)PdMeL and {PPO•B(C_6F_5)$_3$}PdMeL complexes (a) **G**, (b) **H,** (c) **3a-lut**, (d) **4a-lut**, (e) **5a'**, (f) **3b-lut**, and (f) **5b**. The Pd-atom is placed at the center of the xyz coordinate system (right).The P1−Pd1−O1 plane is placed in the xy-plane with the z-axis orthogonal to the xy-plane and passing through the Pd center. The y-axis is through the Pd1–C1 bond and the x-axis is through the P1–Pd1 bond. The 2,6-lutidine (except N1) and Pd1 atoms are omitted.

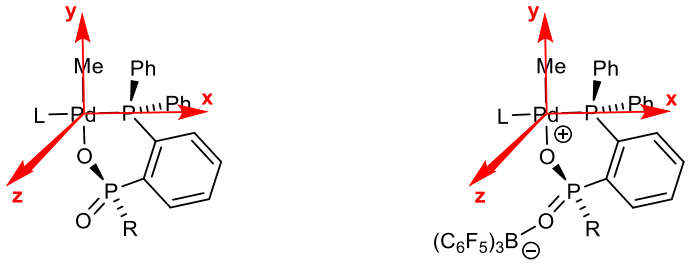

(a) **G** (b) **H**

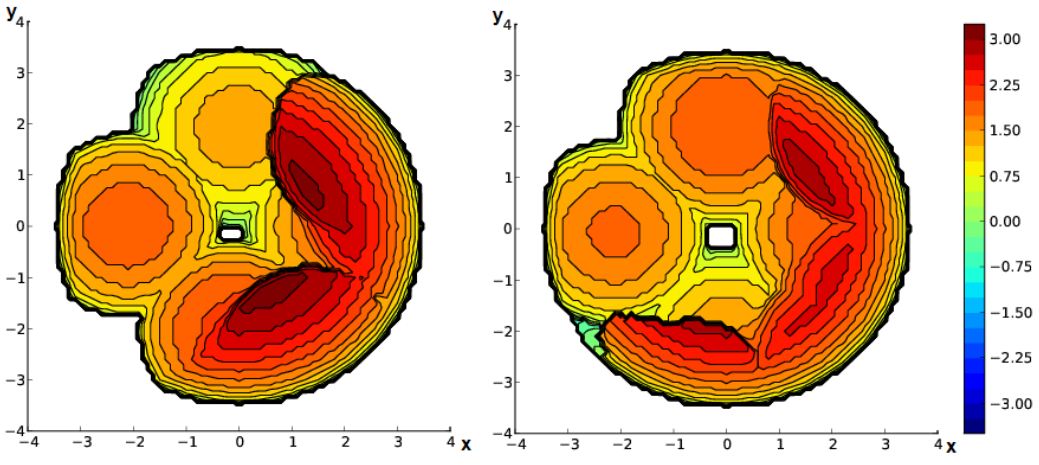

Figure 3.7, continued.

(c) **3a-lut**

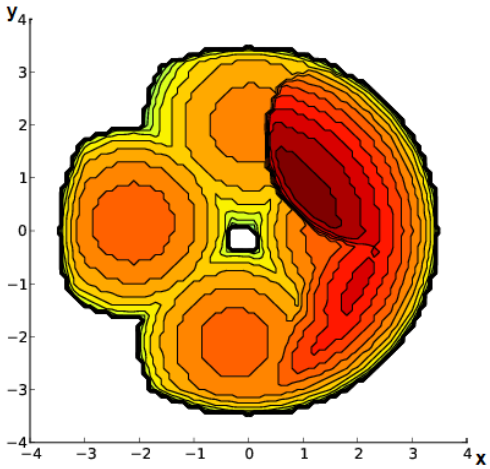

(d) **4a-lut**

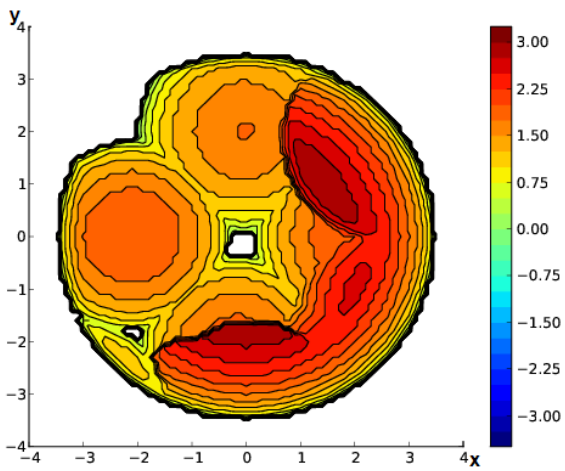

(e) **5a'**

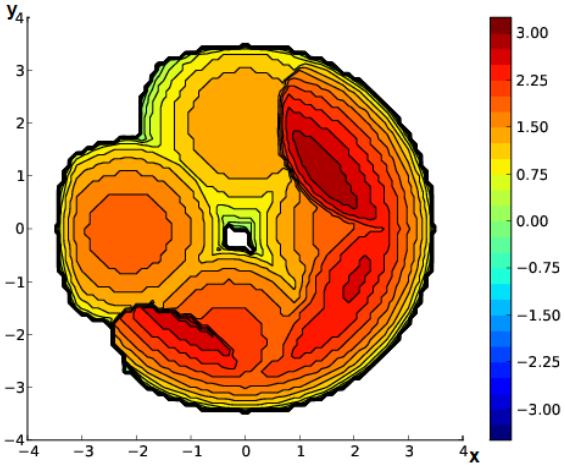

Figure 3.7, continued.

(f) **3b-lut** (g) **5b**

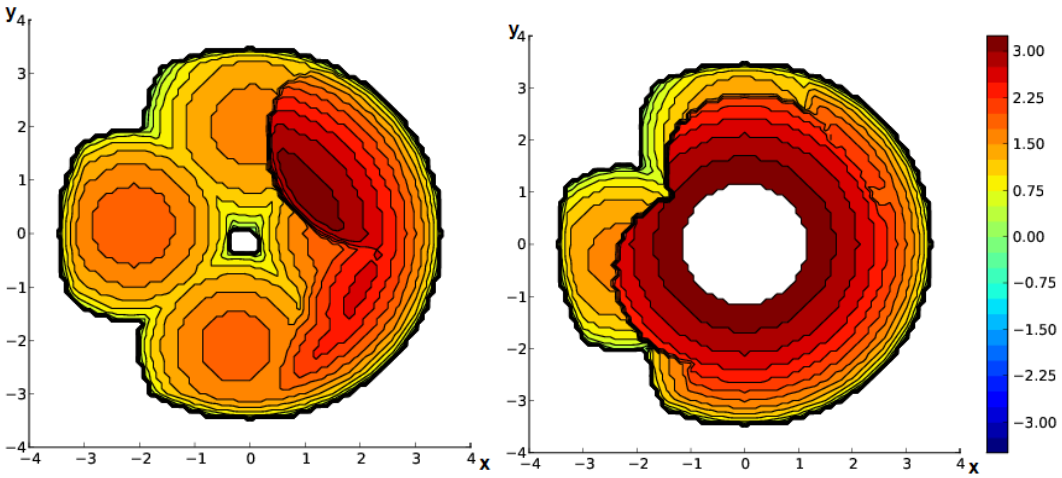

Buried Volume

Table 3.5. Buried volumes of (PPO)PdMeL and {PPO•B(C_6F_5)$_3$}PdMeL complexes.[27]

Complex	% V_{Free}	% V_{Bur}
G	57.6	42.4
H	55.7	44.3
3a-lut	55.4	44.6
4a-lut	56.7	43.3
5a'	53.2	46.8
3b-lut	55.8	44.2
5b	47.7	52.3

3.5 References and Notes

(1) Carrow, B. P.; Nozaki, K. *J. Am. Chem. Soc.* **2012**, *134*, 8802.

(2) Carrow, B. P.; Nozaki, K. *Macromolecules* **2014**, *47*, 2541.

(3) Contrella, N. D.; Sampson, J. R.; Jordan, R. F. *Organometallics* **2014**, *33*, 3546.

(4) Sui, X.; Dai, S.; Chen, C. *ACS Catal.* **2015**, *5*, 5932.

(5) Cai, Z.; Shen, Z.; Zhou, X.; Jordan, R. F. *ACS Catal.* **2012**, *2*, 1187.

(6) Johnson, A. M.; Contrella, N. D.; Sampson, J. R.; Zheng, M.; Jordan, R. F. *Organometallics* **2017**, *36*, 4990.

(7) Vela, J.; Lief, G. R.; Shen, Z.; Jordan, R. F. *Organometallics* **2007**, *26*, 6624.

(8) Shen, Z.; Jordan, R. F. *J. Am. Chem. Soc.* **2010**, *132*, 52.

(9) Reisinger, C. M.; Nowack, R. J.; Volkmer, D.; Rieger, B. *Dalton Trans.* **2007**, 272.

(10) Nowack, R. J. Neutral Nickel and Palladium Complexes as Catalysts in Copolymerizations of Polar and Non-Polar Monomers. Universitat Ulm, 2008.

(11) In a control ethylene polymerization, the catalyst **3a-py** + $2B(C_6F_5)_3$•Et_2O exhibited similar activity and produced PE with similar MW as **5a**/**5a'**, showing that the Et_2O has only a minimal effect on catalyst performance (see Experimental Section for details).

(12) Piche, L.; Daigle, J. C. Rehse, G.; Claverie, J. P. *Chem.—Eur. J.* **2012**, *18*, 3277.

(13) Neuwald, B.; Falivene, L; Caporaso, L.; Cavallo, L.; Mecking, S. *Chem.—Eur. J.* **2013**, *19*, 17773.

(14) Wu, Z.; Chen, M.; Chen, C. *Organometallics* **2016**, *35*, 1472.

(15) Ota, Y.; Ito, S.; Kuroda, J.; Okumura, Y.; Nozaki, K. *J. Am. Chem. Soc.* **2014**, *136*, 11898.

(16) Skupov, K. M.; Marella, P. R.; Simard, M.; Yap, G. P. A.; Allen, N.; Conner, D.; Goodall, B. L.; Claverie, J. P. *Macromol. Rapid Commun.* **2007**, *28*, 2033.

(17) Ittel, S. D.; Johnson, L. K.; Brookhart, M. *Chem. Rev.* **2000**, *100*, 1169.

(18) Nakano, R.; Chung, L. W.; Watanabe, Y.; Okuno, Y.; Okumura, Y.; Ito, S.; Morokuma, K.; Nozaki, K. *ACS Catalysis* **2016**, *6,* 6101.

(19) Noda, S.; Nakamura, A.; Kochi, T.; Chung, L. W.; Morokuma, K.; Nozaki, K. *J. Am. Chem. Soc.* **2009**, *131*, 14088.

(20) The Pd1–O1 distances of **H** and **4a-lut** are very similar to that in **A** (2.164(7) Å; R = Ph; L = py), which suggests that the donor ability of the borane-coordinated phosphinate/phosphonate group is similar to that of the sulfonate group. Piche, L.; Daigle, J-C.; Poli, R.; Claverie, J. P. *Eur. J. Inorg. Chem.* **2010**, 4595.

(21) Wucher, P.; Goldbach, V.; Mecking, S. *Organometallics* **2013**, *32*, 4516.

(22) Kim, Y.; Jordan, R. F. *Organometallics* **2011**, *30*, 4250.

(23) Gott, A. L.; Piers, W. E.; Dutton, J. L.; McDonald, R.; Parvez, M. *Organometallics* **2011**, *30*, 4236.

(24) Liu, W.; Malinoski, J. M.; Brookhart, M. *Organometallics* **2002**, *21*, 2836.

(25) Malinoski, J. M.; Brookhart, M. *Organometallics* **2003**, *22*, 5324.

(26) DiRenzo, G. M.; White, P. S.; Brookhart, M. *J. Am. Chem. Soc.* **1996**, *118*, 6225.

(27) Falivene, L.; Credendino, R.; Poater, A.; Petta, A.; Serra, L.; Oliva, R.; Scarano, V.; Cavallo, L. *Organometallics*, **2016**, *35*, 2286.

(28) Massey, A. G.; Park, A. J. *J. Organomet. Chem.* **1966**, *5*, 218.

(29) Beckett, M. A.; Brassington, D. S.; Coles, S. J.; Hursthouse, M. B. *Inorg. Chem. Commun*. **2000**, 3, 530.

(30) Komon, Z. J. A.; Bazan, G. C.; Fang, C.; Bu, X. *Inorg. Chim. Acta* **2003**, *345*, 95.

(31) Sivaev, I. B.; Bregadze, V. I. *Coord. Chem. Rev.* **2014**, 270-271, 75.

(32) Mendez, M.; Cedillo, A. *Computational and Theoretical Chemistry* **2013**, *1011*, 44.

(33) Jacobsen, H.; Berke, H.; Doring, S.; Kehr, G.; Erker, G.; Frohlich, R.; Meyer, O. *Organometallics* **1999**, *18*, 1724.

(34) Grinshpun, V.; Rudin, A. *Makrom. Chem., Rapid Commun.* **1985**, *6*, 219.

Chapter Four

Studies of the Self-Assembly of Multinuclear Palladium(II) Olefin Polymerization Catalysts

4.1 Introduction

Square planar (Li-OPO)PdMeL complexes (L = py or substituted py) that contain phosphine-*bis*-arenesulfonate (OPO^{2-}) ligands self-assemble to tetrameric structures in which four (Li-OPO)PdMeL units are arranged around the periphery of a central $Li_4S_4O_{12}$ double-four-ring (D4R) core (Scheme 4.1, **A**)[1,2] Complexes of type **A** polymerize ethylene to high-molecular weight polyethylene (PE; M_w > 1000 kDa) and incorporate higher levels of vinyl fluoride in ethylene/vinyl fluoride copolymerizations compared to monomeric (PO)PdMeL complexes that contain phosphine-*mono*-arenesulfonate (PO^-) ligands (Scheme 4.2).[3] However, under typical polymerization conditions (80 ^oC, dilute solution in toluene or slurry in hexanes), **A** partially dissociates to the monomeric (Li-OPO)PdMeL form, which produces PE with lower molecular weight (MW, M_w ~ 10 kDa). The mixture of active catalyst species results in a polyethylene product with a broad bimodal distribution of molecular weights and also makes mechanistic studies under polymerization conditions difficult.

Scheme 4.1. Pd-alkyl complexes containing phosphine-*bis*-arenesulfonate $(OPO)^{2-}$ ligands. The lower (Li-OPO)PdMe(py') units of **A** are denoted by "Pd".

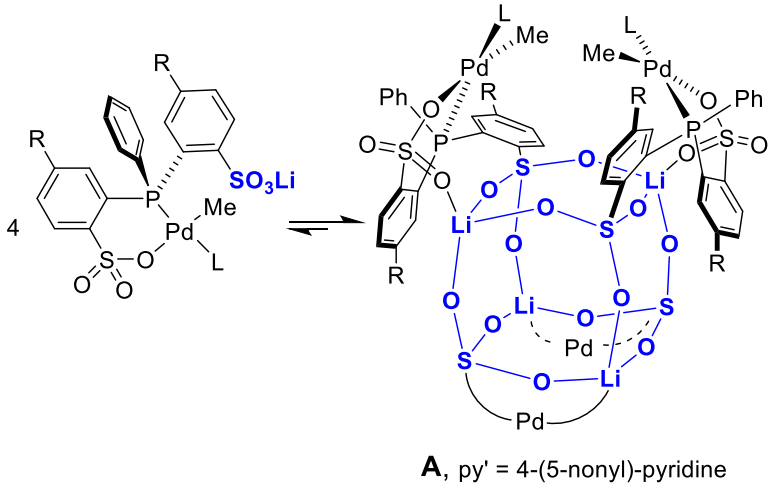

A, py' = 4-(5-nonyl)-pyridine

Scheme 4.2. Olefin polymerization by (PO)PdMeL and $\{(Li\text{-}OPO)PdMeL\}_4$ complexes.

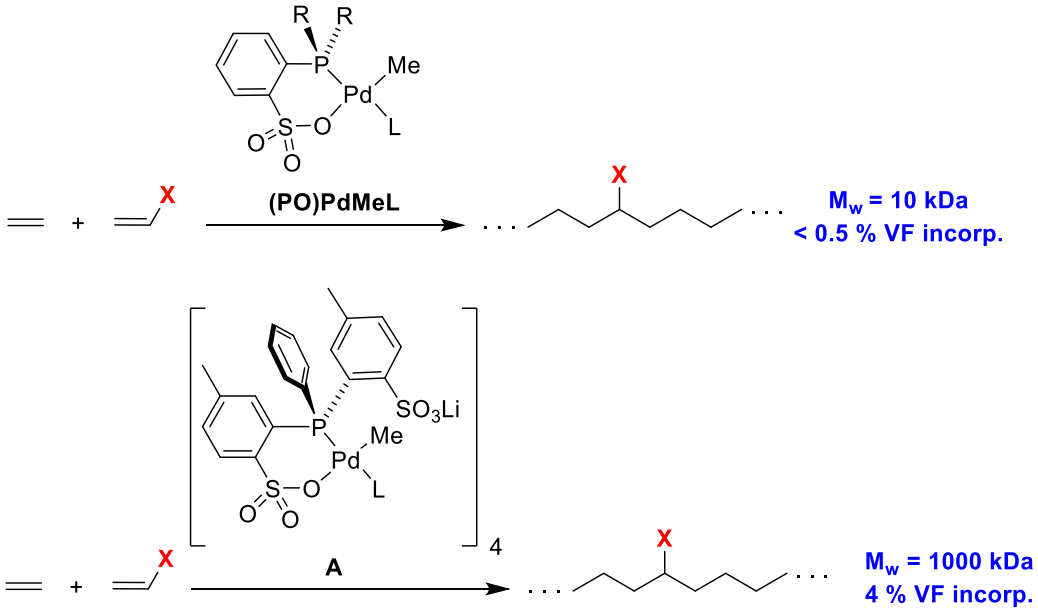

Recently our group reported that the reaction of the phosphine-bis-dimethoxybenzene sulfonate salt (Li_2[**1**]; Li_2[PPh(2-SO_3^--4,5-$(OMe)_2$-Ph)$_2$]) with (COD)PdMeCl results in the self-

assembly of an expanded cage with a central $Li_4S_4O_{12}$•Li_2Cl_2 core (**B**, Scheme 4.3).[4] Complex **B** is significantly more resistant to cage disassembly than **A** under polymerization conditions, and produces high MW PE with a narrow MW distribution (PDI = 2.3, 410 psi ethylene, hexanes solvent, 80 °C, 10 μmol Pd, 2 h).

A current goal in this area is to understand the factors that control the self-assembly process, in order to enable the design of highly robust cage catalysts whose olefin polymerization behavior and mechanisms can be explored without complications from cage disassembly.

Scheme 4.3. Synthesis of expanded $Li_4S_4O_{12}$•Li_2Cl_2 cage structure **B**. The lower (Li-OPO)PdMe(py') units are denoted by "Pd".

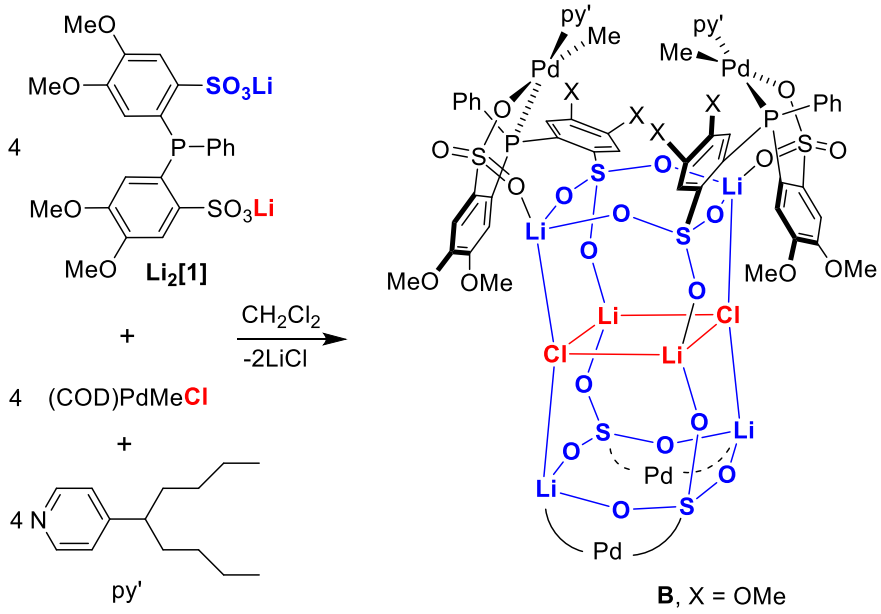

It has been proposed that a key factor that leads to the formation of expanded cage **B** in Scheme 4.3 is the presence of an OMe group *meta* to the sulfonate group on the arene rings,

which creates steric crowding on the cage periphery and prevents a smaller D4R cage like **A** from forming. In **A**, H10 and H17 in the *meta*-positions of the top Pd-bound and bottom non-Pd-bound *Ar*SO_3 groups are close in space to each other (Figure 4.1a). Replacement of those hydrogens with larger methoxy groups would require that the two arene rings be displaced from each other to avoid unreasonable steric crowding (Figure 4.1b). The incorporation of two LiCl units into the central cage of **B** elongates the cage sufficiently to accommodate the steric requirements of the *meta*-OMe groups. In contrast, the substituent that is *para* to the sulfonate group of the *Ar*SO_3 ring (Me in **A**, OMe in **B**) points away from the adjacent arene ring and does not influence the selection for assembly of **A**- or **B**-type structures. (Li-OPO)PdMeL complexes containing $(OPO)^{2-}$ ligands with *para*-R substituents (R = Me, ^{i}Pr, ^{t}Bu, or Cy) all self-assemble to D4R cage structures.[2]

This chapter describes synthetic studies that were undertaken to further probe the factors that influence cage self-assembly. First, the reaction of Li_2[**1**] with $[Pd(C_6H_4CH_2NMe_2)(\mu\text{-}OH)]_2$ in the absence of a chloride source was explored to test if a D4R cage (or some other structure) can form. Second, OPO^{2-} ligands with only a *para*- or *meta*-substituent were synthesized to see how each position individually affects cage self-assembly. Third, the generation of tetrameric Pd assemblies based on a $Li_4S_4O_{12}$•$Li_2(OAc)_2$ cage was explored to determine if the elongation of the cage in **B** can be achieved using other MX units besides LiCl. Finally, an OPO^{2-} ligand with *meta*-^{i}Pr substituents was synthesized to probe whether even more elongated cages with

$Li_4S_4O_{12}$•Li_2Br_2 cores could be generated to accommodate more sterically bulky $(Li\text{-}OPO)^-$ ligands.

Figure 4.1. (a) Space-fill view of **A** highlighting the close contacts between H17 of the Pd-bound arenesulfonate ring and H9 and H10 of the non-Pd-bound arenesulfonate ring (2.552 and 2.940 Å). (b) Space-fill view of **B** highlighting the close contacts between the methoxy groups of the arenesulfonate rings. For both structures, some H atoms and the 5-nonyl groups are omitted.

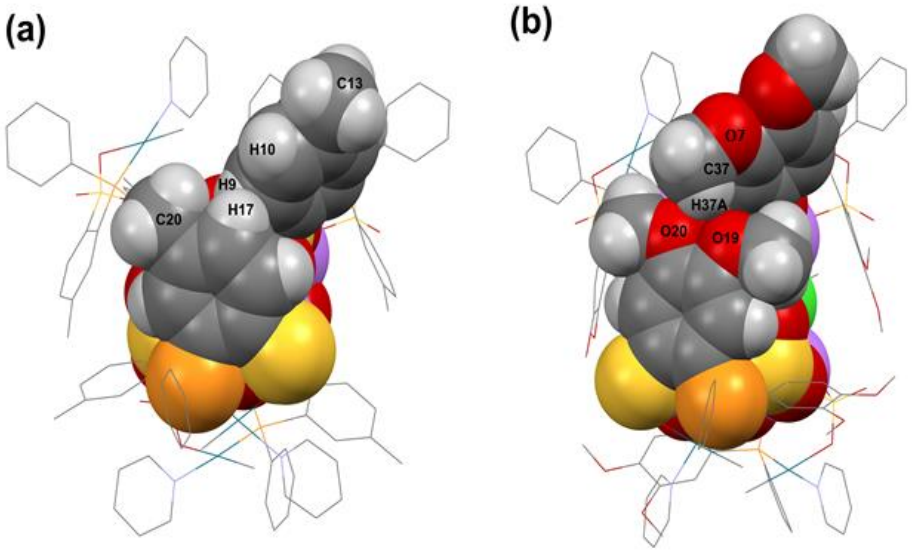

4.2 Results and Discussion

Can (Li-1)PdMeL self-assemble to a D4R cage structure form without chloride present? To investigate whether (Li-**1**)PdLX units can self-assemble to a D4R cage in the absence of a chloride source, Li_2[**1**] was reacted with $[(C_6H_4CH_2NMe_2)Pd(\mu\text{-}OH]_2$ in CH_2Cl_2 (Scheme 4.4a). ^{31}P, ^{7}Li, and ^{1}H NMR analysis of the reaction mixture showed that a complicated

mixture of species is formed. The reaction mixture was subjected to a diffusion-ordered spectroscopy (DOSY) experiment, which differentiates the components of a mixture based on diffusion coefficients, to probe the nuclearity of the $[(\mathbf{1})Pd(C_6H_4CH_2NMe_2)]_n$ aggregates that may be present (Figure 4.2).[5-8] Although there is significant overlap of the peaks in the ^1H NMR spectrum, there is enough separation in the δ 1.5–4.5 region to enable estimation of the diffusion coefficients of the species present in solution. Those values fall in the in the range of 5.1–6.5 10^{-10} m^2/s.

Scheme 4.4. Reaction of $Li_2[\mathbf{1}]$ with $[(C_6H_4CH_2NMe_2)Pd(\mu\text{-}Cl]_2$ and $[(C_6H_4CH_2NMe_2)Pd(\mu\text{-}OH]_2$. The lower (Li-**1**)$PdMe(C_6H_4CH_2NMe_2)$ units in the schematic structure of **2** are denoted by "Pd".

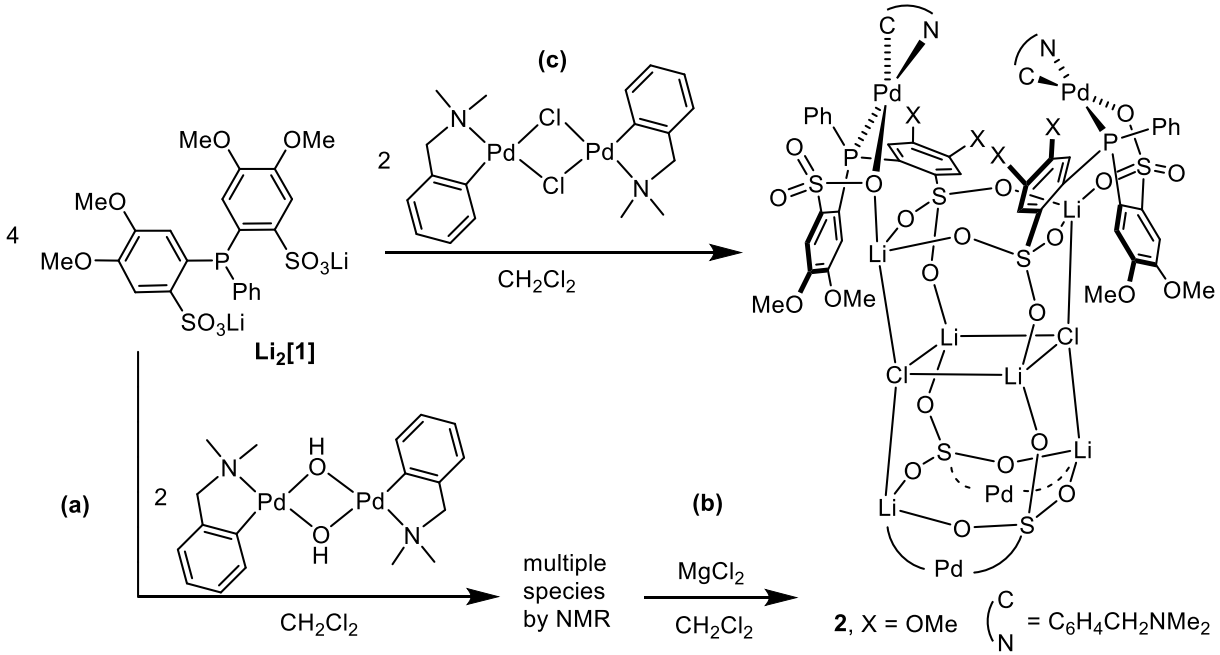

Previous PGSE studies have shown that the diffusion coefficients of dimeric $[(PO)PdR]_2$ species, tetrameric $[(Li\text{-}OPO)PdRL]_4$ species with D4R central cages, and tetrameric [(Li-OPO)]PdRL•Li_2Cl_2 species with expanded cages (Table 4.1)[1,2] fall in reasonably well-defined ranges, as shown in Figure 4.2. The colored regions indicate the range of diffusion coefficients observed for (PO)Pd and (Li-OPO)Pd aggregates: the purple region represents monomeric (Li-OPO)PdMeL complexes, the blue region represents $[(PO)PdMe]_2$ dimers, the green region represents D4R cages, and the red region represents $Li_4S_4O_{12}$•Li_2X_2 cages. Based on these results, the majority of species in the reaction mixture from Scheme 4.4a (>82%) have diffusion coefficients (>5.48 x 10^{-10} m^2/s) that are too large to correspond to D4R cage structures (< 5.26 x 10^{-10} m^2/s). It is likely that the products of Scheme 4.4a are monomeric and dimeric species and that only minor amounts of higher order assemblies are present. Notably, no peaks are observed in the red region which shows that a $Li_4S_4O_{12}$•Li_2OH_2 expanded cage is not formed.

Figure 4.2. DOSY NMR of the products formed by the reaction of **Li_2[1]** and $[(C_6H_4CH_2NMe_2)Pd(\mu\text{-}OH]_2$ in CD_2Cl_2. The purple, blue, green, and red regions demarcate the ranges of diffusion coefficients for monomeric (5.50–6.37 x 10^{-10} m^2/s), dimeric (5.51–5.63 x 10^{-10} m^2/s), D4R tetrameric (4.47–5.26 x 10^{-10} m^2/s), and expanded tetrameric (3.72–4.22 x 10^{-10} m^2/s) (Li-OPO)PdMeL complexes.

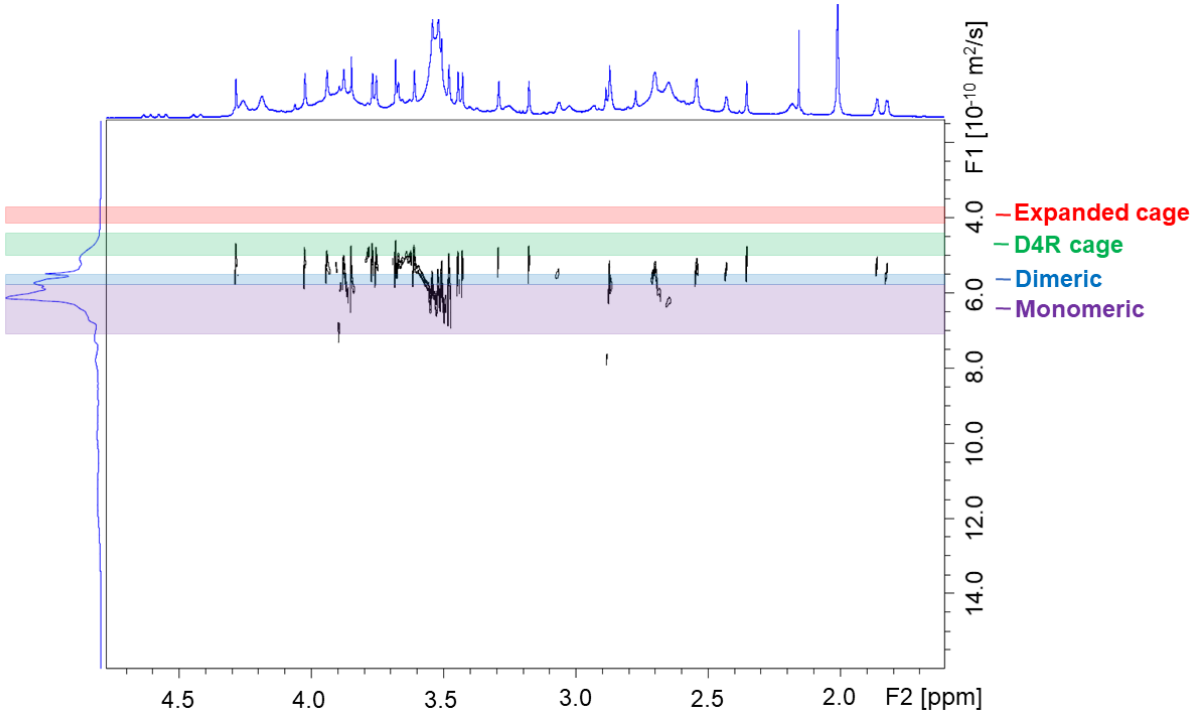

To rule out the possibility that decomposition, the size of the $Pd(C_6H_4CH_2NMe_2)$ unit, or some other factor prevents cage self-assembly in Scheme 4.4a, $MgCl_2$ was added to the complex reaction mixture to provide a source of chloride. This addition resulted in the quantitative formation of expanded cage structure **2** (Scheme 4.4b).

These results suggest that the steric bulk of [Li-**1**]$^-$ precludes formation of a smaller D4R cage core and that a suitable anion, like chloride, is required to form an expanded tetrameric cage with a $Li_4S_4O_{12}$•Li_2X_2 core. A $Li_4S_4O_{12}$•Li_2OH_2 core structure does not form with [Li-**1**]$^-$

(Scheme 4.4a) because OH^- is too small to bridge the top and bottom $Li_2S_2O_6$ rings (ionic radii Cl^- = 1.81 Å vs OH^- = 1.10 Å) and reduce steric crowding around the cage periphery.

Table 4.1. Diffusion coefficients for (PO)PdRL and (Li-OPO)PdRL species determined by PGSE NMR (CD_2Cl_2, 296 K).

Entry	Complex	D (10^{-10} m^2/s)	radius (Å)	V (10^3 $Å^3$)
1	{(PO-3,5-^{t}Bu)PdMe}$_2$(TMEDA)[a]	5.61	9.06	3.12
2	{(PO-3,5-^{t}Bu)PdMe}$_2$[a]	5.49	9.25	3.32
3	**A** (R = Me, L = py')[a]	4.46	11.4	6.21
4	**A** (R = iPr, L = py')[b]	4.77	10.7	5.12
5	**A** (R = iPr, L = py)[b]	5.26	9.70	3.82
6	**A** (R = Cy, L = py)[b]	4.90	10.4	4.67
7	**B**[c]	4.11	12.4	8.00
8	**2**	4.02	12.7	8.60
9	**5b**	4.45	11.4	6.16
10	**6**	3.72	12.8	8.87
11	**7**	4.22	12.1	7.5
12	**5d**	4.11	12.4	8.00

[a] Ref 1 [b] Ref 2 [c] Ref 4.

Alternate synthesis and characterization of 2. Compound **2** was synthesized directly from Li_2[**1**] and [$(C_6H_4CH_2NMe_2)Pd(\mu\text{-}Cl)]_2$ in CH_2Cl_2 (Scheme 4.4c). X-ray quality crystals of **2** were obtained from a $CHCl_2CHCl_2$ solution layered with hexanes at room temperature, and the solid-state structure is shown in Figure 4.3. The solid-state structure of **2** is similar to that of **B** and features a $Li_4S_4O_{12}$•Li_2Cl_2 core with two pairs of Pd centers arranged around the periphery with a Pd–Pd distance of 6.1 Å within each pair. **2** has an *SSSS (ent-RRRR)* configuration at the phosphorus centers. Interestingly, the Pd−$ArSO_3$−Li connectivity in **2** differs from that in **B**. At

the Pd3 unit of **2**, the Pd−$ArSO_3$−Li connectivity , is the same as is observed for cages **A** and **B** (bonding mode A, Figure 4.4a), with one oxygen bound to Pd3, one oxygen bound to the Li corner and one terminal S=O unit. However, the Pd1, Pd2, and Pd4 units have a different Pd−$ArSO_3$−Li connectivity, with one S–*O* bonded to both Pd and the Li corner and two terminal S=O units (bonding mode B, Figure 4.4b). The steric bulk of the Pd($C_6H_4CH_2NMe_2$) unit may favor a more vertical orientation of the Pd square plane relative to the top of the cage, which favors bonding mode B over bonding mode A. Binding mode B was observed previously at one Pd unit in the solid-state structure of **A-*i*Pr** (R = ^{i}Pr, L = py).[2]

Figure 4.3. Molecular structure of **2**. Hydrogen atoms are omitted. Only the nitrogen and Pd–*C* atoms of the $C_6H_4CH_2NMe_2$ ligands are shown for clarity. Selected bond lengths (Å) and angles (deg): Pd1-P1 2.2820(11), Pd1-O1 2.206(3), Pd1-N1 2.130(4), Pd1-C1 1.987(5), S1-O1 1.502(3), O1-Pd1-P1 89.61(7), N1-Pd1-P1 174.58(14), N1-Pd1-O1 92.25(14), C1-Pd1-P1 97.17(14), C1-Pd1-O1 173.18(15), C1-Pd1-N1 80.93(18). Average bond lengths (Å) and angles (deg) related with Li1: Li-O 1.95, Li-Cl 2.43, O-Li-O 103.8, O-Li-Cl 115.0. Average bond lengths (Å) and angles (deg) related with Li3: Li-O 1.877, Li-Cl 2.399, O-Li-O 103.7, Cl-Li-Cl 96.8, O-Li-Cl 114.1.

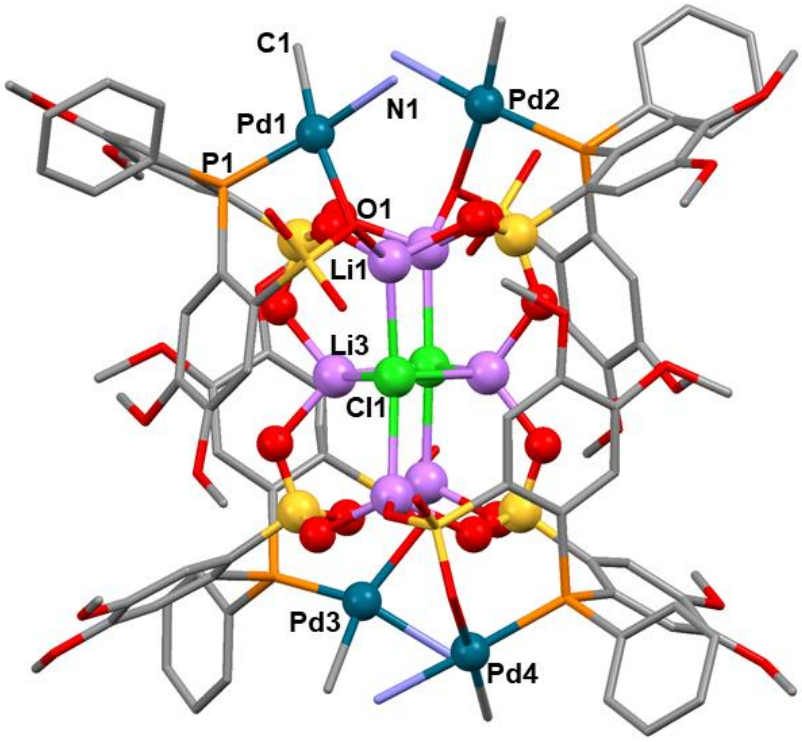

Figure 4.4. Different Pd−$ArSO_3$−Li connectivity in **2**. a) Binding mode A in Pd1 unit and b) Binding mode B in Pd3 unit.

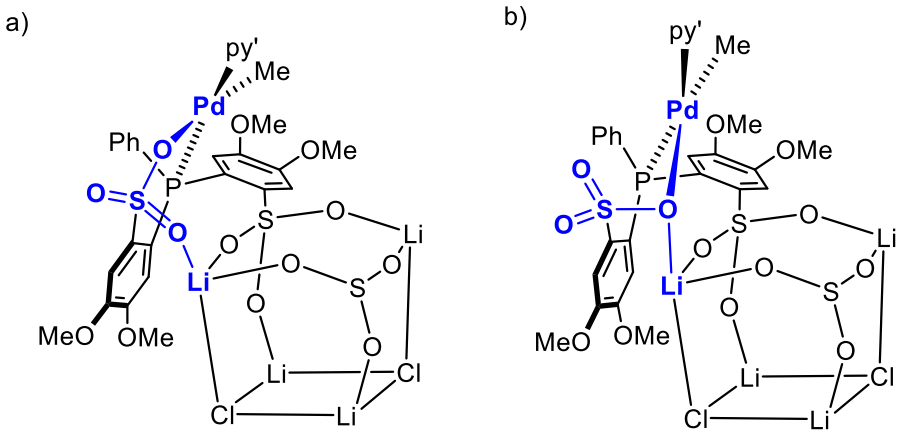

For compound **2**, one sharp resonance is observed by ^{31}P NMR (δ 27.9) and one set of resonances is observed by ^{1}H and ^{13}C NMR, indicating that all four Pd units are equivalent. The ^{1}H NMR spectrum establishes that there are two inequivalent 4,5-OMe_2*Ar* groups and four inequivalent OMe groups per Pd unit, which is consistent with cage formation. One methyl resonance from the NMe_2 group is shifted to high field in the ^{1}H NMR spectrum (δ 2.11 vs 2.60) which is ascribed to anisotropic shielding by the neighboring Pd–*Ar* group. This is analogous to the anisotropic shielding of the Pd–*Me* group by the neighboring py ligand in **A** and **B** and is indicative of cage formation.[1,2,4] Two sharp resonances in a 2:1 intensity ratio are observed by ^{7}Li NMR, corresponding to the two types of Li in the solid-state structure. The hydrodynamic volume of **2** in CD_2Cl_2 determined by PGSE is consistent with an expanded cage structure (Table 4.1, entry 8). NMR data for **2** at room temperature and low (down to –50 ^{o}C) temperature ^{1}H

NMR show that the (Li-**1**)Pd($C_6H_4CH_2NMe_2$) units are equivalent on the NMR timescale, consistent with fast exchange between binding modes A and B.

These results show that the expanded $Li_4S_4O_{12}$•Li_2Cl_2 cage can support different (Li-OPO)PdRL units and Pd−$ArSO_3$−Li connectivity modes, while maintaining the same structure.

Is the *meta*-OMe group really important? As noted above, steric crowding between the *meta*-OMe groups of the Pd-bound and non-Pd-bound *Ar*SO_3 groups on the top and bottom layers of the cage is proposed to prevent the self-assembly of the D4R cage structure and favor the formation of the expanded $Li_4S_4O_{12}$•Li_2Cl_2 cage.[4] To test whether the D4R cage self-assembles without the *meta*-OMe substituent, a Li_2[OPO] ligand with only *para*-OMe substituents (Li_2[PPh(2-SO_3^--5-(OMe)-Ph]; Li_2[**4a**]) was synthesized by a former group member Qian Liu, as shown in Scheme 4.5. The reaction of Li_2[**4a**], (COD)PdMeCl and a pyridine ligand (L) in CH_2Cl_2 produces either an insoluble product (L = py; no signal observed in the ^{31}P NMR spectrum) or results in the formation of Pd black (L = py' or 4-^{t}Bu-py). Therefore, Li_2[PPh(2-SO_3^--5-$(NEt)_2$-Ph]; Li_2[**4b**]), which contains *para*-NEt_2 substituents that are electronically similar to OMe, was synthesized by James Earl, an undergraduate student who carried out the synthetic work under the supervision of the author (Scheme 4.5). The reaction of Li_2[**4b**], (COD)PdMeCl and 4-^{t}Bu-py in CH_2Cl_2 results in the self-assembly of tetrameric compound **5b**, which has a D4R cage structure (Scheme 4.6).

Scheme 4.5. Synthesis of $(OPO)^{2-}$ ligands.

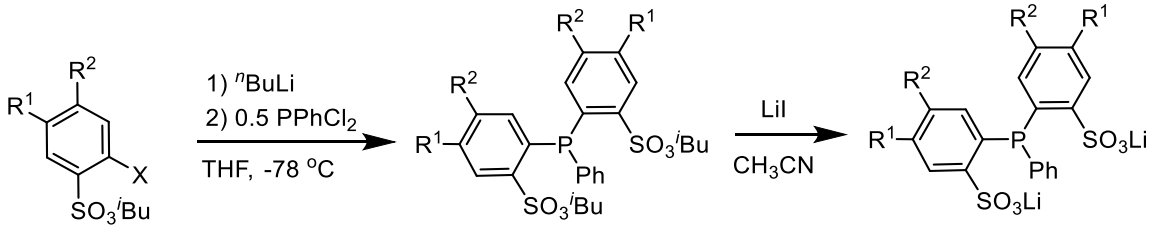

3a-*i*Bu (R^1=H, R^2=OMe, X=H) **4a-*i*Bu** **Li_2[4a]**
3b-*i*Bu (R^1=H, R^2=NEt_2, X=H) **4b-*i*Bu** **Li_2[4b]**
3c-*i*Bu (R^1=OMe, R^2=H, X=Br) **4c-*i*Bu** **Li_2[4c]**
3d-*i*Bu (R^1=*i*Pr, R^2=H, X=H) **4d-*i*Bu** **Li_2[4d]**

Scheme 4.6. Synthesis of **5b**. The lower (Li-**4b**)PdMe(py') units in the schematic structure of **5b** are denoted by "Pd".

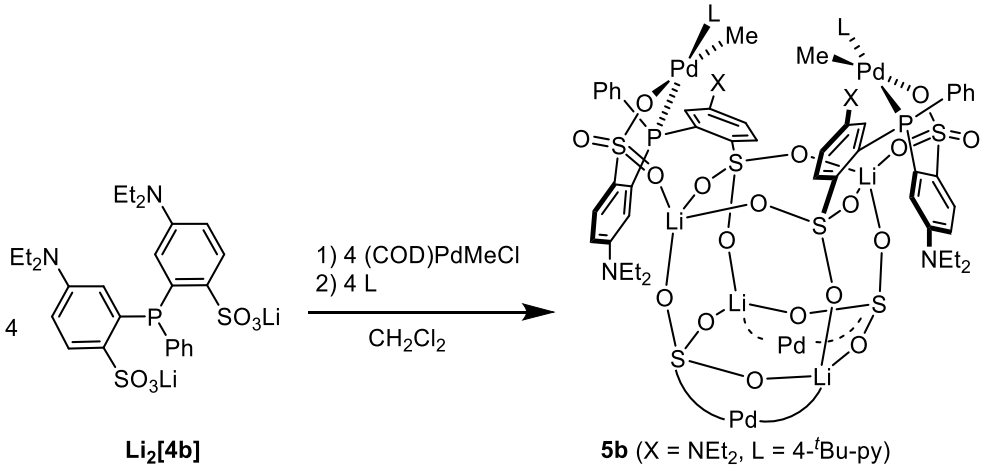

Li_2[4b] **5b** (X = NEt_2, L = 4-*t*Bu-py)

X-ray quality crystals were grown by layering hexanes onto a CH_2Cl_2 solution at –10 °C. The solid-state structure of **5b** (Figure 4.5) is similar to that of **A**, and contains two pairs of (Li-**4b**)PdMe(4-*t*Bu-py) units arranged on the periphery of a D4R $Li_4S_4O_{12}$ cage with a Pd–Pd distance of 5.8 Å within each pair. The cage has S_4-symmetry and an *RRSS* configuration at the

phosphorus centers. The Pd−$ArSO_3$−Li units are coordinated through binding mode A at all four Pd units.

Figure 4.5. Molecular structure of **5b**. Hydrogen atoms and ^{t}Bu groups removed and bottom units for clarity.

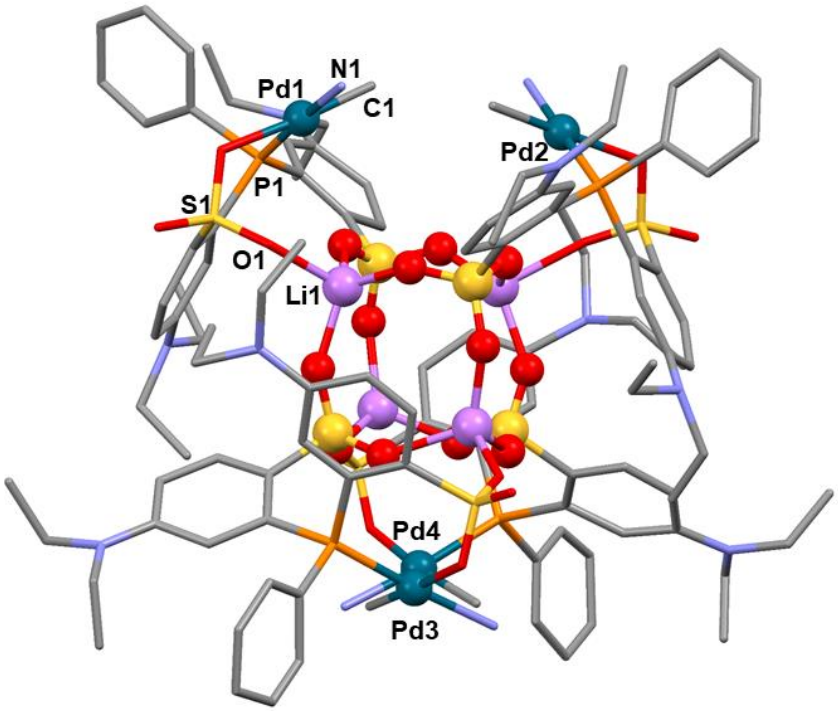

The solution behavior of **5b** is consistent with the solid-sate structure. The hydrodynamic volume (6.16×10^3 Å^3) determined by PGSE NMR in CD_2Cl_2 is consistent with a D4R cage structure (Table 4.1, entry 9). One resonance is observed by ^{31}P (δ 39.2) and ^{7}Li NMR (δ –1.0), indicating that **5b** is highly symmetric in solution and does not contain a Li_2Cl_2 unit in the core. A high-field Pd–C*H*$_3$ resonance (δ –0.32) in the ^{1}H NMR is consistent with anisotropic shielding by the neighboring 4-^{t}Bu-py ligand.

Based on the space-filling model of **5b** (Figure 4.6), the *para* NEt_2 substituents are directed away from the cage and so the size of these substituents does not prevent the assembly of the D4R cage. As noted above, previous self-assembly reactions of (Li-OPO)PdMeR units containing OPO^{2-} ligands with *para*-alkyl substituents (R = Cy, ^{i}Pr, Me, ^{t}Bu) also form D4R cages.[2]

Figure 4.6. Space-fill view of **5b** highlighting the close contacts between H102 of the bottom Pd-bound arenesulfonate ring and H56 of the top non-Pd-bound arenesulfonate ring.

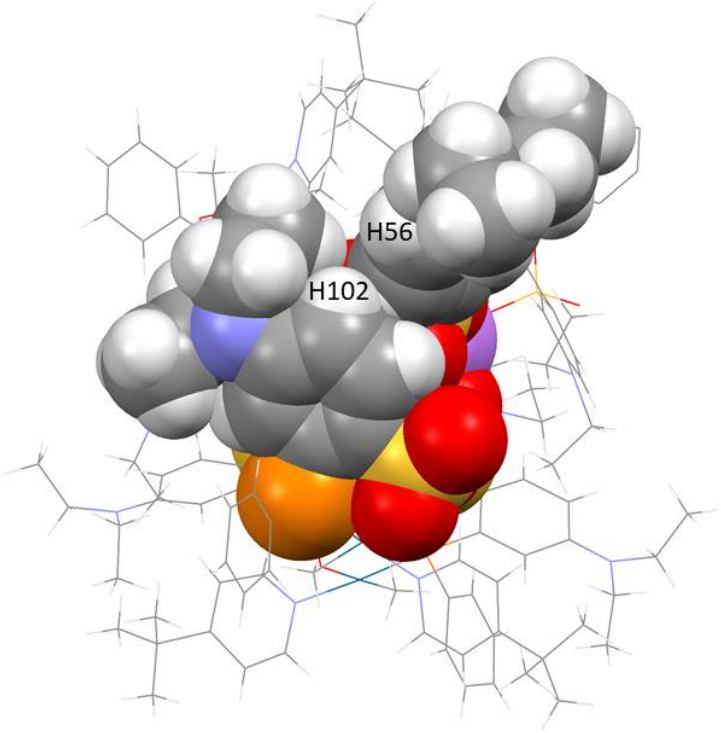

However, the *meta* hydrogens (H102 and H56) in Figure 4.6 are directed towards each other and in close proximity. The incorporation of *meta* substituents would likely preclude

formation of a D4R cage. To test this hypothesis, a Li_2[OPO] ligand with only *meta*-OMe substituents (Li_2[PPh(2-SO_3^--4-(OMe)-Ph]; Li_2[**4c**]) was synthesized, as shown in Scheme 4.5. The reaction of Li_2[**4c**], (COD)PdMeCl and py' in CH_2Cl_2 results in a mixture of products with the tetrameric expanded $Li_4S_4O_{12}$•Li_2Cl_2 cage **5c** as the major species (52 %, Scheme 4.7).

Scheme 4.7. Synthesis of **5c**. The lower (Li-**4c**)PdMe(py') units in the schematic structure of **5c** are denoted by "Pd".

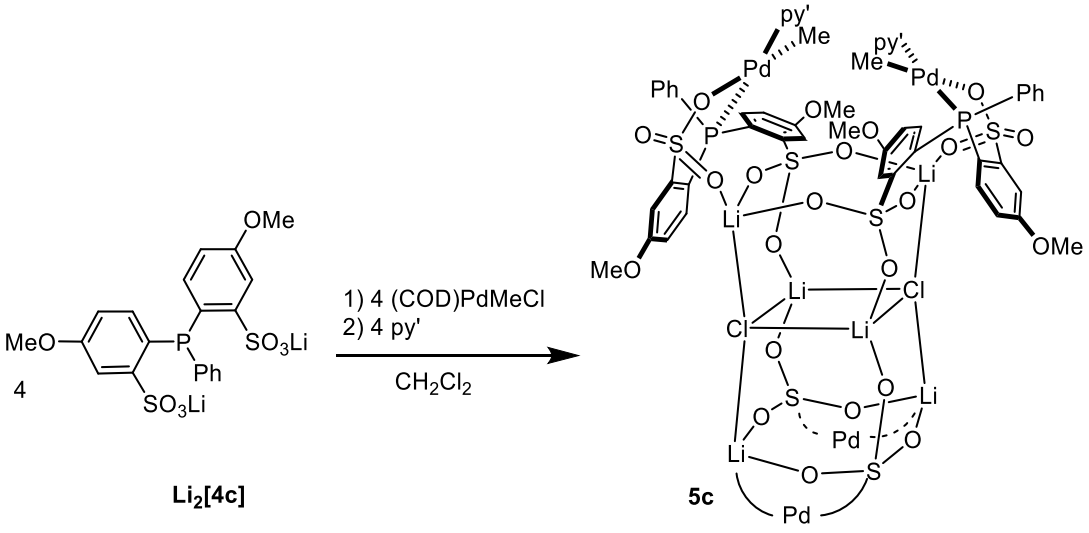

The NMR data of **5c** in CD_2Cl_2 is consistent with an expanded $Li_4S_4O_{12}$•Li_2Cl_2 cage structure. One major resonance is observed by ^{31}P NMR (δ 32.2) and two sharp resonances are observed by ^{7}Li NMR (δ –0.4 and –0.8) in a 2:1 intensity ratio, indicating that **5c** is highly symmetric in solution and contains a Li_2Cl_2 unit between the top and bottom $Li_2S_2O_6$ layers. A high-field Pd–C*H*$_3$ resonance (δ –0.18) in the ^{1}H NMR is consistent with anisotropic shielding by the neighboring py' ligand. These results confirm that the *meta*-OMe substituent of Li_2[**1**]

necessitates the formation of an expanded cage core structure because of steric crowding around the cage periphery.

Can the Li_2X_2 layer in the expanded $Li_4S_4O_{12}$•Li_2X_2 cage be replaced with other ionic units? If the role of the inner Li_2Cl_2 layer in the core structure of **2** is simply to elongate the cage to accommodate the large Li[**1**]$^-$ ligand, then other MX salts should self-assemble with (**1**)PdLX units to form analogous $Li_4S_4O_{12}$•M_2X_2 expanded cage structure. To test this proposal, the self-assembly of $Li_4S_4O_{12}$•Li_2OAc_2 cages was investigated. The reaction of Li_2[**1**] and $[(C_6H_4CH_2NMe_2)Pd(\mu\text{-}OAc)]_2$ in CH_2Cl_2 results in the self-assembly of {(Li-**1**)Pd($C_6H_4CH_2NMe_2$)}$_4Li_2(OAc)_2$ (**6**), which adopts a $Li_4S_4O_{12}$•$Li_2(OAc)_2$-expanded cage structure, as shown in Scheme 4.8. Similarly, Li_2[**1**], (COD)PdMeCl, silver(I) acetate, and py' self-assemble in CH_2Cl_2 to {(Li-**1**)PdMe(py')}$_4Li_2(OAc)_2$ (**7**) in which four (**1**)PdMepy' units are arranged around an expanded $Li_4S_4O_{12}$•$Li_2(OAc)_2$ core (Scheme 4.8).

X-ray quality crystals of **6** and **7** were grown from a $CHCl_2CHCl_2$ solution layered with hexanes at room temperature (Figures 4.7 and 4.8). The cage cores of **6** and **7** are similar to that of **2** except that acetate has replaced chloride in the Li_2X_2 unit between the top and bottom $Li_2S_2O_6$ rings of the cage. As in **2** and **B**, the Pd-bound *Ar*SO_3^- rings are closely packed with the non-Pd-bound *Ar*SO_3^- rings. The $Li_2(OAc)_2$ units are fully sterically blocked by these *Ar*SO_3^- groups. The $Li_4S_4O_{12}$•$Li_2(OAc)_2$ cage cores of **6** and **7** are more vertically elongated than the

$Li_4S_4O_{12}$•Li_2Cl_2 cage cores of **2** and **B**, and the O–Li–O angles that form two sides of the cage core expand to accommodate the acetate anion (Table 4.2).

Scheme 4.8. Synthesis of **6** and **7**. The lower (Li-OPO)PdRL units in the schematic structure of **6** and **7** are denoted by "Pd".

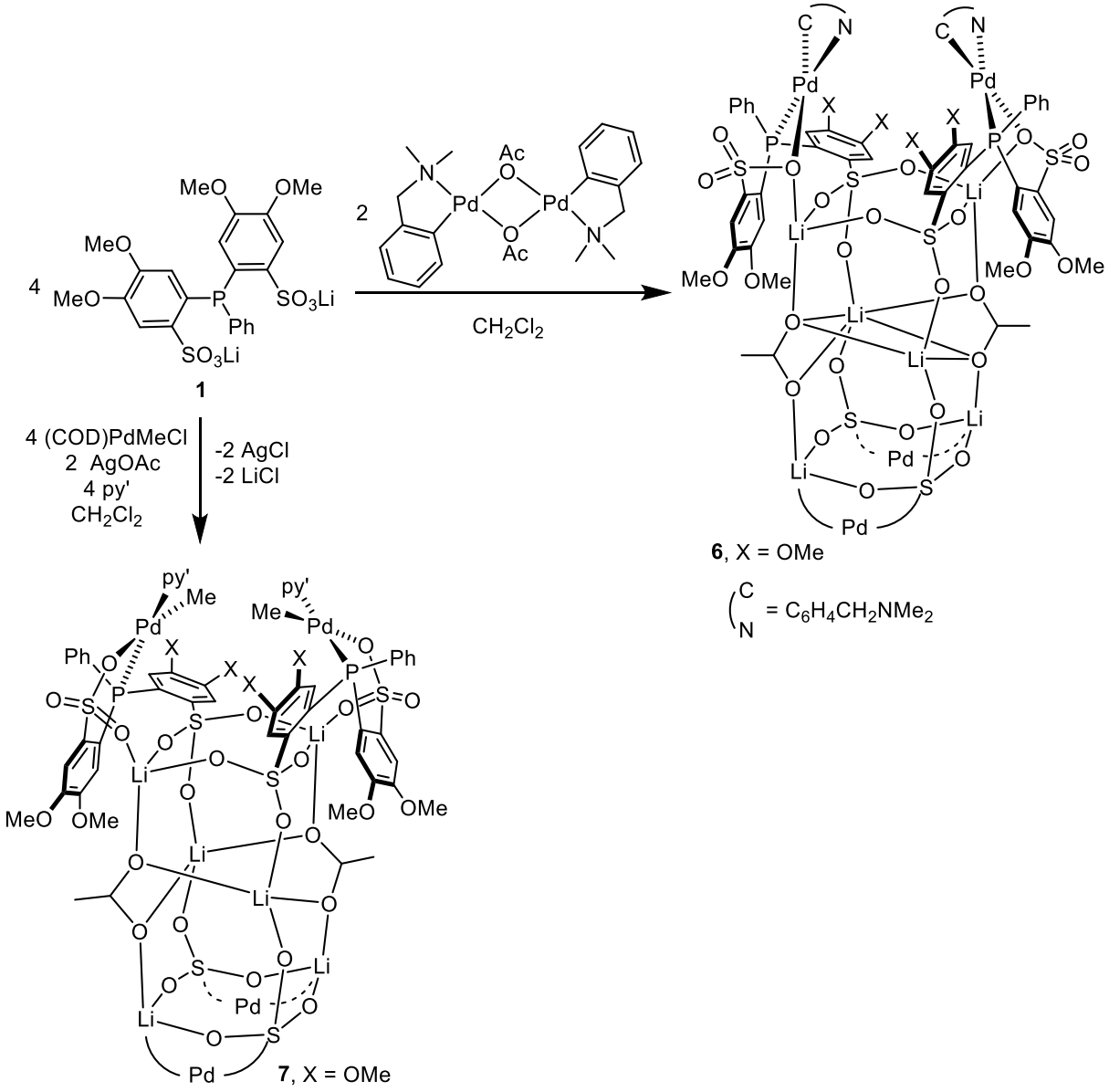

Figure 4.7. Molecular structure of **6**. Hydrogen atoms are omitted. Only the nitrogen and Pd–*C* atoms of the $C_6H_4CH_2NMe_2$ ligands are shown for clarity.

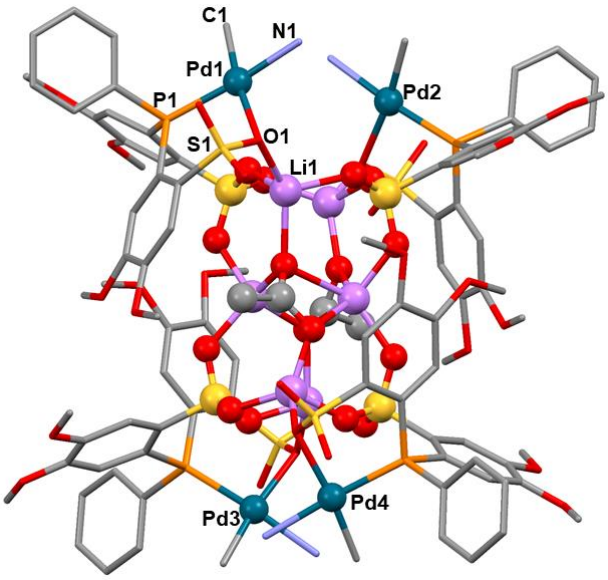

Figure 4.8. Molecular structure of **7**. Hydrogen atoms are omitted. Only of the nitrogen atoms of the py' ligands are shown for clarity.

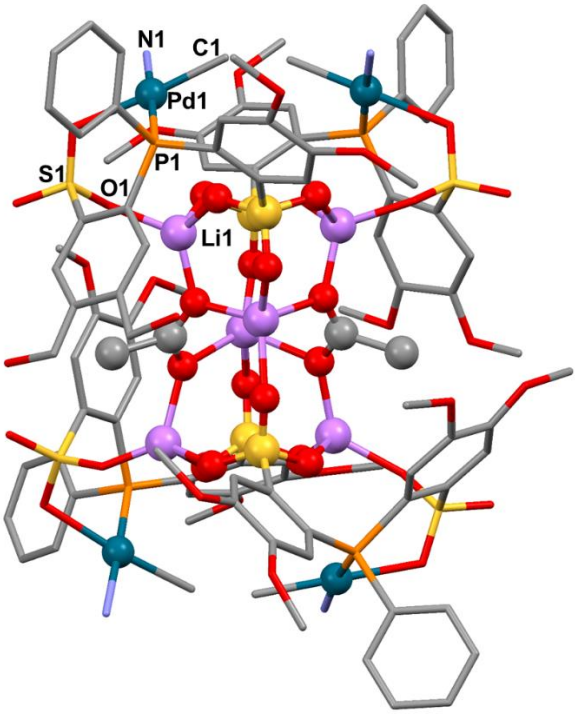

Several differences in the μ-OAc bridging modes and Pd−$ArSO_3$−Li connectivity in the solid-state structures of **6** and **7** exist, which may be related to the different steric requirements of the PdMepy' and Pd($C_6H_4CH_2NMe_2$) units in those compounds. In **6**, the acetate ions bridge in a 4.32 mode to neighboring Li atoms in the cage core, as described in Harris notation.[9] In contrast, in **7**, the acetate ions exhibit a 4.22 binding mode to neighboring Li atoms in the cage core. The acetate ions are twisted in the cage core, resulting in an oblique prismatic core.

All four Pd units of **6** are linked to the cage through binding mode B, as observed in **2**, whereas all four Pd units of **7** are linked by binding mode A, as observed in **B**. This trend supports the proposal that the Pd unit structures Pd($C_6H_4CH_2NMe_2$) and PdMepy' favor binding modes B and A, respectively.

Table 4.2. Comparison of distances and angles in expanded $Li_4S_4O_{12}$•Li_2X_2 cage structures.

Entry	Complex	$Li_2S_2O_6$– $Li_2S_2O_6$ interplane distance (Å)[a]	O–Li–O angle (deg)
1	**B**	5.785	102
2	**2**	5.752	99–103
3	**6**	6.227	107
4	**7**	6.050	121

[a]plane-to-plane distances between $Li_2S_2O_6$ rings

NMR studies show that **6** and **7** exist in several forms in solution. The major isomer of **7** in CD_2Cl_2 solution (>80 %) exhibits one ^{31}P NMR resonance (δ 32.0), one major Pd–CH_3 ^1H NMR resonance at high field (δ –0.02) and two sharp ^7Li NMR resonances in a 2:1 intensity

ratio. These data are consistent with the solid-state structure. Two minor species are present (< 20 %) that are likely stereosiomers of **7**. One of the minor species exhibits four equal-intensity Pd–C*H*$_3$ ^{1}H NMR resonances and four equal-intensity ^{31}P NMR resonances with chemical shifts similar to that of the major isomer of **7**. The other minor species exhibits two Pd–*CH*$_3$ ^{1}H NMR resonances (1:1 intensity ratio) and two ^{31}P NMR resonances (1:1 intensity ratio). Two possible stereoisomers can be formed by inverting the configurations of the phosphorous (and sulfur) atoms in one or two Pd units of the tetramer—from *SSSS* to *SRSS* and *SRSR* at P (Experimental Section, Figure 4.41). An *SRSS* configuration would produce four inequivalent Pd units and an *SRSR* configuration would produce two inequivalent Pd units, consistent with the symmetries of the two minor species observed by NMR. Importantly, dissolution of **7** in the coordinating solvent CD_3OD, which solvates the ionic groups that form the cage, cleanly generates the monomeric (Li-**1**)PdMepy' species, which was identified by ^{31}P, ^{1}H, ^{7}Li and ^{13}C NMR. This result shows that **7** is chemically pure and supports the proposal that the minor species are stereoisomers of **7**.

The major isomer of **6** in CD_2Cl_2 solution exhibits one ^{31}P resonance (δ 28.8), –N*Me*$_2$ ^{1}H NMR resonances at δ 2.01 and 2.58, and two sharp ^{7}Li NMR resonances in a 2:1 intensity ratio, consistent with the solid state structure. In addition to the sharp resonances for the major species, broad peaks are present in the ^{31}P, ^{1}H, and ^{7}Li NMR spectra of **6**. These broad resonances may be due to unsymmetrical isomers of **6** that feature different Pd−$ArSO_3$−Li connectivities (binding

modes A or B) or acetate bridging modes and are dynamic, or to smaller aggregates formed by cage disassembly.[2] One species is observed by NMR in CD_3OD solution, indicating **6** is chemically pure.

The hydrodynamic volumes of the major species of **6** and **7** (8.9×10^3 Å^3 and 7.5×10^3 Å^3, Table 4.1, entry 10 and 11) were calculated from PGSE experiments and confirm that both complexes are larger than D4R cages and similar in hydrodynamic volume to **2** and **B** in solution. Although the bridging motifs of acetate and chloride are very different, both ions can bridge the top and bottom $Li_2S_2O_6$ rings and provide the necessary expansion to accommodate a sterically bulky ligand.

Can cage structure be expanded further to accommodate *meta*-substituents larger than OMe? As noted above, the *meta*-OMe substituents of the (Li-**1**)$^-$ and (Li-**4c**)$^-$ ligands preclude formation of a D4R cage core. Similarly, increasing the size of the *meta*-substituent of the $(OPO)^{2-}$ ligand further, may preclude formation of an expanded $Li_4S_4O_{12}$•Li_2Cl_2 cage core and necessitate a larger M_2X_2 inner layer. To explore the self-assembly of expanded cages with larger M_2X_2 units, where M = Li and X = Br, the lithium salt of a phosphine-*bis*-arenesulfonate ligand with *meta*-^{i}Pr substituents was synthesized (Li_2[**4d**], Scheme 4.5).

The reaction of Li_2[**4d**], (COD)PdMeBr, and py' in CD_2Cl_2 forms one product that is highly symmetric in solution (Scheme 4.9). One sharp resonance is observed by ^{31}P NMR (δ

34.1) and one set of resonances is observed by ^{1}H and ^{13}C NMR, indicating that all four Pd units are equivalent. The ^{1}H NMR spectrum establishes that there are two inequivalent 5-^{i}Pr$_2$*Ar* groups and two inequivalent ^{i}Pr groups per Pd unit which is consistent with cage formation. The Pd–*Me* resonance is shifted to high field in the ^{1}H NMR spectrum (δ –0.37) which is ascribed to anisotropic shielding by the neighboring py' ligand. Two sharp resonances in a 2:1 intensity ratio are observed by ^{7}Li NMR (δ –0.5 and –1.0), corresponding to the two types of Li in the solid-state structure. The hydrodynamic volume of **8** in CD_2Cl_2 (8.0×10^3 Å) determined by PGSE is consistent with an expanded cage structure (Table 4.1, entry 12).

As noted above, the O–Li–O angle that forms two sides of the cage is flexible and varies from 99–121 ^{o} in the solid-state structures of **B**, **2**, **6**, and **7**. In **5d**, the O–Li–O angles likely expand to accommodate the larger bromide anion. The shallow potential energy surface associated with varying the O–Li–O allows for a variety of X^- to be incorporated in the cage core structure.[10]

Scheme 4.9. Synthesis of **5d**. The lower (Li-**4d**)PdMe(py') units in the schematic structure of **5d** are denoted by "Pd".

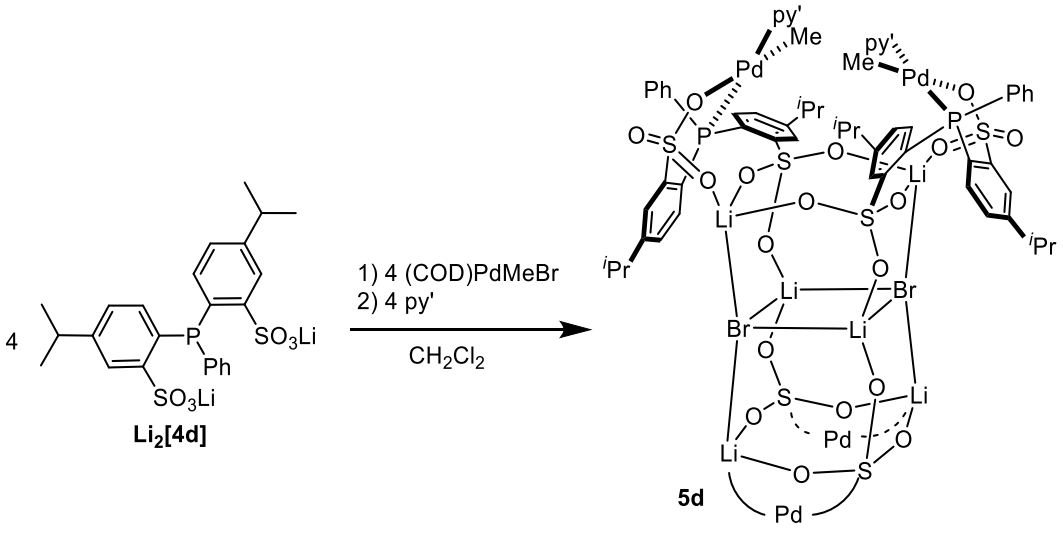

4.3 Conclusion

Steric saturation around the cage periphery is likely a controlling factor in the self-assembly process. (**1**)PdLX units cannot form smaller D4R cage cores, but instead self-assemble to expanded cage structures with inner Li_2Cl_2 or $Li_2(OAc)_2$ units. *Meta*-substituents (OMe or ^{i}Pr) have been shown to inhibit formation of D4R cage structures whereas *para*-substituents do not. As the size of the *meta*-substituent increases, the cage core must correspondingly expand, and as a result the *meta*-substituent can be chosen in order to control which type of cage core assembles ($Li_4S_4O_{12}$ or $Li_4S_4O_{12}$•M_2X_2). Flexibility in the interior O–Li–O angles allows for a variety of anions to be incorporated in the M_2X_2 unit (X = Cl, Br, OAc).

The synthesis of complexes **2** and **6** shows that the cage structures can accommodate different types of Pd units (Pd($C_6H_4CH_2NMe_2$) vs PdMe(py')). However, different Pd units were

shown to favor different binding modes (A or B) for Pd−$ArSO_3$−Li connectivity. During polymerization with **A** and **B**, in which the Pd unit in the active form of the catalyst is Pd(alkyl)(C_2H_4), it is unknown if one or both binding modes is utilized. If binding modes A and B are exchanging, it may cause broadening of the MW distribution of the polymer produced. A broad MW distribution is observed for **A** and **B**.

4.4 Experimental Section

General Procedures. All experiments were performed under a nitrogen atmosphere using drybox or Schlenk techniques. Nitrogen was purified by passage through Q-5 oxygen scavenger and activated molecular sieves. Methylene chloride, diethyl ether and THF were dried by passage over activated alumina. Toluene, pentane and hexane were purified by passage through BASF R3-11 oxygen scavenger and activated alumina. $CDCl_2CDCl_2$ and $CHCl_2CHCl_2$ were dried over 4 Å molecular sieves. CD_2Cl_2 was dried over P_2O_5. The following materials were obtained from commercial sources and used without further purification: 4-bromo-3-nitroanisole (Alfa Aesar, 96 %), ammonium chloride (Aldrich, 99 %), iron powder (Aldrich, 97 %), sodium nitrite (Aldrich, 99 %), thionyl chloride (Aldrich, 99 %), cuprous chloride (Fisher, 95 %), 2-methyl-1-propanol (Aldrich, 99 %), 3-isopropylbenzenesulfonyl chloride (AstaTech, 95 %), pyridine (Aldrich, 99.8 %), P,P-dichlorophenylphosphine (Aldrich, 97 %), ^{n}BuLi solution (Aldrich, 2.5 M in hexanes), HCl solution (Aldrich, 2 M in diethyl ether), lithium iodide (Aldrich, 99.9 %), 4-(5-

nonyl)pyridine (TCI, 98 %), 4-*tert*-butyl-pyridine (Aldrich, 96 %), and silver(I) acetate (Aldrich, 98 %). The following compounds were prepared by literature procedures: (COD)PdMeCl,[11] (COD)PdMeBr,[12] **1**,[4] $[(PhCH_2NMe_2)Pd(\mu\text{-}Cl)]_2$,[13] $[(PhCH_2NMe_2)Pd(OAc)]_2$,[14] and $[(PhCH_2NMe_2)Pd(\mu\text{-}OH)]_2$.[15]

NMR spectra were acquired on Bruker DRX-500 or Bruker DRX-400 spectrometers at ambient temperatures unless otherwise indicated. ^1H and ^{13}C chemical shifts are reported relative to $SiMe_4$ and are internally referenced to residual ^1H and ^{13}C solvent resonances. ^{31}P chemical shifts are reported relative to externally referenced 85% H_3PO_4. ^7Li chemical shifts are reported relative to externally referenced LiCl in D_2O. NMR resonances were assigned based on COSY, HMQC, and $^1H\{^{31}P\}$ experiments, as well as trends in chemical shifts and coupling constants derived from these experiments. Coupling constants are given in Hz. Mass spectrometry was performed on an Agilent 6224 TOF-MS (high resolution) instrument.

$[(1)Pd(PhCH_2NMe_2)]_4 \bullet Li_2Cl_2$ (2). 1 (0.080 g, 0.14 mmol) and $[(PhCH_2NMe_2)PdCl]_2$ (39 mg, 0.14 mmol) were weighed out in a vial and dissolved in CH_2Cl_2 (10 mL). The mixture was stirred for 1 h. **2** was isolated by layering pentane onto the CH_2Cl_2 solution and cooling to -40 °C. The resulting white solid was collected by filtration and dried under vacuum (0.05 g, 44 %). X-ray quality crystals were grown from $CHCl_2CHCl_2$ and hexanes at room temperature. $^{31}P\{^1H\}$ NMR (CD_2Cl_2): δ 27.9. ^1H NMR (CD_2Cl_2): δ 7.98 (d, $^4J_{PH}$ = 4, 1H, H^3), 7.75 (d, $^4J_{PH}$ = 5, 1H, $H^{3'}$), 7.44 (t, $^3J_{HH}$ = 8, 1H, H^{10}), 7.35 (t, $^3J_{HH}$ = 7, 2H, H^9), (the H^8 resonance is broadened into

the baseline due to restricted rotation around the P-C^7 bond), 6.75 (t, $^3J_{HH}$ = 8, 1H, H^{13}), 6.47 (d, $^3J_{PH}$ = 11, 1H, H^6), 6.45 (d, $^3J_{HH}$ = 8, 1H, H^{14}), 6.41 (t, $^3J_{HH}$ = 8, 1H, H^{12}), 6.38 (d, $^3J_{PH}$ = 11, 1H, $H^{6'}$), 5.94 (t, $^3J_{HH}$ = 8, 1H, H^{11}), 4.18 (s, 3H, $H^{19'}$), 4.15 (s, 3H, H^{19}), 3.73 (d, $^2J_{HH}$ = 13, 1H, H^{17}), 3.46 (s, 3H, H^{20}), 3.37 (d, $^2J_{HH}$ = 12, 1H, $H^{17'}$), 3.27 (s, 3H, $H^{20'}$), 2.60 (d, $^3J_{HH}$ = 2, 3H, H^{18}), 2.11 (d, $^3J_{HH}$ = 2, 3H, $H^{18'}$). $^{13}C\{^1H\}$ NMR (CD_2Cl_2): δ 151.9 (d, $^4J_{PC}$ = 2, C^4), 151.4 (d, $^4J_{PC}$ = 2, $C^{4'}$), 150.4 (d, $^3J_{PC}$ = 8, $C^{5'}$), 149.5 (d, $^3J_{PC}$ = 9, C^5), 149.1 (d, $^2J_{PC}$ = 2, C^{16}), 142.0 (s, C^{15}), 139.7 (d, $^2J_{PC}$ = 15, C^2), 139.1 (d, $^2J_{PC}$ = 10, $C^{2'}$), 135.1 (d, $^2J_{PC}$ = 11, C^{11}), 131.5 (s, C^8), 130.7 (d, $^1J_{PC}$ = 43, C^7), 129.0 (s, C^9), 128.9 (C^{10}), 125.0 (d, J_{PC} = 6, C^{12}), 124.3 (s, C^{13}), 123.6 (s, C^{14}), 120.0 (s, C^6), 118.6 (d, $^1J_{PC}$ = 19, C^1), 118.0 (d, $^1J_{PC}$ = 27, $C^{1'}$), 117.9 (d, $^2J_{PC}$ = 8, $C^{6'}$), 114.6 (d, $^3J_{PC}$ = 7, C^3), 113.7 (d, $^3J_{PC}$ = 10, $C^{3'}$), 70.9 (s, C^{17}), 57.3 (s, C^{19}), 56.6 (s, $C^{20'}$), 56.4 (s, $C^{19'}$), 55.8 (s, C^{20}), 50.1 (s, C^{18}), 49.2 (s, $C^{18'}$). $^7Li\{^1H\}$ NMR (CD_2Cl_2): δ -0.7, -1.0. $^{31}P\{^1H\}$ NMR (CD_3OD): δ 28.8. ^1H NMR (CD_3OD): δ 7.90 (br, 2H, H^8, this resonance is broad due to the restricted rotation around the P-C^7 bond), 7.62 (d, $^4J_{PH}$ = 4, 2H, $H^{3,3'}$), 7.49 (t, $^3J_{HH}$ = 8, 1H, H^{10}), 7.42 (t, $^3J_{HH}$ = 7, 2H, H^9), 6.93 (d, $^3J_{HH}$ = 7, 1H, H^{14}), 6.77 (m, 1H, H^{13}), 6.68 (d, $^3J_{PH}$ = 9, 2H, $H^{6,6'}$), 6.37 (m, 2H, H^{11} and H^{12}), 4.03 (br, 2H, $H^{17,17'}$), 3.89 (s, 6H, $H^{19,19'}$), 3.55 (s, 6H, $H^{20,20'}$), 2.80 (d, $^3J_{HH}$ = 3, 6H, $H^{18,18'}$). $^{13}C\{^1H\}$ NMR (CD_3OD): δ 151.7 (br), 150.6 (br), 150.3 (s), 144.0 (s), 137.9 (s), 137.8 (s), 137.7 (br), 132.1 (s), 131.7 (s), 129.5 (d, J_{PC} = 11), 125.7 (d, J_{PC} = 6), 125.0 (s), 123.5 (s), 118.9 (s), 113.9 (br), 72.0 (d, J_{PC} = 3, C^{17}), 56.5 (s, C^{19}), 56.3 (s, C^{20}), 50.1 (s, C^{28}).

$^{7}Li\{^{1}H\}$ NMR (CD_3OD): δ 0.2. HRMS (ESI; *m/z*): Calcd. for [$C_{62}H_{66}N_2O_{20}P_2Pd_2S_4Li_2$•LiCl + 2H]$^{+}$ 1620.09668, Found: 1620.0931.[16]

Figure 4.9. Numbering scheme for **2**.

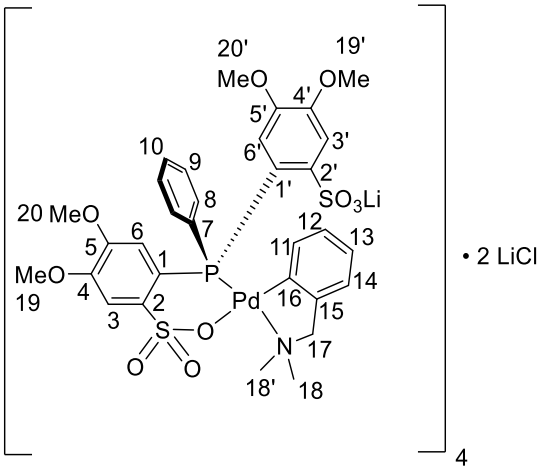

Figure 4.10. NMR spectra of **2**.

(a) $^{31}P\{^{1}H\}$ NMR (CD_2Cl_2, 202 MHz):

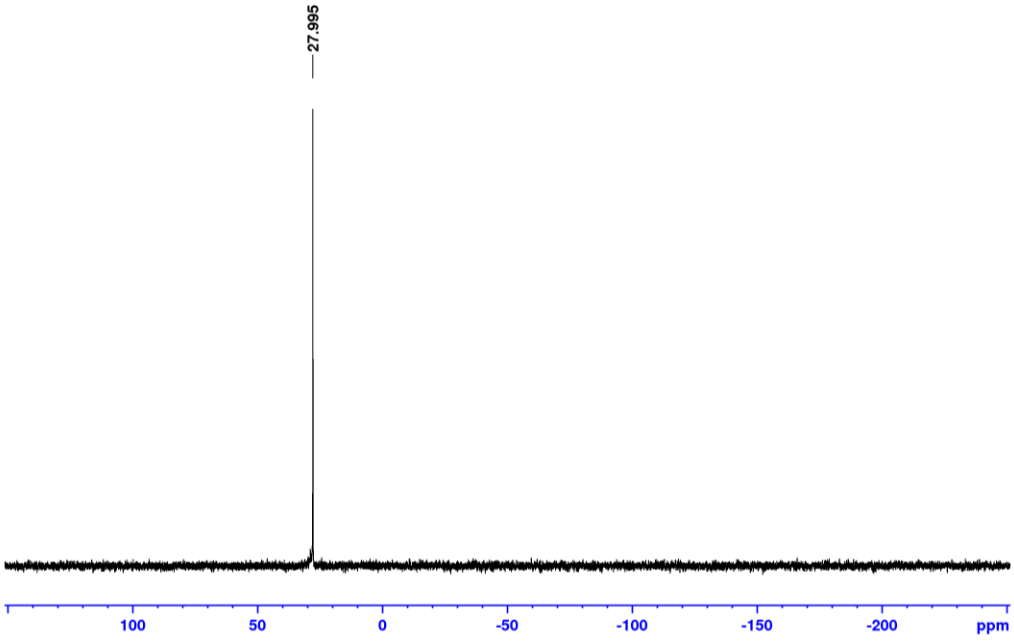

Figure 4.10, continued.

(b) ^{1}H NMR (CD_2Cl_2, 500 MHz):

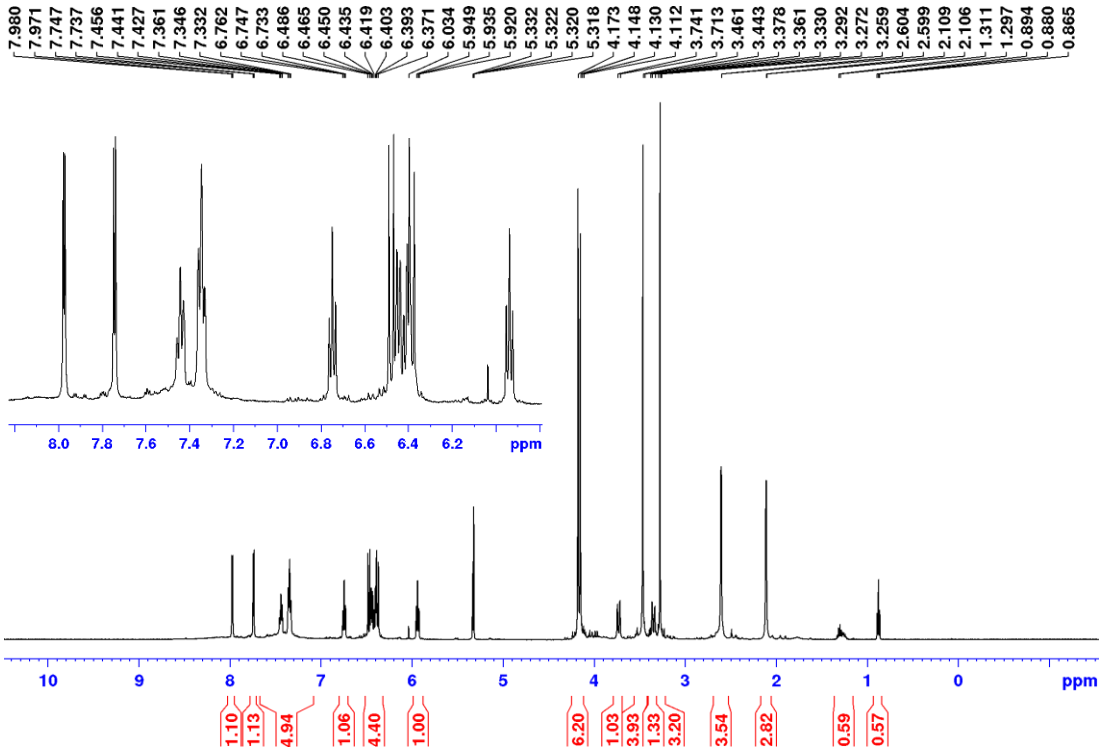

(c) ^{13}C{^{1}H} NMR (CD_2Cl_2, 125 MHz):

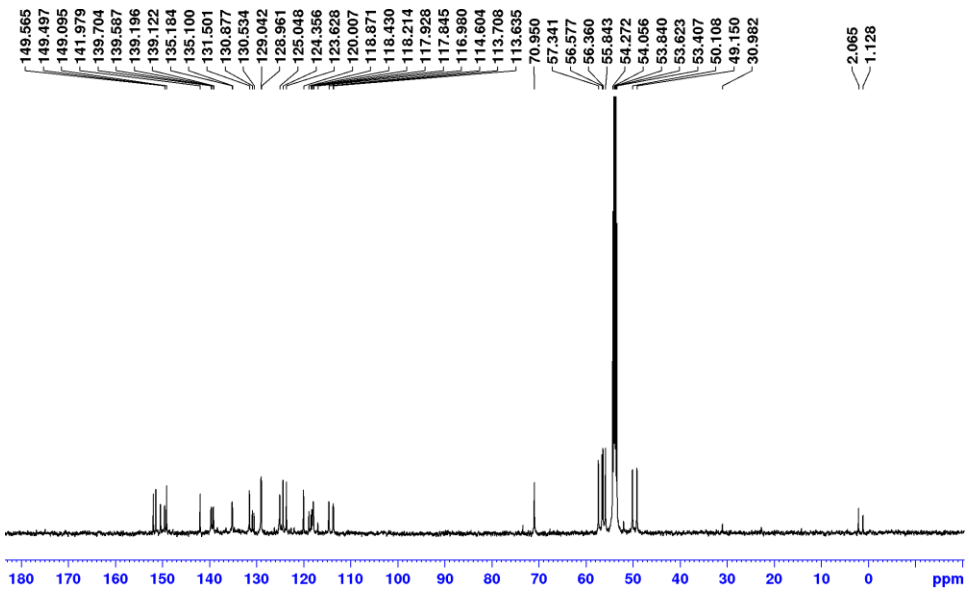

Figure 4.10, continued.

(d) $^{13}C\{^{1}H\}$ NMR (CD_2Cl_2, 125 MHz), aromatic region:

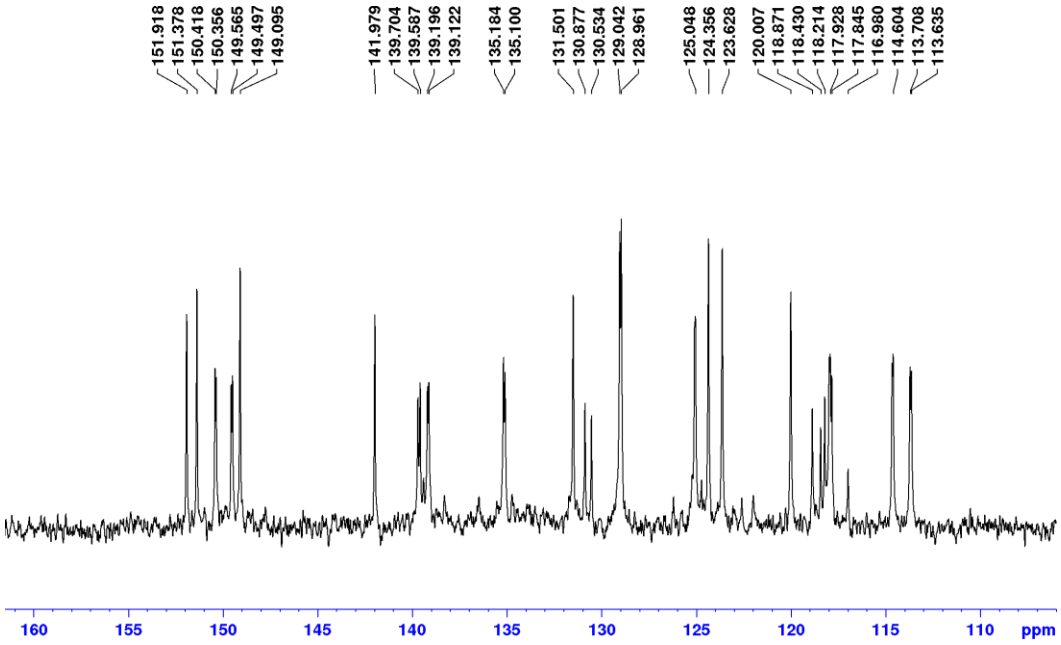

(e) $^{7}Li\{^{1}H\}$ NMR (CD_2Cl_2, 155 MHz):

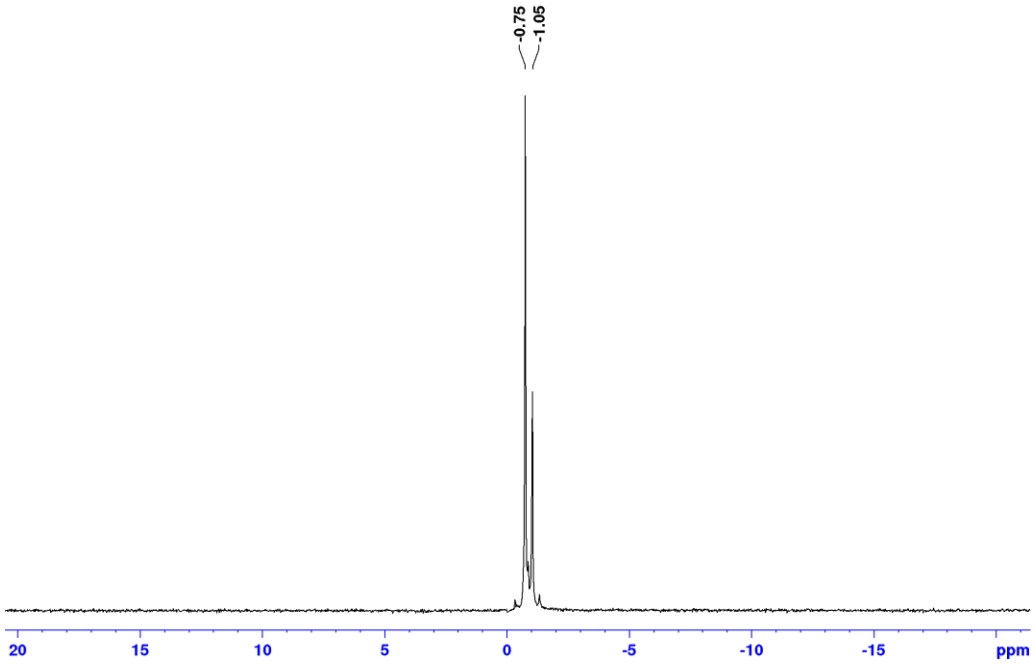

Figure 4.10, continued.

(f) COSY (CD_2Cl_2, 500 MHz):

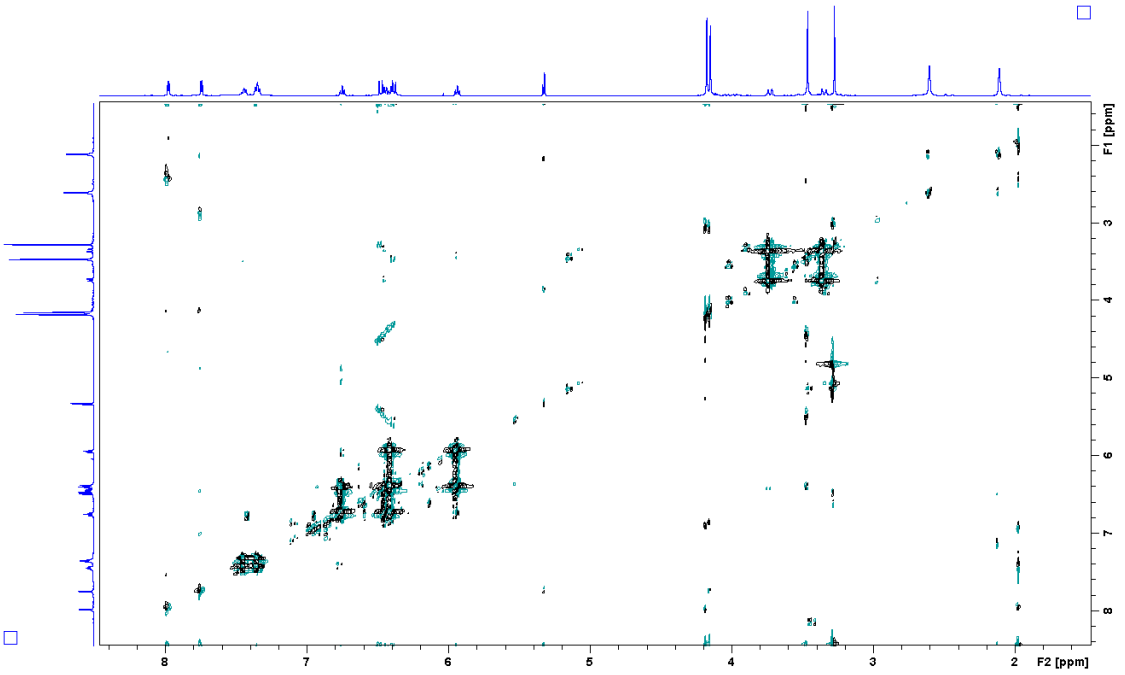

(g) COSY (CD_2Cl_2, 500 MHz), aromatic region:

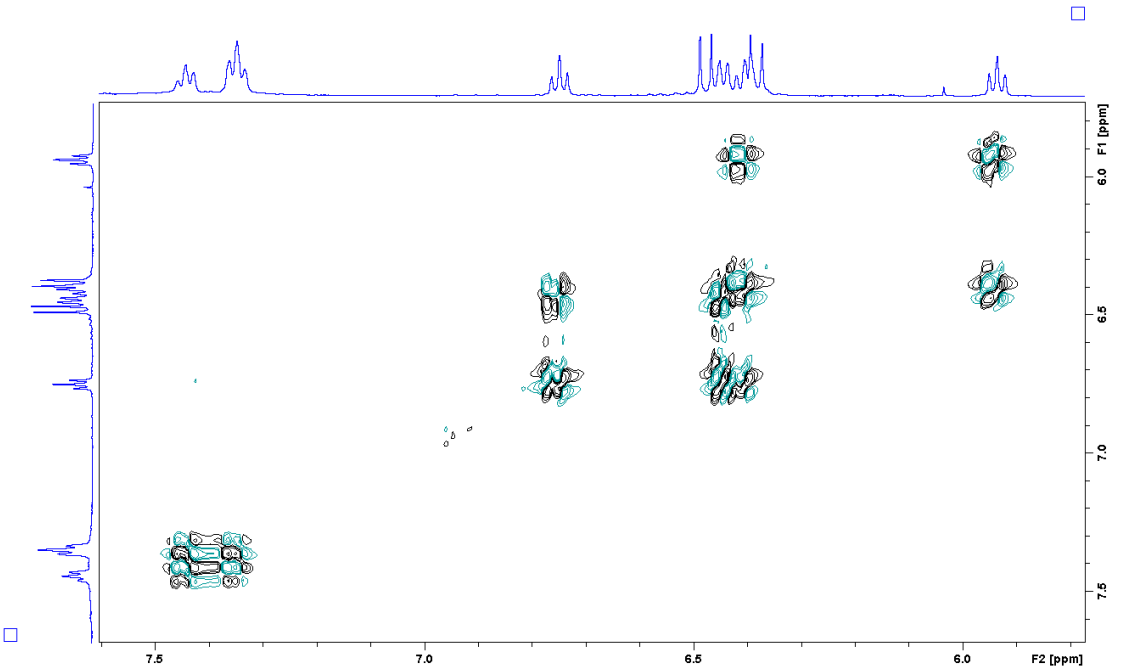

Figure 4.10, continued.

(h) HMQC ($(CD_2Cl_2$, 500 MHz, 125 MHz):

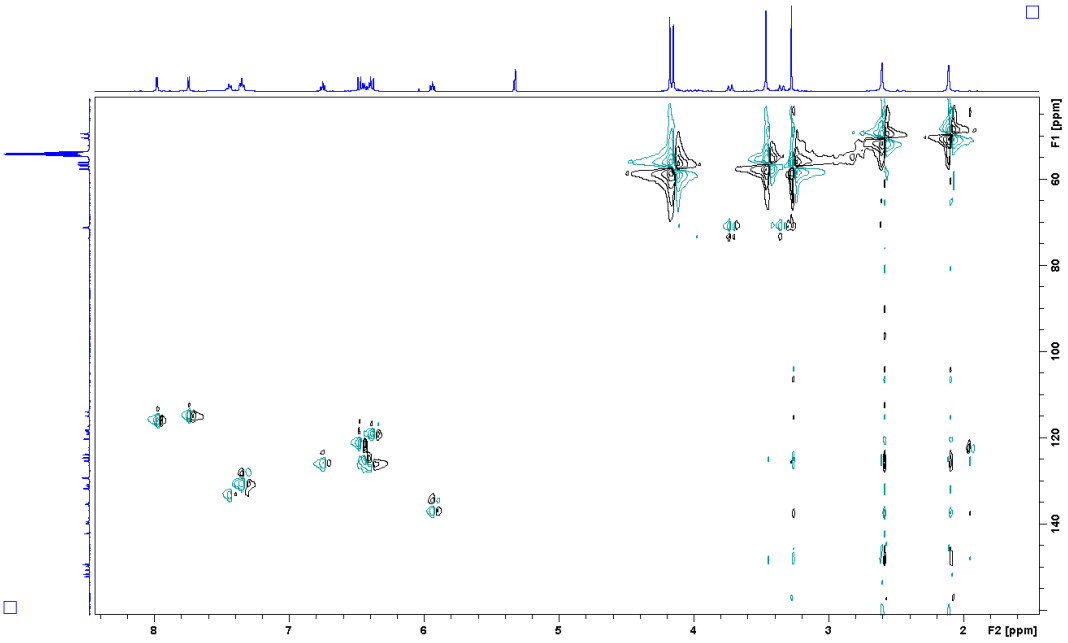

(i) $^{31}P\{^1H\}$ NMR (CD_3OD, 202 MHz):

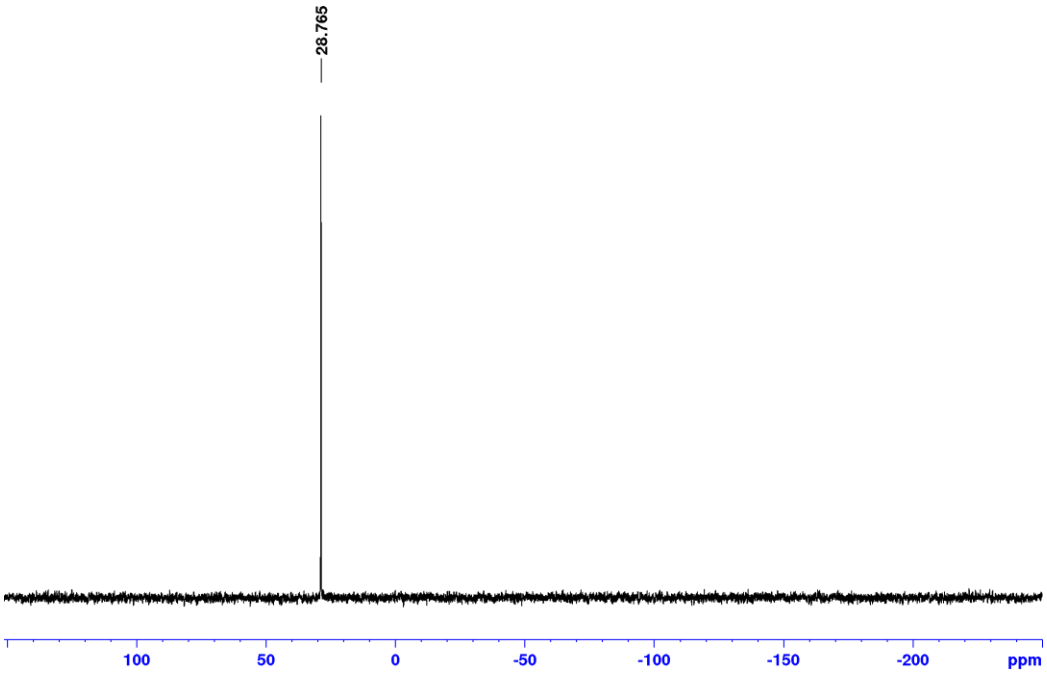

Figure 4.10, continued.

(j) ^{1}H NMR (CD_3OD, 500 MHz):

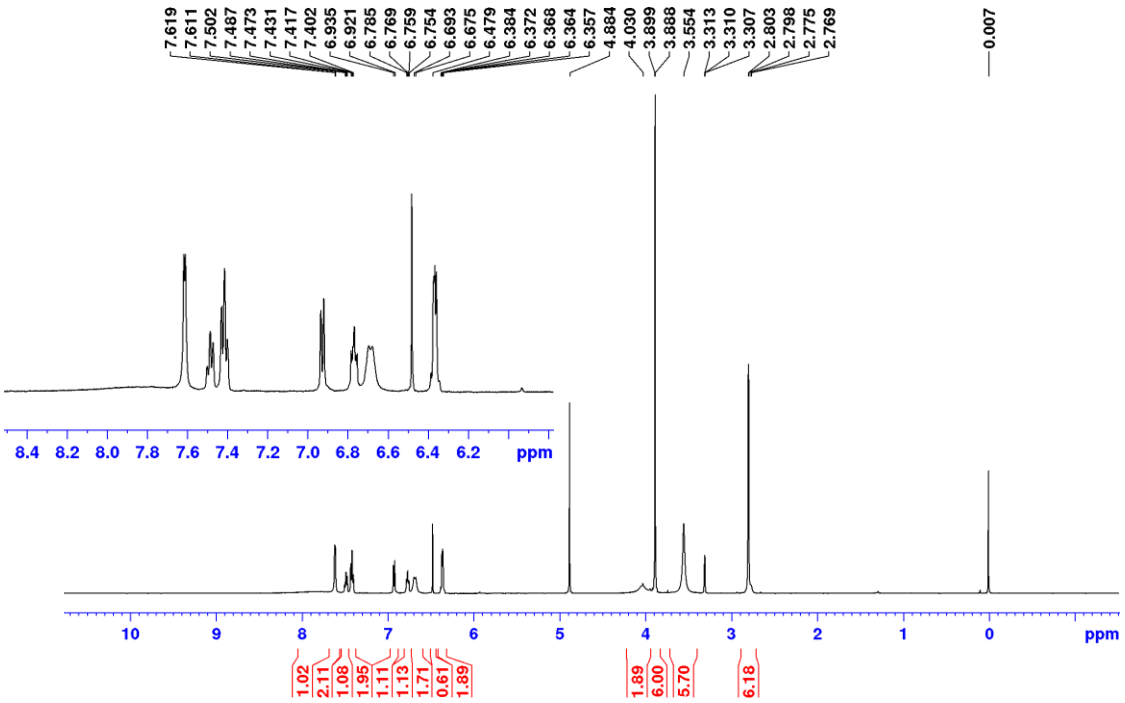

(k) ^{13}C{^{1}H} NMR (CD_3OD, 125 MHz):

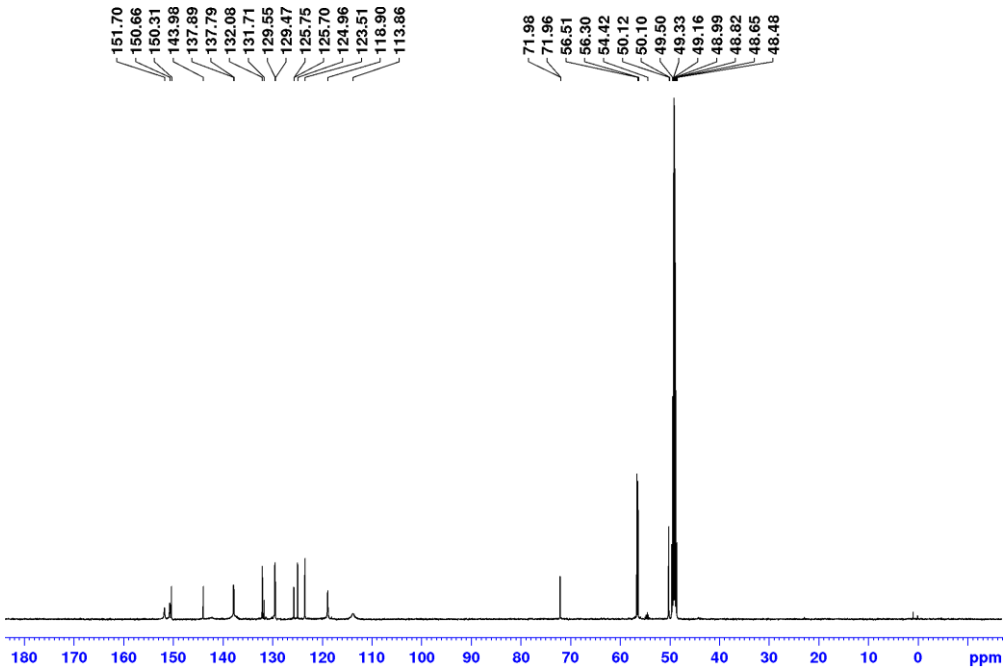

Figure 4.10, continued.

(l) $^{13}C\{^{1}H\}$ NMR (CD_3OD, 125 MHz), aromatic region:

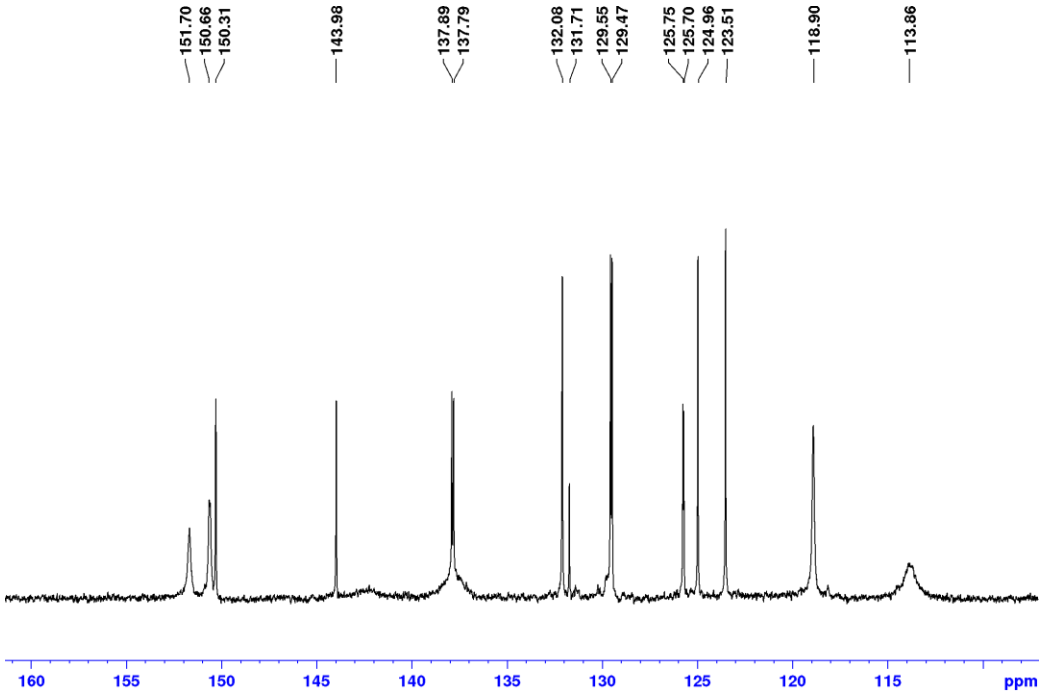

(m) $^{7}Li\{^{1}H\}$ NMR (CD_3OD, 155 MHz):

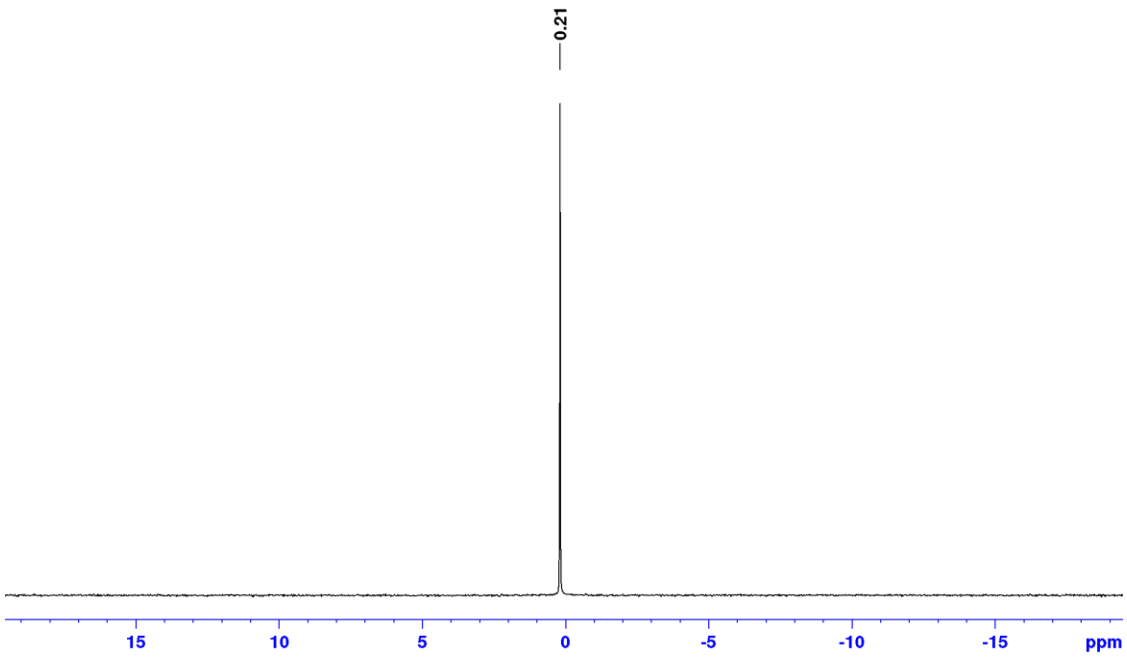

Scheme 4.10. Synthesis of 2-bromo-5-methoxybenzenesulfonyl chloride.

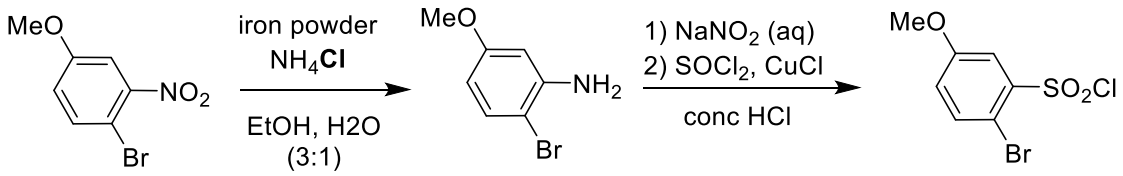

2-bromo-5-methoxybenzenesulfonyl chloride. 2-bromo-5-methoxybenzenesulfonyl chloride was synthesized using a procedure adapted from Refs 17, 18, and 19. 4-bromo-3-nitroanisole (7.5 g, 32 mmol) was dissolved in EtOH (30 mL) and H_2O (22 mL). NH_4Cl (6.7 g, 130 mmol) and iron powder (8.8 g, 160 mmol) were added. The mixture was refluxed for 5 h. The black reaction mixture was filtered through Celite and extracted with diethyl ether (6 x 100 mL). The combined organic layers were dried over $MgSO_4$ and the volatiles were removed under vacuum. 3-amino-4-bromoanisole was purified by silica gel chromatography using a 9:1 hexanes:ethyl acetate solution as the eluent to afford a yellow oil, with data as reported.[17]

Thionyl chloride (3.77 mL, mmol) was slowly added to H_2O (22 mL) and cooled to 0 ^oC in a round bottom flask over 45 min. The solution was stirred for 1 h at 0 ^oC. The solution was allowed to warm to 18 ^oC and CuCl (ca. 120 mg) was added. The yellow solution was cooled to –5 ^oC. Meanwhile, 4-bromo-3-aminoanisole (2.45 g, mmol) was cooled to –5 ^oC in a second round bottom flask and concentrated HCl (12 mL) was added to form a gray slurry. An aqueous solution of $NaNO_2$ (0.92 g, mmol in 5 mL H_2O) was slowly added over 45 min. The resulting orange slurry was stirred for 20 min at –5 ^oC. The diazonium salt was slowly added to the first

flask over 30 minr, resulting in a dark yellow solution. After the addition was completed a yellow slurry formed. The mixture was agitated at 0 ^{o}C for 1 h. The aqueous layer was extracted with ethyl acetate (6 x 50 mL) and the combined layers were dried over $MgSO_4$. The volatiles were removed under vacuum resulting in a dark red oil (1.2 g, 29 %). ^{1}H NMR (CD_2Cl_2): δ 7.74 (d, $^{3}J_{HH}$ = 9, 1H, H^5), 7.69 (d, $^{4}J_{HH}$ = 3, 1H, H^2), 7.12 (dd, $^{3}J_{HH}$ = 9, $^{4}J_{HH}$ = 3; 1H, H^4), 3.88 (s, 3H, -OCH_3). ^{13}C{^{1}H} NMR (CD_2Cl_2): δ 159.4 (s), 143.6 (s), 137.5 (s), 122.6 (s), 116.2 (s), 110.5 (s), 56.6 (s, –OCH_3).

Figure 4.11. Numbering scheme for 2-bromo-5-methoxybenzenesulfonyl chloride.

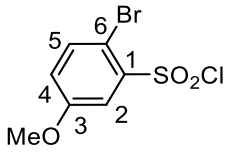

Figure 4.12. NMR spectra of 2-bromo-5-methoxybenzenesulfonyl chloride.

(a) ^{1}H NMR (CD_2Cl_2, 500 MHz):

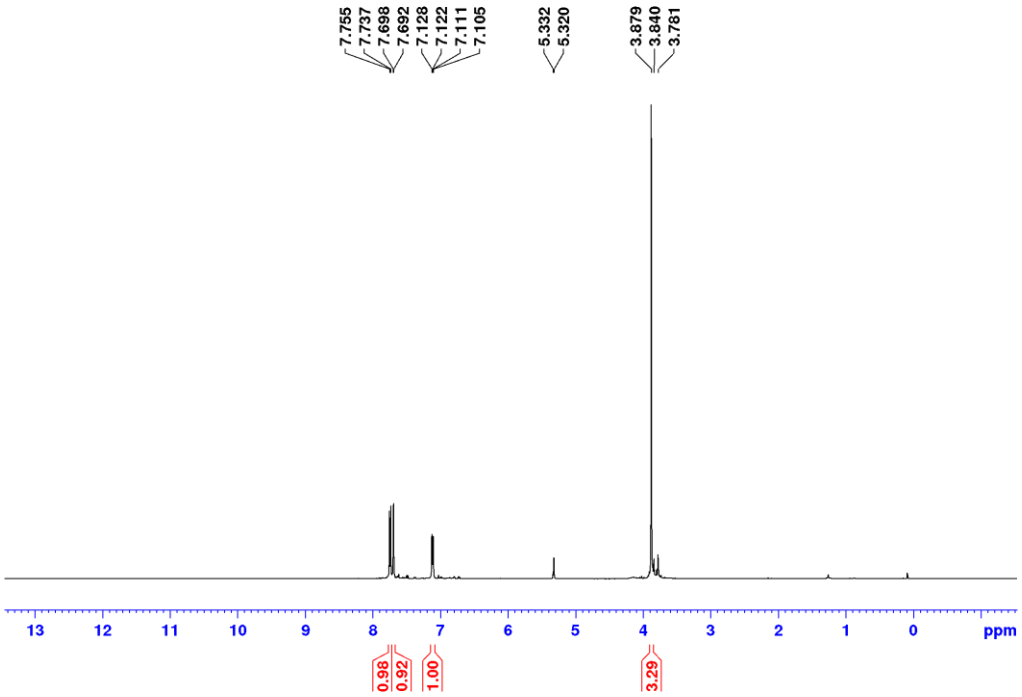

(b) $^{13}C\{^{1}H\}$ NMR (CD_2Cl_2, 126 MHz):

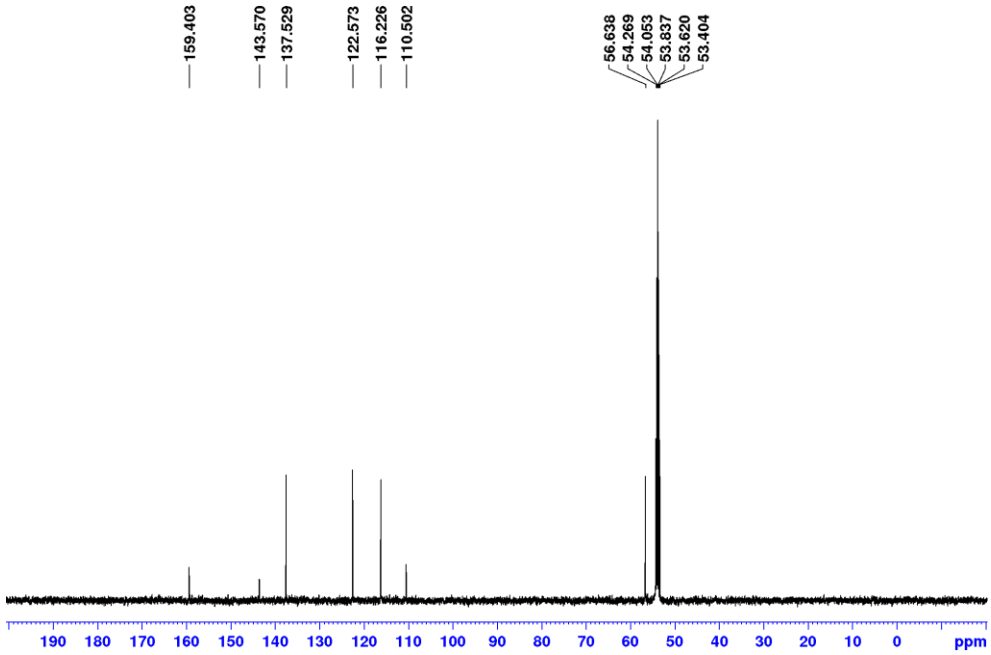

3c-^{i}Bu. A flask was charged with ^{i}BuOH (0.4 mL, 4.3 mmol), pyridine (0.7 mL, 0.08 mol) and $CHCl_3$ (10 mL), and cooled to 0 ^{o}C for 30 min. A solution of 2-bromo-5-methoxybenzenesulfonyl chloride (1.0 g, 3.5 mmol) in $CHCl_3$ (5 mL) was added, and the mixture was stirred for 20 h. HCl solution (0.1 M in H_2O, 40 mL) was added, and the mixture was stirred for 5 min and transferred to a separatory funnel. The $CHCl_3$ layer was washed with H_2O (3 × 50 mL) and brine (10 mL), and dried over $MgSO_4$. The volatiles were removed under vacuum to yield an orange oil. The crude product was purified by silica gel chromatography using 1:2 hexanes/CH_2Cl_2 as the eluent. The product was isolated as a yellow oil (0.64 g, 64 %). The ethyl ester of 2-bromo-5-methoxybenzenesulfonate, which is formed by the reaction with EtOH instead of ^{i}BuOH, was present as a minor impurity. Commercial $CHCl_3$ contains EtOH as stabilizer. ^{1}H NMR (CD_2Cl_2): δ 7.66 (t, $^{3}J_{HH}$ = 9, 1H, H^5), 7.61 (d, $^{4}J_{HH}$ = 3, 1H, H^2), 7.02 (dd, $^{3}J_{HH}$ = 9, $^{4}J_{HH}$ = 3, 1H, H^4), 4.15 (q, $^{3}J_{HH}$ = 7, 2H, $–SO_3CH_2CH_3$), 3.85 (s, 3H, $–OCH_3$), 3.84 (d, $^{3}J_{HH}$ = 7, 2H, $–SO_3CH_2CH(CH_3)_2$), 1.99 (sept, $^{3}J_{HH}$ = 7, 1H, $–SO_3CH_2CH(CH_3)_2$), 1.34 (t, $^{3}J_{HH}$ = 7, 3H, $–SO_3CH_2CH_3$), 0.94 (d, $^{3}J_{HH}$ = 7, 6H, $–SO_3CH_2CH(CH_3)_2$). $^{13}C\{^{1}H\}$ NMR (CD_2Cl_2): δ 159.2 (s), 137.3 (s, C^1), 136.7 (s), 120.8 (s), 117.8 (s), 110.6 (s), 77.8 (s, $–SO_3CH_2CH(CH_3)_2$), 68.5 (s, $–SO_3CH_2CH_3$), 56.4 (s, $–OCH_3$), 28.5 (s, $–SO_3CH_2CH(CH_3)_2$), 18.8 (s, $–SO_3CH_2CH(CH_3)_2$), 14.9 (s, $–SO_3CH_2CH_3$). GCMS Calcd. for $[C_{11}H_{16}O_4SBr + H]^+$ 322.0, Found: 321.9.

Figure 4.13. Numbering scheme for **3c-^{i}Bu**.

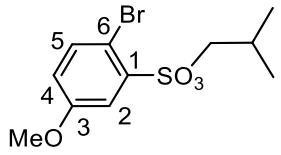

Figure 4.14. NMR spectra of 3c-^{i}Bu.

(a) ^{1}H NMR (CD_2Cl_2, 500 MHz):

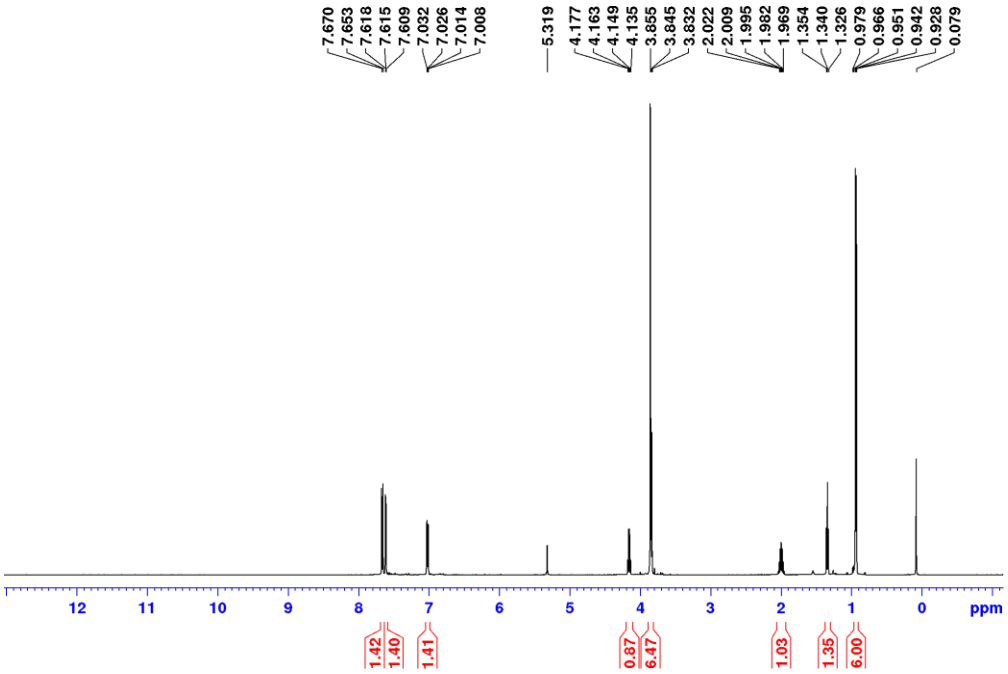

Figure 4.14, continued.

(b) $^{13}C\{^{1}H\}$ NMR ($CDCl_3$, 125 MHz):

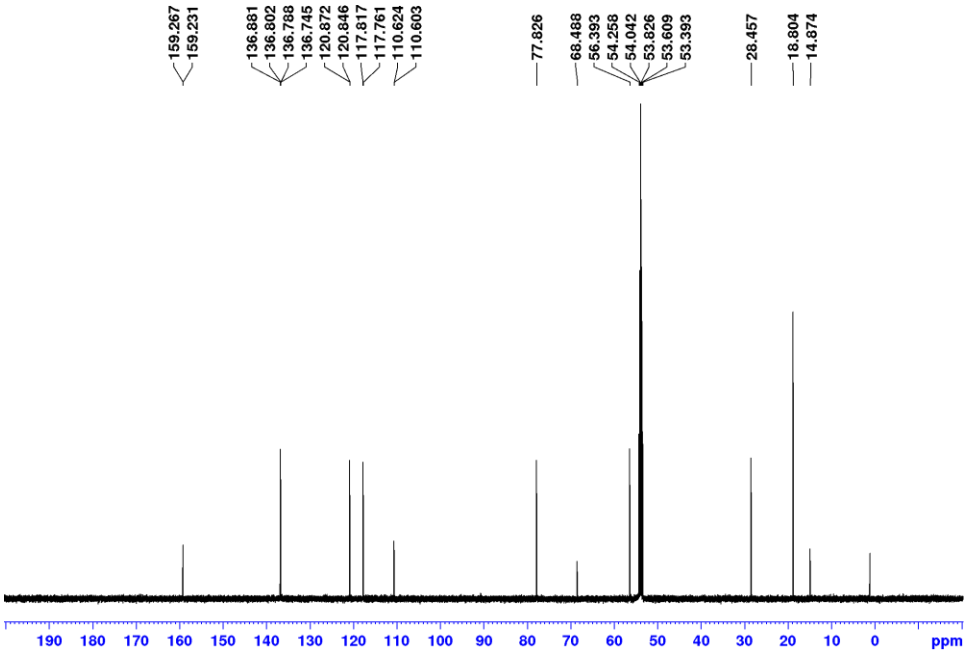

3d-^{i}Bu. 3d-^{i}Bu was synthesized analogously to **3c-^{i}Bu** from ^{i}BuOH (2.3 mL, 25 mmol), pyridine (3.8 mL, 50 mmol) and 3-isopropylbenzenesulfonyl chloride (5.0 g, 23 mmol). HCl solution (0.1 M in H_2O, 40 mL) was added, and the mixture was stirred for 5 min and transferred to a separatory funnel. The $CHCl_3$ layer was washed with H_2O (3 × 50 mL) and brine (10 mL), and dried over $MgSO_4$. The volatiles were removed under vacuum to yield a colorless oil (4.9 g, 88 %). The ethyl ester of 3-isopropylbenzenesulfonate, which is formed by the reaction with EtOH instead of ^{i}BuOH, was present as a minor impurity. Commercial $CHCl_3$ contains EtOH as stabilizer. ^{1}H NMR (CD_2Cl_2): δ 7.74 (dd, $^{4}J_{HH}$ = 1.7, 1H, H^2), 7.70 (ddd, $^{3}J_{HH}$ = 7, $^{4}J_{HH}$ = 1.4, 1H,

H^4), 7.39 (d, $^3J_{HH}$ = 7, 1H, H^6), 7.48 (t, $^3J_{HH}$ = 8, 1H, H^5), 3.78 (d, $^3J_{HH}$ = 7, 2H, –$SO_3CH_2CH(CH_3)_2$), 3.01, (sept, $^3J_{HH}$ = 7, 1H, –$CH(CH_3)_2$), 1.91 (sept, $^3J_{HH}$ = 7, 1H, –$SO_3CH_2CH(CH_3)_2$), 1.28 (d, $^3J_{HH}$ = 7, 6H, –$CH(CH_3)_2$), 0.87 (d, $^3J_{HH}$ = 6, 6H, –$SO_3CH_2CH(CH_3)_2$). $^{13}C\{^1H\}$ NMR ($CDCl_3$): δ 151.0 (s), 136.4 (s), 132.4 (s), 129.6 (s), 126.0 (s), 125.6 (s, C^6), 76.9 (s, -$SO_3CH_2CH(CH_3)_2$), 34.5 (s, –$CH(CH_3)_2$), 28.4 (s, -$SO_3CH_2CH(CH_3)_2$), 23.9 (s, –$CH(CH_3)_2$), 18.7 (s, -$SO_3CH_2CH(CH_3)_2$). HRMS (APCI/ESI-Mixed mode; *m*/*z*): Calcd. for $[2(C_{13}H_{20}O_3S) + Na]^+$ 535.21643, Found: 535.2161.

Figure 4.15. Numbering scheme for **3d-^{i}Bu**.

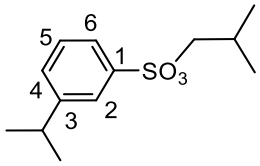

Figure 4.16. NMR spectra of 3d-^{i}Bu

(a) ^{1}H NMR (CD_2Cl_2, 500 MHz):

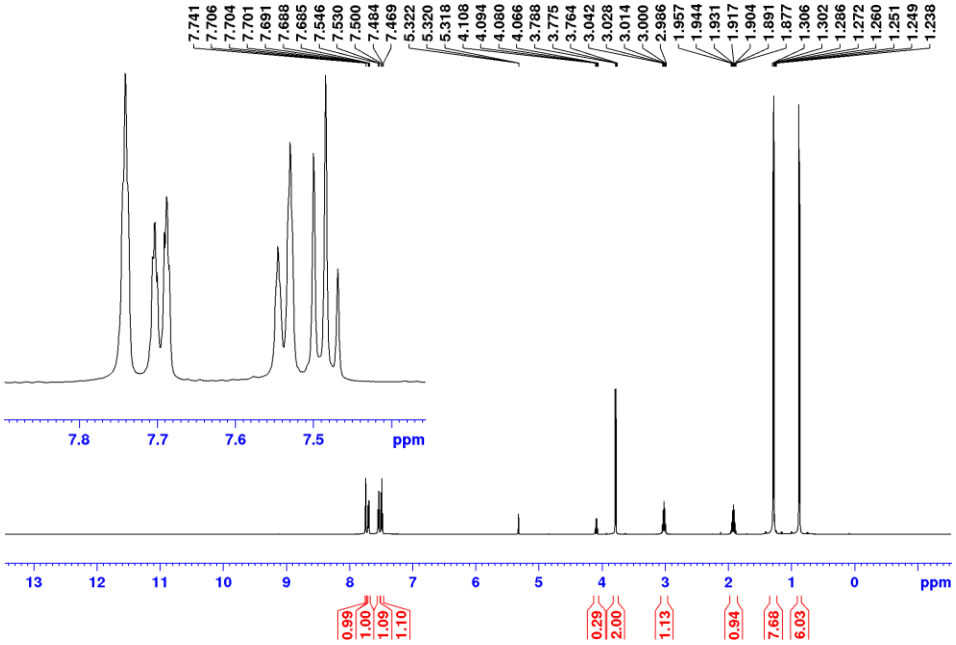

(b) ^{13}C{^{1}H} NMR (CD_2Cl_2, 125 MHz):

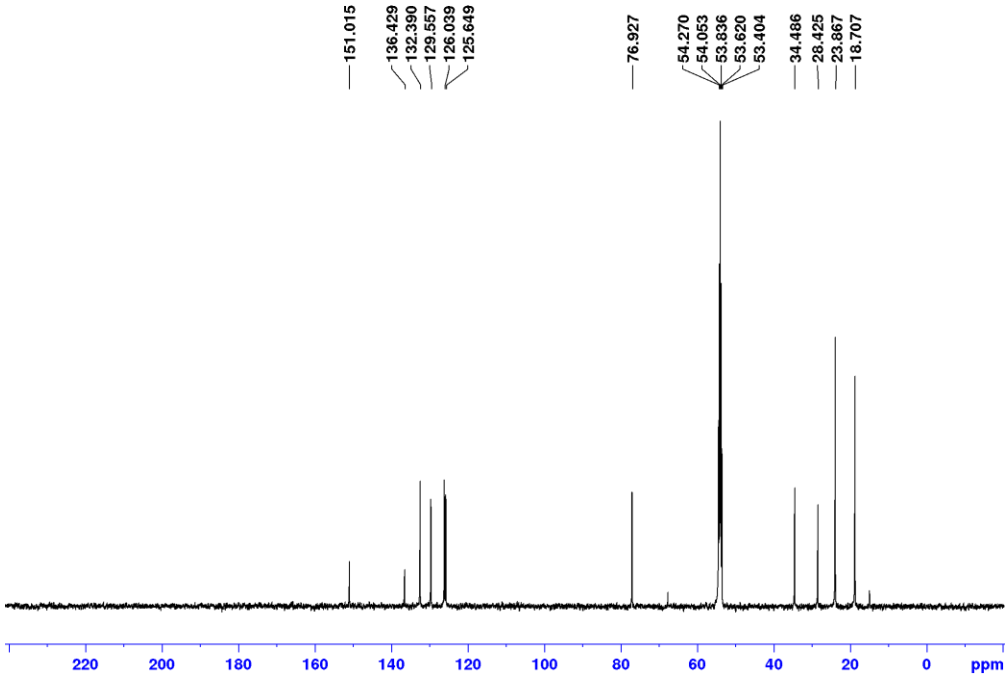

4c-^{i}Bu. A Schlenk flask was charged with **3c-^{i}Bu** (0.62 g, 2.0 mmol) and THF (20 mL) and cooled to –78 ^{o}C. ^{n}BuLi (2.5 M solution in hexanes, 0.8 mL, 2.0 mmol) was added dropwise via syringe. The mixture was stirred at –78 ^{o}C for 1 h, and $PPhCl_2$ (0.14 mL, 1.0 mmol) was added. The volatiles were removed under vacuum, and the resulting orange oil was taken up in H_2O (50 mL) and extracted with Et_2O (3 × 50 mL). The combined organic fractions were washed with brine (15 mL) and dried over $MgSO_4$, and the volatiles were removed under vacuum to yield a white solid. The crude product was purified by crystallization from a CH_2Cl_2 solution layered with hexanes at –10 ^{o}C. The product was isolated as a white solid (0.3 g, 38 %). The ethyl sulfonate esters $(2\text{-}SO_3Et\text{-}4\text{-}OMe\text{-}Ph)_2PPh$ and $(2\text{-}SO_3Et\text{-}4\text{-}OMe\text{-}Ph)(2\text{-}SO_3{}^{i}Bu\text{-}4\text{-}OMe\text{-}Ph)PPh$, which are formed from the 2-bromo-5-methoxybenzenesulfonate ethyl ester impurity in **3c-^{i}Bu**, are present as minor impurities. $^{31}P\{^{1}H\}$ NMR (CD_2Cl_2): δ –13.7. ^{1}H NMR (CD_2Cl_2): δ 7.65 (dd, $^{4}J_{HH}$ = 3, $^{4}J_{PH}$ = 3, 2H, H^{3}), 7.34 (m, 3H, H^{9} and H^{10}), 7.11 (dd, $^{3}J_{HH}$ = 6, $^{4}J_{PH}$ = 6, 2H, H^{5}), 7.00 (dd, $^{3}J_{HH}$ = 9, $^{4}J_{HH}$ = 3, 2H, H^{8}), 6.89 (dd, $^{3}J_{HH}$ = 7, $^{4}J_{PH}$ = 3, 2H, H^{6}), 3.95 (dd, $^{2}J_{HH}$ = 9, $^{3}J_{HH}$ = 6, 2H, H^{12}), 3.87 (s, 6H, H^{11}), 3.84 (dd, $^{2}J_{HH}$ = 9, $^{3}J_{HH}$ = 6, 2H, $H^{12'}$), 1.95 (sept, $^{3}J_{HH}$ = 7, 2H, H^{13}), 0.94 and 0.93 (d, $^{3}J_{HH}$ = 7, 12H, H^{14} and $H^{14'}$). $^{13}C\{^{1}H\}$ NMR (CD_2Cl_2): δ 160.5 (s), 141.7 (d, $^{2}J_{PC}$ = 28), 138.4 (d, $^{1}J_{PC}$ = 29), 138.3 (s), 134.0 (d, $^{1}J_{PC}$ = 22), 129.2 (d, $^{2}J_{PC}$ = 3), 128.9 (s), 119 (s), 117.0 (s), 77.6 (d, $^{5}J_{PC}$ = 3, $C^{13,13'}$), 56.2 (s, –O*C*H_3), 28.5 (C^{14}), 19.0 and 18.8 ($C^{15,15'}$). ESI-MS (1/1 CH_3OH/H_2O; *m/z*): Calcd. for $[C_{28}H_{35}O_8PS_2 + H]^{+}$ 595.2, Found: 595.1.

Figure 4.17. Numbering scheme for **4c-^{i}Bu**.

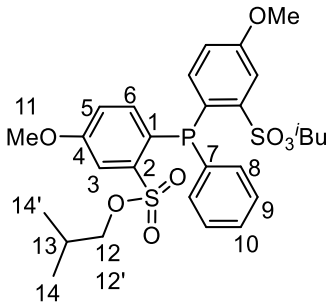

Figure 4.18. NMR spectra of 4c-^{i}Bu.

(a) $^{31}P\{^{1}H\}$ NMR (CD_2Cl_2, 202 MHz):

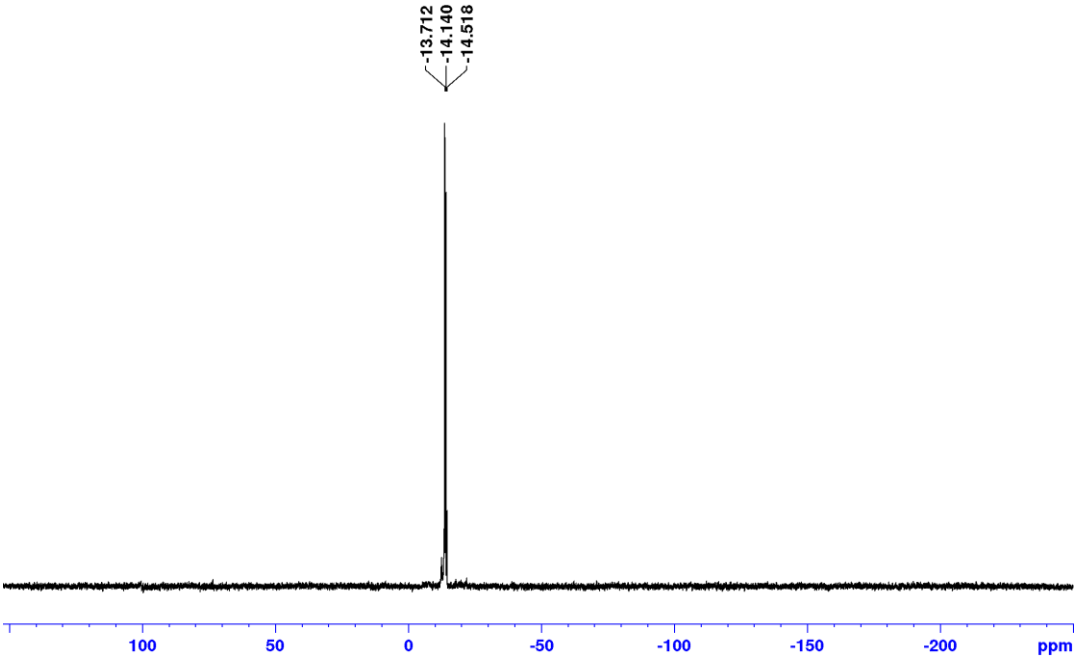

Figure 4.18, continued.

(b) ^{1}H NMR (CD_2Cl_2, 500 MHz):

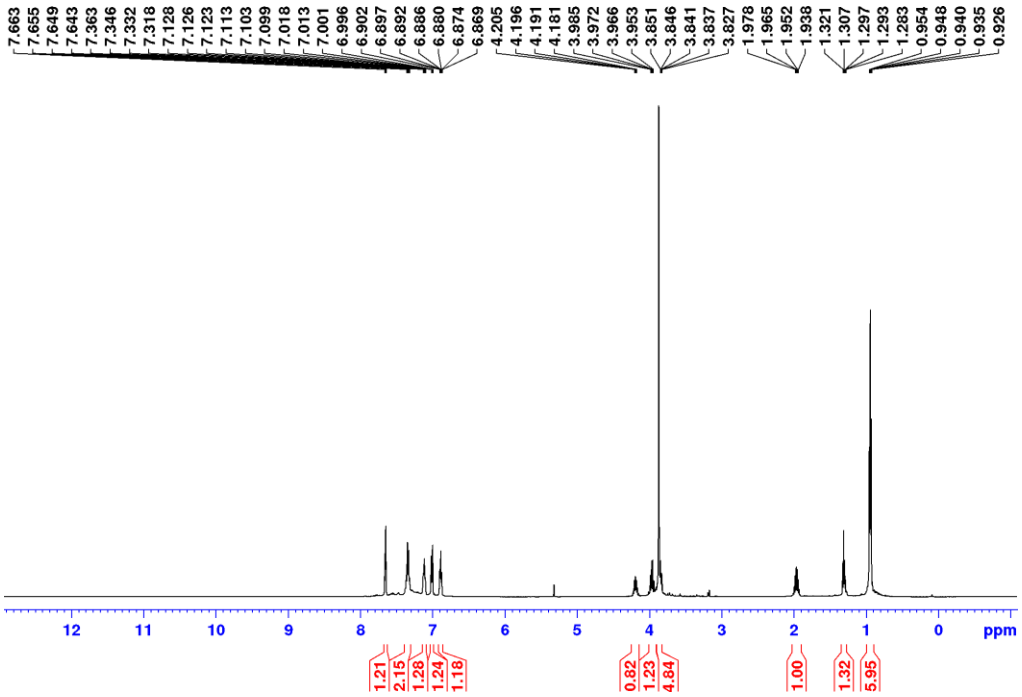

(c) $^{13}C\{^{1}H\}$ NMR (CD_2Cl_2, 125 MHz):

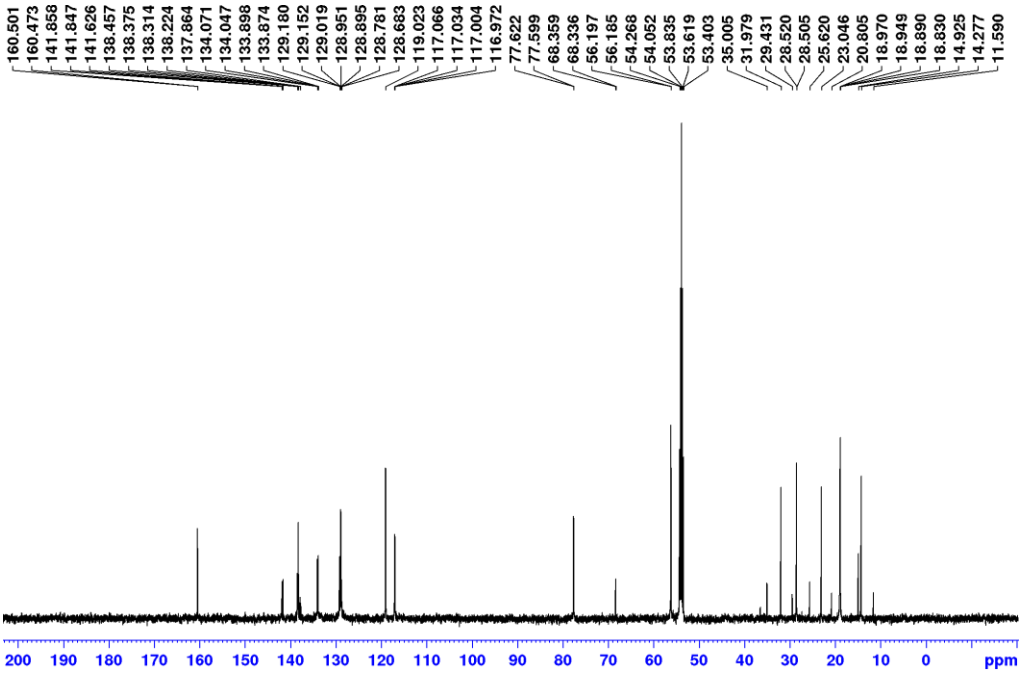

4d-^{i}Bu. 4d-^{i}Bu was synthesized analogously to **4c-^{i}Bu** from **3d-^{i}Bu** (3.1 g, 12 mmol) and $PPhCl_2$ (0.82 mL, 6.0 mmol). The volatiles were removed under vacuum, and the resulting orange oil was taken up in H_2O (50 mL) and extracted with Et_2O (3 × 50 mL). The combined organic fractions were washed with brine (15 mL) and dried over $MgSO_4$, and the volatiles were removed under vacuum to yield an orange oil. The crude product was purified by silica gel chromatography using a 9:1 hexanes/ethyl acetate mixture as the eluent. The product isolated as a white solid by layering a CH_2Cl_2 solution with hexanes at –40 ^{o}C (2.4 g, 63 %). The ethyl sulfonate ester (2-SO_3Et-4-^{i}Pr-Ph)(2-$SO_3{}^{i}$Bu-4-^{i}Pr-Ph)PPh, which is formed from the 3-isopropylbenzenesulfonate ethyl ester impurity in **3d-^{i}Bu**, is present as a minor impurity. $^{31}P\{^{1}H\}$ NMR (CD_2Cl_2): δ –11.6. ^{1}H NMR (CD_2Cl_2): δ 7.97 (dd, $^{4}J_{HH}$ = 2, $^{4}J_{PH}$ = 4, 2H, H^{3}), 7.4–7.3 (m, 5H, H^{8}, H^{9} and H^{10}), 7.12 (ddd, $^{3}J_{HH}$ = 8, $^{4}J_{HH}$ = 2, $^{4}J_{PH}$ = 7, 2H, H^{5}), 6.89 (dd, $^{3}J_{HH}$ = 8, $^{3}J_{PH}$ = 3, 2H, H^{6}), 3.92 and 3.82 (dd, $^{3}J_{HH}$ = 7, $^{2}J_{HH}$ = 9, 4H, $H^{13,13'}$), 3.00 (sept, $^{3}J_{HH}$ = 7, 2H, H^{11}), 1.93 (sept, $^{3}J_{HH}$ = 7, 2H, H^{14}), 1.28 (d, $^{3}J_{HH}$ = 7, 12H, H^{12}), 0.93 and 0.92 (d, $^{3}J_{HH}$ = 6, 12H, $H^{15,15'}$). $^{13}C\{^{1}H\}$ NMR ($CDCl_3$): δ 151.0 (C^{4}), 140.4 (d, $^{2}J_{PC}$ = 26, C^{2}), 137.5 (d, $^{1}J_{PC}$ = 13, C^{7}), 137.0 (C^{6}), 135.4 (d, $^{1}J_{PC}$ = 31, C^{1}), 134.2 (d, $^{2}J_{PC}$ = 22, C^{8}), 131.7 (C^{5}), 129.5 (d, $^{3}J_{PC}$ = 3, C^{3}), 129.3 (C^{10}), 128.9 (d, $^{3}J_{PC}$ = 7, C^{9}), 77.3 (d, $^{5}J_{PC}$ = 3, $C^{13,13'}$), 34.5 (C^{11}), 28.5 (C^{14}), 23.7 ($C^{12,12'}$), 19.0 and 18.9 ($C^{15,15'}$). HRMS (ESI; *m*/*z*): Calcd. for $[C_{32}H_{43}O_6PS_2 + H]^{+}$ 619.231697, Found: 619.2425.

Figure 4.19. Numbering scheme for **4d-^{i}Bu**.

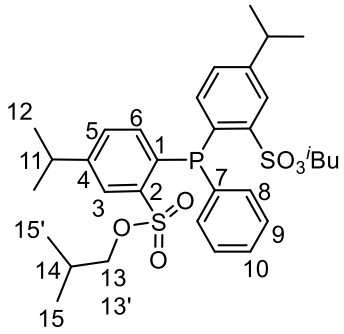

Figure 4.20. NMR spectra of 4d-^{i}Bu.

(a) $^{31}P\{^{1}H\}$ NMR (CD_2Cl_2, 202 MHz):

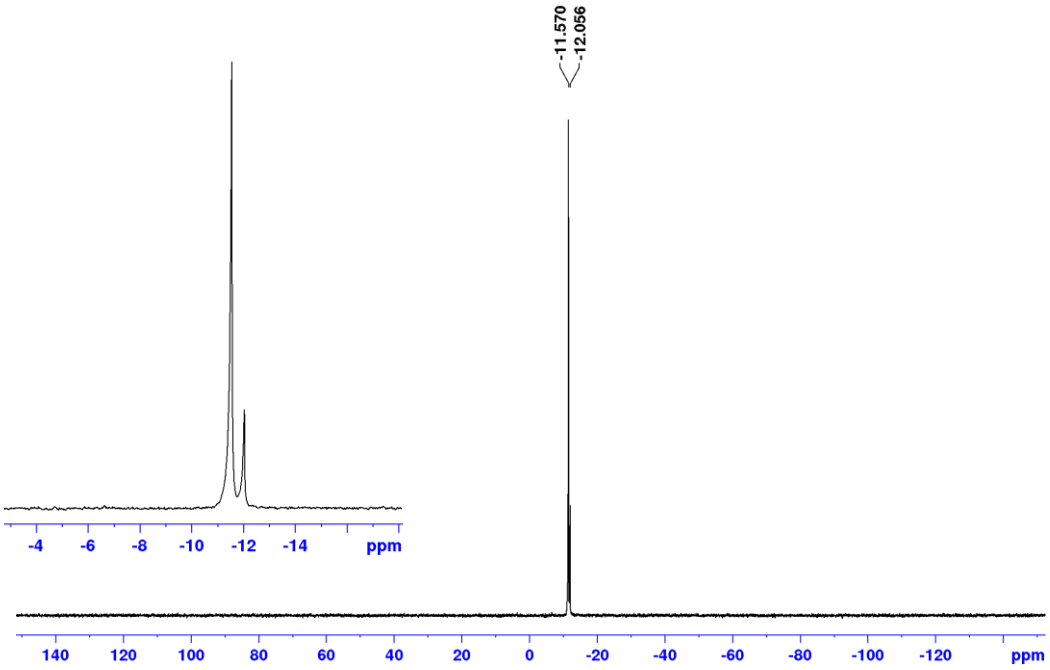

Figure 4.20, continued.

(b) ^{1}H NMR (CD_2Cl_2, 500 MHz):

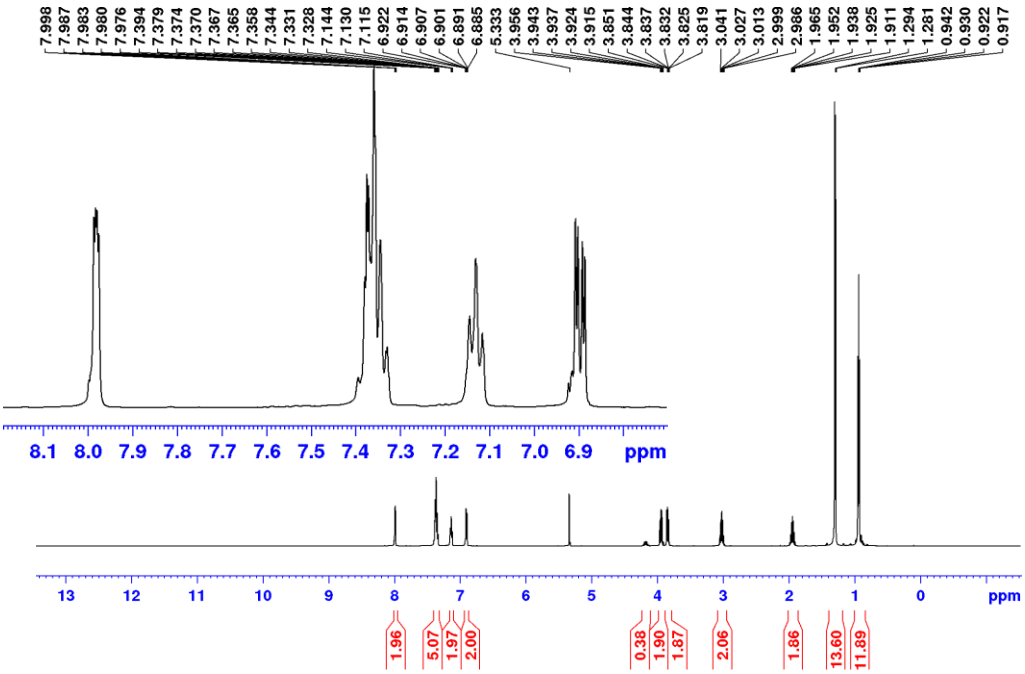

(c) ^{13}C{^{1}H} NMR (CD_2Cl_2, 125 MHz):

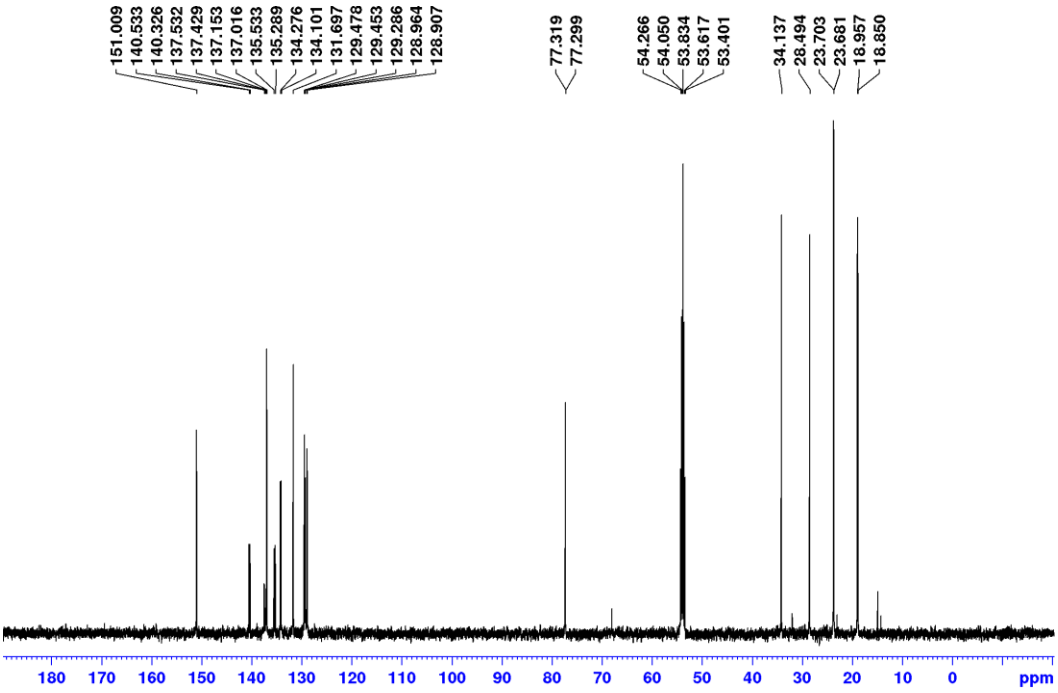

Li_2[4c]. A flask was charged with **4c-^{i}Bu** (0.2 g, 0.3 mmol) and LiI (0.2 g, 1.0 mmol) and dissolved in acetonitrile (4 mL). The mixture was covered in foil and stirred for 2 d. A white solid precipitated. The mixture was filtered and the solid was rinsed with acetonitrile (5 mL) and dried under vacuum to afford a white solid (0.14 g, 84 %). $^{31}P\{^1H\}$ NMR (CD_3OD): δ –17.4. ^1H NMR (CD_3OD): δ 7.63 (br, 2H, H^3), 7.22 (br, 3H, H^9 and H^{10}), 7.10 (br, 2H, H^8), 6.86 (br, 4H, H^5 and H^6), 3.82 (s, 6H, H^{11}). $^{13}C\{^1H\}$ NMR (CD_3OD): δ 161.2 (s), 151.1 (d, J_{PC} = 28), 141.4 (d, J_{PC} = 14), 138.5 (s), 134.5 (d, J_{PC} = 20), 128.9 (d, J_{PC} = 6), 128.6 (s), 127.9 (d, J_{PC} = 24), 116.5 (s), 114.7 (J_{PC} = 5), 55.9 (C^{11}). $^7Li\{^1H\}$ NMR (CD_3OD): δ 0.2. ESI-MS (1/1 CH_3OH/H_2O; *m/z*): Calcd. for $[C_{20}H_{17}O_8PS_2 + 3H]^+$ 483.0, Found: 483.1.

Figure 4.21. Numbering scheme for **Li_2[4c]**.

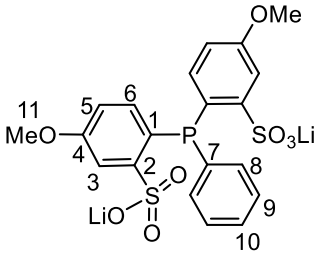

Figure 4.22. NMR spectra of Li_2[4c].

(a) $^{31}P\{^{1}H\}$ NMR (CD_3OD, 202 MHz):

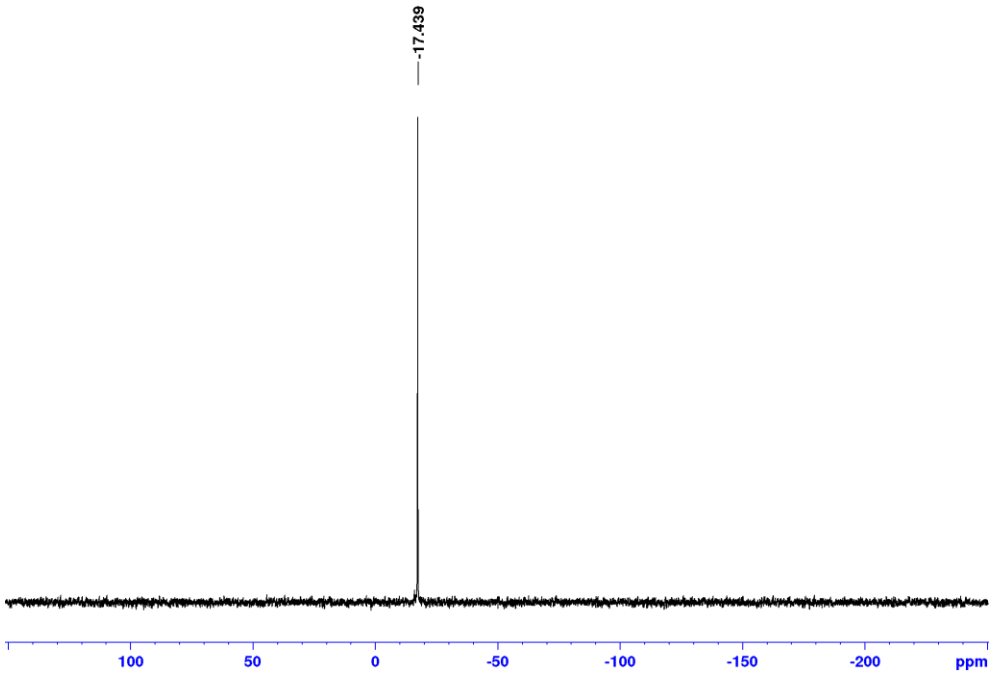

(b) ^{1}H NMR (CD_3OD, 500 MHz):

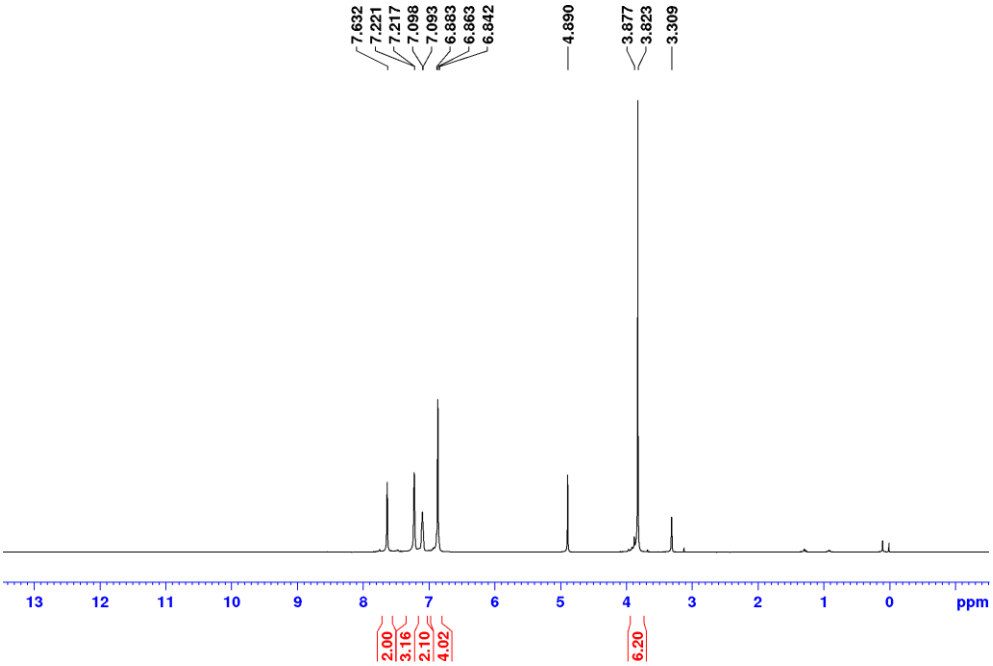

Figure 4.22, continued.

(c) $^{13}C\{^{1}H\}$ NMR (CD_3OD, 125 MHz):

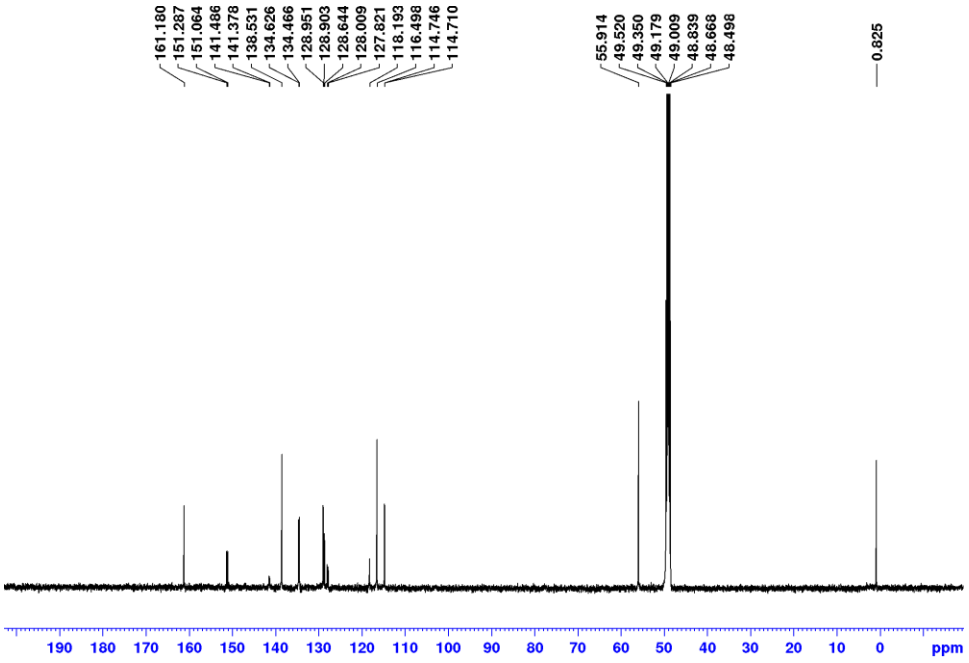

(d) $^{7}Li\{^{1}H\}$ NMR (CD_3OD, 156 MHz):

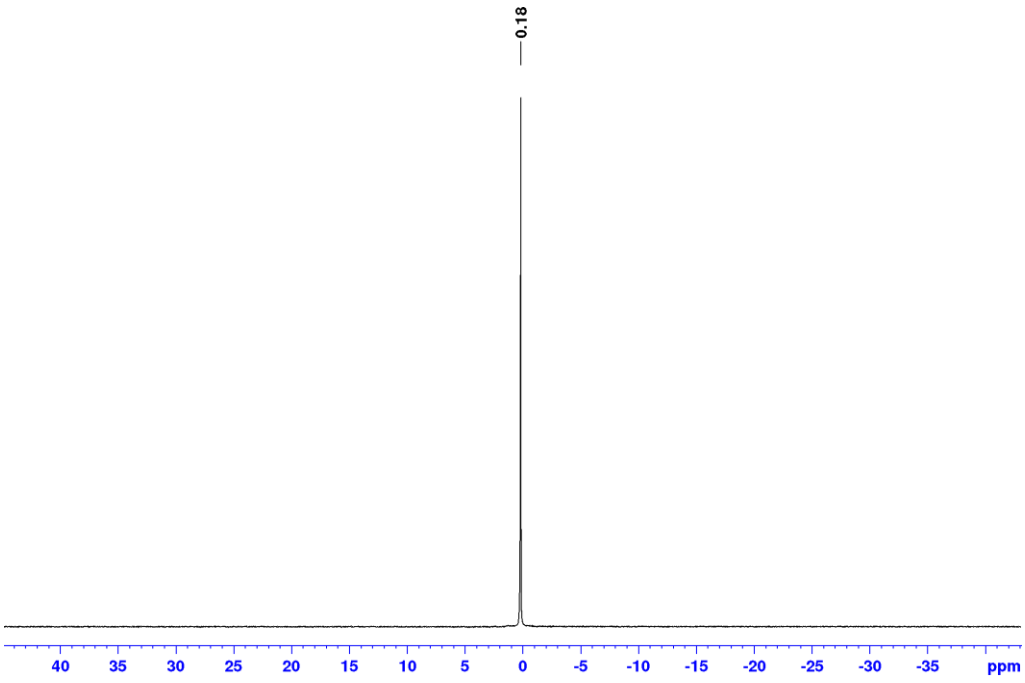

Li_2[4d]. Li_2[4d] was prepared analogously to **Li_2[4c]** from **4d-^{i}Bu** (0.5 g, 0.8 mmol) and LiI (0.41 g, 3.1 mmol) in acetonitrile (8 mL). The mixture was covered in foil and stirred for 18 h. A white solid precipitated. The mixture was filtered and the solid was rinsed with acetonitrile (20 mL) and dried under vacuum to afford a white solid (0.4 g, 95 %). $^{31}P\{^{1}H\}$ NMR (CD_3OD): δ –16.5. ^{1}H NMR (CD_3OD): δ 7.96 (d, $^{4}J_{PH}$ = 2, 2H, H^{3}), 7.23 (br, 3H, H^{9}, H^{10}), 7.16 (d, $^{3}J_{HH}$ = 8, 2H, H^{8}), 7.09 (m, 2H, H^{5}), 6.86 (dd, $^{3}J_{HH}$ = 8, $^{3}J_{PH}$ = 3, 2H, H^{6}), 2.94 (sept, $^{3}J_{HH}$ = 7, 2H, H^{11}), 1.26 (t, $^{3}J_{HH}$ = 7, 12H, H^{12}). $^{13}C\{^{1}H\}$ NMR (CD_3OD): δ 150.7 (C^{4}), 149.7 (d, $^{2}J_{PC}$ = 27, C^{2}), 140.9 (d, $^{1}J_{PC}$ = 14, C^{7}), 137.2 (C^{5}), 134.7 (d, $^{2}J_{PC}$ = 20, C^{8}), 134.3 (d, $^{1}J_{PC}$ = 25, C^{1}), 129.2 (C^{6}), 128.9 (d, $^{3}J_{PC}$ = 6, C^{9}), 128.8 (C^{10}), 127.0 (d, $^{3}J_{PC}$ = 4, C^{3}), 35.1 (C^{11}), 24.1 ($C^{12,12'}$). $^{7}Li\{^{1}H\}$ NMR (CD_3OD): δ 0.1. ESI-MS (1/1 CH_3OH/H_2O; *m/z*): Calcd. for $[C_{24}H_{28}O_6S_2P + H) - 2Li]^{+}$ 507.1, Found: 507.1.

Figure 4.23. Numbering scheme for **Li_2[4d]**.

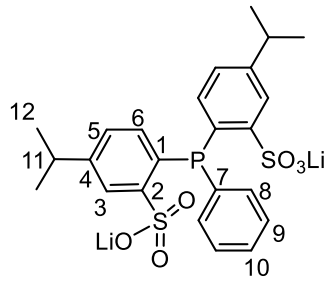

Figure 4.24. NMR spectra of Li_2[4d].

(a) $^{31}P\{^1H\}$ NMR (CD_3OD, 202 MHz):

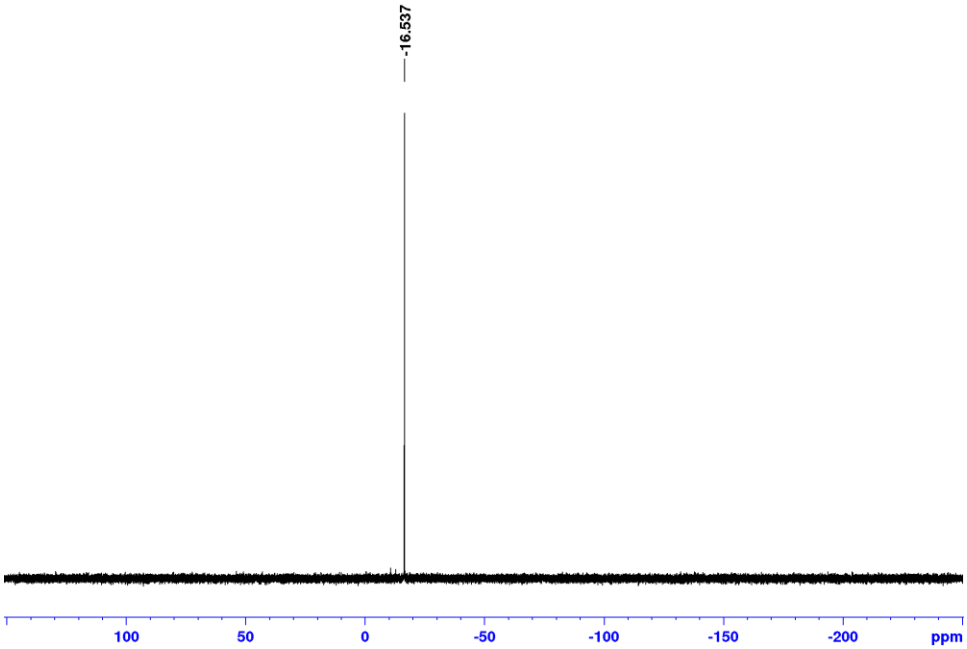

(b) ^1H NMR (CD_3OD, 500 MHz):

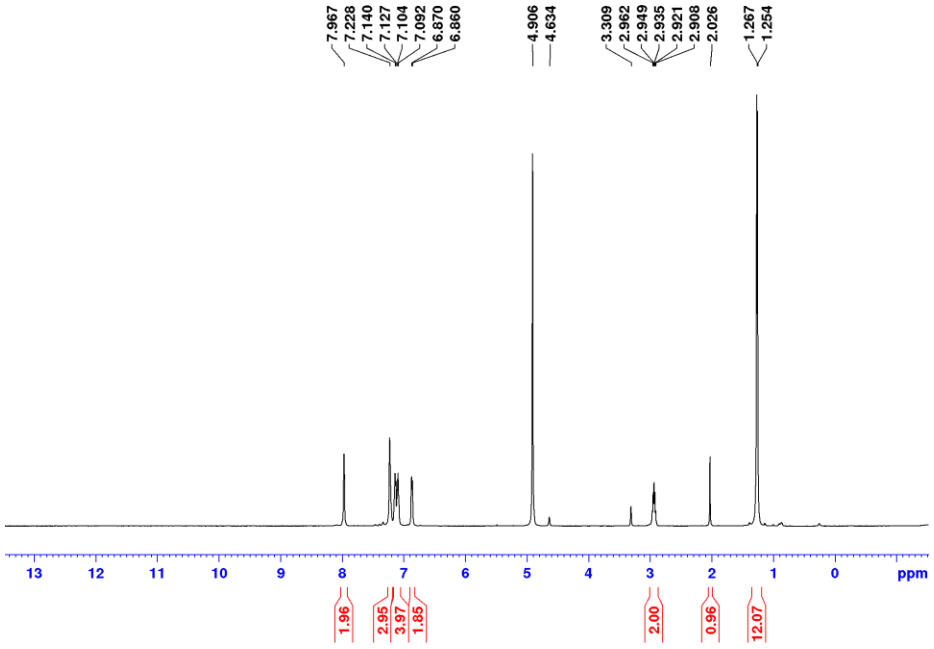

Figure 4.24, continued.

(c) $^{13}C\{^{1}H\}$ NMR (CD_3OD, 125 MHz):

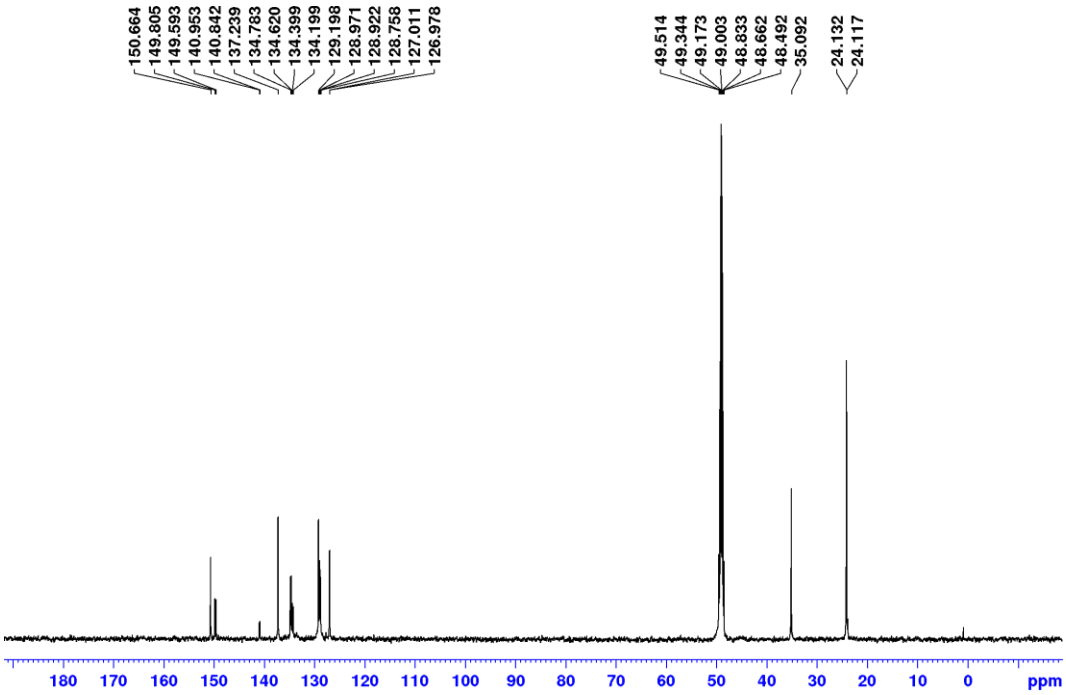

(d) $^{7}Li\{^{1}H\}$ NMR (CD_3OD, 156 MHz):

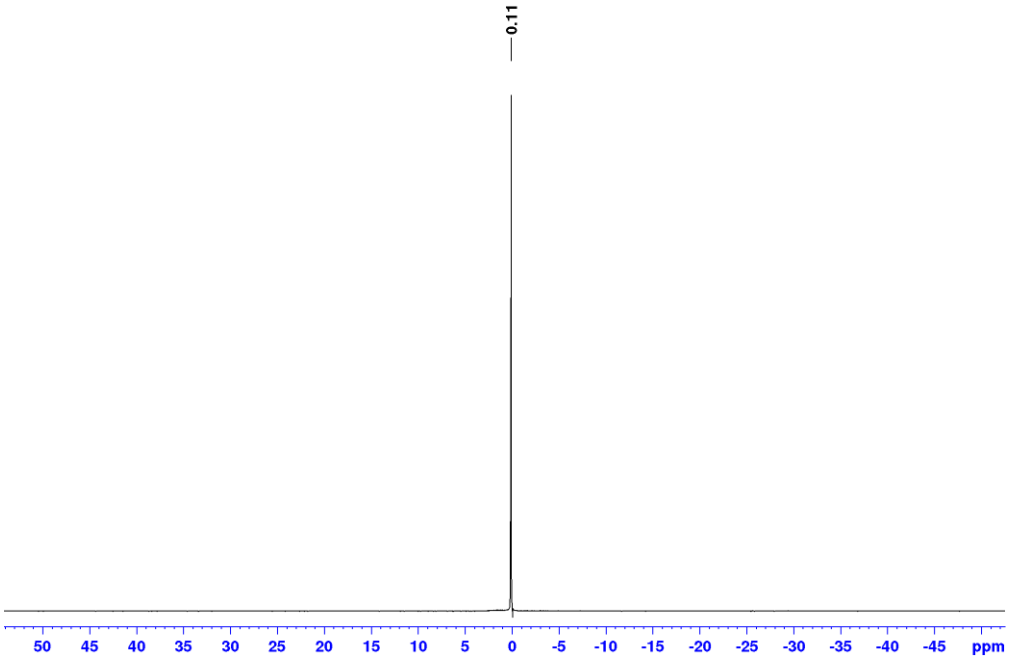

{[κ^2-P,O-PPh(2-SO$_3$-4-OMe-Ph)(2-SO$_3$Li-4-OMe-Ph)]PdMe(py')}$_4$•Li$_2$Cl$_2$ (5c).

Li_2[**4c**] (50 mg, 0.10 mmol), (COD)PdMeCl (31 mg, 0.10 mmol) and CH_2Cl_2 (5 mL) were added to a vial. The vial was wrapped with foil, and the mixture was stirred for 1 h at room temperature. 4-(5-nonyl)pyridine (23.4 µL, 0.101 mmol) was added and the mixture was stirred overnight at room temperature. The solution was filtered and the solvent was removed under vacuum to afford a pale yellow powder. This material was dissolved in CH_2Cl_2 (2 mL) and layered with hexanes (4 mL) to afford an off-white powder that was collected by filtration (28 mg, 33% yield). $^{31}P\{^1H\}$ NMR (CD_2Cl_2): δ 32.2. ^1H NMR (CD_2Cl_2): δ 8.69 (d, $^3J_{HH}$ = 6, 1H, H^5), 8.61 (d, $^3J_{HH}$ = 5, 2H, H^{11}), 7.99 (br, 1H, H^3), 7.80 (br, 1H, $H^{3'}$), 7.56–7.42 (m, 5H, H^8, H^9 and H^{10}; the H^8 resonance is broadened into the baseline due to restricted rotation around the P-C^7 bond), 7.14 (d, $^3J_{PH}$ = 6, 1H, $H^{5'}$), 7.00 (d, $^3J_{PH}$ = 6, 1H, H^6), 6.93 (d, $^3J_{PH}$ = 9, 1H, $H^{6'}$), 6.69 (d, $^3J_{HH}$ = 5, 2H, H^{12}), 4.16 (s, H^{19}), 4.05 (s, $H^{19'}$), 2.27 (sept, $^3J_{HH}$ = 5, 1H, H^{14}), 1.25–0.84 (m, 18H, H^{15}, H^{16}, H^{17} and H^{18}), –0.18 (d, $^3J_{PH}$ = 3, 3H, Pd–CH_3). $^7Li\{^1H\}$ NMR (CD_2Cl_2): δ –0.4, –0.8. $^{31}P\{^1H\}$ NMR (CD_3OD): δ 29.9. ^1H NMR (CD_3OD): δ 8.73 (br, 2H, H^{11}), 7.75 (br, 2H, H^8, this resonance is broad due to the restricted rotation around the P-C^7 bond), 7.68 (d, $^4J_{HH}$ = 1.5, $^4J_{PH}$ = 4, 2H, H^3), 7.48 (d, $^3J_{HH}$ = 7, $^4J_{HH}$ = 1.5, 1H, H^{10}), 7.43 (dd, $^3J_{HH}$ = 7, 2H, H^9), 7.35 (d, $^3J_{HH}$ = 6, 2H, H^{12}), 6.99 (dd, $^3J_{HH}$ = 8, $^3J_{PH}$ =11, 2H, $H^{6,6'}$), 6.93 (dd, $^3J_{HH}$ = 8, $^4J_{HH}$ = 1, 2H, $H^{5,5'}$), 3.85 (s, 6H, $H^{19,19'}$), 2.63 (sept, $^3J_{HH}$ = 5, 1H, H^{14}), 1.75–1.57 (m, 4H, H^{15}), 1.36–1.02 (m, 8H, H^{16} and H^{17}), 0.85 (t, $^3J_{HH}$ = 7, 6H, H^{18}), 0.53 (d, $^3J_{PH}$ = 3, 3H, Pd-CH_3). $^{13}C\{^1H\}$ NMR (CD_3OD): δ 162.7 (s),

151.5 (s), 150.3 (d, J_{PC} = 14), 137.1 (d, J_{PC} = 4), 136.8 (br), 133.2 (d, J_{PC} = 49), 131.7 (s), 129.6 (s), 129.5 (s), 125.6 (s), 125.1 (s), 116.4 (d, J_{PC} = 8), 115.8 (d, J_{PC} = 8), 56.1 ($C^{19,19'}$), 46.9 (C^{14}), 36.9 (C^{15}), 30.7 (C^{16}), 23.7 (C^{17}), 14.3 (C^{18}), –1.7 (d, $^{2}J_{PC}$ = 4, Pd-CH_3). ^{7}Li{^{1}H} NMR (CD_3OD): δ 0.1.

Figure 4.25. Numbering scheme for **5c.**

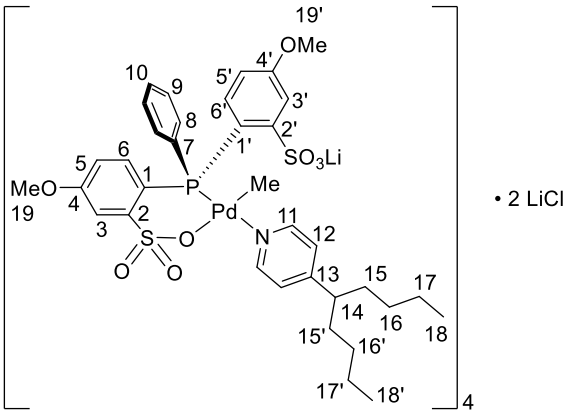

Figure 4.26. NMR spectra of 5c.

(a) ^{31}P{^{1}H} NMR (CD_2Cl_2, 202 MHz):

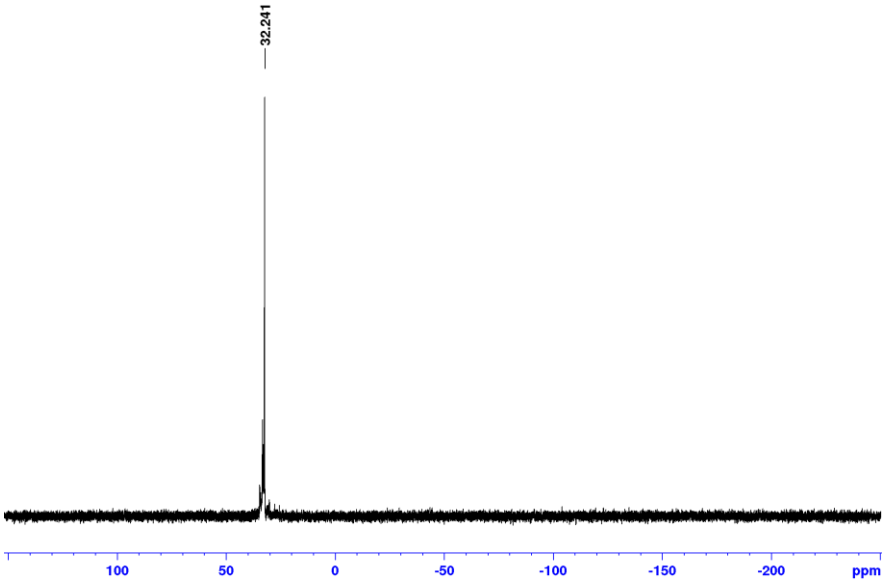

Figure 4.26, continued.

(b) ^{1}H NMR (CD_2Cl_2, 500 MHz):

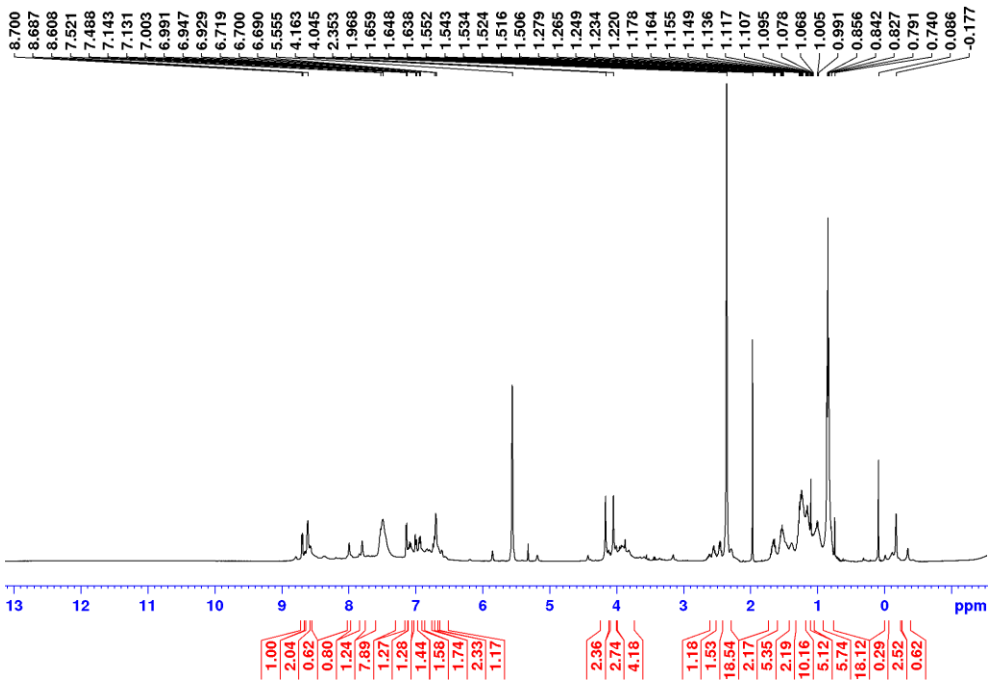

(c) ^{7}Li{^{1}H} NMR (CD_2Cl_2, 155 MHz):

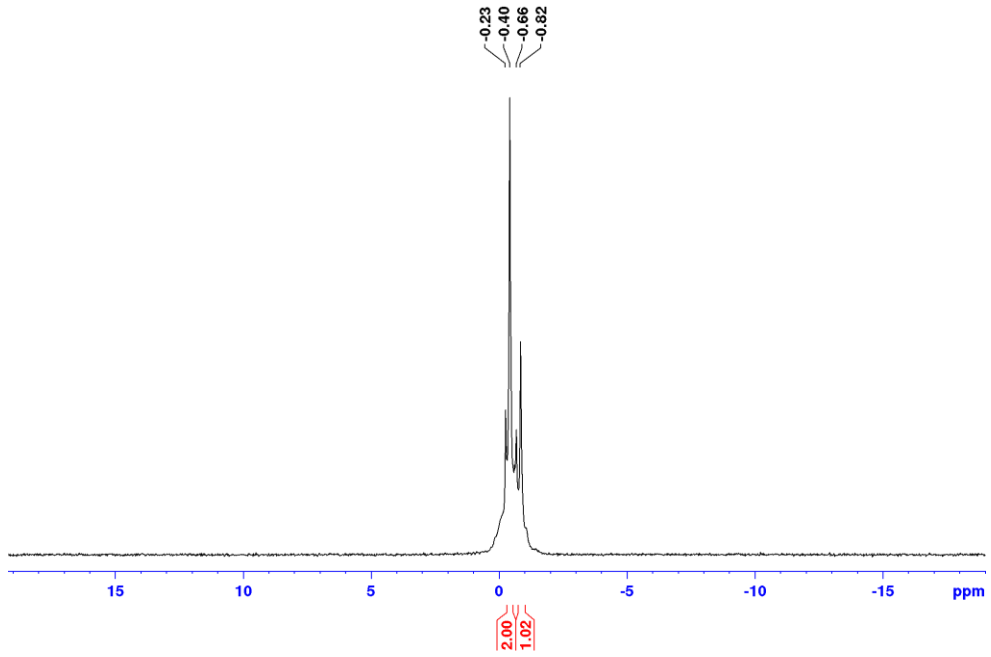

Figure 4.26, continued.

(d) $^{31}P\{^{1}H\}$ NMR (CD_3OD, 202 MHz):

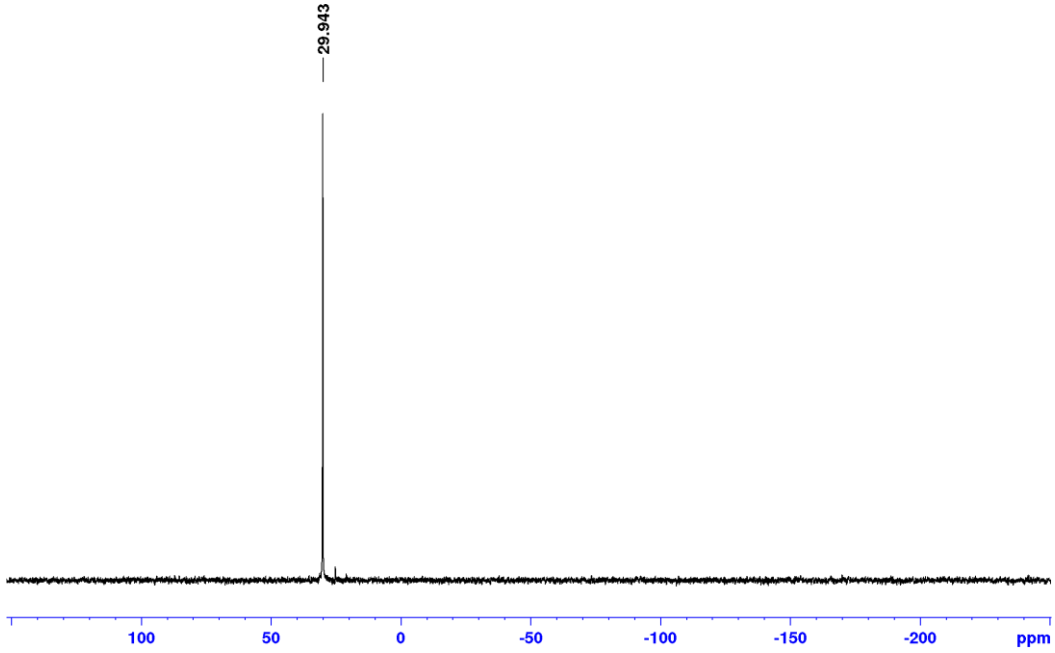

(e) ^{1}H NMR (CD_3OD, 500 MHz):

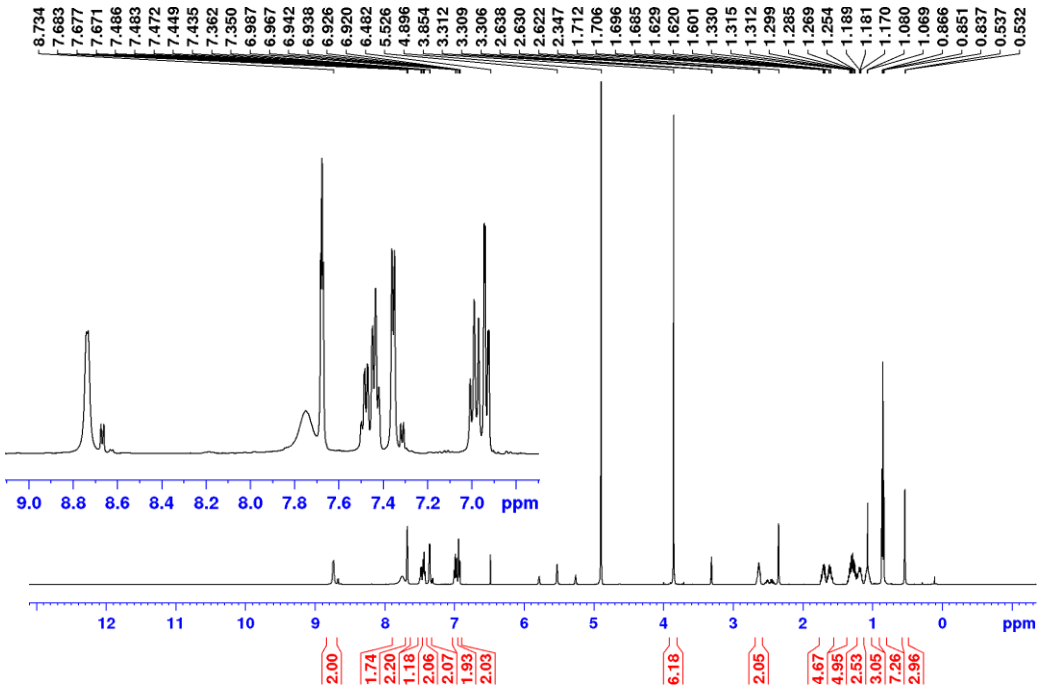

Figure 4.26, continued.

(f) $^{13}C\{^{1}H\}$ NMR (CD_3OD, 126 MHz):

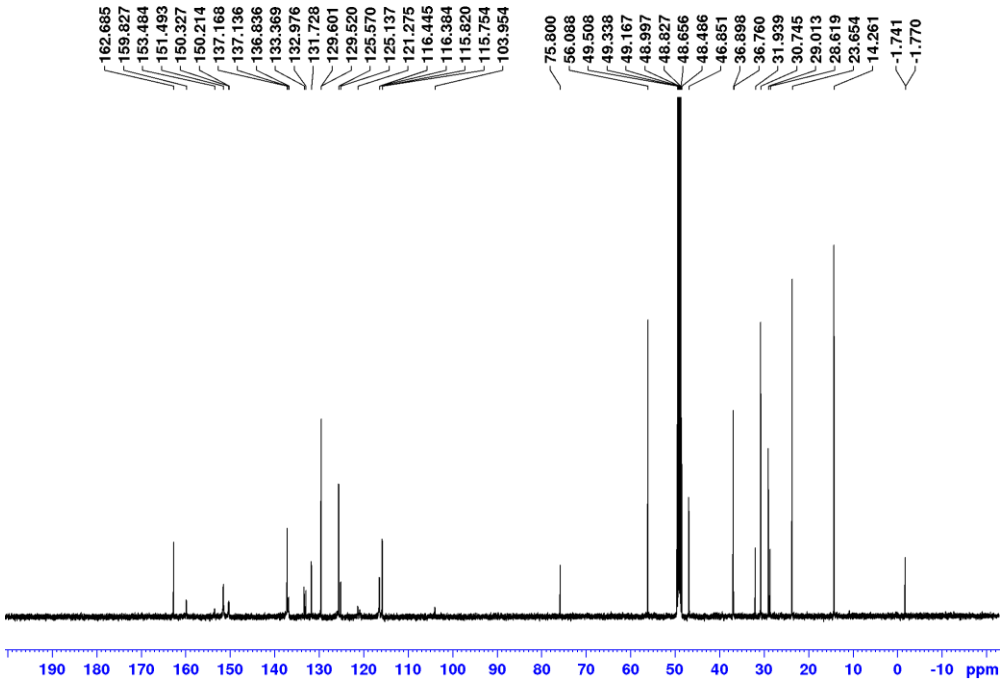

(g) $^{7}Li\{^{1}H\}$ NMR (CD_3OD, 155 MHz):

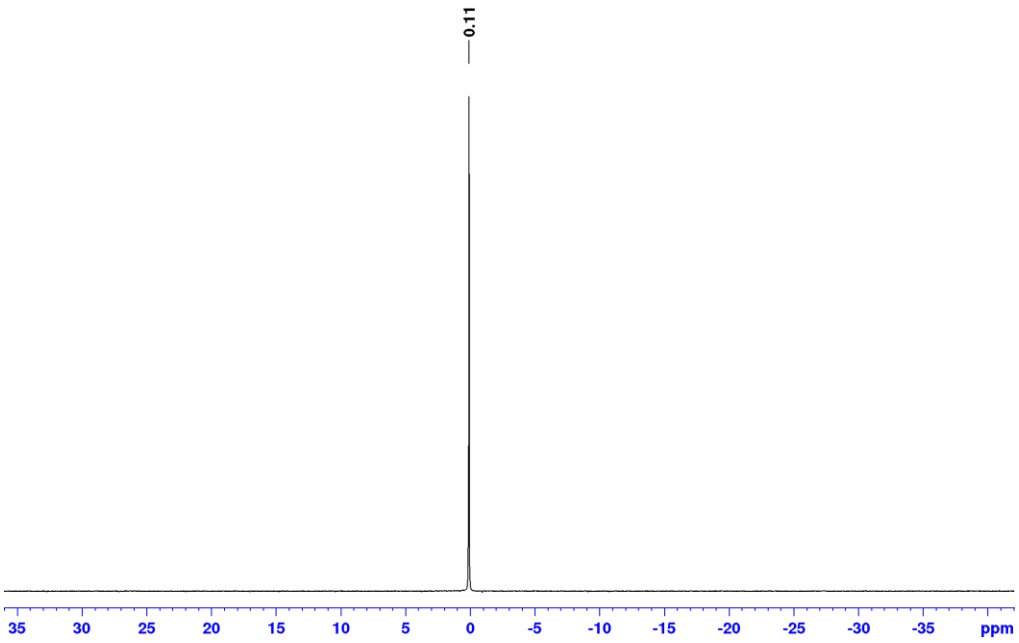

[(1)Pd(PhCH$_2$NMe$_2$)]$_4$•Li$_2$OAc$_2$ (6). 6 was synthesized analogously to **2** from **1** (0.15 g, 0.27 mmol), [(PhCH$_2$NMe$_2$)Pd(OAc)]$_2$ (81 mg, 0.14 mmol), and CH_2Cl_2 (8 mL). **6** was crystallized by layering hexanes onto the CH_2Cl_2 solution and cooling to -40 °C and collected by filtration. The filtrate was dried under vacuum to afford an off-white solid (0.142 g, 64 %). X-ray quality crystals were grown by layering hexanes onto a $CHCl_2CHCl_2$ solution at room temperature. $^{31}P\{^1H\}$ NMR (CD_2Cl_2): δ 28.8. ^1H NMR (CD_2Cl_2): δ 7.91 (d, $^4J_{PH}$ = 4, 1H, H^3), 7.57 (d, $^4J_{PH}$ = 5, 1H, $H^{3'}$), 7.39 (t, $^3J_{HH}$ = 7, 1H, H^{10}), 7.29 (t, $^3J_{HH}$ = 7, 2H, H^9), (the H^8 resonance is broadened into the baseline due to restricted rotation around the P-C^7 bond), 6.83 (t, $^3J_{HH}$ = 7, 1H, H^{13}), 6.67 (d, $^3J_{PH}$ = 8, 1H, H^{14}), 6.57 (d, $^3J_{HH}$ = 11, 1H, H^6), 6.44 (d, $^3J_{PH}$ = 11, 1H, $H^{6'}$), 6.42 (t, 1H, H^{12}), 5.99 (t, $^3J_{HH}$ = 7, 1H, H^{11}), 4.13 (s, 3H, $H^{19'}$), 3.98 (s, 3H, H^{19}), 3.75 (d, $^2J_{HH}$ = 14, 1H, H^{17}), 3.46 (s, 3H, H^{20}), 3.27 (s, 3H, $H^{20'}$), 3.06 (d, $^2J_{HH}$ = 13, 1H, $H^{17'}$), 2.58 (d, 3H, H^{18}), 2.01 (d, 3H, $H^{18'}$), 1.52 (s, 1.5H, C*H*$_3$COO). $^{13}C\{^1H\}$ NMR (CD_2Cl_2): δ 183.6 (s, *C*O$_2$CH$_3$), 151.5 (s, C^4), 151.2 (s, $C^{4'}$), 150.2 (d, $^3J_{PC}$ = 9, $C^{5'}$), 149.4 (d, obscured by C^{16}, C^5), 149.3 (s, C^{16}), 141.9 (s, C^{15}), 140.9 (d, $^2J_{PC}$ = 10, $C^{2'}$), 139.7 (d, $^2J_{PC}$ = 15, C^2), 135.6 (d, $^2J_{PC}$ = 12, C^{11}), 131.5 (d, $^1J_{PC}$ = 42, C^7), 131.3 (s, C^8), 128.9 (s, C^9), 128.8 (C^{10}), 125.2 (br, C^{12}), 124.5 (s, C^{13}), 123.6 (s, C^{14}), 120.1 (d, $^1J_{PC}$ = 55, C^1), 119.1 (s, C^6), 116.8 (d, $^1J_{PC}$ = 47, $C^{1'}$), 118.2 (d, $^2J_{PC}$ = 8, $C^{6'}$), 115.0 (d, $^3J_{PC}$ = 8, C^3), 112.8 (d, $^3J_{PC}$ = 10, $C^{3'}$), 70.9 (s, C^{17}), 57.1 (s, C^{19}), 56.7 (s, $C^{20'}$), 56.2 (s, $C^{19'}$), 55.9 (s, C^{20}), 50.2 (s, C^{18}), 49.3 (s, $C^{18'}$), 25.4 (s, CO$_2$*C*H$_3$). $^7Li\{^1H\}$ NMR (CD_2Cl_2): δ -0.7, -1.6. $^{31}P\{^1H\}$ NMR (CD_3OD): δ 30.7. ^1H NMR (CD_3OD): δ 7.90 (br, 2H, H^8,

this resonance is broad due to the restricted rotation around the P-C[7] bond), 7.62 (d, $^{4}J_{PH}$ = 4, 2H, H[3,3']), 7.48 (t, $^{3}J_{HH}$ = 7, 1H, H[10]), 7.41 (t, $^{3}J_{HH}$ = 7, 2H, H[9]), 6.93 (d, $^{3}J_{HH}$ = 7, 1H, H[24]), 6.76 (m, 1H, H[23]), 6.68 (d, $^{3}J_{PH}$ = 9, 2H, H[6,6']), 6.36 (m, 2H, H[21] and H[22]), 4.02 (br, 2H, H[27] and H[27']), 3.88 (s, 6H, H[19,19']), 3.55 (s, 6H, H[20,20']), 2.80 (d, $^{3}J_{HH}$ = 2, 6H, H[28] and H[28']), 1.90 (s, CO_2CH_3). $^{13}C\{^{1}H\}$ NMR (CD_3OD): δ 180.3 (s, CO_2CH_3), 151.8 (br), 150.7 (br), 150.4 (d, J_{PC} = 2), 144.1 (s), 138.0 (s), 137.9 (s), 137.6 (br), 132.2 (s), 132.1 (s), 131.7 (s), 129.5 (d, J_{PC} = 11), 125.8 (d, J_{PC} = 6), 125.0 (s), 123.5 (s), 118.8 (s), 113.9 (br), 72.0 (s, C[17]), 56.5 (s, C[19]), 56.2 (s, C[20]), 50.1 (s, C[28]), 24.2 (s, CO_2CH_3). $^{7}Li\{^{1}H\}$ NMR (CD_3OD): δ 0.1. HRMS (ESI; *m*/*z*): Calcd. for $[C_{64}H_{69}N_2O_{22}P_2Pd_2S_4 + H]^+$ 1622.08545, Found: 1622.0841.[16]

Figure 4.27. Numbering scheme for **6**.

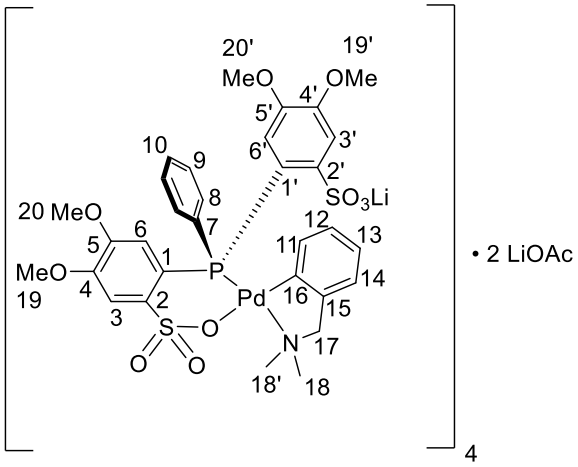

Figure 4.28. NMR spectra of 6.

(a) $^{31}P\{^{1}H\}$ NMR (CD_2Cl_2, 202 MHz):

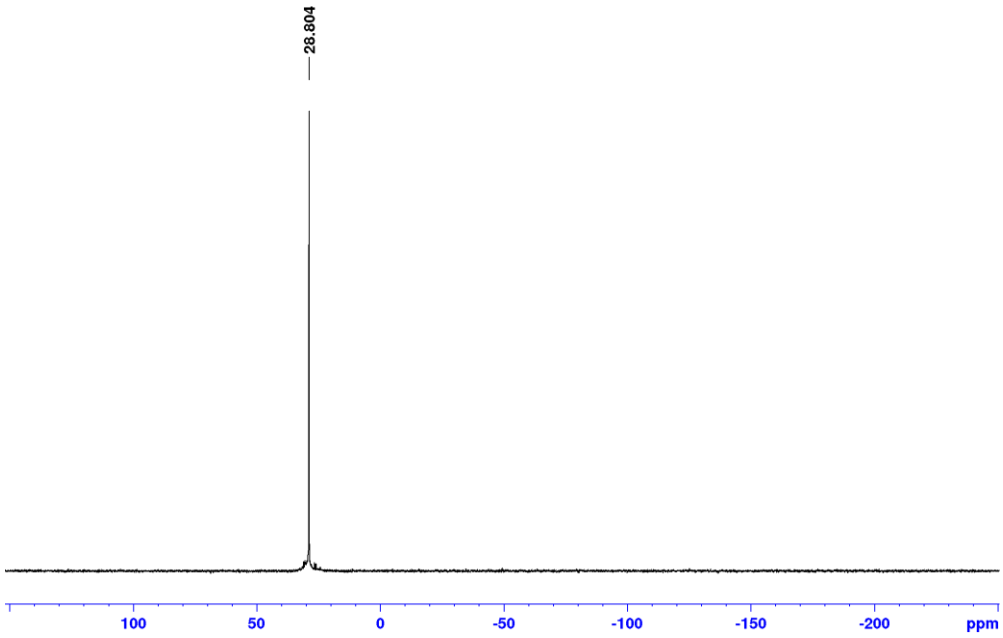

(b) ^{1}H NMR (CD_2Cl_2, 500 MHz):

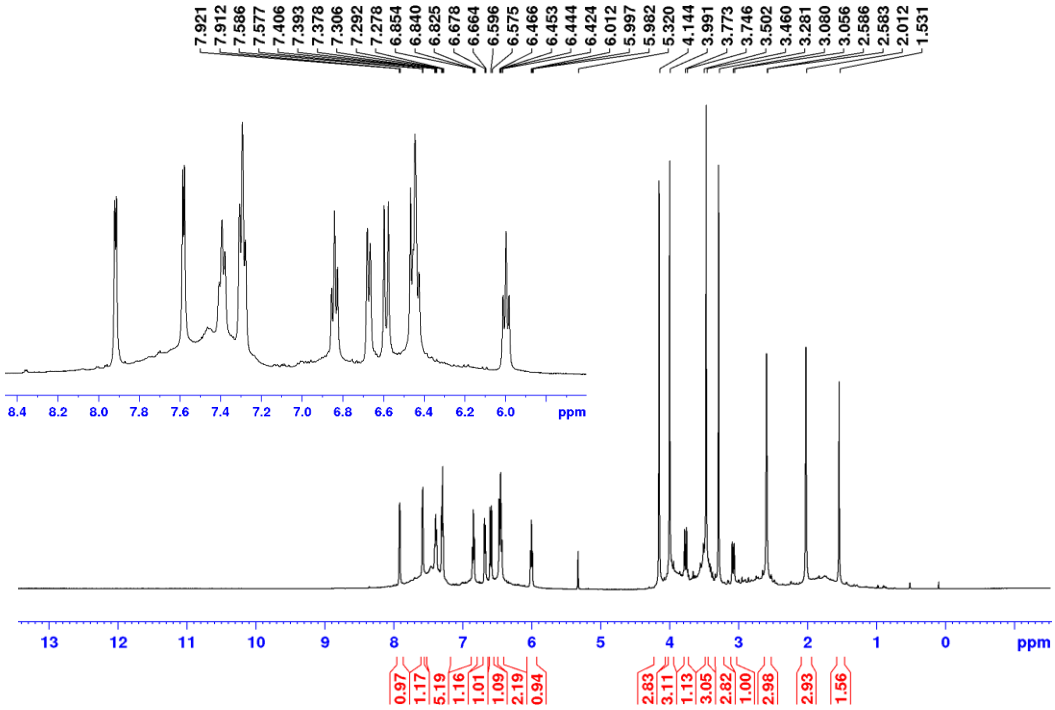

Figure 4.28, continued.

(c) $^{13}C\{^{1}H\}$ NMR (CD_2Cl_2, 125 MHz):

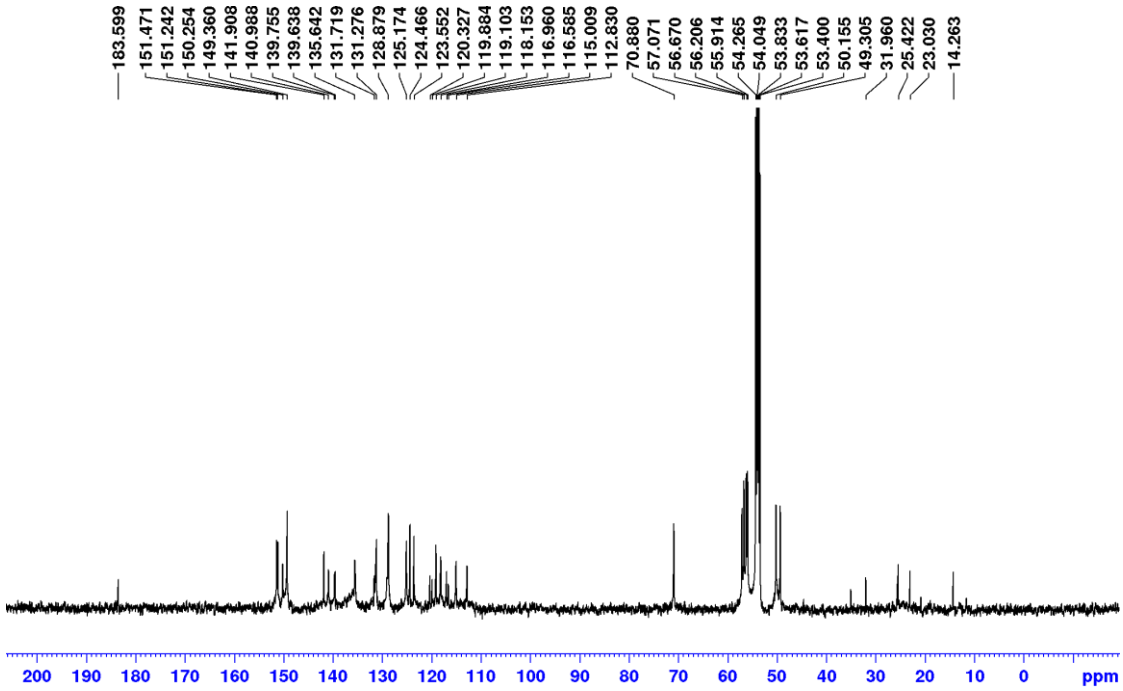

(a) $^{13}C\{^{1}H\}$ NMR (CD_2Cl_2, 125 MHz), aromatic region:

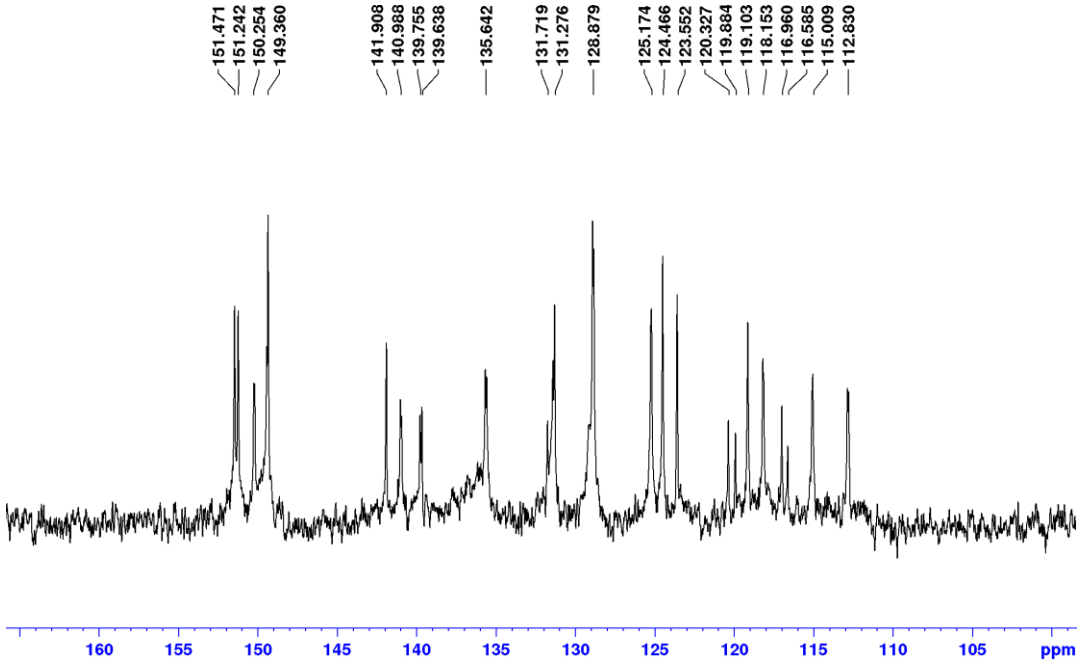

Figure 4.28, continued.

(b) $^{7}Li\{^{1}H\}$ NMR (CD_2Cl_2, 155 MHz):

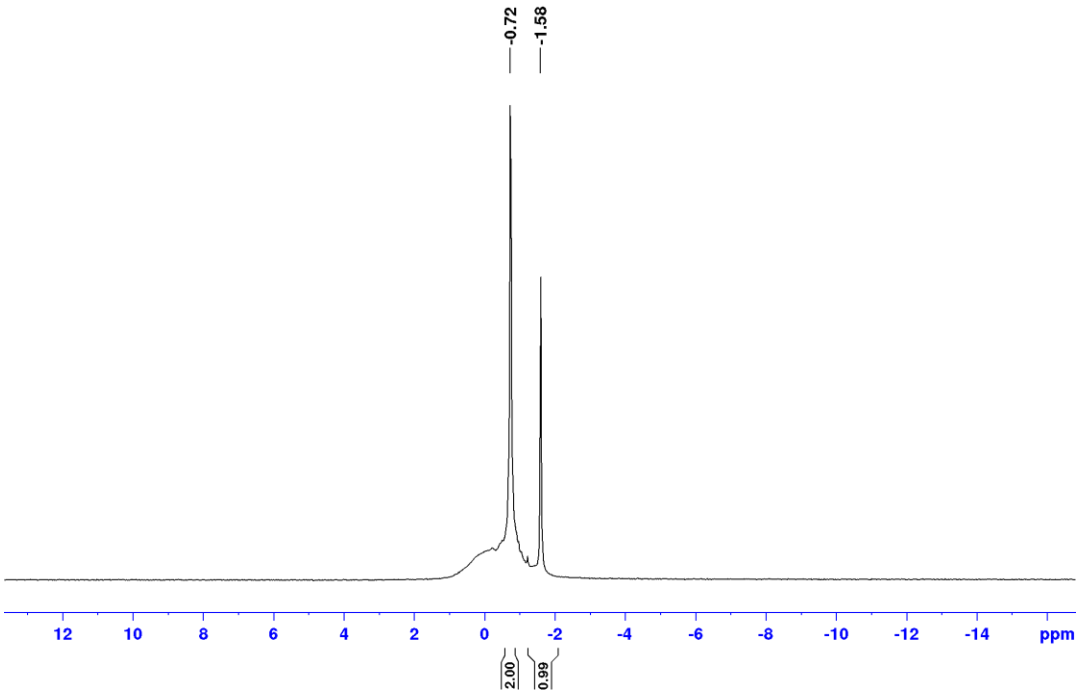

(c) $^{31}P\{^{1}H\}$ NMR (CD_3OD, 202 MHz):

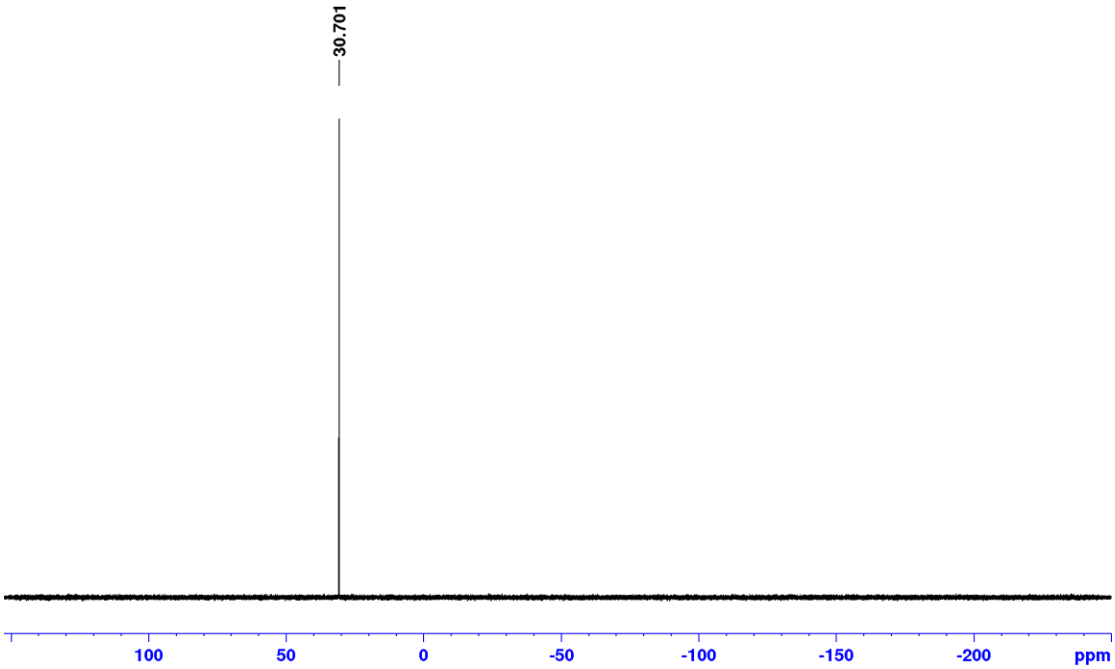

Figure 4.28, continued.

(d) ^{1}H NMR (CD_3OD, 500 MHz):

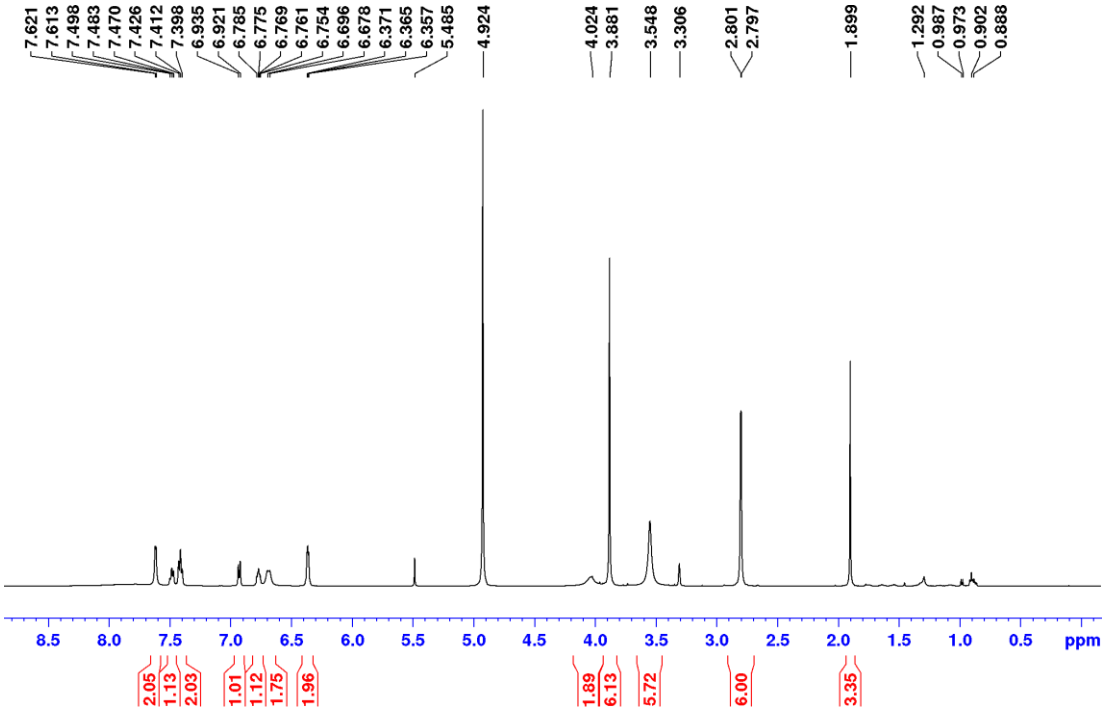

(e) ^{13}C{^{1}H} NMR (CD_3OD, 125 MHz):

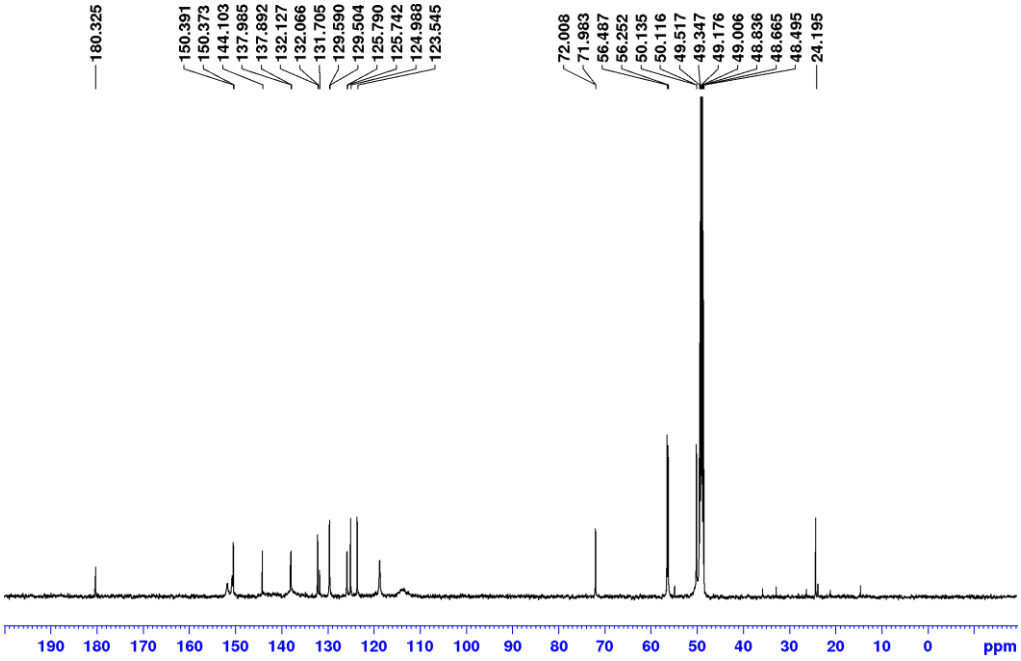

Figure 4.28, continued.

(d) $^{13}C\{^{1}H\}$ NMR (CD_3OD, 125 MHz), aromatic region:

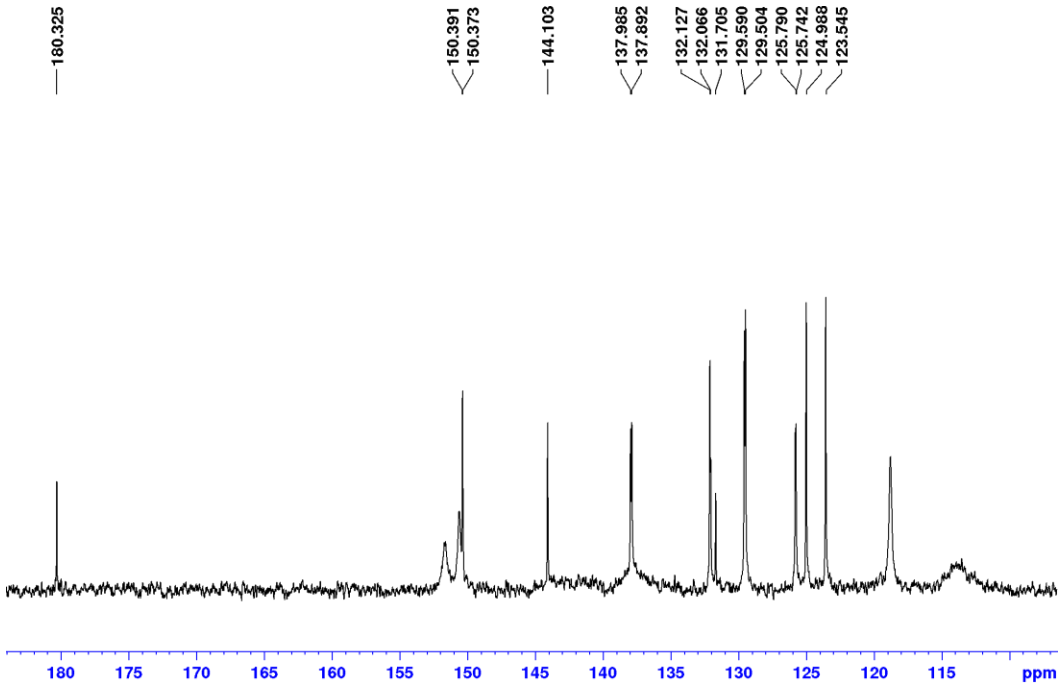

(f) $^{7}Li\{^{1}H\}$ NMR (CD_3OD, 155 MHz):

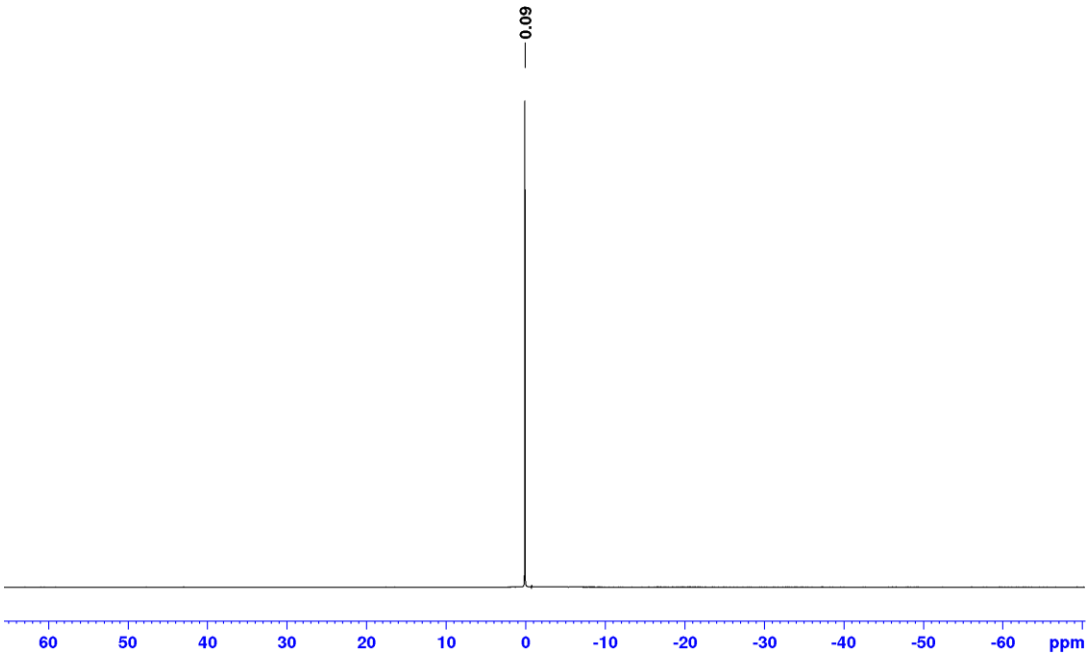

[(1)PdMe(py')]$_4$•Li$_2$OAc$_2$ (7). **1** (0.11 g, 0.20 mmol), (COD)PdMeCl (53 mg, 0.20 mmol), and AgOAc (17 mg, 0.10 mmol) were weighed out to a vial and dissolved in CH_2Cl_2 (8 mL). The mixture was stirred for 1 h and py' (46 µL, 0.20 mmol) was added. The mixture was stirred for 1 h. Hexanes were layered onto the CH_2Cl_2 solution and the mixture was cooled to -40 °C. **7** was collected by filtration and dried under vacuum to afford a white solid (0.10 g, 57 %). X-ray quality crystals were grown by layering hexanes onto a $CHCl_2CHCl_2$ solution at room temperature. $^{31}P\{^1H\}$ NMR (CD_2Cl_2): δ 32.0. ^1H NMR (CD_2Cl_2): δ 8.61 (d, $^3J_{HH}$ = 5, 2H, H^{11}), 7.95 (d, $^4J_{PH}$ = 4, 1H, H^3), 7.67 (d, $^4J_{PH}$ = 5, 1H, $H^{3'}$), 7.51–7.4 (m, 5H, H^8, H^9 and H^{10}; the H^8 resonance is broadened into the baseline due to restricted rotation around the P-C^7 bond), 6.77 (d, $^3J_{HH}$ = 6, 1H, H^{12}), 6.50 (d, $^3J_{PH}$ = 11, 1H, H^6), 6.19 (d, $^3J_{PH}$ = 11, 1H, $H^{6'}$), 4.17 (s, 3H, $H^{19'}$), 4.03 (s, 3H, H^{19}), 3.41 (s, 3H, H^{20}), 3.37 (s, 3H, $H^{20'}$), 2.32 (sept, $^3J_{HH}$ = 5, 1H, H^{14}), 1.73 (s, 1.5H, C*H*$_3$COO), 1.5–0.84 (m, 18H, H^{15}, H^{16}, H^{17} and H^{18}), -0.02 (d, $^3J_{PH}$ = 3, 3H, Pd-C*H*$_3$). $^{13}C\{^1H\}$ NMR (CD_2Cl_2): δ 183.7 (s, O_2CCH_3), 158.0 (s, C^{13}), 151.4 (d, $^4J_{PC}$ = 2, C^4), 151.2 (s, C^{11}), 151.1 (d, $^4J_{PC}$ = 2, $C^{4'}$), 150.3 (d, $^3J_{PC}$ = 8, $C^{5'}$), 149.5 (d, $^3J_{PC}$ = 9, C^5), 140.9 (d, $^2J_{PC}$ = 9, $C^{2'}$), 140.4 (d, $^2J_{PC}$ = 15, C^2), 133.6 (d, $^1J_{PC}$ = 42, C^7), 131.2 (s, C^8), 129.1 (br, C^9 and C^{10}), 124.5 (s, C^{12}), 119.7 (d, $^1J_{PC}$ = 57, C^1), 118.1 (s, C^6), 117.6 (d, $^1J_{PC}$ = 52, $C^{1'}$), 116.4 (d, $^2J_{PC}$ = 7, $C^{6'}$), 114.2 (d, $^3J_{PC}$ = 8, C^3), 113.4 (d, $^3J_{PC}$ = 10, $C^{3'}$), 57.3 (s, C^{19}), 56.7 (s, $C^{20'}$), 56.3 (s, $C^{19'}$), 55.4 (s, C^{20}), 46.0 (s, C^{14}), 36.1 and 36.0 (s, $C^{15,15'}$), 30.0 and 29.9 (s, $C^{16,16'}$), 25.5 (s, O_2CCH_3), 23.2 and 23.1 (s, $C^{17,17'}$), 14.3 and 14.2 (s, $C^{18,18'}$), -1.2 (s, Pd-*C*H$_3$). $^7Li\{^1H\}$ NMR (CD_2Cl_2): δ –0.7, –1.5.

$^{31}P\{^{1}H\}$ NMR (CD_3OD): δ 31.6. ^{1}H NMR (CD_3OD): δ 8.73 (s, 2H, H^{11}), 7.79 (br, 2H, H^{8}, this resonance is broad due to the restricted rotation around the P-C^{7} bond), 7.68 (d, $^{4}J_{PH}$ = 4, 2H, $H^{3,3'}$), 7.53–7.46 (m, 3H, H^{9} and H^{10}), 7.35(d, $^{3}J_{HH}$ = 6, 2H, H^{12}), 6.53 (d, $^{3}J_{PH}$ = 9, 2H, $H^{6,6'}$), 3.91 (s, 6H, $H^{19,19'}$), 3.51 (s, 6H, $H^{20,20'}$), 2.64 (sept, $^{3}J_{HH}$ = 5, 1H, H^{14}), 1.90 (s, 3H, $O_2C_2H_3$), 1.75–1.57 (m, 4H, H^{15}), 1.36–1.02 (m, 8H, H^{16} and H^{17}), 0.85 (t, $^{3}J_{HH}$ = 7, 6H, H^{18}), 0.55 (br, 3H, Pd–CH_3). $^{13}C\{^{1}H\}$ NMR (CD_3OD): δ 180.3 (s, CO_2CH_3), 159.9 (s), 151.5 (s), 150.6 (d, J_{PC} = 9), 142.2 (br), 136.8 (br), 133.8 (s), 133.4 (s), 132.0 (s), 129.7 (d, J_{PC} = 11), 125.6 (s), 121.6 (br), 118.3 (d, J_{PC} = 5), 113.9 (d, J_{PC} = 9), 56.5 (C^{19}), 56.1 (C^{20}), 46.8 (C^{14}), 36.9 (C^{15}), 30.7 (C^{16}), 24.2 (s, CO_2CH_3), 23.7 (C^{17}), 14.3 (C^{18}), –1.9 (d, $^{2}J_{PC}$ = 4, Pd-CH_3). $^{7}Li\{^{1}H\}$ NMR (CD_3OD): δ 0.2. HRMS (ESI; *m*/*z*): Calcd. for $[C_{76}H_{97}N_2O_{22}P_2Pd_2S_4Li_3]^{+}$ 1814.34468, Found: 1814.3484.[16]

Figure 4.29. Numbering scheme for **7**.

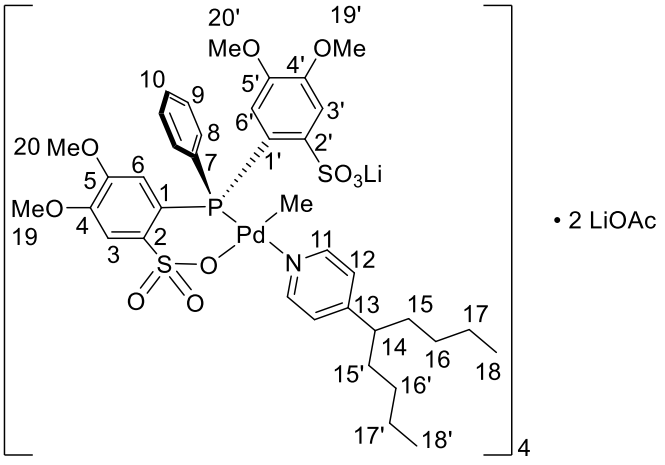

Figure 4.30. NMR spectra of 7.

(a) $^{31}P\{^{1}H\}$ NMR (CD_2Cl_2, 202 MHz):

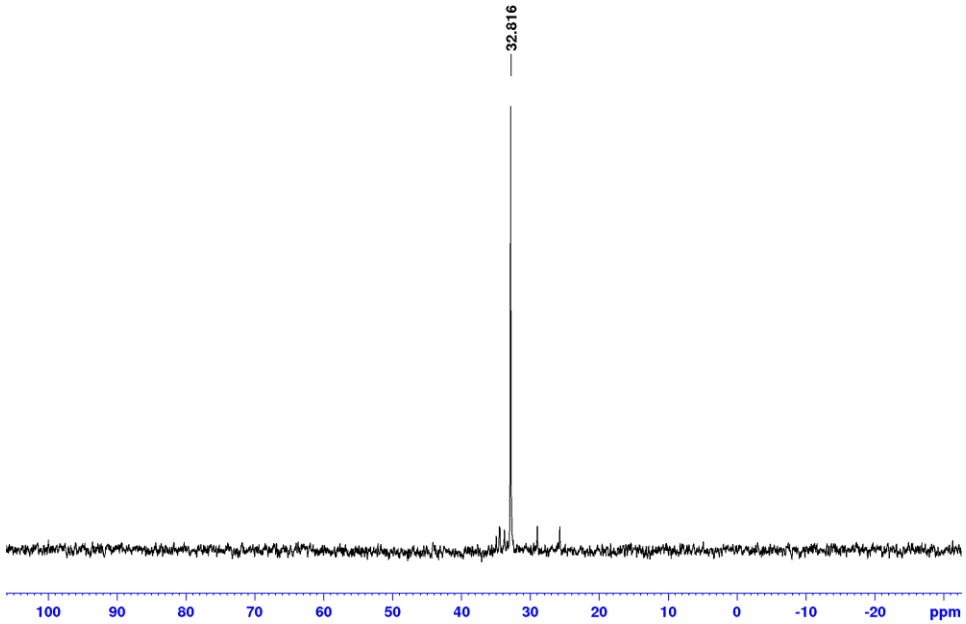

(b) ^{1}H NMR (CD_2Cl_2, 500 MHz):

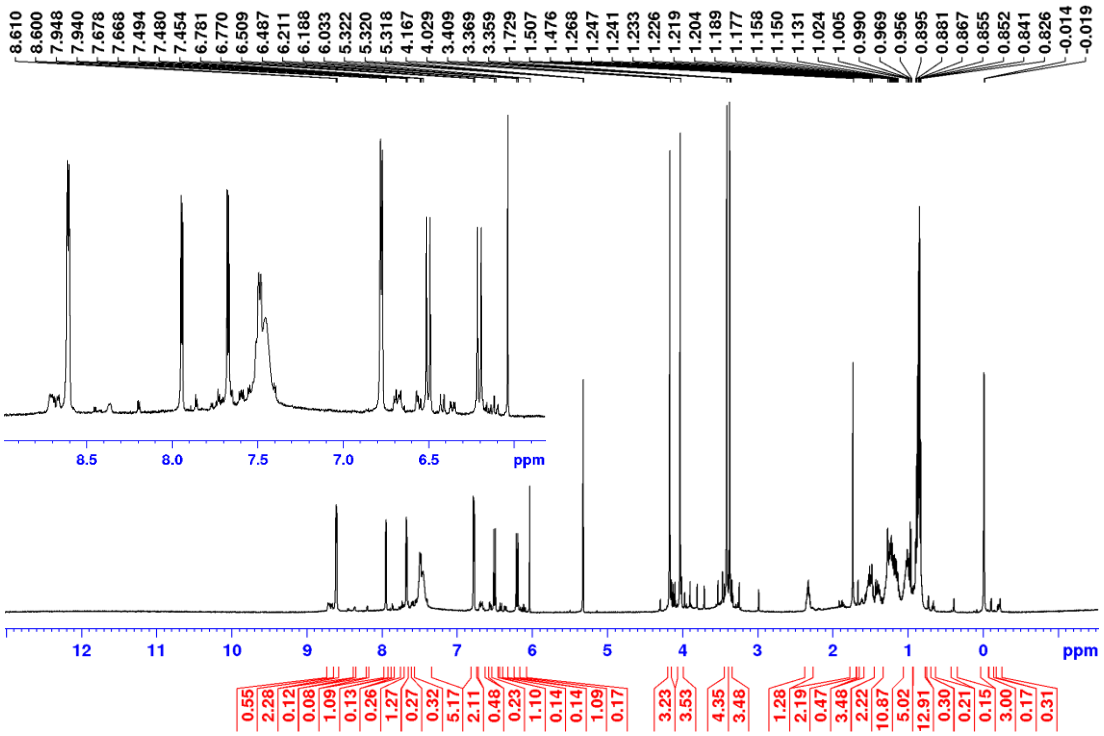

Figure 4.30, continued.

(c) $^{13}C\{^{1}H\}$ NMR (CD_2Cl_2, 125 MHz):

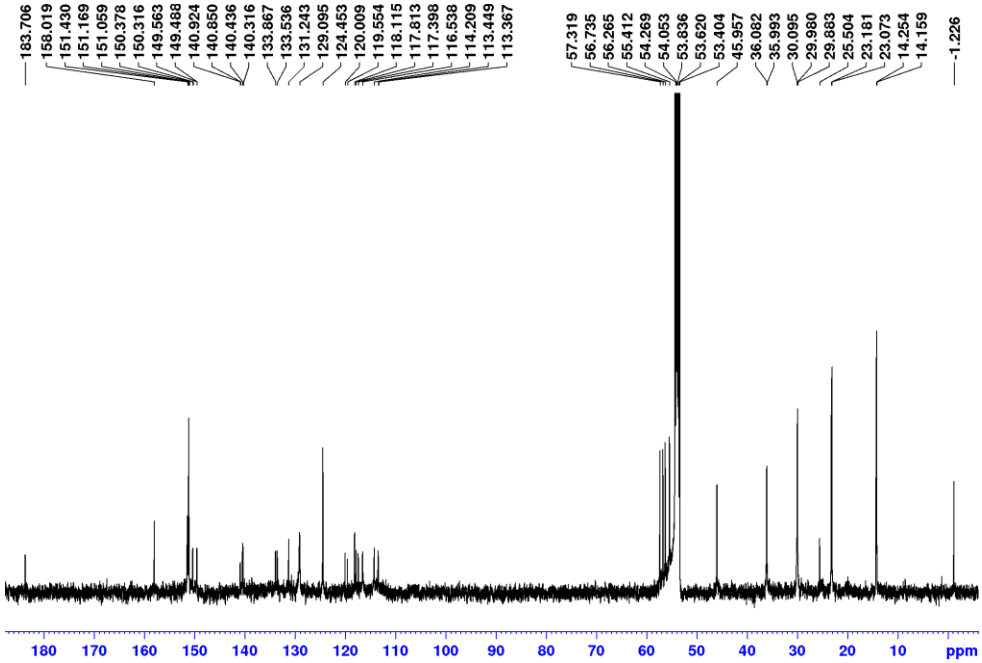

(d) $^{13}C\{^{1}H\}$ (CD_2Cl_2, 125 MHz), aryl region:

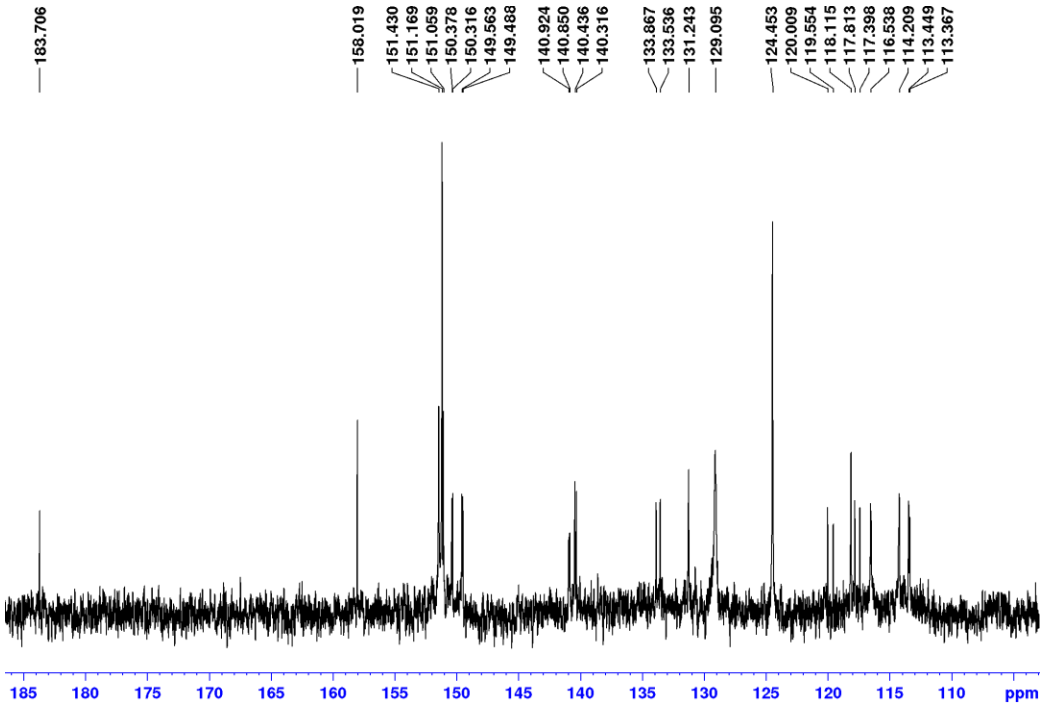

Figure 4.30, continued.

(e) $^{7}Li\{^{1}H\}$ NMR (CD_2Cl_2, 155 MHz):

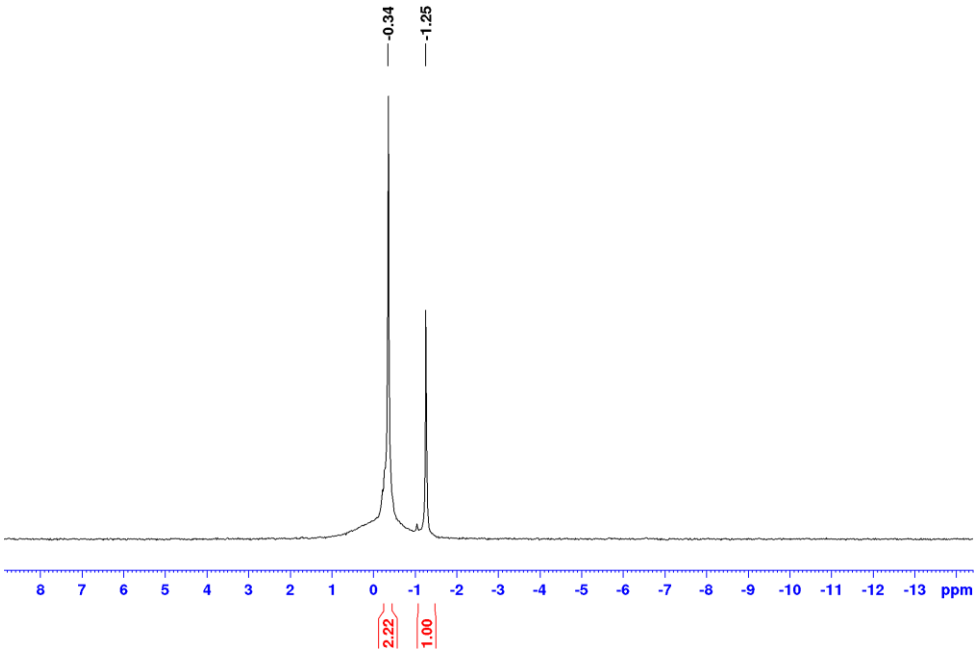

(f) $^{31}P\{^{1}H\}$ NMR (CD_3OD, 202 MHz):

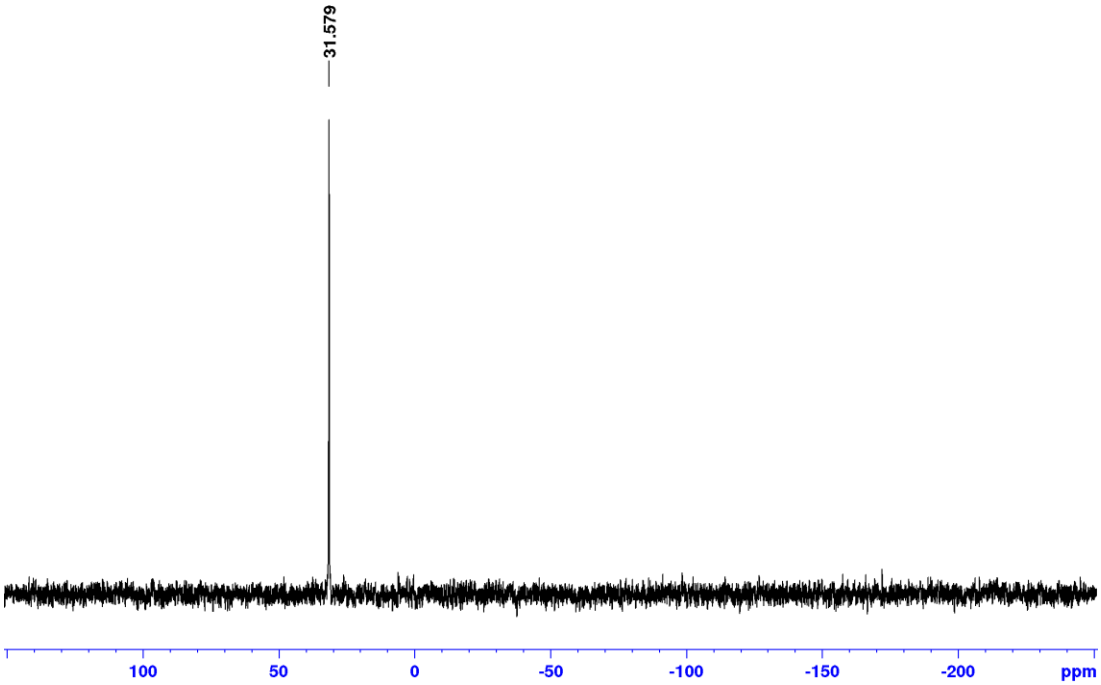

Figure 4.30, continued.

(g) ^{1}H NMR (CD_3OD, 500 MHz):

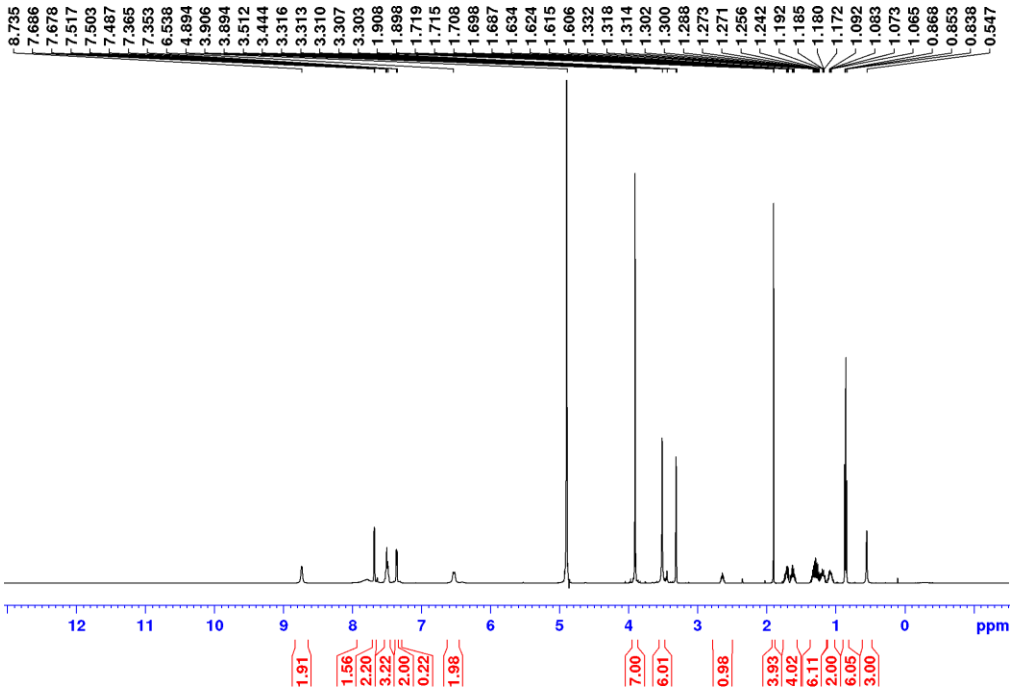

(h) ^{13}C{^{1}H} NMR (CD_3OD, 125 MHz):

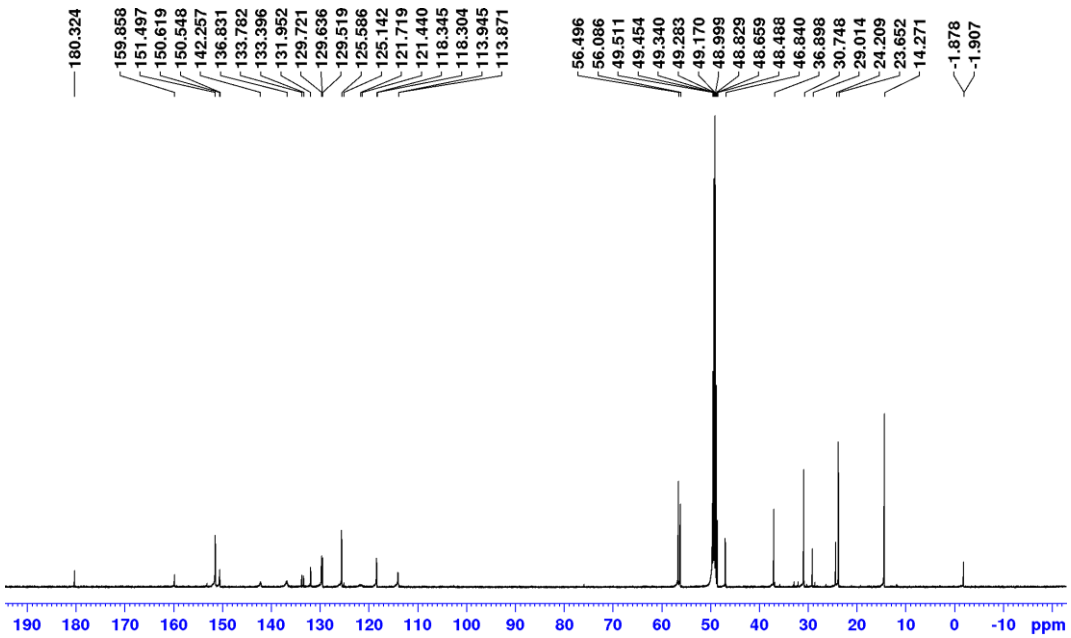

Figure 4.30, continued.

(i) $^{7}Li\{^{1}H\}$ NMR (CD_3OD, 155 MHz):

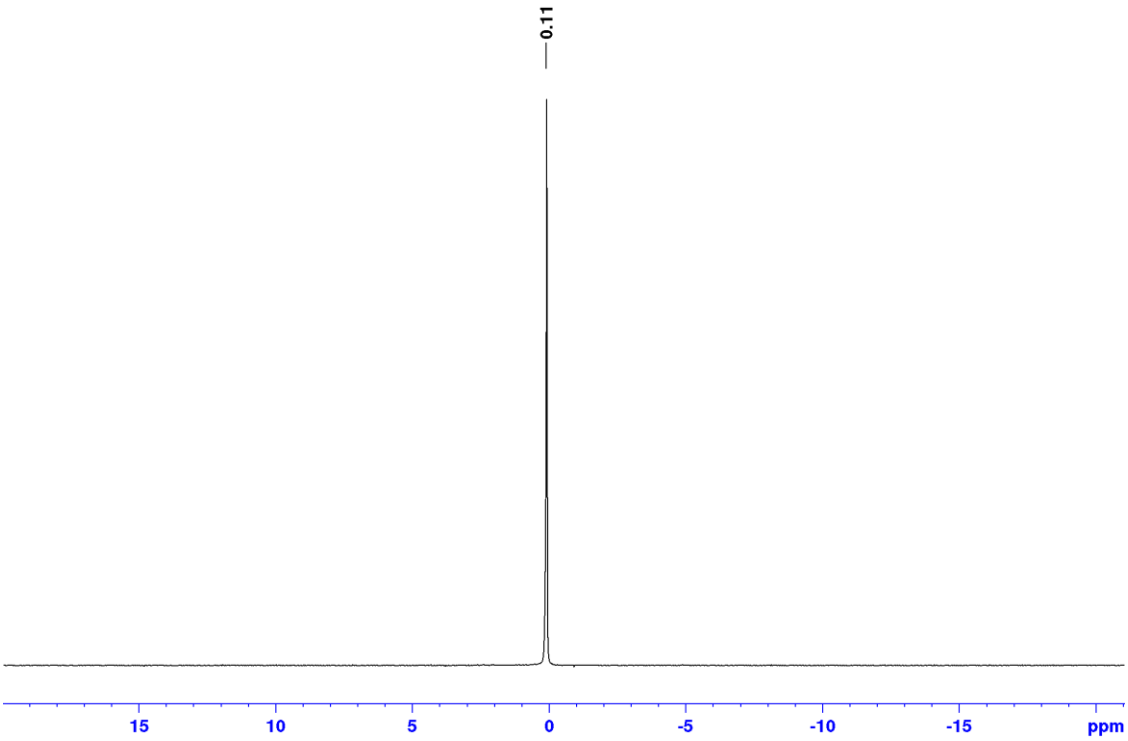

5d. Li_2[**4d**] (0.100 g, 0.191 mmol), (COD)PdMeBr (59 mg, 0.191 mmol) and CH_2Cl_2 (10 mL) were added to a vial. The vial was wrapped with foil, and the mixture was stirred for 0.5 h at room temperature. 4-(5-nonyl)-pyridine (44.1 µL, 0.191 mmol) was added and the mixture was stirred overnight at room temperature. The solution was filtered, concentrated, and layered with hexanes to afford a white powder (87 mg, 52% yield). $^{31}P\{^{1}H\}$ NMR (CD_2Cl_2): δ 34.8. ^{1}H NMR (CD_2Cl_2): δ 8.53 (d, $^{3}J_{HH}$ = 5, 2H, H^{11}), 8.14 (d, $^{4}J_{PH}$ = 4, 1H, H^{3}), 8.12 (d, $^{4}J_{PH}$ = 5, 1H, $H^{3'}$), 7.51–7.4 (m, 5H, H^{8}, H^{9} and H^{10}; the H^{8} resonance is broadened into the baseline due to

restricted rotation around the P-C^{7} bond), 7.37 (d, $^{3}J_{HH}$ = 8, 2H, H^{5}), 7.29 (d, $^{3}J_{HH}$ = 8, 2H, H$^{5'}$), 7.07 (dd, $^{3}J_{PH}$ = 11, $^{3}J_{HH}$ = 8, 2H, H^{6}), 6.71 (dd, $^{3}J_{PH}$ = 11, $^{3}J_{HH}$ = 8, 1H, H$^{6'}$), 6.62 (d, J = 6, 2H, H^{12}), 3.33 (sept, $^{3}J_{HH}$ = 7, 1H, H^{19}), 3.16 (sept, $^{3}J_{HH}$ = 6, 1H, H$^{19'}$), 2.22 (sept, $^{3}J_{HH}$ = 5, 1H, H^{14}), 1.67 (d, $^{3}J_{HH}$ = 7, 6H, H^{20}), 1.47 (d, $^{3}J_{HH}$ = 5, 6H, H^{21}), 1.5–0.84 (m, 18H, H^{15}, H^{16}, H^{17} and H^{18}), 0.82 (d, $^{3}J_{HH}$ = 7, 6H, H$^{20'}$), 0.81 (d, $^{3}J_{HH}$ = 7, 6H, H$^{21'}$), –0.38 (d, $^{3}J_{PH}$ = 3, 3H, Pd-CH_3). ^{13}C{^{1}H} NMR (CD_2Cl_2): δ 157.8 (C^{13}), 154.1 (C$^{4/4'}$), 152.4 (C$^{4/4'}$), 151.3 (C^{11}), 146.5 (d, J_{PC} = 9, C$^{2/2'}$), 146.2 (d, J_{PC} = 14, C$^{2/2'}$), 134.7 (d, J_{PC} = 7, C$^{6/6'}$), 134.2 (C$^{6/6'}$), 131.9 (d, J_{PC} = 45, C$^{1,1'}$), 131.4 (C^{8}), 129.7 (d, J_{PC} = 8, C$^{3/3'}$), 129.5 (d, J_{PC} = 6, C$^{5/5'}$), 129.1 (br, C^{9} and C^{10}), 128.5 (d, J_{PC} = 8, C$^{3/3'}$), 127.9 (d, J_{PC} = 6, C$^{5/5'}$), 124.7 (d, J_{PC} = 35, C$^{1/1'}$), 124.3 (s, C^{12}), 46.3 (s, C^{14}), 36.3 and 36.0 (s, C$^{15,15'}$), 34.5 (s, C^{19}), 34.3 (C$^{19'}$), 30.1 and 29.9 (s, C$^{16,16'}$), 25.4 and 24.4 (C^{20}), 23.7 and 23.6 (C$^{20'}$), 23.2 and 23.1 (s, C$^{17,17'}$), 14.3 and 14.2 (s, C$^{18,18'}$), –0.8 (s, Pd-CH$_3$). ^{7}Li{^{1}H} NMR (CD_2Cl_2): δ –0.5, –1.0. ^{31}P{^{1}H} NMR (CD_3OD): δ 31.7. ^{1}H NMR (CD_3OD): δ 8.74 (br, 2H, H^{11}), 8.02 (d, $^{4}J_{HH}$ = 1.5, $^{4}J_{PH}$ = 4, 2H, H^{3}), 7.75 (br, 2H, H^{8}, this resonance is broad due to the restricted rotation around the P-C^{7} bond), 7.49 (d, $^{3}J_{HH}$ = 7, ^{4}J$_{HH}$ = 1.5, 1H, H^{10}), 7.43 (dd, $^{3}J_{HH}$ = 7, 2H, H^{9}), 7.36 (d, $^{3}J_{HH}$ = 6, 2H, H^{12}), 7.27 (d, $^{3}J_{HH}$ = 8, $^{4}J_{HH}$ = 1, 2H, H$^{5,5'}$), 6.98 (dd, $^{3}J_{HH}$ = 8, $^{3}J_{PH}$ =11, 2H, H$^{6,6'}$), 2.99 (sept, $^{3}J_{HH}$ = 7, 2H, H^{19}), 2.64 (sept, $^{3}J_{HH}$ = 5, 1H, H^{14}), 1.75–1.57 (m, 4H, H^{15}), 1.28 (d, $^{3}J_{HH}$ = 7, 12H, H$^{20,20'}$), 1.36–1.02 (m, 8H, H^{16} and H^{17}), 0.86 (t, $^{3}J_{HH}$ = 7, 6H, H^{18}), 0.52 (d, $^{3}J_{PH}$ = 3, 3H, Pd-CH_3). ^{13}C{^{1}H} NMR (CD_3OD): δ 159.8 (s), 152.9 (s), 151.5 (br), 148.6 (br), 137.0 (br), 135.6 (d, J_{PC} = 3), 132.6 (d, J_{PC} = 49), 131.8 (d, J_{PC} = 2), 129.6 (d, J_{PC} =

11), 129.5 (s), 128.9 (d, J_{PC} = 7), 128.5 (br), 125.6 (s), 46.8 (C^{14}), 36.9 (C^{15}), 35.2 (C^{19}), 30.8 (C^{16}), 23.9 ($C^{20,20'}$), 23.7 (C^{17}), 14.3 (C^{18}), –2.0 (d, Pd-CH_3). $^{7}Li\{^{1}H\}$ NMR (CD_3OD): δ 0.1.

Figure 4.31. Numbering scheme for **5d**.

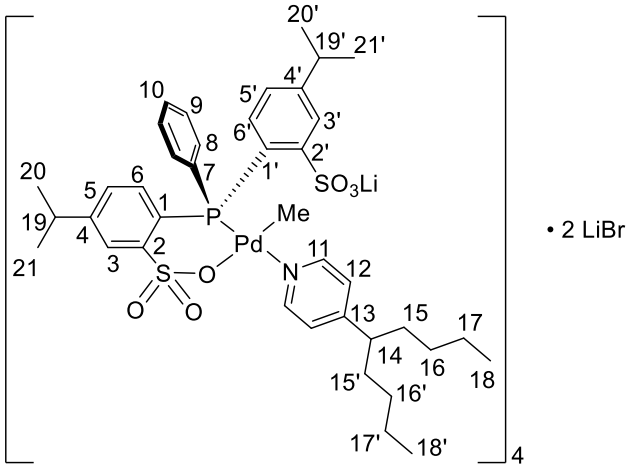

Figure 4.32. NMR spectra of 5d.

(a) $^{31}P\{^{1}H\}$ NMR (CD_2Cl_2, 202 MHz):

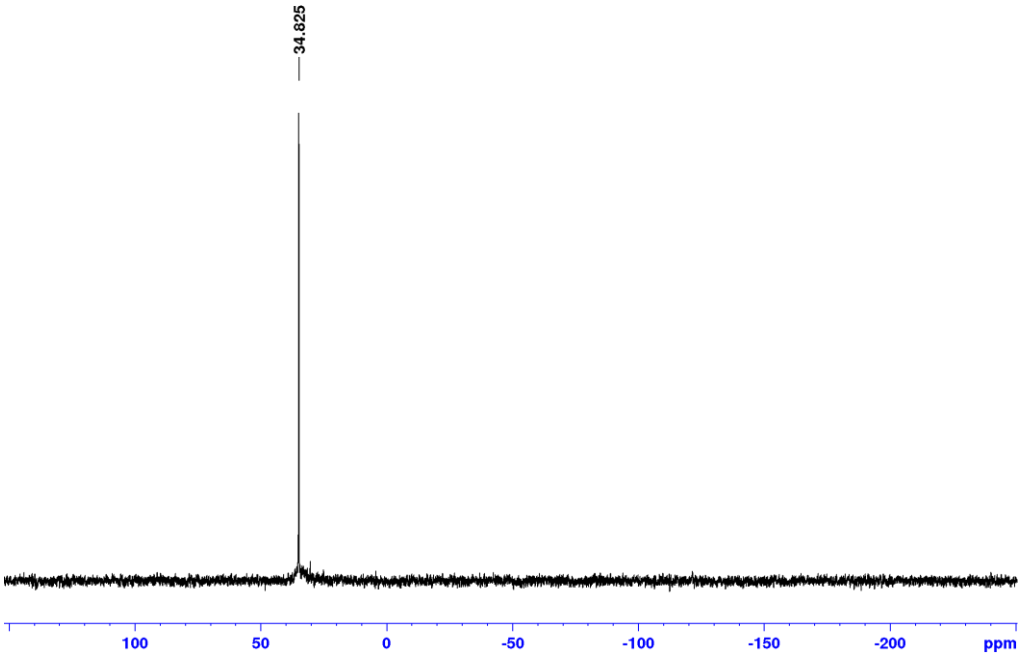

Figure 4.32, continued.

(b) ^{1}H NMR (CD_2Cl_2, 500 MHz):

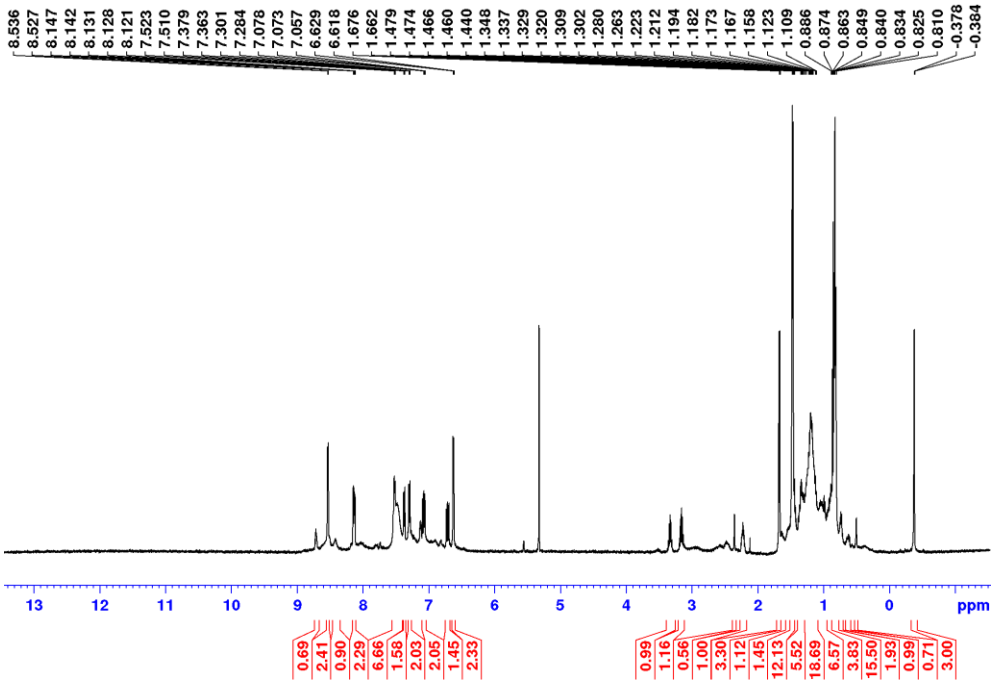

(c) $^{13}C\{^{1}H\}$ NMR (CD_2Cl_2, 126 MHz):

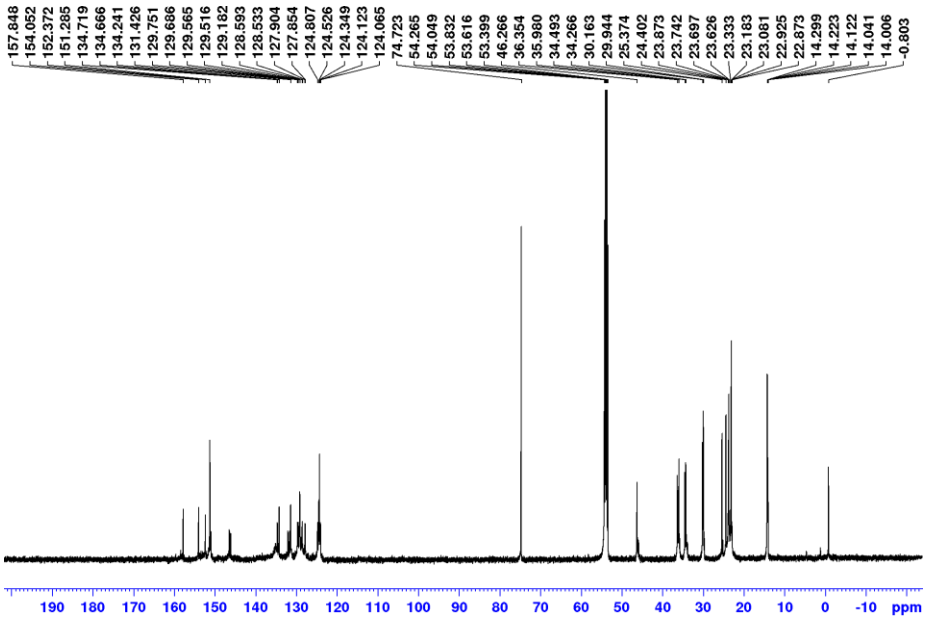

Figure 4.32, continued.

(d) $^{7}Li\{^{1}H\}$ NMR (CD_2Cl_2, 155 MHz):

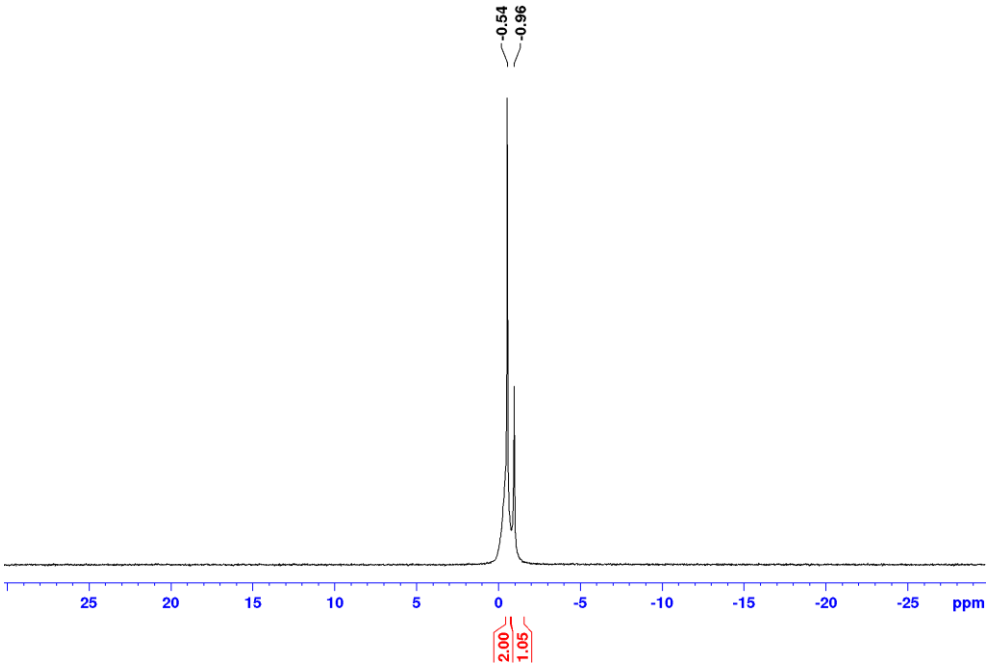

(e) $^{31}P\{^{1}H\}$ NMR (CD_3OD, 202 MHz):

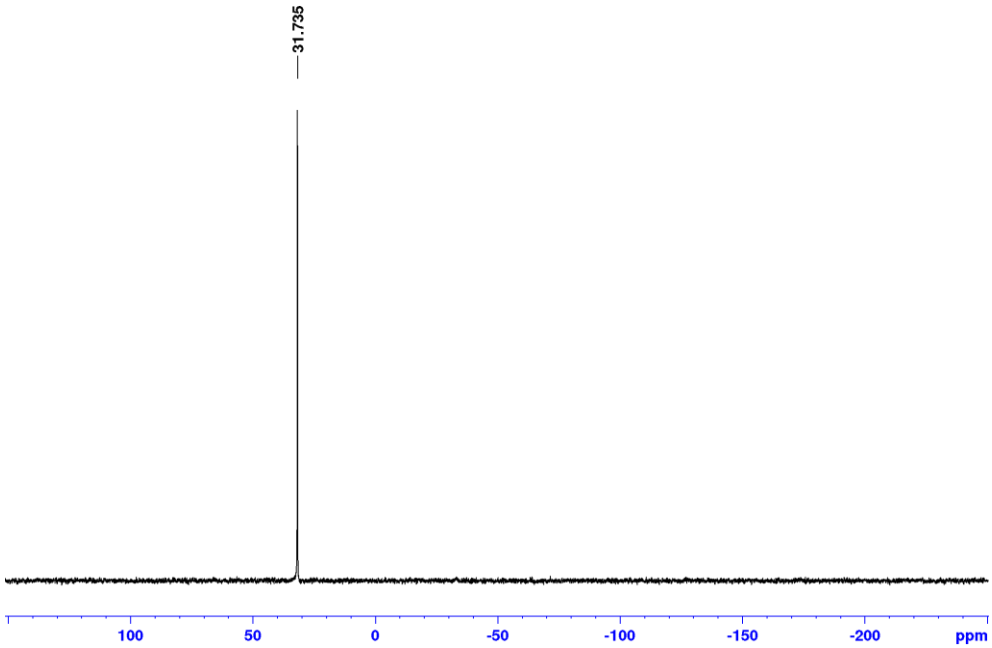

Figure 4.32, continued.

(f) ^{1}H NMR (CD_3OD, 500 MHz):

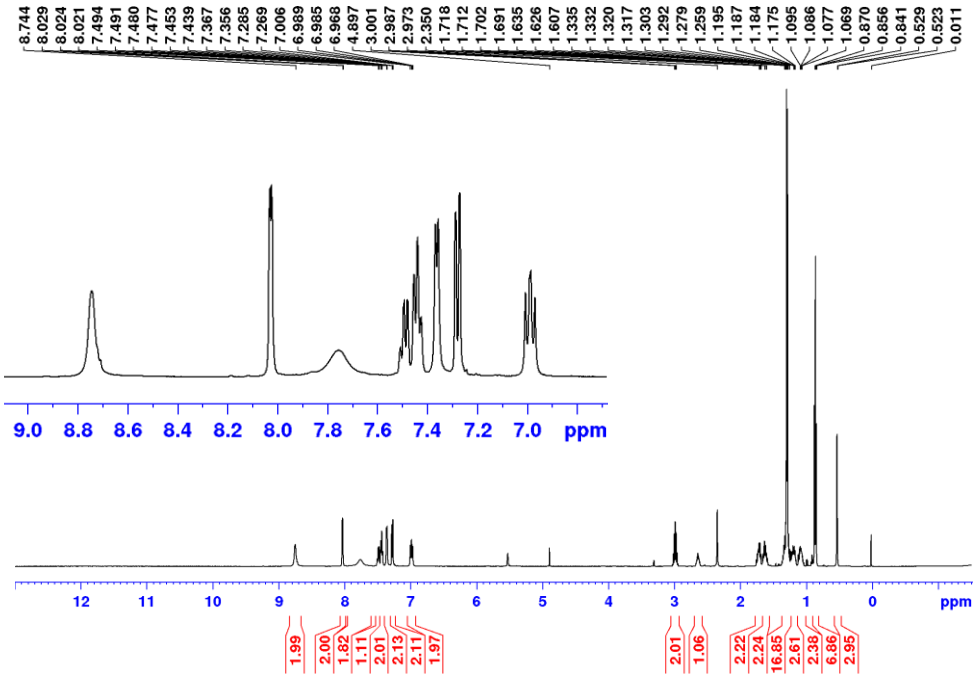

(g) ^{13}C{^{1}H} NMR (CD_3OD, 126 MHz):

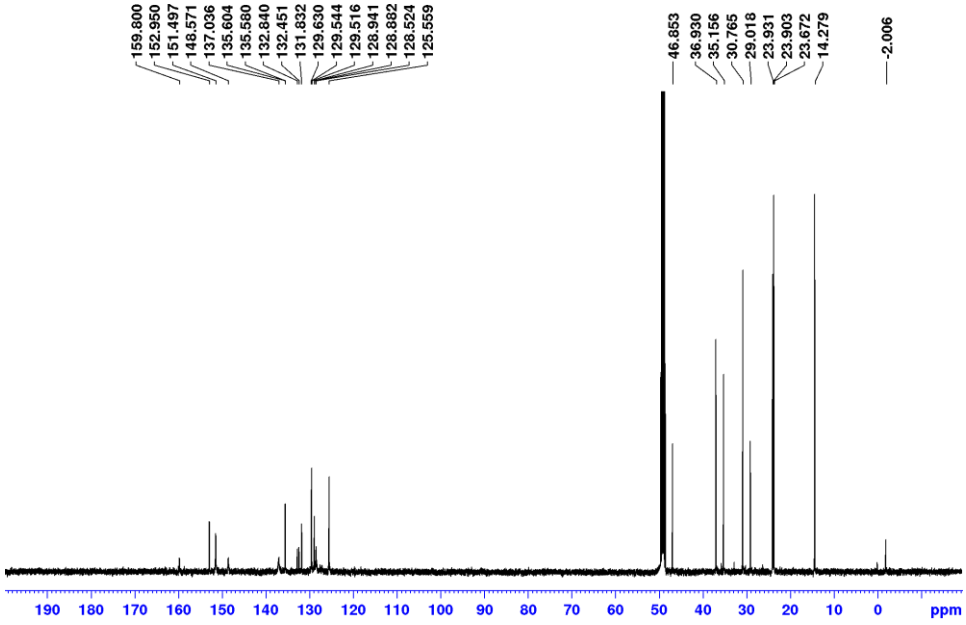

Figure 4.32, continued.

(h) $^{7}Li\{^{1}H\}$ NMR (CD_3OD, 155 MHz):

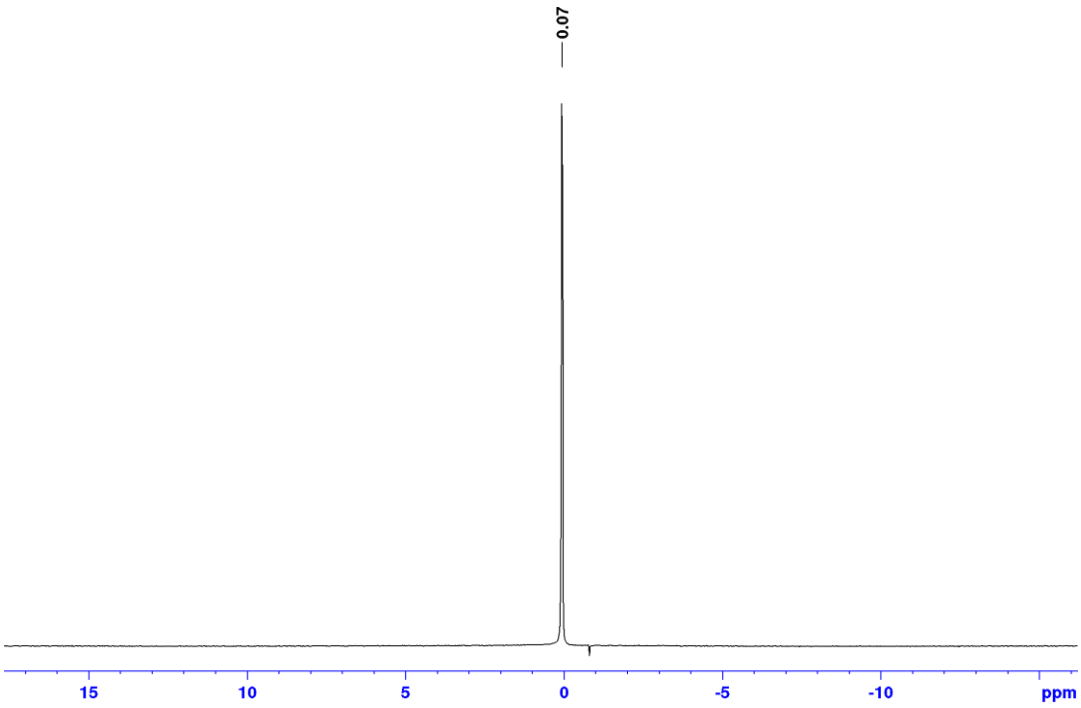

3b-^{i}Bu. Compound **3b-^{i}Bu** was prepared analogously to **3c-^{i}Bu** from ^{i}BuOH (3.54 mL, 3.85 mmol), pyridine (6.2 mL, 7.7 mmol), and **3b-Cl** (8.7 g, 3.5 mmol) in $CHCl_3$ (70 mL). The reaction was allowed to warm slowly to room temperature overnight, and was quenched with 0.1M HCl (50 mL). The organic layer was extracted sequentially with 0.1M HCl (50 mL), H_2O (3 x 50 mL), and brine (50 mL). The organic layer was dried over $MgSO_4$, filtered, and the solvent was removed under vacuum. Column chromatography was performed twice using 70:29:1 hexanes:acetone:NEt_3 and 95:5 hexanes:acetone. The product was obtained as a pale

yellow solid. (7.5 g, 57% yield). ^{1}H NMR ($CDCl_3$): δ 7.70 (d, $^{3}J_{HH}$ = 6, 2H, H^{2}), 6.67 (d, $^{3}J_{HH}$ = 6, 2H, H^{3}), 3.76 (d, $^{3}J_{HH}$ = 6, 2H, H^{7}), 3.43 (q, $^{2}J_{HH}$ = 7, 4H, H^{5}), 1.97 (seq, $^{3}J_{HH}$ = 7, 1H, H^{8}), 1.23 (t, $^{3}J_{HH}$ = 7, 6H, H^{6}), 0.92 (d, $^{3}J_{HH}$ = 7, 6H, H^{9}). $^{13}C^{7}$ NMR (CD_2Cl_2): δ 151.7 (C^{4}), 130.2 (C^{3}), 120.0 (C^{1}), 110.7 (C^{2}), 75.9 (C^{7}), 45.0 (C^{5}), 28.4 (C^{8}), 18.8 (C^{9}), 12.4 (C^{6}). HRMS (ESI; *m*/*z*): Calcd. for $[C_{14}H_{23}NO_3S + H]^+$ 286.1477, Found: 286.1476.

Figure 4.33. Numbering scheme for **3b-^{i}Bu**.

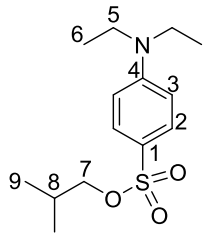

Figure 4.34. NMR spectra of 3b-^{i}Bu.

(a) ^{1}H NMR ($CDCl_3$, 500 MHz):

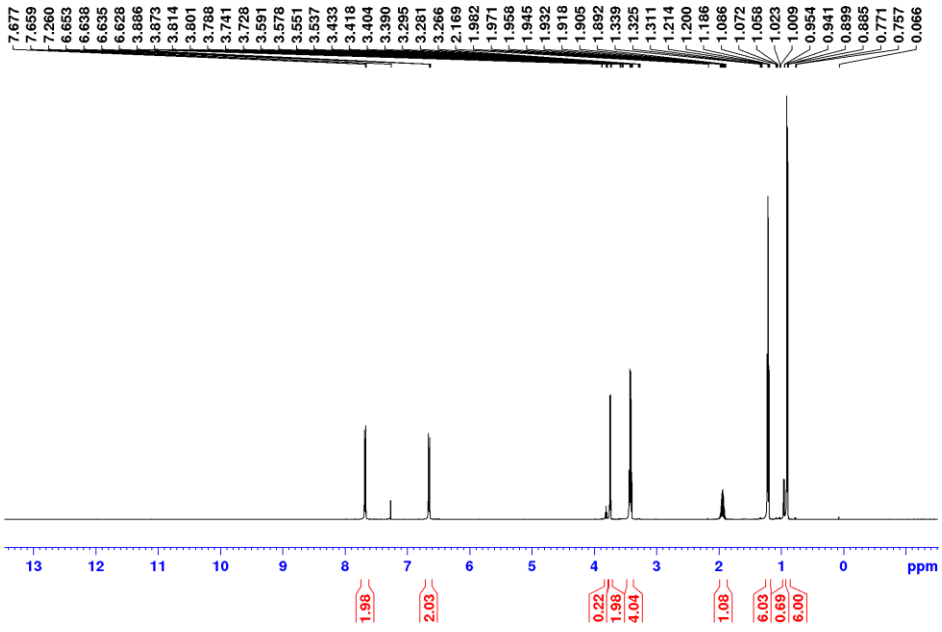

Figure 4.34, continued.

(b) $^{13}C\{^{1}H\}$ NMR ($CDCl_3$, 126 MHz):

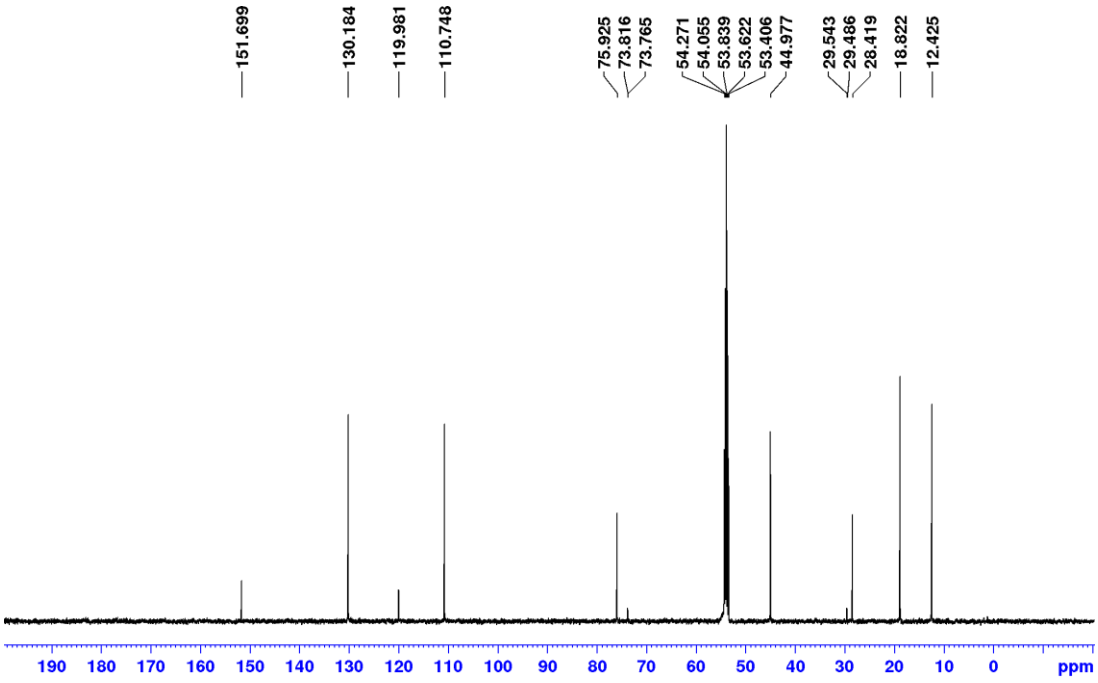

4b-^{i}Bu. Compound **4b-^{i}Bu** was synthesized analogously to **4c-^{i}Bu** from a solution of **3b-^{i}Bu** (2.10 g, 7.34 mmol) in THF (30 mL), ^{n}BuLi (4.58 mL, 7.34 mmol), and $PPhCl_2$ (0.484 mL, 3.67 mmol). The mixture was stripped of solvent affording a white solid. The solid was dissolved in EtOAc (30 mL) and washed with H_2O (30 mL). The aqueous layer was extracted with EtOAc (3 x 20 mL). The combined organic layers were washed with brine (30 mL), dried over $MgSO_4$ and stripped under vacuum. **4b-^{i}Bu** was purified by column chromatography (silica; 78:20:2 hexanes:acetone:NEt_3). The solvent was removed under vacuum to afford a white solid (1.83 g,

74% yield). ^{31}P NMR (CD_2Cl_2): δ –6.1. ^{1}H NMR (CD_2Cl_2): δ 7.83 (d, $^{3}J_{HH}$ = 10, $^{4}J_{PH}$ = 5, 2H, H^{3}), 7.36 (br, 3H, H^{9} and H^{10}), 7.23 (br, 2H, H^{8}), 6.60 (dd, $^{3}J_{HH}$ = 9, $^{5}J_{PH}$ = 3, 2H, H^{4}), 6.09 (s, 2H, H^{6}), 3.86 (dd, $^{2}J_{HH}$ = 10, $^{3}J_{HH}$ = 7, 2H, H^{13}), 3.76 (dd, $^{2}J_{HH}$ = 9, $^{3}J_{HH}$ = 7, 2H, $H^{13'}$), 3.11 (q, 8H, H^{11}), 1.94 (sept, $^{3}J_{HH}$ = 7, 2H, H^{14}), 0.91 (m, 24H, $H^{15/15'}$ and H^{12}). $^{13}C\{^{1}H\}$ NMR (CD_2Cl_2): δ 150.7 (C^{5}), 140.3 (d, $^{1}J_{PC}$ = 30, C^{1}), 138.3 (d, $^{1}J_{PC}$ = 14, C^{7}), 134.2 (d, $^{2}J_{PC}$ = 22, C^{8}), 133.3 (d, $^{2}J_{PC}$ = 4, C^{4}), 129.1 (C^{10}), 128.8 (d, $^{3}J_{PC}$ = 7, C^{9}), 124.1 (d, $^{2}J_{PC}$ = 24, C^{2}), 119.3 (C^{6}), 109.8 (C^{3}), 76.3 (d, $^{5}J_{PC}$ = 3, C^{13}), 44.8 (C^{11}), 28.5 (C^{14}), 19.0 and 18.8 (C^{15} and $C^{15'}$), 12.4 (C^{12}). HRMS (ESI; *m*/*z*): Calcd. for $[C_{34}H_{49}N_2O_6S_2P + H]^+$ 677.28482, Found: 677.2844.

Figure 4.35. Numbering scheme for **4b-*i*Bu**.

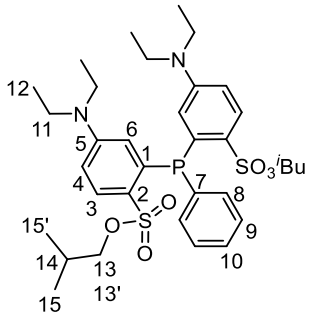

Figure 4.36. NMR spectra of 4b-^{i}Bu.

(a) $^{31}P\{^{1}H\}$ NMR (CD_2Cl_2, 202 MHz):

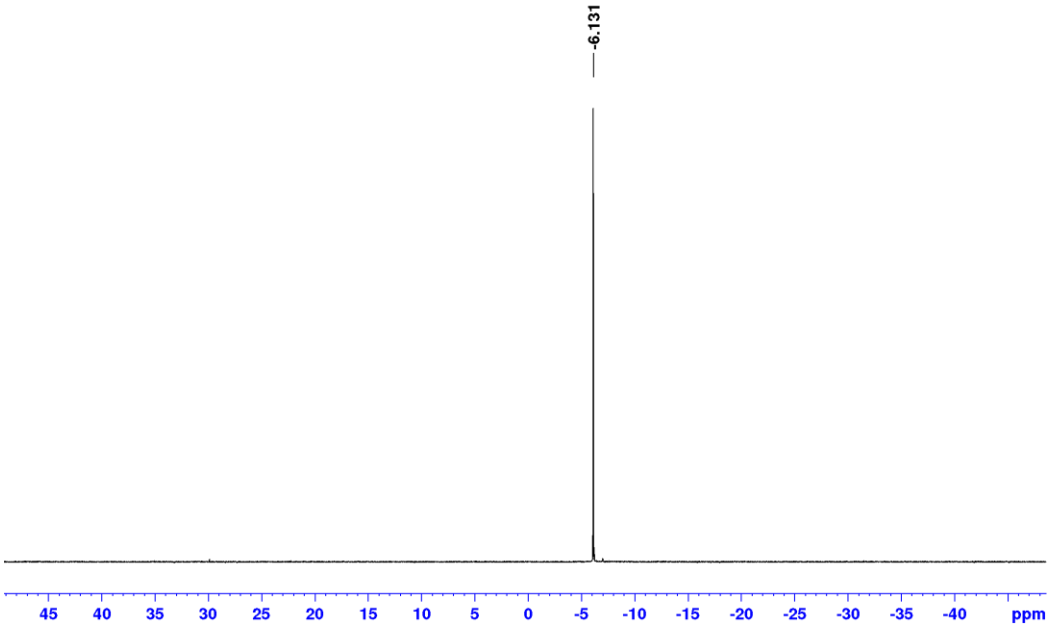

(b) ^{1}H NMR (CD_2Cl_2, 500 MHz):

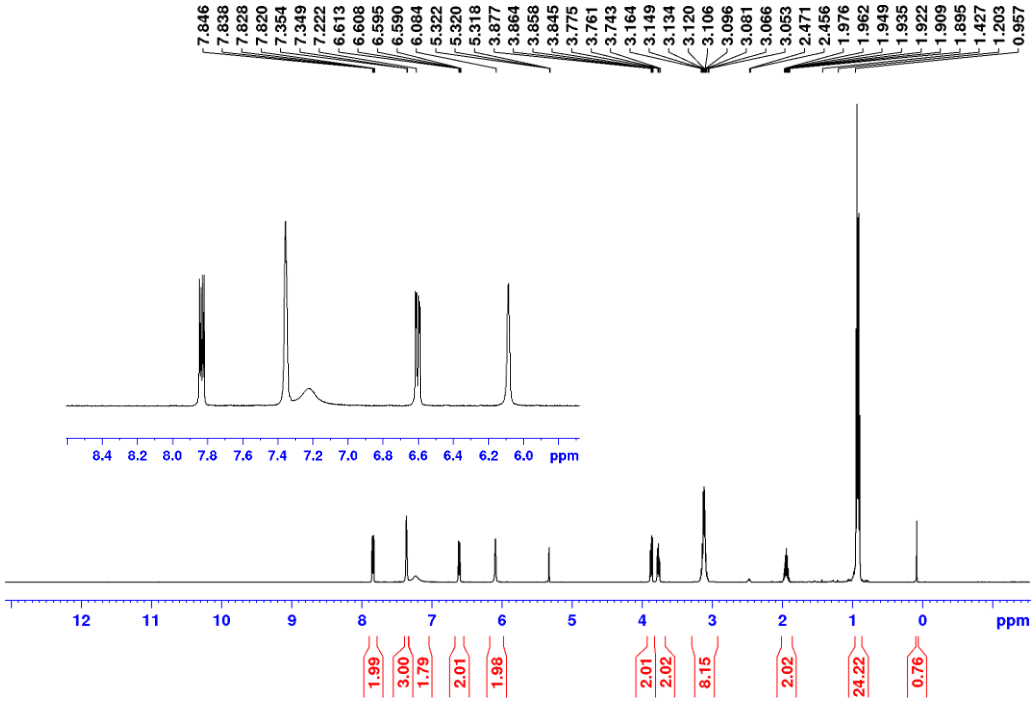

Figure 4.36, continued.

(c) $^{13}C\{^{1}H\}$ NMR (CD_2Cl_2, MHz):

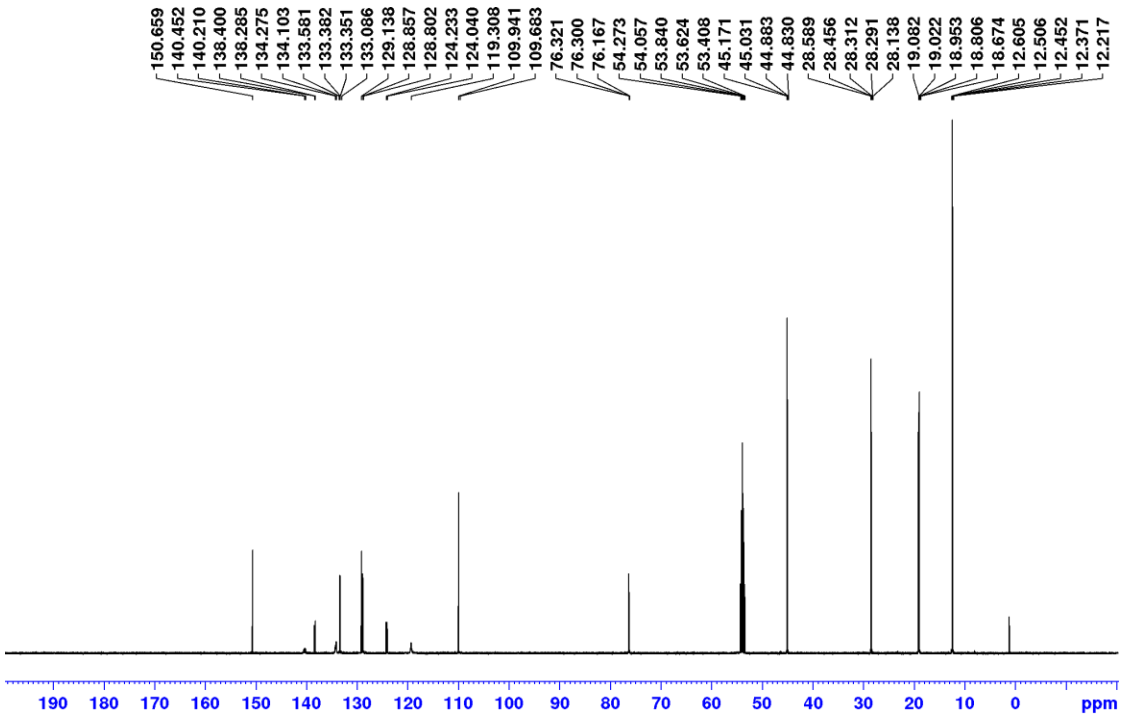

Li_2[4b]. A flask was charged with **4b-^{i}Bu** (1.2 g, 1.8 mmol), LiI (0.713 g, 5.32 mmol) and acetonitrile (10 mL). The mixture was covered in foil, stirred and refluxed overnight. A white solid precipitated. The mixture was filtered and the solid was rinsed with acetonitrile (20 mL) and dried under vacuum to afford a white solid (1.01g, 98% yield). ^{31}P NMR (CD_3OD): δ –10.5. ^{1}H NMR (CD_3OD): δ 7.81 (d, $^{3}J_{HH}$ = 9, $^{4}J_{PH}$ = 4, 2H, H^3), 7.3–7.15 (br, 5H, H^8, H^9, H^{10}), 6.60 (d, $^{3}J_{HH}$ = 9, 2H, H^4), 6.21 (s, 2H, H^6), 3.12 (m, 8H, H^{11}), 0.89 (t, $^{3}J_{HH}$ = 7, 12H, H^{12}). $^{13}C\{^{1}H\}$ NMR (CD_3OD): δ 149.6 (C^5), 141.3 (d, $^{1}J_{PC}$ = 16, C^7), 138.3 (d, $^{1}J_{PC}$ = 25, C^1), 135.7 (d, $^{2}J_{PC}$ =

25, C^2), 134.9 (d, $^2J_{PC}$ = 20, C^8), 130.5 (C^{10}), 128.9 (d, $^3J_{PC}$ = 6, C^9), 128.7 (C^2), 120.2 (C^6), 110.8 (C^3), 76.3 (d, $^5J_{PC}$ = 3, C^{13}), 44.8 (C^{11}), 28.5 (C^{14}), 19.0 and 18.8 (s, C^{15} and $C^{15'}$), 12.4 (C^{12}). $^7Li^7$ NMR (DMSO-d_6): δ -0.6. HRMS (ESI; *m*/*z*): Calcd. for [2($C_{26}H_{32}N_2O_6S_2P$ + 2H) + Li]$^+$ 1081.32295, Found: 1081.321.

Figure 4.37. Numbering scheme for Li_2[**4b**].

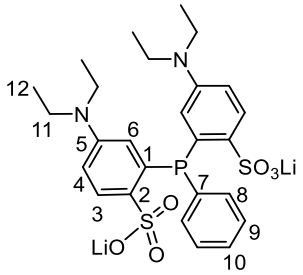

Figure 4.38. NMR spectra of 4b-^{i}Bu.

(a) $^{31}P\{^1H\}$ NMR (CD_3OD, 202 MHz):

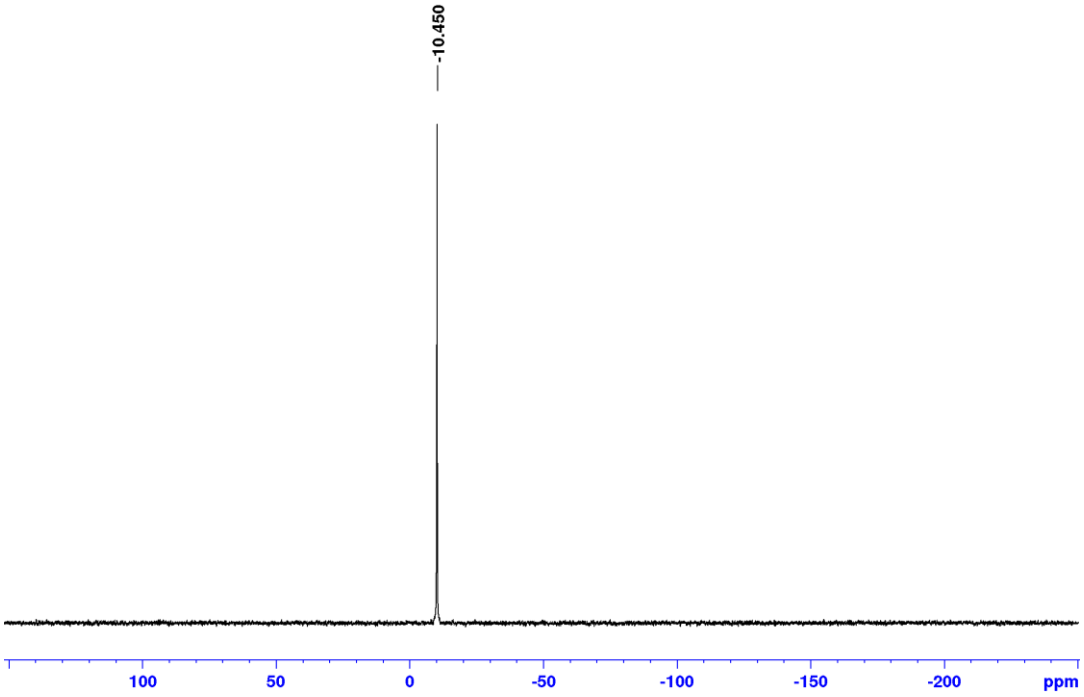

Figure 4.38, continued.

(b) ^{1}H NMR (CD_3OD, 500 MHz):

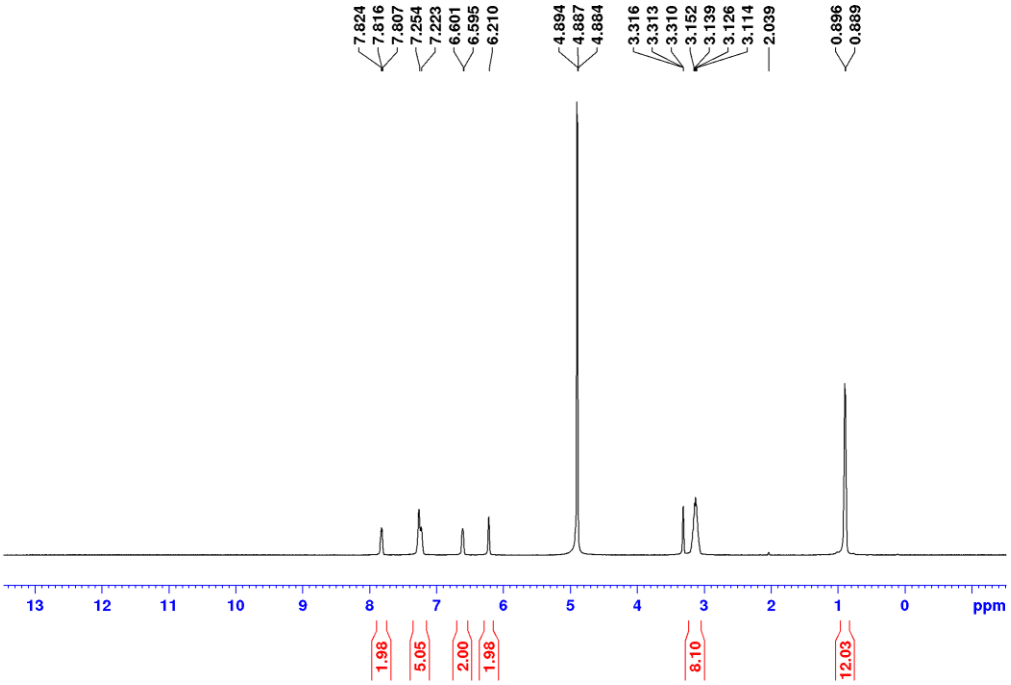

(c) ^{13}C{^{1}H} NMR (CD_3OD, 126 MHz):

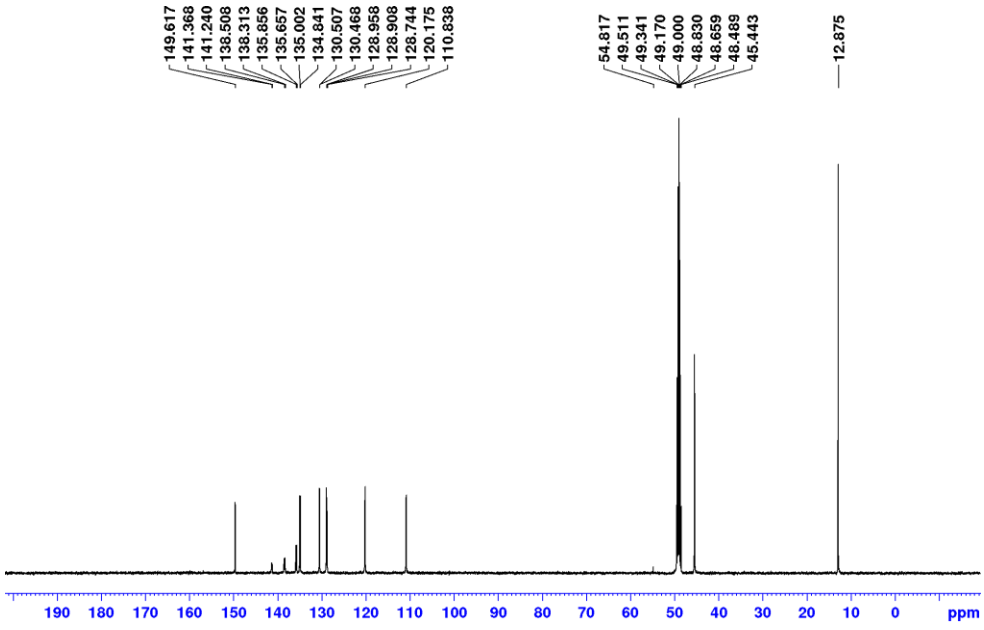

Figure 4.38, continued.

(d) $^{7}Li\{^{1}H\}$ NMR (CD_3OD, 155 MHz):

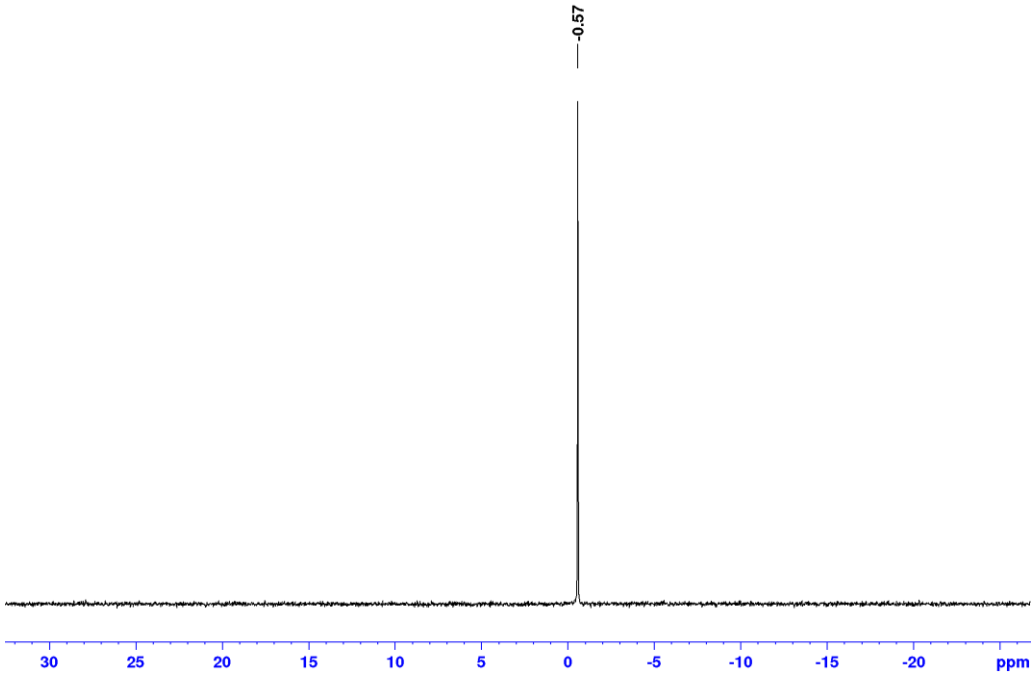

(e) COSY (CD_3OD, 500 MHz):

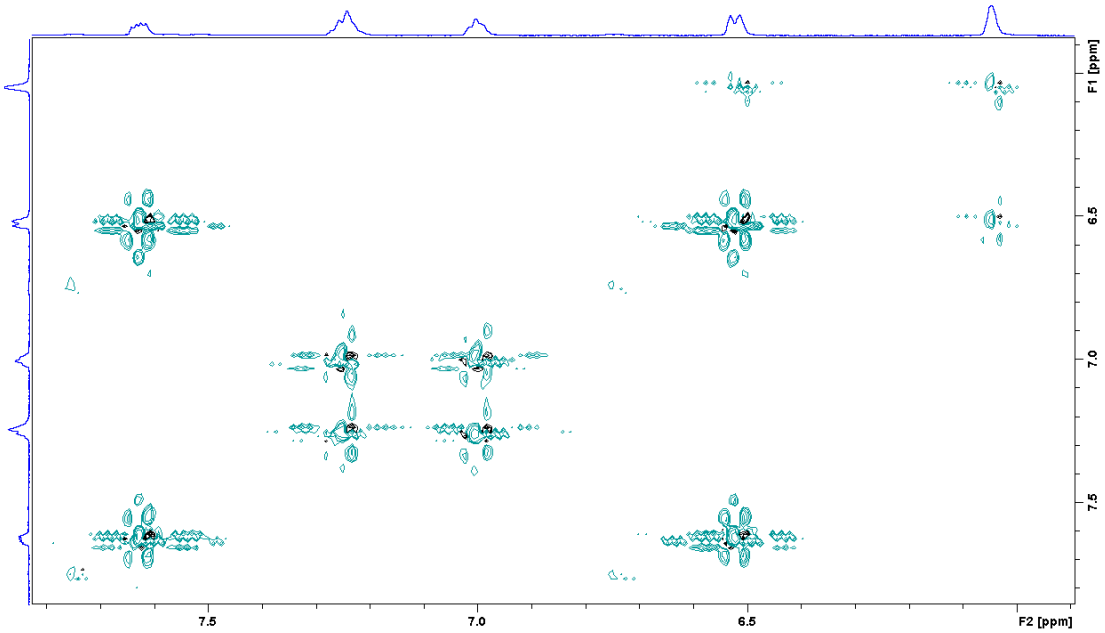

5b. Li_2[**4b**] (0.200 g, 0.347 mmol), (COD)PdMeCl (91.5 mg, 0.345 mmol) and CH_2Cl_2 (10 mL) were added to a vial. The vial was wrapped with foil, and the mixture was stirred for 1 h at room temperature. 4-^{t}Butylpyridine (50.9 µL, 0.347 mmol) was added and the mixture was stirred overnight at room temperature. The solution was filtered and the solvent was removed under vacuum to afford a pale yellow powder. This material was dissolved in CH_2Cl_2 (2 mL) and layered with hexanes (4 mL) to afford a white powder (0.131 g, 56% yield). X-ray quality crystals were grown from a CH_2Cl_2 solution layered with hexanes at -10 ^oC over 4 d. $^{31}P^7$ NMR (CD_2Cl_2): δ 39.2. ^{1}H NMR (CD_2Cl_2): δ 8.57 (d, $^3J_{HH}$ = 5, 2H, H^{11}), 8.12 (dd, $^4J_{PH}$ = 5, $^3J_{HH}$ = 9, 1H, H^3), 7.76 (dd, $^4J_{PH}$ = 5, $^3J_{HH}$ = 9, 1H, $H^{3'}$), 7.55–7.3 (m, 5H, H^8, H^9 and H^{10}; the H^8 resonance is broadened into the baseline due to restricted rotation around the P-C^7 bond), 6.95 (d, $^3J_{HH}$ = 8, 1H, H^4), 6.89 (d, $^3J_{PH}$ = 8, 1H, $H^{4'}$), 6.74 (d, $^3J_{HH}$ = 6, 2H, H^{12}), 6.35 (dd, $^5J_{PH}$ = 2, $^3J_{HH}$ = 14, 1H, H^6), 5.72 (dd, $^5J_{PH}$ = 3, $^3J_{HH}$ = 13, 1H, $H^{6'}$), 3.4–3.0 (m, 8H, $H^{16,16'}$ and $H^{18,18'}$), 1.05 (s, 9H, H^{15}), 1.04 (t, $^3J_{HH}$ = 7, 6H, H^{17}), 0.93 (t, $^3J_{HH}$ = 7, 6H, $H^{17'}$), -0.32 (d, $^3J_{PH}$ = 3, 3H, Pd-CH_3). $^{13}C\{^1H\}$ NMR (CD_2Cl_2): δ 160.9 (C^{13}), 151.6 (C^{11}), 149.3 (d, $^3J_{PC}$ = 7, $C^{5'}$), 147.7 (d, $^3J_{PC}$ = 9, C^5), 135.9 (d, $^2J_{PC}$ = 9, $C^{2'}$), 134.7 (d, 30, C^1), 134.4 ($C^{1'}$), 132.5 (d, $^1J_{PC}$ = 14, C^7), 130.7 (d, 8, C^6), 130.6 (C^8), 117.6 (d, $^1J_{PC}$ = 52, $C^{1'}$), 129.0 (br, C^9 and C^{10}), 121.6 (C^{12}), 118.1 (C^6), 116.6 (d, $^3J_{PC}$ = 9, $C^{6'}$), 111.0 (C^3), 110.3 ($C^{3'}$), 45.2 (C^{16}), 44.8 (C^{14}), 34.8 ($C^{16'}$), 30.4 (C^{15}), 13.0 (C^{16} and C^{17}), 12.7 ($C^{16'}$ and $C^{17'}$), –2.3 (s, Pd-CH_3). $^7Li^7$ NMR (CD_2Cl_2): δ -1.0. ^{31}P NMR (CD_3OD): δ 35.2. ^{1}H NMR (CD_3OD): δ 8.78 (s, 2H, H^{11}), 7.87 (br, 2H, $H^{4,4'}$), 7.55 (dd, $^3J_{HH}$ = 6, $^4J_{PH}$ = 2, 2H,

$H^{3,3'}$), 7.5-7.45 (m, 3H, $H^{9,9'}$ and H^{10}), (the H^{8} resonance is broadened into the baseline due to restricted rotation around the P-C^{7} bond), 6.75 (d, $^{3}J_{HH}$ = 9, 2H, H^{12}), 6.21 (br, 2H, $H^{6,6'}$), 3.16 m, 8H, $H^{16,16'}$ and $H^{18,18'}$), 1.36 (s, 9H, H^{15}), 0.94 (t, $^{3}J_{HH}$ = 7, 6H, $H^{17,17'}$ and $H^{19,19'}$), 0.65 (br, 3H, Pd-CH_3). HRMS (ESI; *m*/*z*): Calcd. for $[C_{76}H_{97}N_2O_{22}P_2Pd_2S_4Li_3]^+$ 1814.34462, Found: 1814.3479.[a]

Figure 4.39. Numbering scheme for **5b**.

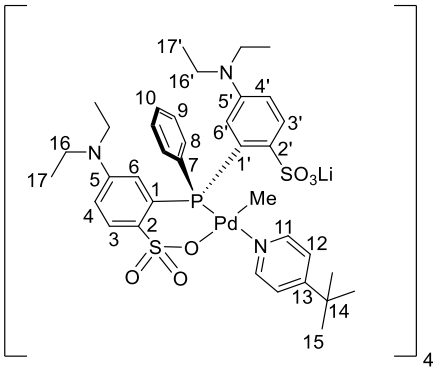

Figure 4.40. NMR spectra of 5b.

(a) $^{31}P\{^{1}H\}$ NMR (CD_2Cl_2, 500 MHz):

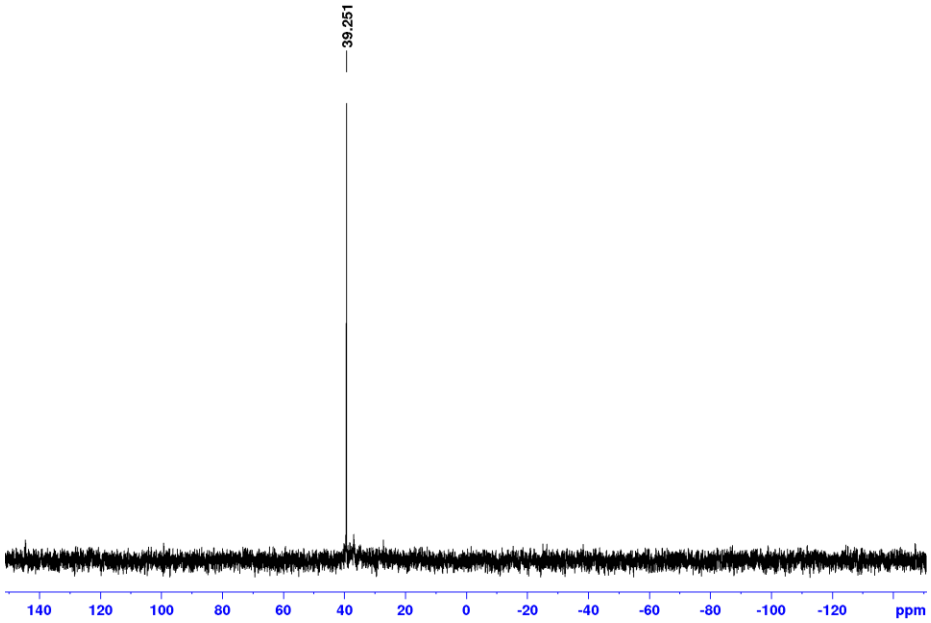

(b) ^{1}H NMR (CD_2Cl_2, 500 MHz):

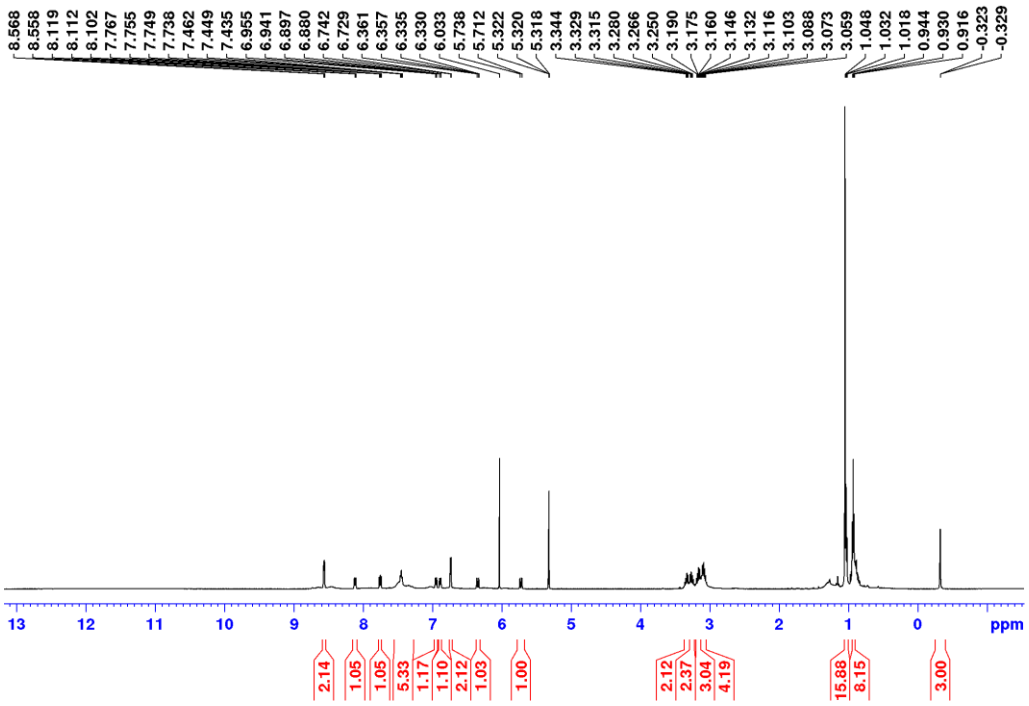

Figure 4.40, continued.

(c) $^{13}C\{^{1}H\}$ NMR (CD_2Cl_2, 126 MHz):

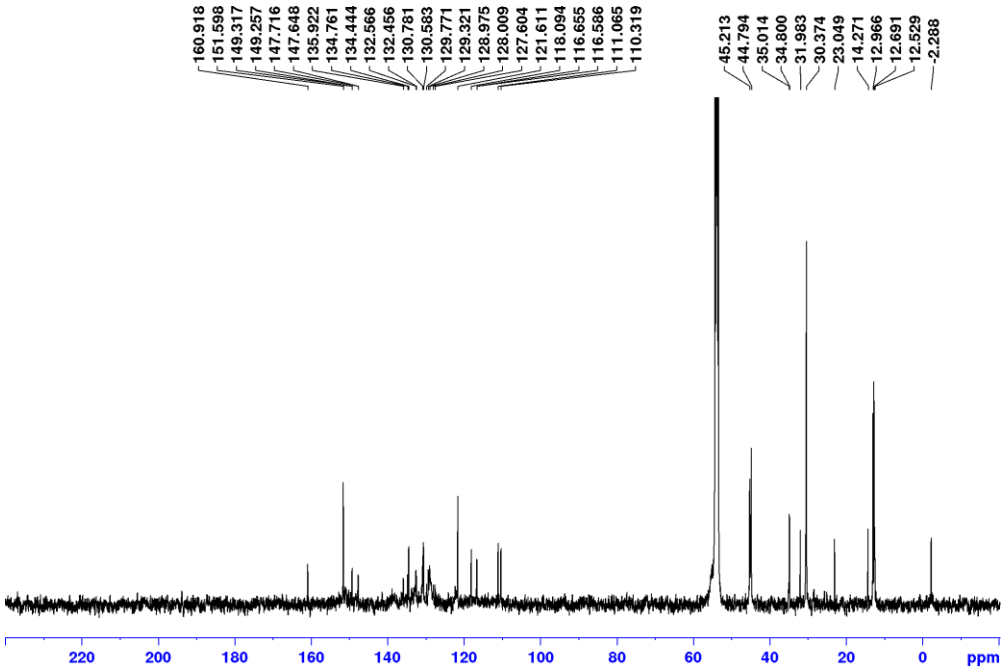

(d) $^{7}Li\{^{1}H\}$ NMR (CD_2Cl_2, 155 MHz):

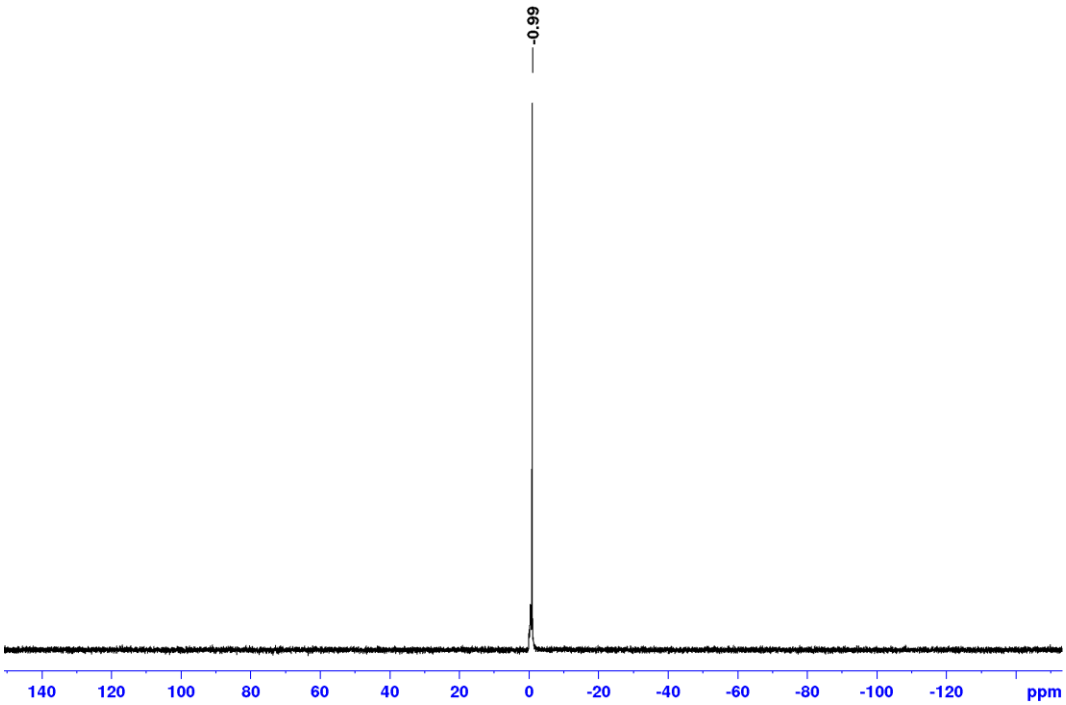

Figure 4.40, continued.

(e) $^{31}P\{^{1}H\}$ NMR (CD_3OD, 202 MHz):

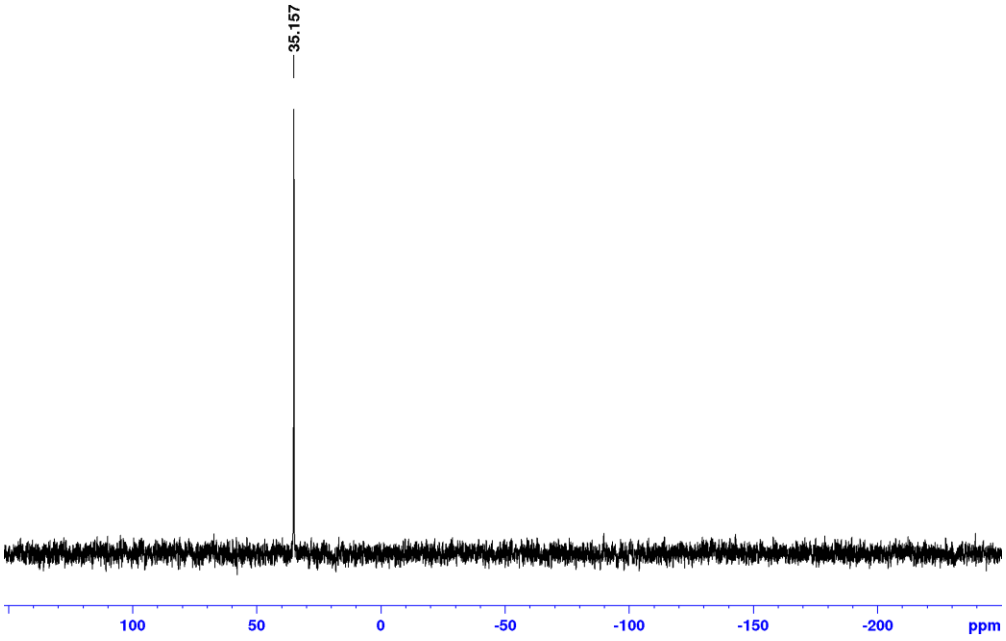

(f) ^{1}H NMR (CD_3OD, 500 MHz):

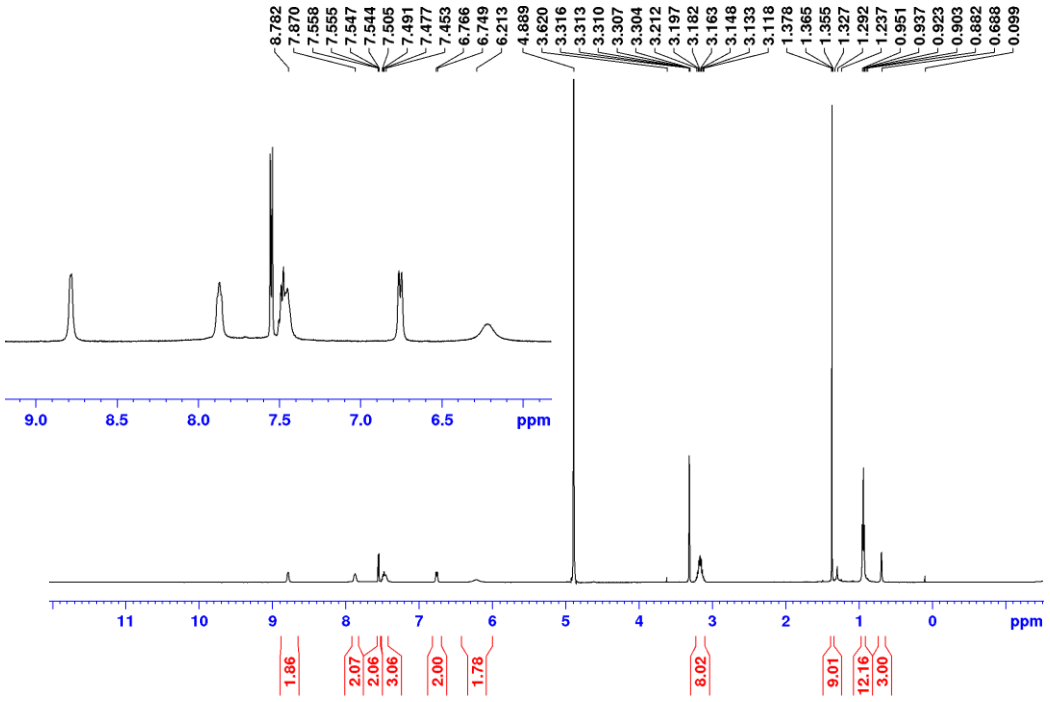

Pulsed-Gradient Spin-Echo (PGSE) NMR Experiments. All PGSE measurements were performed on a Bruker 500 MHz spectrometer using the SteJskal-Tanner method.[7] Two identical pulsed field gradients with duration δ = 0.004 s separated by a delay time Δ = 0.01418 s were incorporated into a spin-echo sequence, one before and the other after the 180° pulse. ^{1}H NMR spectra were recorded in CD_2Cl_2 or CD_3OD at 295.5 K without sample spinning. During each experiment, the gradient strength (G) was varied between 0 and 26 G/cm while keeping all other factors constant. The gradient was calibrated using a solution of 2% H_2O in D_2O. After obtaining the spectra, careful integration was carried out. In all studies, the integral of the Pd–Me resonance, if present, or a Pd–NMe_2 or Ar–H resonance was used to evaluate signal intensity. A linear plot of $\ln(I/I_0)$ (I = integral of a peak in the presence of G; I_0 = integral of the peak without a gradient) versus G^2 was generated. According to eq 1, the slope of this line is proportional to the diffusion coefficient and thus inversely proportional to the hydrodynamic radius of the molecule according to the Stokes-Einstein equation (eq 2). Hydrodynamic volumes were estimated by eq 3.

$$\ln(I/I_0) = -\gamma_H^2 \delta^2 G^2 (\Delta - \delta/3) D \quad (1)$$

where γ_H = magnetogyric ratio of ^{1}H; δ = length of the gradient pulse; Δ = delay between the midpoints of the gradients; D = diffusion coefficient.

$$r_H = k_B T/(6\pi\eta D) \quad (2)$$

where r_H = hydrodynamic radius, k_B = Boltzmann constant; T = temperature; η = viscosity of the solvent.

$$V_H = 4\pi r_H^3/3 \quad (3)$$

where V_H = hydrodynamic volume.

Figure 4.41. Linear plot of PGSE data (eq 1) for **2** in CD_2Cl_2 solution at 25 °C. Δ = 0.01418 s. The intrinsic viscosity of CD_2Cl_2 at 25 °C is 0.41 × 10^{-6} Pa•s. From eq 1-3, V_H = 8.6 × 10^3 Å.

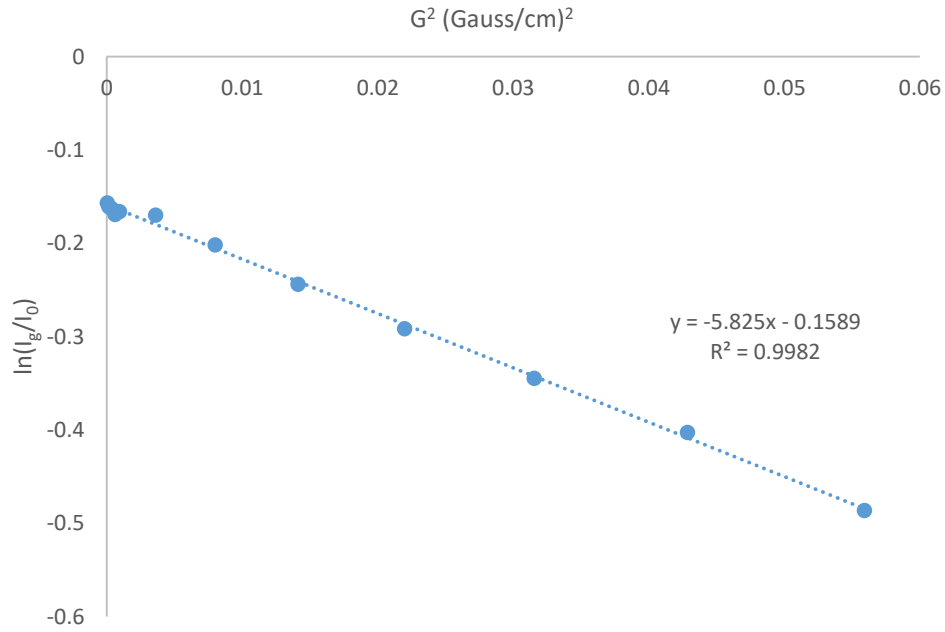

Figure 4.42. Linear plot of PGSE data (eq 1) for **2** in CD_3OD solution at 25 °C. Δ = 0.01418 s. The intrinsic viscosity of CD_3OD at 25 °C is 0.543 × 10^{-6} Pa•s. From eq 1-3, V_H = 3.2 × 10^3 Å.

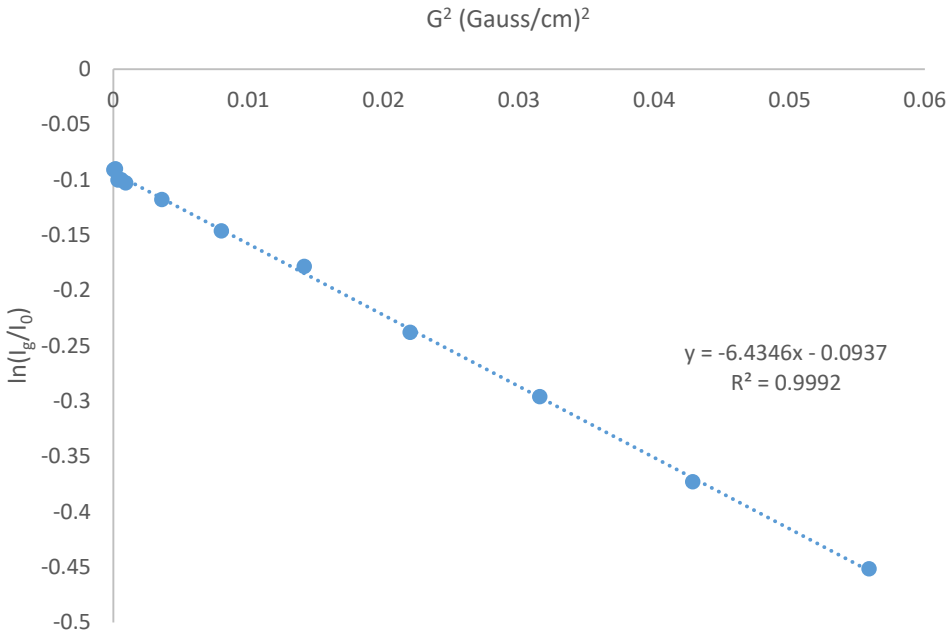

Figure 4.43. Linear plot of PGSE data (eq 1) for **6** in CD_2Cl_2 solution at 25 °C. Δ = 0.01418 s. The intrinsic viscosity of CD_2Cl_2 at 25 °C is 0.41 × 10^{-6} Pa•s. From eq 1-3, V_H = 8.87 × 10^3 Å.

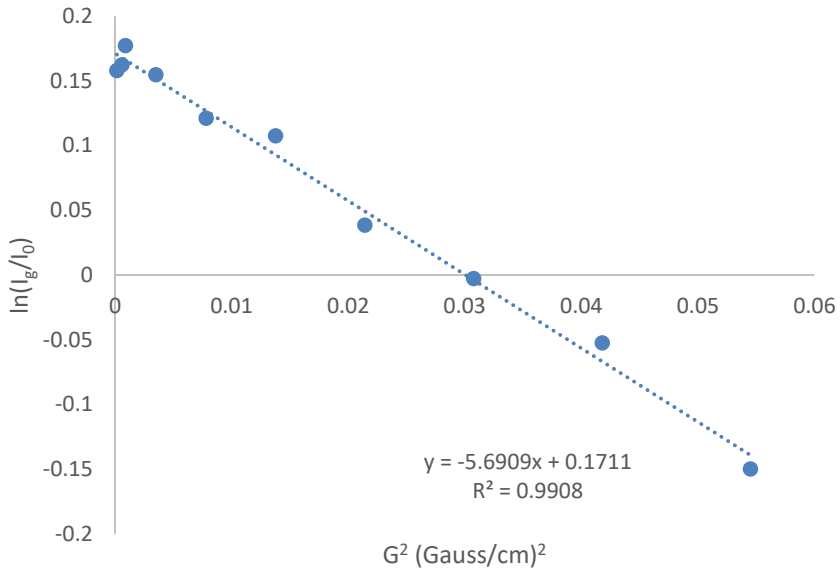

Figure 4.44. Linear plot of PGSE data (eq 1) for **6** in CD_3OD solution at 25 °C. Δ = 0.01418 s. The intrinsic viscosity of CD_3OD at 25 °C is 0.543 × 10^{-6} Pa•s. From eq 1-3, V_H = 5.4 × 10^3 Å.

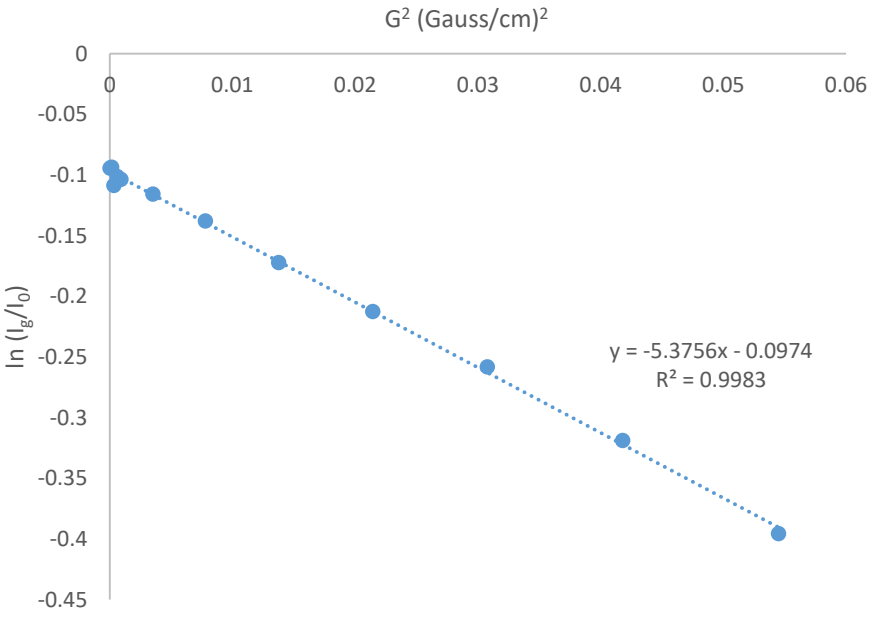

Figure 4.45. Linear plot of PGSE data (eq 1) for **7** in CD_2Cl_2 solution at 25 °C. Δ = 0.01418 s. The intrinsic viscosity of CD_2Cl_2 at 25 °C is 0.41 × 10^{-6} Pa•s. From eq 1-3, V_H = 7.5 × 10^3 Å.

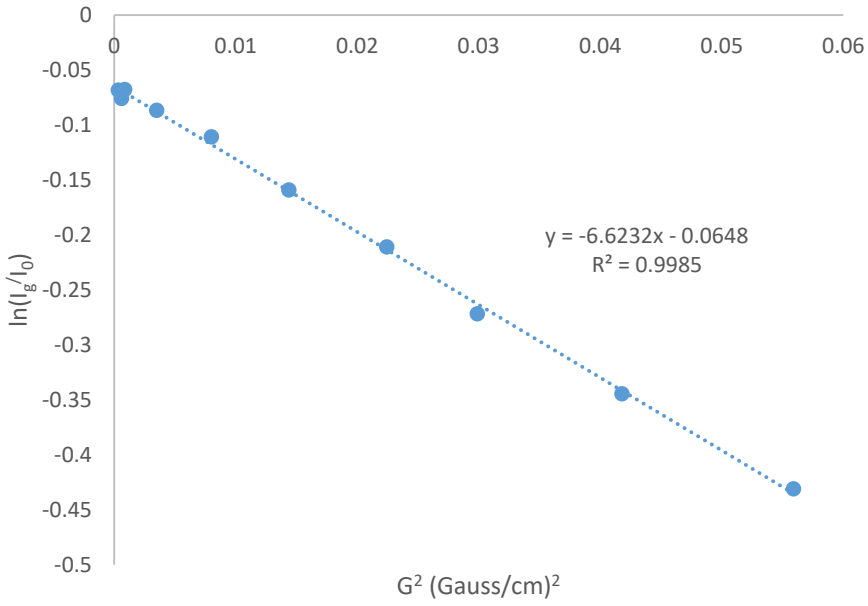

Figure 4.46. Linear plot of PGSE data (eq 1) for **5d** in CD_2Cl_2 solution at 25 °C. Δ = 0.01418 s. The intrinsic viscosity of CD_2Cl_2 at 25 °C is 0.41 × 10^{-6} Pa•s. From eq 1-3, V_H = 8.0 × 10^3 Å.

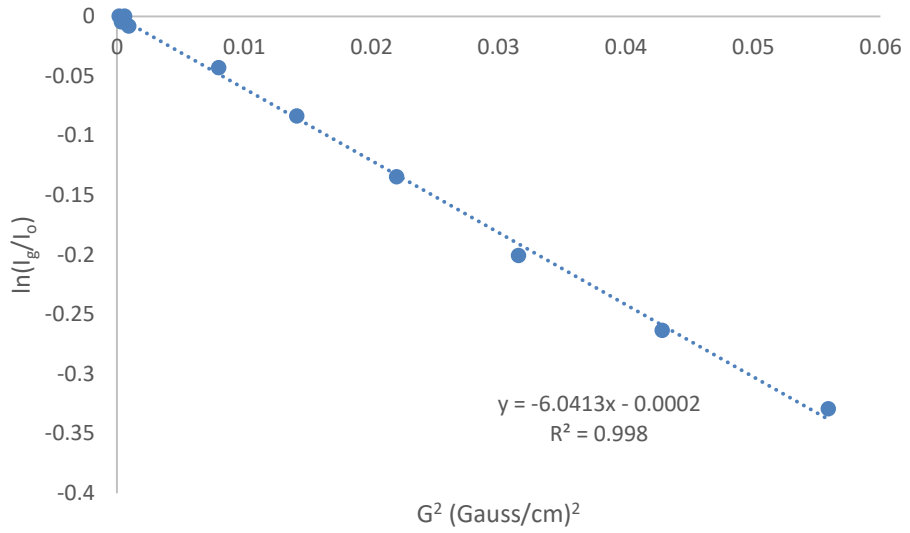

Figure 4.47. Linear plot of PGSE data (eq 1) for **5d** in CD_3OD solution at 25 °C. Δ = 0.01418 s. The intrinsic viscosity of CD_3OD at 25 °C is 0.543 × 10^{-6} Pa•s. From eq 1-3, V_H = 4.9 × 10^3 Å.

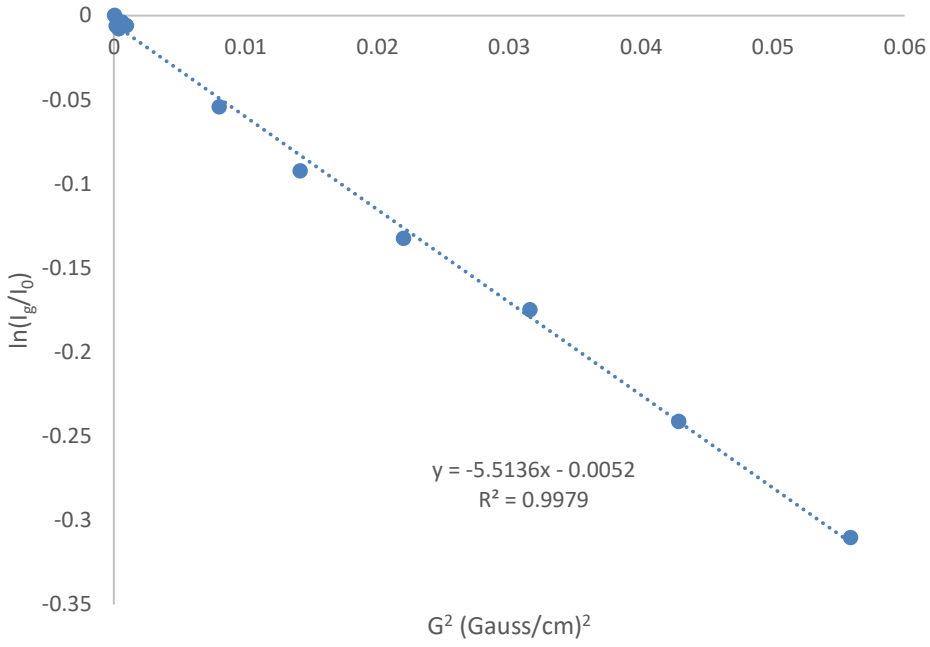

X-ray Crystallography. Data were collected on a Bruker D8 Venture diffractometer using Mo Kα radiation (0.71073 Å). Direct methods were used to locate many atoms from the E-map. Repeated difference Fourier maps enabled location of all expected non-hydrogen atoms. Following anisotropic refinement of all non-H atoms, ideal H atom positions were calculated. Final refinement was anisotropic for all non-H atoms and isotropic-riding for H atoms.

Specific details for structure refinement of 2. All elements were refined with anisotropic thermal parameters. Hydrogen atoms were included in idealized positions for structure factor calculations. The large molecular cluster consists of 4 of the same Pd-containing subunits, and one of the subunits is whole body disordered. Disorder was modelled using additional restraints, such as RIGU, DELU, FLAT, SADI. The ratio of major/minor parts refined to ca. 0.6. All structures are drawn with thermal ellipsoids at 50% probability. Anomalous scattering and absorption coefficients for λ = 0.41328 Å used (SHELX format): DISP C 0.0001 0.0005 5.2; DISP Cl 0.0554 0.053 141.4; DISP H 0 0 0.6; DISP Li 0.0001 0 1.9; DISP N 0.0005 0.001 7.2; DISP O 0.0017 0.0018 10.2; DISP P 0.0349 0.0309 86.6; DISP Pd -0.5286 2.5733 6120.5; DISP S 0.0444 0.0409 111.4.

Table 4.3. X-ray crystallographic parameters of **2**.

Empirical formula $C_{124}H_{132}Cl_2Li_6N_4O_{40}P_4Pd_4S_8$
Formula weight 3236.83
Temperature/K 100
Crystal system triclinic
Space group P-1
a/Å 20.527(3)
b/Å 20.970(2)
c/Å 25.175(3)
α/° 91.513(2)
β/° 105.892(2)
γ/° 118.807(2)
Volume/Å3 8969.9(18)
Z 2
ρcalcg/cm3 1.198
μ/mm-1 0.606
F(000) 3296.0
Crystal size/mm3 0.02 × 0.02 × 0.01
Radiation synchrotron (λ = 0.41328)
2Θ range for data collection/° 2.484 to 30.624
Index ranges $-26 \leq h \leq 26$, $-26 \leq k \leq 26$, $-31 \leq l \leq 32$
Reflections collected 197672
Independent reflections 35933 [Rint = 0.0515, Rsigma = 0.0375]
Data/restraints/parameters 35933/705/2040
Goodness-of-fit on F2 1.027
Final R indexes [I>=2σ (I)] R1 = 0.0504, wR2 = 0.1375
Final R indexes [all data] R1 = 0.0638, wR2 = 0.1450
Largest diff. peak/hole / e Å-3 2.08/-0.89

Stereoisomers of 7. As noted in the text, ^{1}H NMR spectra of **7** contain variable amounts of two sets of minor Pd–Me resonances (total <20%) comprising in one case four equal intensity signals (d, $^{3}J_{PH}$ = 3–4 Hz) and in the other case two equal intensity signals (d, $^{3}J_{PH}$ = 3 Hz), as illustrated in Figure 4.40.

Figure 4.48. Pd–Me region of ^{1}H NMR spectrum of **7.** Red and blue asterisks indicate Pd-Me resonances of two minor species.

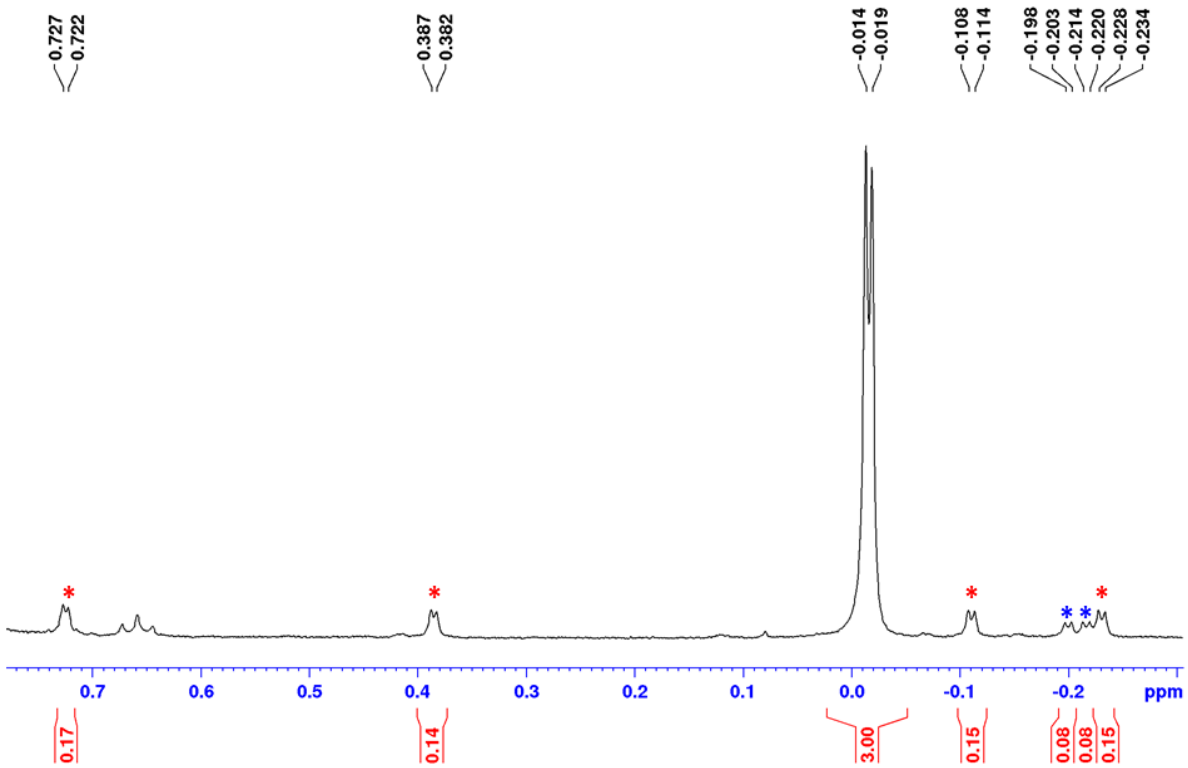

These minor species have not been conclusively identified but are likely to be diastereomers of **7** with different relative configurations at the phosphine P atoms. The configurations at the phosphine P atoms in the two pairs of Pd units in the major S_4-symmetric isomer are *SS* and *RR*. Analysis of molecular models suggests that inversion of

configuration of one phosphine P atom within each pair is possible. Therefore the minor diastereomers are likely to have *SSSR* and *SRSR* configurations at the phosphine P atoms. Analysis of molecular models shows that diastereomers generated by inversion of configuration of both phosphine P atoms within a pair are likely to be strongly disfavored due to extreme steric crowding.

4.5 Acknowledgements

As noted in the text, ligand Li_2[**4a**] was prepared by Qian Liu, and ligand Li_2[**4b**] and complex **5b** were prepared by James Earl under the supervision of the author. This work is included in this Chapter for completeness.

4.6 References and Notes

(1) Shen, Z.; Jordan, R. F. *J. Am. Chem. Soc.* **2010,** *132*, 52.

(2) Wei, J.; Shen, Z.; Filatov, A. S.; Liu, Q.; Jordan, R. F. *Organometallics* **2016,** *35*, 3557.

(3) Shen, Z.; Jordan, R. F. *Macromolecules* **2010,** *43*, 8706.

(4) Liu, Q., Multinuclear Palladium Catalysts for Ethylene Polymerization. University of Chicago, **2016**.

(5) Cohen, Y.; Avram, L.; Frish, L. *Angew. Chem., Int. Ed.* **2005,** *44*, 520.

(6) Johnson, C. S. *Progress in Nuclear Magnetic Resonance Spectroscopy* **1999,** *34*, 203.

(7) Stejskal, E. O.; Tanner, J. E. *The Journal of Chemical Physics* **1965,** *42*, 288.

(8) Hori, A.; Kumazawa, K.; Kusukawa, T.; Chand, D. K.; Fujita, M.; Sakamoto, S.; Yamaguchi, K. *Chem. – Eur. J.* **2001,** *7*, 4142.

(9) Coxall, R. A.; Harris, S. G.; Henderson, D. K; Parsons, S.; Tasker, P. A.; Winpenny, R. E. P. *J. Chem. Soc., Daton Trans.* **2000**, 2349.

(10) Lyubartsev, A. P.; Laasonen, K.; Laaksonen, A. *J. Chem. Phys.* **2001**, *114*, 3120.

(11) Rulke, R. E.; Ernsting, *J*. M.; Spek, A. L.; Elsevier, C. *J*.; van Leeuwen, P. W. N. M.; Vrieze, K. *Inorg. Chem.* **1993,** *32*, 5769.

(12) (COD)PdMeBr was synthesized analagously to (COD)PdMeCl from (COD)$PdBr_2$. See Ref. 9.

(13) Feng, R.; Yao, *J*.; Liang, Z.; Liu, Z.; Zhang, Y. *J. Org. Chem.* **2013,** *78*, 3688.

(14) Cockburn, B. N.; Howe, D. V.; Keating, T.; *J*ohnson, B. F. G.; Lewis, *J. J. Chem. Soc., Dalton Trans.* **1973**, 404.

(15) Ruiz, *J*.; Cutillas, N.; Rodríguez, V.; Sampedro, *J*.; López, G.; A. Chaloner, P.; B. Hitchcock, P. *J. Chem. Soc., Dalton Trans.* **1999**, 2939.

(16) The mass spectroscopy analysis is very challenging for the tetrameric complexe**s**, which is due to the cage fragmentation under the APCI/ES MS conditions. The highest intensity peak was assigned to $Pd_2\{[(Li\text{-}OPO)Pd]_2 \bullet LiX + H^+\}$ signal.

(17) Khalifa, A.; Conway, L.; Geoghegan, K.; Evans, P. *Tetrahedron Lett.* **2017**, *58*, 4559.

(18) Hogan, P. J.; Cox, B. G. *Org. Process Res. Dev.* **2009**, *13*, 875.

(19) Miyaji, R.; Asano, K.; Matsubara, S. *Chem. Eur. J.* **2017**, *23*, 9996.